

**Catalytic Carbon-Carbon Bond Hydrogenation
of Hydrocarbons with Water Catalyzed by
Group 9 Metalloporphyrins**

TO, Ching Tat

A Thesis Submitted in Partial Fulfilment
of the Requirements for the Degree of
Doctor of Philosophy
in
Chemistry

The Chinese University of Hong Kong
March 2015

Thesis Assessment Committee

Professor MAK Thomas Chung Wai (Chair)

Professor CHAN Kin Shing (Thesis Supervisor)

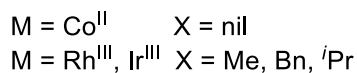
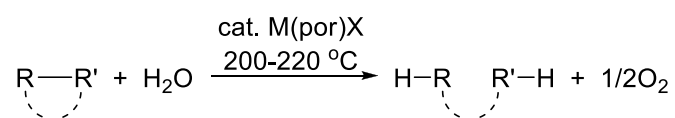
Professor WONG Nai Ching (Committee Member)

Professor Ma Jing (External Examiner)

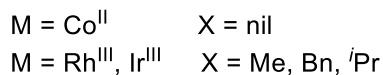
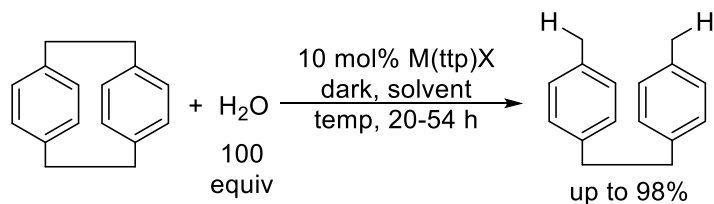
Professor Kwong Hoi-lun (External Examiner)

Abstract

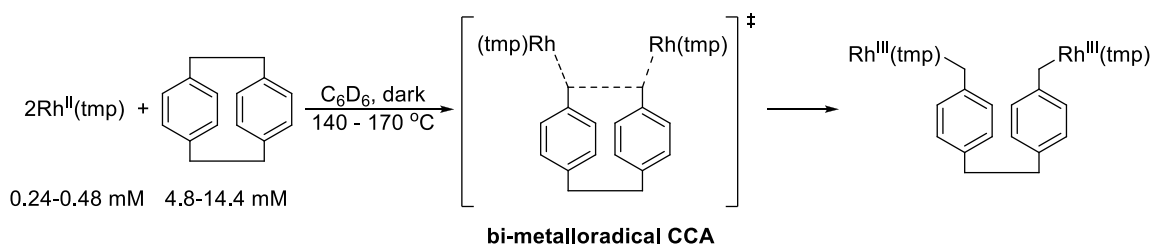
This thesis focuses on the mechanistic investigation of catalytic carbon-carbon σ -bond hydrogenation of hydrocarbons using water as the convenient hydrogen source under neutral conditions by group 9 metallocporphyrins M(por)X.



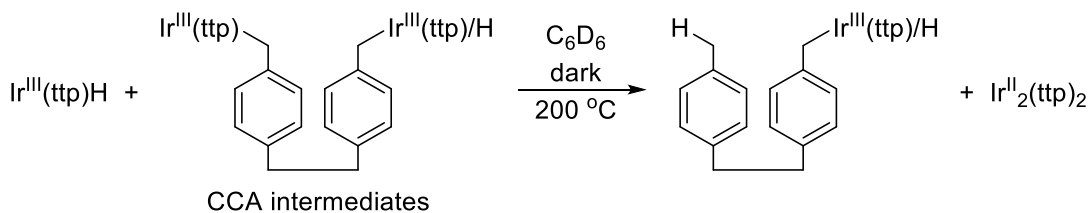
The benzylic carbon-carbon bond of [2.2]paracyclophane (PCP) was catalytically hydrogenated to give 4,4'-dimethylbibenzyl up to 98% yield using water with 10 mol% M(tpp)X pre-catalyst (tpp = 5,10,15,20-tetratolylporphyrinato dianion, M = Rh^{III} and Ir^{III}, X = Me, Bn and *i*Pr) at 200 °C in C₆D₆. Deuterium labeling experiments using D₂O supported water as the hydrogen source. Preliminary screening with Co^{II}(tpp) catalyst in polar DMF solvent at 220 °C also yielded the hydrogenation product selectively. The role of DMF is proposed to promote the hydrolysis of cobalt(III) porphyrin benzyl intermediates and increase the solubility of H₂O.



Kinetic studies on the stoichiometric benzylic CCA of PCP with $\text{Rh}^{\text{II}}(\text{tmp})$ metalloradical ($\text{tmp} = 5,10,15,20\text{-tetramesitylporphyrinato dianion}$) gave the rate law as $\text{rate} = k[\text{Rh}^{\text{II}}(\text{tmp})]^2[\text{PCP}]$. The 2nd order dependence on $\text{Rh}^{\text{II}}(\text{tmp})$ radical suggests a bi-metalloradical CCA mechanism via a four-centered transition state.



In the iridium catalyzed system, $\text{Ir}^{\text{III}}(\text{ttp})\text{H}$ was found to have promoting role in the hydrogenation process. The bi-molecular reductive elimination between $\text{Ir}^{\text{III}}(\text{ttp})\text{H}$ and the CCA intermediates speeded up the hydrogenation process. It is estimated that this process gave the hydrogenated alkyl fragment 3 times faster than hydrolysis of the CCA intermediates.



摘要

本論文主要探討在中性反應條件下，利用水作為一個方便的氫來源，以第 9 族金屬卟啉， $M(\text{por})X$ ，催化碳氫化合物中的碳碳單鍵加氫反應的反應機制。

在 200 °C 及溶有 10 mol% $M(\text{ttp})X$ ($M = \text{Rh}^{\text{III}}$ 和 Ir^{III} ， $X = \text{Me}$ ， Bn 和 $i\text{Pr}$) 預催化劑的氬代苯中，利用水把[2.2]二聚對二甲苯的苄基碳碳鍵進行催化加氫，生成高達 98% 的 4,4'-二甲基聯苄 (下稱 PCP)。利用氬代水的氬標記實驗支持了氫的來源為水。另一方面，經過以 $\text{Co}^{\text{II}}(\text{ttp})$ 催化劑進行了初步篩選後，能在 220 °C 及 DMF 極性溶劑中使加氫產物選擇性地生成。DMF 的作用被提議為促進鈷卟啉苄基的水解及增加了水的溶解度。

在進行了 $\text{Rh}^{\text{II}}(\text{tmp})$ 與 PCP 的當量苄基碳碳鍵活化動力學實驗後，得出速率方程 $\text{rate} = k[\text{Rh}^{\text{II}}(\text{tmp})]^2[\text{PCP}]$ 。 $\text{Rh}^{\text{II}}(\text{tmp})$ 的二級反應級數反映了一個經由四中心過渡態的雙金屬自由基碳碳鍵活化反應機制。

在由銨催化的系統中，發現了 $\text{Ir}^{\text{III}}(\text{ttp})\text{H}$ 在加氫過程中的促進作用。 $\text{Ir}^{\text{III}}(\text{ttp})\text{H}$ 與碳碳鍵活化中間體的雙分子還原消除反應把加氫過程加快。根據估計，這個雙分子還原消除反應比碳碳鍵活化中間體的水解要快 3 倍。

Acknowledgement

I would like to take this opportunity to express my hearty gratitude and sincere thanks to Professor Kin Shing Chan for his continuous encouragement, valuable comments and providing me an excellent research environment since I joined the group in 2008. I have experienced exciting adventures to look for solutions to difficulties and challenges in chemical research. Prof. Chan enthusiastically shares his authoritative knowledge on my research work, as well as in various areas of chemistry. This greatly enriched my understanding on those topics.

Thanks are given to my senior group members for their support on me, especially Dr. Yun Wai Chan, Dr. Yin Ki Jenkins Tsang and Dr. Kwong Shing Choi who guided my experimental works when I was undergraduate. I also thanks my current groupmates for their useful discussion and friendship.

I appreciate so much the technical support from all members of the Department of Chemistry to help me on the documentation work and instrumental analysis.

Finally, I am heavily indebted to my family members. Their care and understanding on me allow me to stay focus on the research work. I am very grateful to my family.

January, 2015.

Ching Tat To

Department of Chemistry

The Chinese University of Hong Kong

Table of Contents

	Page
Abstract	i
Acknowledgement	iv
Table of Contents	v
Abbreviations	ix
Structural Abbreviations for Porphyrins	x
Chapter 1 General Introduction	1
1.1 General Introduction of Hydrocarbons	1
1.2 Hydrocarbons as Fuel	1
1.3 [2.2]Paracyclophane	2
1.3.1 General Introduction to Cyclophane	2
1.3.2 Properties of [2.2]Paracyclophane	3
1.3.3 Organic Examples of Carbon(sp ³)-Carbon(sp ³) Bond Clevage of PCP	3
1.3.3.1 Thermolysis	3
1.3.3.2 Photolysis	4
1.3.3.3 Oxidative Clevage	5
1.4 Carbon-Carbon Bond Activation by Transition Metal Complexes	5
1.4.1 General Strategies	6
1.4.2 Carbon-Carbon Bond Activation of Hydrocarbons	7
1.4.2.1 1972 and Before	7
1.4.2.2 1974-1988	9
1.4.2.3 1988 and After	11
1.5 Water as Hydrogenation Agent	26
1.5.1 Titanium/H ₂ O System	27
1.5.2 Cobalt/H ₂ O System	29
1.5.3 Borane/H ₂ O System	29
1.6 Porphyrins and Group 9 Metalloporphyrins	30
1.6.1 Porphyrin Ligands	30
1.6.2 Metalloporphyrins	31
1.6.3 Chemistry of Group 9 Metalloporphyrins	33
1.6.3.1 M ^I (por) Chemistry	34
1.6.3.2 M ^{II} (por) Chemistry	35
1.6.3.3 M ^{III} (por) Chemistry	40
1.6.4 Equilibrium Between M ^I (por), M ^{II} (por) and M ^{III} (por)	42

1.7	Scope of Thesis	43
Chapter 2	Catalytic Carbon-Carbon Bond Hydrogenation of [2.2]Paracyclophane with Water by Rhodium Porphyrin Complexes	53
2.1	Introduction	53
2.2	Objectives of the Work	55
2.3	Preparation of Starting Materials	55
2.3.1	Synthesis of Porphyrins	55
2.3.2	Synthesis of Metalloporphyrins	56
2.3.2.1	Synthesis of Rhodium(III) Porphyrin Halides	56
2.3.2.2	Synthesis of Rhodium(III) Porphyrin Alkyls	57
2.3.2.3	Synthesis of Rh ^{II} (tmp)	57
2.4	Optimization of Catalytic PCP Hydrogenation with H ₂ O	58
2.4.1	Initial Screenings	58
2.4.2	Porphyrin Ligand Electronic Effects	60
2.4.3	Additive Effects	62
2.5	Mechanistic Investigations	62
2.5.1	Deuterium Labeling Experiments	63
2.5.2	CCA via CHA Intermediates	65
2.5.3	¹ H NMR Kinetics of Stoichiometric CCA	67
2.5.3.1	Determination of Reaction Orders	68
2.5.3.2	Activation Parameters	70
2.5.4	Mechanistic Implications	73
2.5.4.1	Rh ^{II} (tmp) as a Trap	73
2.5.4.2	PCP Homolysis Rate at 200 °C	75
2.5.4.3	Possible CCA Transition State	77
2.5.4.4	Computational Study	77
2.5.5	Hydrolysis of Rh ^{III} (ttp)R	79
2.6	Proposed Mechanism	80
2.7	Conclusions	82
	Experimental Section	87
Chapter 3	Catalytic Carbon-Carbon Bond Hydrogenation of [2.2]Paracyclophane with Water by Iridium Porphyrin Complexes	110
3.1	Introduction	110
3.2	Objectives of the Work	111
3.3	Preparation of Starting Materials	111
3.3.1	Synthesis of Metalloporphyrins	111
3.3.1.1	Synthesis of Iridium(III) Porphyrin Halides	111
3.3.1.2	Synthesis of Iridium(III) Porphyrin Alkyls	111

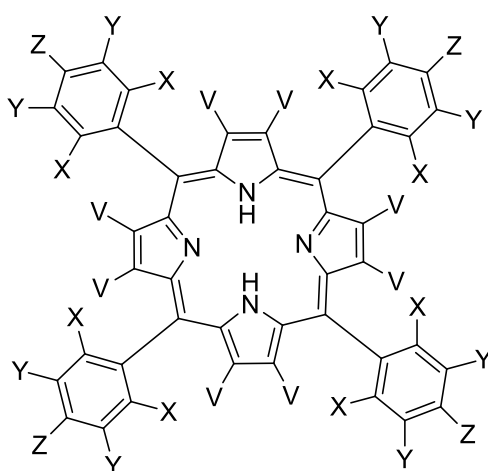
	3.3.1.3	Synthesis of Ir ^{III} (ttp)H and Ir ^{II} ₂ (ttp) ₂	112
3.4		Optimization of Catalytic PCP Hydrogenation with H ₂ O	112
	3.4.1	With Ir ^{III} (ttp)R Pre-Catalysts	112
	3.4.2	Ir ^{III} (ttp) ⁱ Pr Pre-Catalyst Loading	114
	3.4.3	Water Loading Effects	115
	3.4.4	Additive Effects	117
3.5		Mechanistic Investigations	118
	3.5.1	Deuterium Labeling Experiments	118
	3.5.2	CCA vis CHA Intermediate	120
	3.5.3	Hydrolysis of Ir ^{III} (ttp)R	122
		3.5.3.1 Investigation with Ir ^{III} (ttp)CD ₃	123
		3.5.3.2 Investigation with Ir ^{III} (ttp) ⁱ Pr	125
	3.5.4	Reaction of Ir ^{II} ₂ (ttp) ₂ with PCP	128
	3.5.5	Reaction of Ir ^{III} (ttp)H with PCP	128
		3.5.5.1 Ir ^{II} (ttp)-Catalyzed 1,2-Addition of Ir ^{III} (ttp)H	131
		3.5.5.2 Bi-molecular Reductive Elimination with Ir ^{III} (ttp)H	134
	3.5.6	Reaction of Ir ^{II} ₂ (ttp) ₂ with H ₂ O	138
3.6		Proposed Mechanism	141
3.7		Conclusions	143
		Experimental Section	147
Chapter 4		Catalytic Carbon-Carbon Bond Hydrogenation of [2.2]Paracyclophane with Water by Cobalt Porphyrin Complexes	169
	4.1	Introduction	169
	4.2	Objectives of the Work	169
	4.3	Preparation of Cobalt(II) Porphyrins	169
	4.4	Discovery of Selective Hydrogenation of PCP in DMF Solvent	170
	4.5	Optimization of Catalytic Hydrogenation of PCP with H ₂ O	172
		4.5.1 Porphyrin Ligand Electronic Effects	172
		4.5.2 Solvent Effects	173
		4.5.3 Catalyst Loading Effects	174
		4.5.4 Temperature Effects	176
		4.5.5 Improved Catalytic Hydrogenation of PCP at Higher Temperatures	177
	4.6	Mechanistic Investigations	179
		4.6.1 Pre-coordination of DMF to Co ^{II} (ttp)	179
		4.6.2 Stability Test of Co ^{II} (ttp) with H ₂ O in DMF	179
	4.7	Proposed Mechanism	181

4.8	Co ^{II} (ttp) Catalyzed Carbon-Carbon Bond Hydration in DMSO	182
4.9	Conclusions	182
	Experimental Section	185
Chapter 5	Analysis on the Carbon-Carbon Bond Activation with Group 9 Metalloporphyrins	200
5.1	Introduction	200
5.2	Thermodynamics	200
	5.2.1 Equilibrium Concentration of M ^{II} (ttp) Metalloradical	200
	5.2.2 Reaction Free Energy Estimations	201
5.3	Kinetics	204
5.4	Bi-molecular Reductive Elimination with M ^{III} (ttp)H	207
5.5	Redox Potentials of Group 9 Metalloporphyrins	208
5.6	Conclusions	210

Abbreviations

δ	: chemical Shift	J	: coupling constant
Anal	: analytical	K	: equilibrium constant
Ar	: Aryl	k	: rate constant
OAc	: acetate	m	: multiplet (NMR)
Bn	: benzyl	M^+	: molecular ion
PhCN	: benzonitrile	M	: molarity
BDE	: bond dissociation energy	Me	: methyl
br	: broad singlet (NMR)	mg	: milligram (s)
t Bu	: <i>tert</i> -butyl	min	: minute (s)
Bn	: benzyl	mL	: milliliter (s)
Calcd.	: calculated	mM	: millimolar (s)
CCA	: carbon carbon bond activation	mmol	: millimole (s)
CHA	: carbon hydrogen bond activation	nm	: nanometer
COD	: 1,5-cyclooctadiene	NMR	: nuclear magnetic resonance
Cp	: cyclopentadienyl	por	: porphyrin dianion
d	: day (s)	ppm	: part per million
$^{\circ}$ C	: degree Celsius	Ph	: phenyl
K	: degree Kelvin	n Pr	: <i>n</i> -propyl
d	: doublet (NMR)	i Pr	: isopropyl
DMF	: <i>N,N</i> -dimethylformamide	py	: pyridine
H	: enthalpy	q	: quartet (NMR)
S	: entropy	quin	: quintet (NMR)
Et	: ethyl	R	: alkyl group
equiv	: equivalent (s)	R_f	: retention factor
ESI	: electrospray ionization	r.t.	: room temperature
FAB	: fast atom bombardment	s	: second (s)
g	: gram (s)	s	: singlet (NMR)
G	: Gibbs free energy	sept	: septet (NMR)
GC/MS	: gas chromatography/mass spectrometry	sext	: sextet (NMR)
h	: hour (s)	THF	: tetrahydrofuran
HRMS	: highest resolution mass spectrometry	t	: triplet (NMR)
Hz	: Hertz	TLC	: thin-layer chromatography
IR	: infrared	TMS	: tetramethylsilane

Structural Abbreviations for Porphyrins



Nomenclature of Porphyrins

Abbreviation	Porphyrin	Substituent			
		V	X	Y	Z
H ₂ (tpp)	5,10,15,20-tetraphenylporphyrin	H	H	H	H
H ₂ (ttp)	5,10,15,20-tetratolylporphyrin	H	H	H	Me
H ₂ (tap)	5,10,15,20-tetraanisylporphyrin	H	H	H	OMe
H ₂ (t _p -CF ₃ pp)	5,10,15,20-tetra(<i>p</i> -trifluoromethylphenyl)porphyrin	H	H	H	CF ₃
H ₂ (t _p -Clpp)	5,10,15,20-tetra(<i>p</i> -chlorophenyl)porphyrin	H	H	H	Cl
H ₂ (tmp)	5,10,15,20-tetramesitylporphyrin	H	Me	H	Me
H ₂ (ocp)	2,3,7,8,12,13,17,18-octachloro- 5,10,15,20-tetraphenylporphyrin	Cl	H	H	H
H ₂ (bocp)	5,10,15,20-tetrakis(<i>p</i> - ^t butyl- phenyl)porphyrin	Cl	H	H	^t Bu
H ₂ (tspp)	5,10,15,20-tetra(<i>p</i> -sulfonatophenyl)porphyrin	H	H	H	SO ₃ ⁻
H ₂ (oep)	2,3,7,8,12,13,17,18-octaethylporphyrin	Et	--	--	--

Chapter 1 General Introduction

1.1 General Introduction of Hydrocarbons

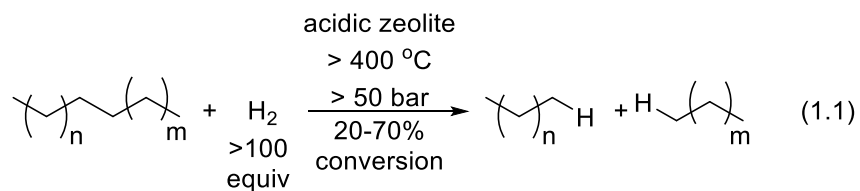
Hydrocarbons are compounds made of carbon and hydrogen only, and the most basic class of organic compounds.¹ They are non-polar in nature. Hydrocarbons can generally be divided into 4 classes based on bonding structure: (1) alkane; (2) alkene; (3) alkyne; and (4) aromatics, which contain C-C, C=C, C≡C bonds and benzene ring in their carbon skeletons, respectively.

1.2 Hydrocarbons as Fuel

Combustion of fuel is an exothermic reaction, where energy is released. Hydrocarbons are fossil fuels and exist in the form of coal, oil or natural gas with varying H:C ratio (Table 1.1).¹ Hydrocarbons with higher H:C ratio are considered as clean fuel as they tend to burn completely, or alternatively with more C-H bonds to be oxidized. Therefore, short chain hydrocarbons are ideal fuel, e.g. petrol. In petroleum industry, heavier hydrocarbons are converted to lower molecular weight fragments via hydrocracking process to increase their H:C ratio (eq 1.1).² This process involves the cleavage of aliphatic carbon-carbon bonds followed by hydrogenation.

Table 1.1 H:C Ratio of Different Hydrocarbon Sources.

Hydrocarbon Sources	Average H:C Ratio
Methane	4.0
Natural Gas	3.8
Petroleum Crude	1.8
Shale oil (raw)	1.5
Bituminous coal	0.8



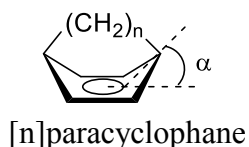
1.3 [2.2]Paracyclophane

1.3.1 General Introduction to Cyclophane

Cyclophanes are a type of hydrocarbon containing at least one aromatic ring bridged with carbon side chains of various lengths.³ The aromatic ring, with benzene as the simplest form, is distorted into a boat form unless the side chain is sufficiently long. Table 1.2 summarizes the relationships between the bridge length n , distortion angle α and the theoretical heat of formation ΔH_f using $[n]$ paracyclophane as the example.^{3b} In general, the shorter the bridge length, the more distorted the aromatic ring, and therefore more strain.

Table 1.2 Relationships between bridge length, distortion angle and heat of formation in $[n]$ paracyclophane.

	n	α ($^\circ$)	ΔH_f (kcal/mol) ^a
	9	9.6	-18.9
	8	13.4	-8.7
	7	16.4	5.1
	6	22.3	26.2
	5	28.6	53.8
	4	35.6	87.8
	3	79.4	117.8

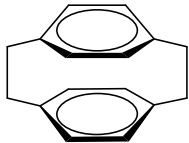


^a Calculation at AM1 level.

1.3.2 Properties of [2.2]Paracyclophane

[2.2]Paracyclophane (PCP) contains two benzene rings bridged by two *para* -CH₂CH₂- groups. It is first prepared by Brown and Farthing in 1949 in the pyrolysis of *p*-xylene.⁴ Table 1.3 summarizes some properties of PCP.

Table 1.3 Properties of [2.2]Paracyclophane.

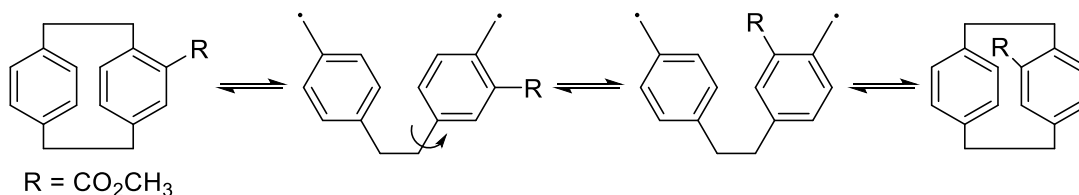
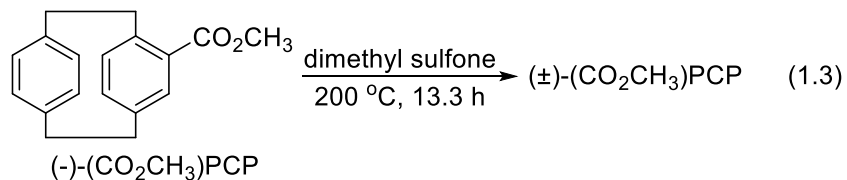
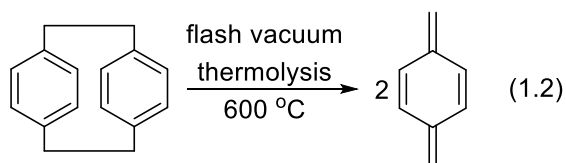
	$\Delta H_f(\text{gas})^5$	57.7 kcal/mol
	Melting point ⁴	285 °C
	CH ₂ -CH ₂ length ⁶	1.558 Å (93K), 1.630 Å (291K),
	Angle of bending of benzene ⁶	14° (93 K and 291 K)
	Strain Energy ⁵	31 kcal/mol
	1 st oxidation potential ⁷	1.52 V
	2 nd oxidation potential ⁷	1.80 V

1.3.3 Organic Examples of Carbon(sp³)-Carbon(sp³) Bond Cleavage of PCP

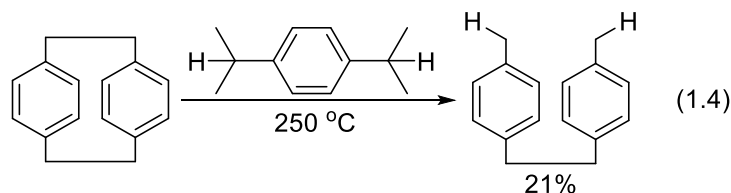
There are three types of C(sp³)-C(sp³) bond cleavage of PCP: (1) thermolysis; (2) photolysis; and (3) oxidative cleavage.

1.3.3.1 Thermolysis

Flash vacuum thermolysis of PCP at 600 °C resulted in cleavage of two bridging carbon-carbon bonds to give *p*-xylylene (eq 1.2).⁸ Racemization of (-)-4-carbomethoxy[2.2]paracyclophane at 200 °C has been reported to go through a benzylic diradical intermediate (eq 1.3 and Scheme 1.1).⁹ The diradical character was further supported by trapping using H atom donor solvent *p*-diisopropylbenzene. 4,4-Dimethylbibenzyl was formed in 21% yield when PCP was heated in *p*-diisopropylbenzene at 250 °C, together with oligomeric *p*-xylyl co-products (eq 1.4).⁹

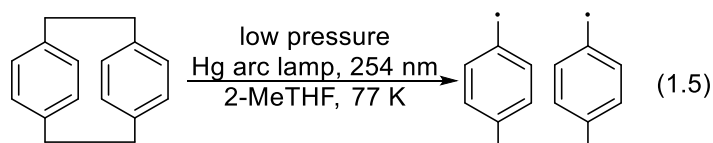


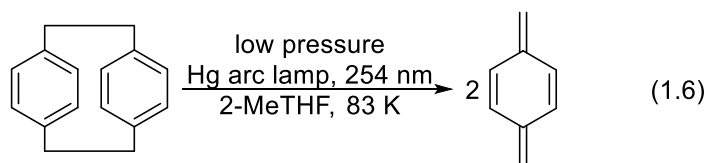
Scheme 1.1 Racemization of (-)-4-Carbomethoxy[2.2]paracyclophane via Diradical Intermediate



1.3.3.2 Photolysis

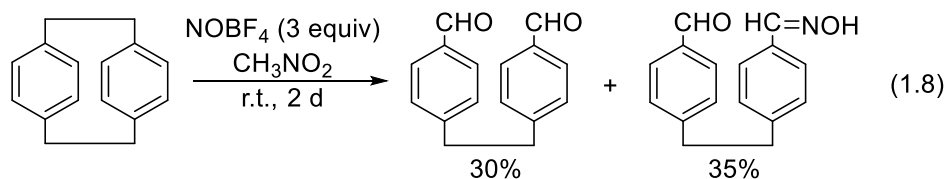
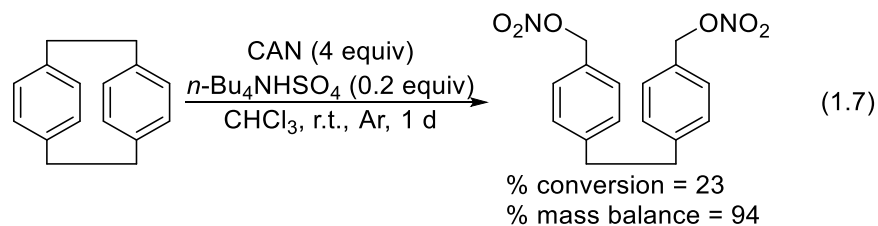
Kaupp has reported the CH₂-CH₂ bridge cleavage in PCP by photolysis. Irradiation of PCP in 2-methyltetrahydrofuran organic glass with 254 nm low pressure mercury arc lamp yielded the benzylic diradical at 77 K (eq 1.5).¹⁰ At 83 K, *p*-xylylene was formed instead (eq 1.6).¹⁰





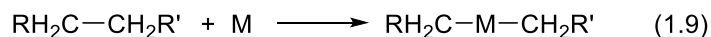
1.3.3.3 Oxidative Cleavage

The ethylene bridge is cleaved heterolytically in the presence of strong oxidizing agents. PCP underwent ring opening under the action of cerium(IV) ammonium nitrate (CAN) in CHCl_3 to form the nitroxymethyl substituted product (eq 1.7).¹¹ NOBF_4 oxidized PCP successfully with ring cleavage to yield a mixture of aldehyde and oxime products (eq 1.8).¹²



1.4 Carbon-Carbon Bond Activation by Transition Metal Complexes

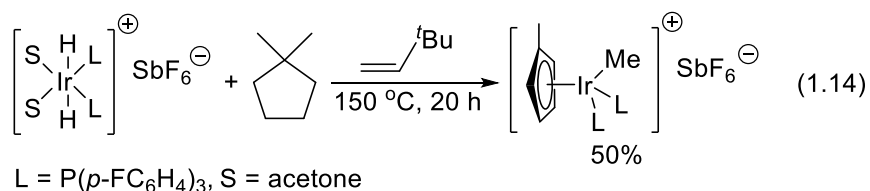
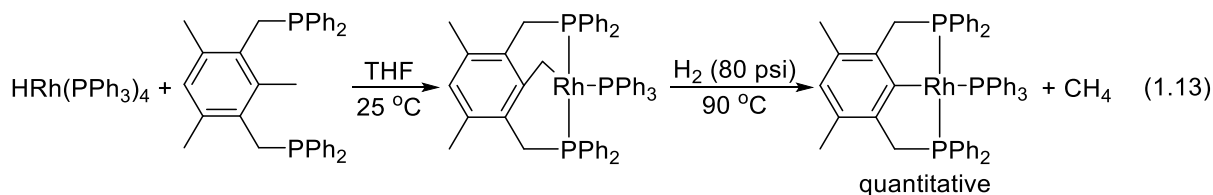
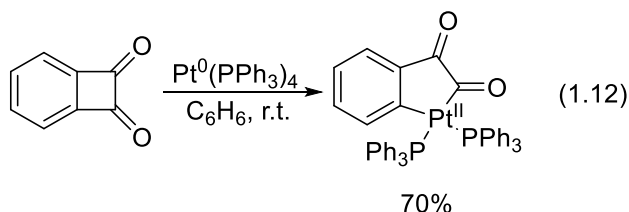
Carbon-carbon bond activation (CCA) of hydrocarbons by transition metal complexes involves the cleavage of C-C bond followed by the formation of M-C bond (eqs 1.9 and 1.10).¹³ In catalytic CCA, the M-C bond is further functionalized to give desired product (eq 1.11).

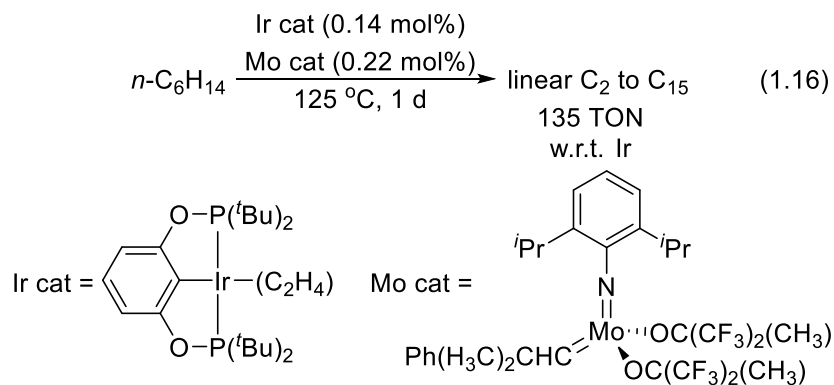
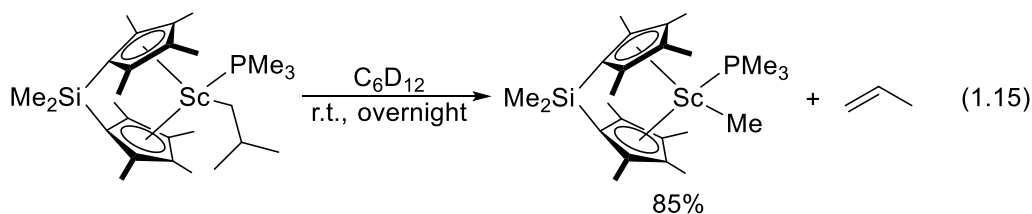


Homogeneous carbon-carbon bond activation of hydrocarbons with transition metal complexes is very challenging, mainly accounted by two reasons: (1) kinetically inaccessibility of the C-C bond due to the surrounding C-H bonds; and (2) competitive C-H bond activation because of forming stronger M-H bond than M-C bond.^{14,15}

1.4.1 General Strategies

Several common strategies have been observed in the homogeneous CCA of organic substrates, including ring strain relief (eq 1.12),¹⁶ chelation assistance (eq 1.13),¹⁷ aromatization (eq 1.14),¹⁸ β -alkyl elimination (eq 1.15)¹⁹ and alkane metathesis (eq 1.16).²⁰ Since the scope of this thesis focus on CCA of hydrocarbons, the mechanistic details for functionalized substrates will not be discussed.



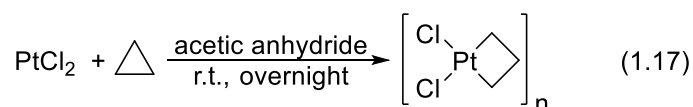


1.4.2 Carbon-Carbon Bond Activation of Hydrocarbons

Table 1.4 summarizes the stoichiometric and catalytic CCA of hydrocarbons with transition metal complexes in chronological order. Most of the examples reported are associated with ring strained hydrocarbons. From the table, the development of CCA of hydrocarbons can generally be divided into three eras: (1) 1972 and before; (2) 1974-1988; and (3) 1988 and after. They will be discussed one by one accompanied with representative examples in details.

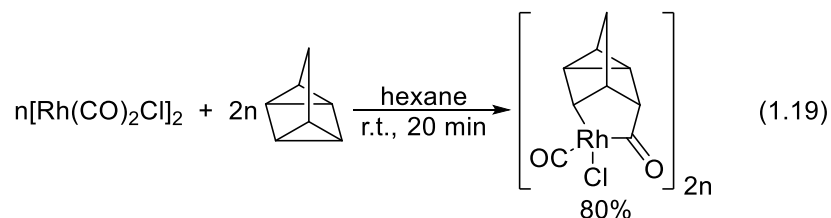
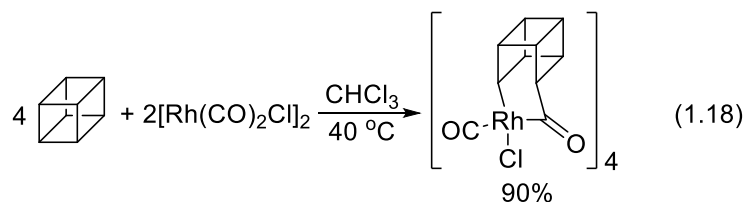
1.4.2.1 1972 and Before

In 1955, Tipper reported the first CCA of hydrocarbon by reacting cyclopropane with PtCl_2 to yield the platinumacyclobutane complex (eq 1.17).²¹ It is proposed to go through an oxidative addition mechanism.

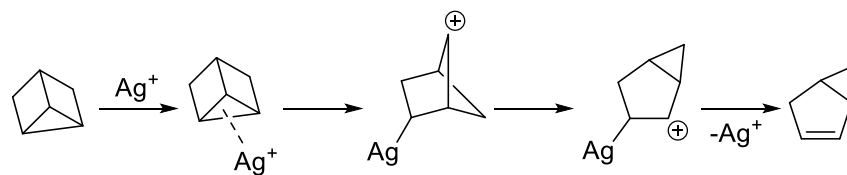


Most reports later on are restricted to the catalytic rearrangement of strained cyclopropyl and cyclobutyl ring systems. These rearrangements usually fall into either mechanism: (1) rearrangement by initial oxidative addition of metal to the C-C bond followed by retro-oxidative C-C coupling or (2) symmetry forbidden rearrangement catalyzed by metal with suitable d orbitals for interaction (Lewis acidic metal ion like Ag^+).

The oxidative addition mechanism is supported by the CO insertion in stoichiometric reactions investigated by Halpern. The low valent $[\text{Rh}(\text{CO})_2\text{Cl}]_2$ inserts into the C-C bond of cubane at 40 °C in CHCl_3 to yield 90% of the 6-membered metallocycle (eq 1.18).²⁸ The cyclopropane ring in quadricyclane reacted similarly with $[\text{Rh}(\text{CO})_2\text{Cl}]_2$ to yield 80% of the 5-membered metallocycle (eq 1.19).²⁹

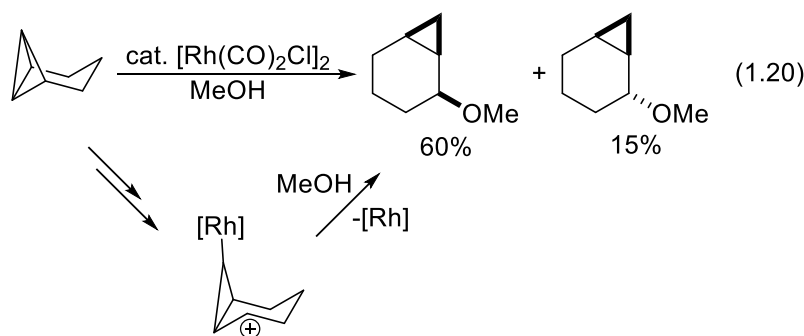


The metal catalyzed symmetry forbidden rearrangements are usually triggered by silver(I) complexes. It is suggested that the weak coordination of silver(I) to the strained C-C bond with partial π -bond character is involved in the first step, followed by intermediate formation with Ag-C bond and carbocation. For example, the rearrangement of tricyclohexane by AgPF_6 reported by Katz goes through the proposed mechanism depicted in Scheme 1.2.³⁵



Scheme 1.2 Proposed Mechanism for the Ag^+ Catalyzed Rearrangement of Tricyclohexane

Interestingly, heterolytic cleavage of C-C bond to form M-C bond and carbocation intermediate in protic solvent by low valent $[\text{Rh}(\text{CO})_2\text{Cl}]_2$ has also been proposed. In the $[\text{Rh}(\text{CO})_2\text{Cl}]_2$ catalyzed rearrangement of tricyclo[4.1.0.0]heptane carried out in MeOH, trapping products by the solvent were isolated (eq 1.20 and Scheme 1.3).³⁴ A carbocation intermediate is likely formed.

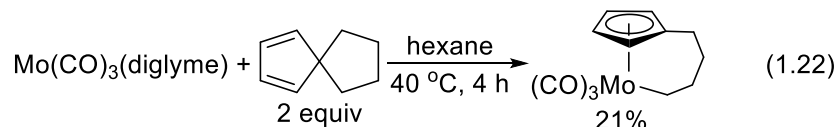
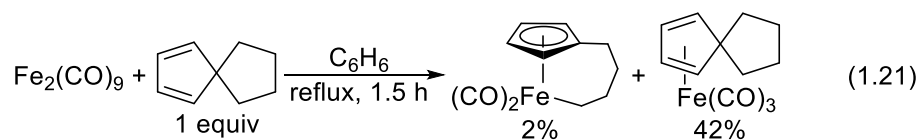


Scheme 1.3 $[\text{Rh}(\text{CO})_2\text{Cl}]_2$ Catalyzed Rearrangement of Tricyclo[4.1.0.0]heptane in MeOH.

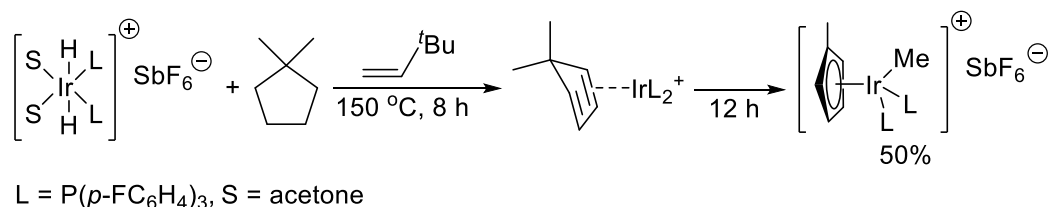
1.4.2.2 1974-1988

In 1974-1988, the investigations on CCA are stoichiometric based with greatly broadened substrate scopes. There are successful reports on CCA of unstrained hydrocarbons.

Eilbracht reported the stoichiometric CCA of spiro[4.4]nona-1,3-diene with iron and molybdenum carbonyl complexes (eqs 1.21 and 1.22).⁴¹ The relatively unstrained cyclopentane ring was cleaved driven by pre-coordination of metal to the diene moiety and subsequent aromatization.

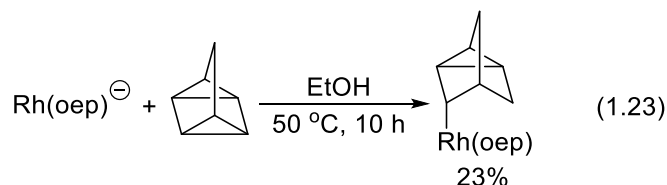


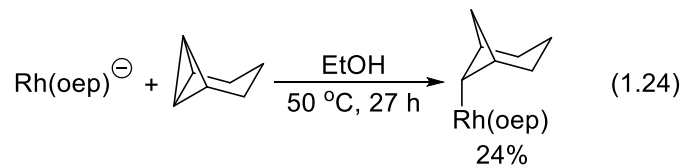
Crabtree in 1984 reported the CCA of 1,1-dimethylcyclopentane with iridium complex (Scheme 1.4).¹⁸ The alkane first undergoes dehydrogenation with *t*-butylethylene as acceptor to form the iridium-diene π complex intermediate. Further heating results in methyl transfer and aromatization to give CCA product.



Scheme 1.4 Proposed Mechanism for the CCA of 1,1-Dimethylcyclopentane

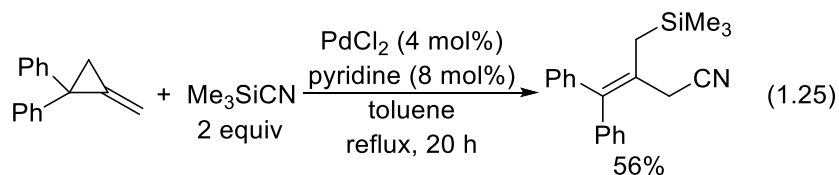
Ogoshi reported an interesting finding on stoichiometric CCA by nucleophilic substitution. Rh^I(oep)[−] anion undergoes nucleophilic attack at the tri-bridged carbon in quadricyclane and [4.1.0.0]tricycloheptane followed by rapid protonation with solvent to give the corresponding Rh^{III}(oep)(alkyl) product in 23% and 24% yields, respectively (eqs 1.23 and 1.24).^{40,44}



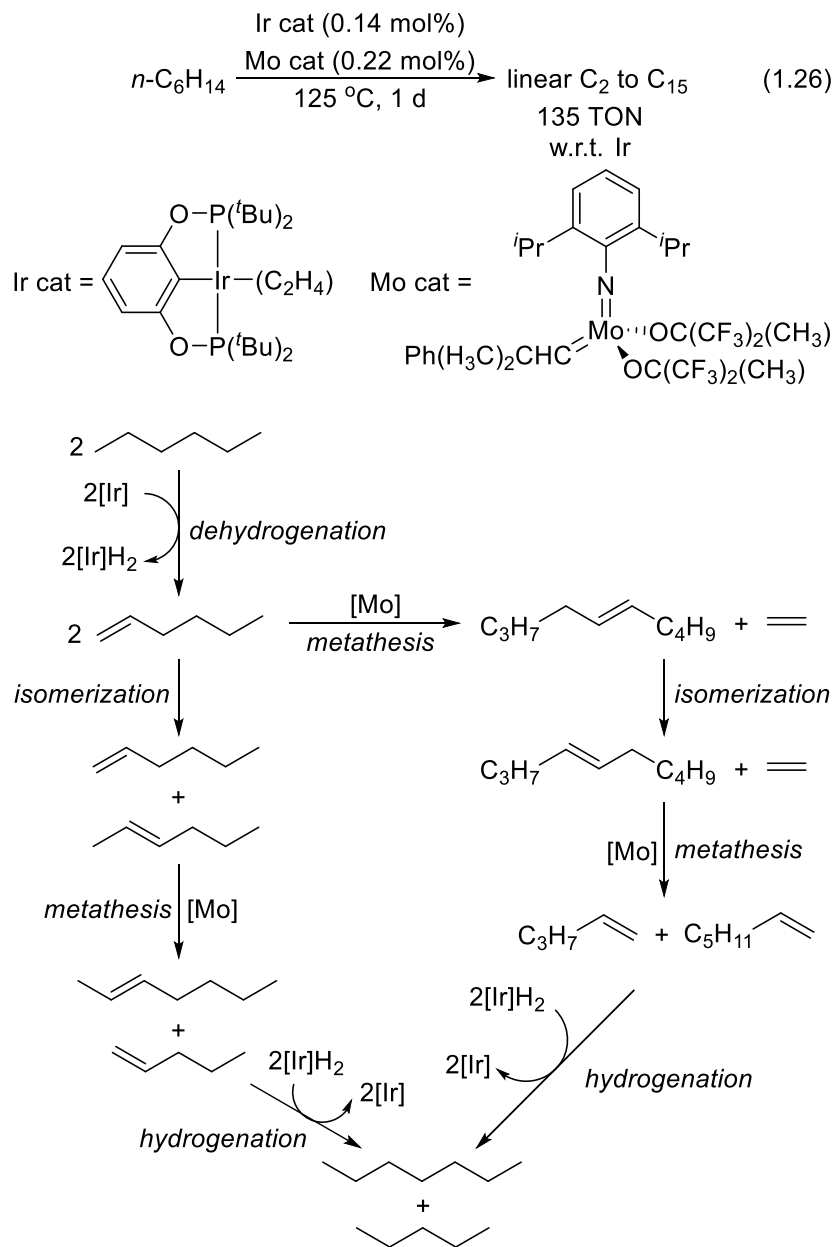


1.4.2.3 1988 and After

In 1988, Chatani reported the first catalytic CCA with insertion of another reagent to construct new carbon-carbon bond and carbon-heteroatom bond, which established the foundation of catalytic CCA development. In this report, Chatani described the palladium catalyzed ring opening of various substituted methylenecyclopropanes with Me_3SiCN to give β -(cyanomethyl)allylsilanes (eq 1.25).⁴⁸ Followed by this initial discovery, formation of new C-N,^{67,80} C-O,^{68,82,89} C-C(heteroaryl),^{72,78} C-B⁷³ and C-Sn⁸⁴ bonds based on substituted methylenecyclopropane skeletons have been reported.

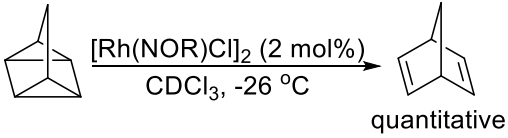
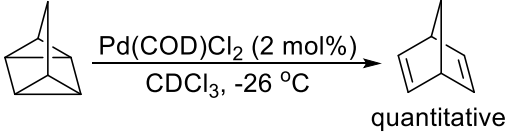
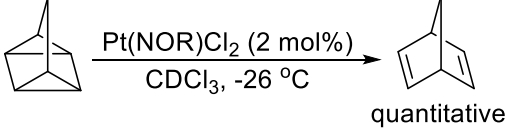
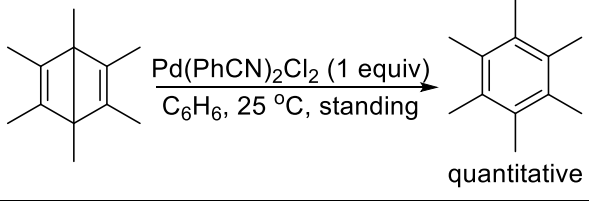
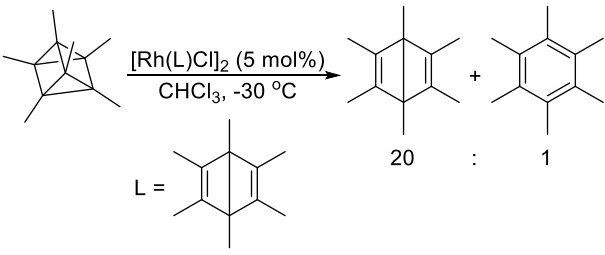
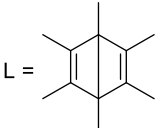
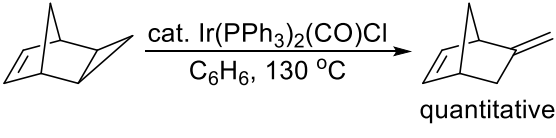
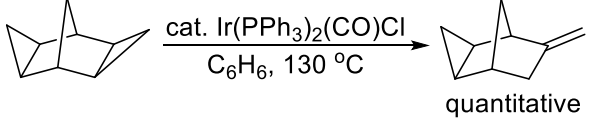


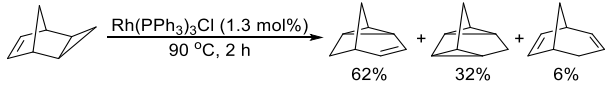
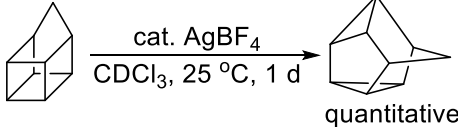
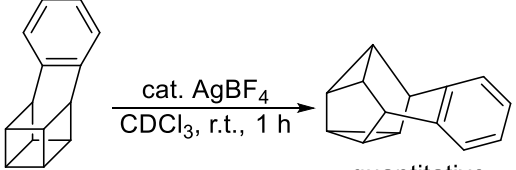
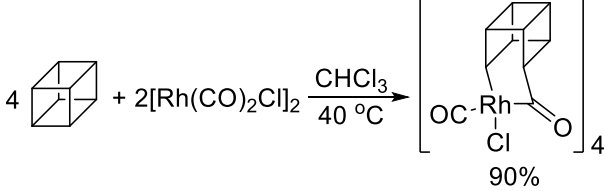
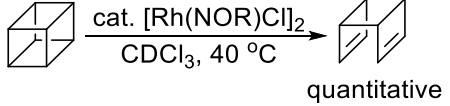
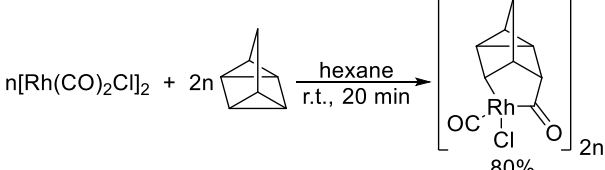
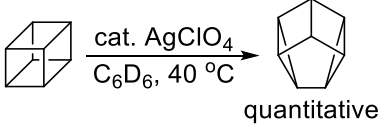
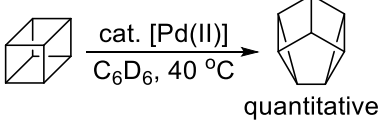
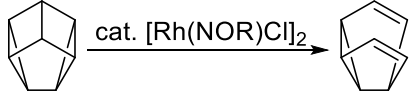
Goldman designed an elegant catalytic alkane metathesis which transformed *n*-hexane into a distribution of C_2 to C_{15} *n*-alkanes (eq 1.26).²⁰ The reaction is proposed to go through acceptorless dehydrogenation, isomerization, olefin metathesis and hydrogenation by the cooperation of hydrogenation/dehydrogenation catalyst and Schrock type metathesis catalyst (Scheme 1.5).

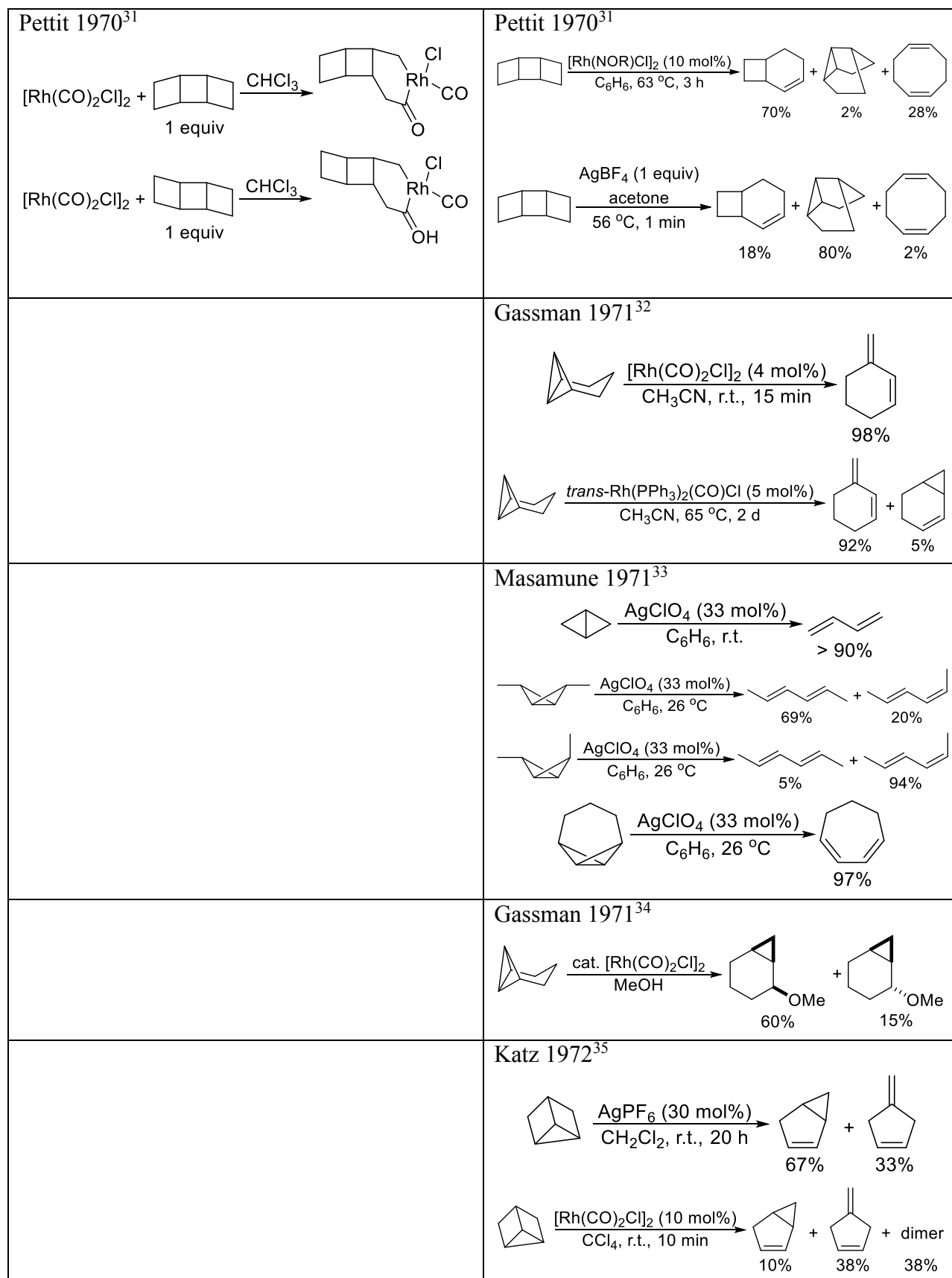


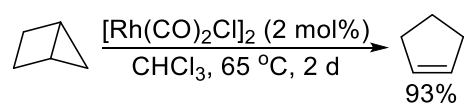
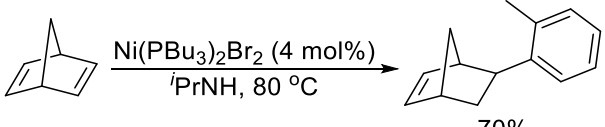
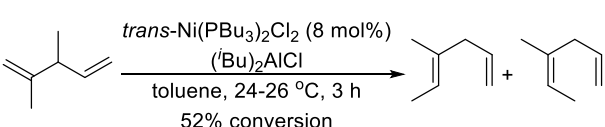
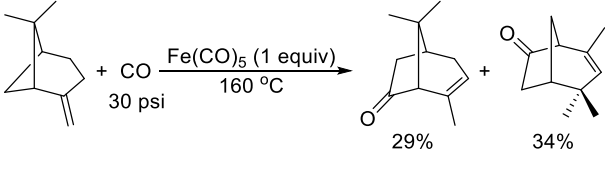
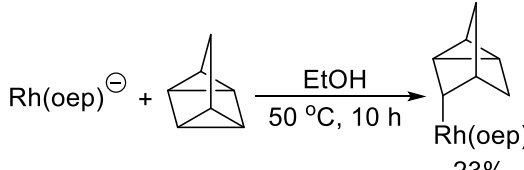
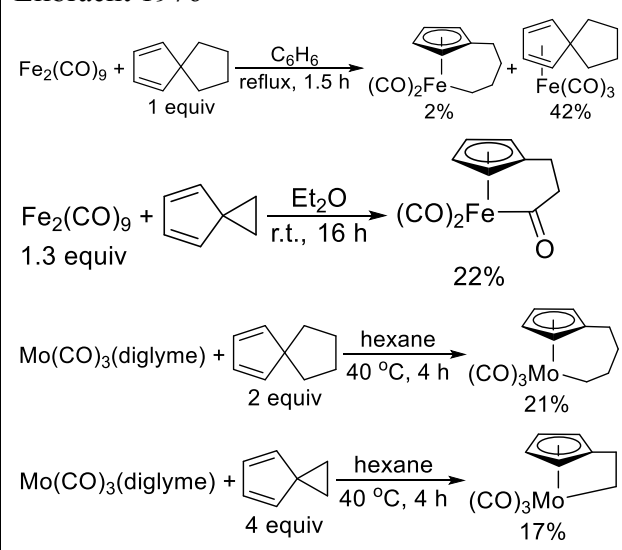
Scheme 1.5 Proposed Mechanism for the Catalytic Alkane Metathesis

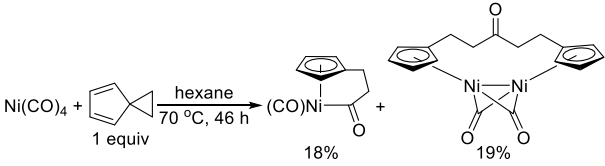
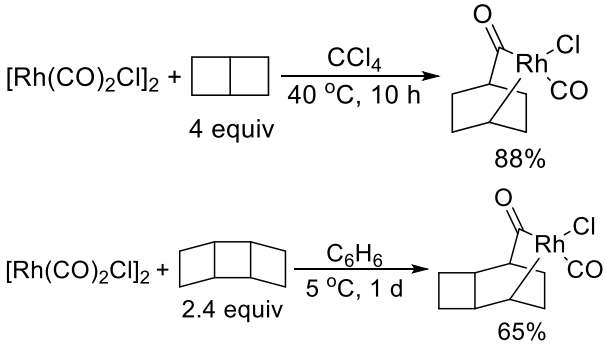
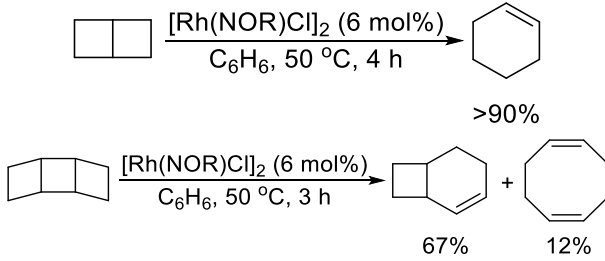
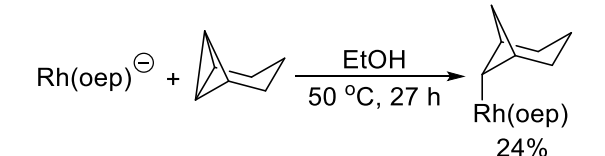
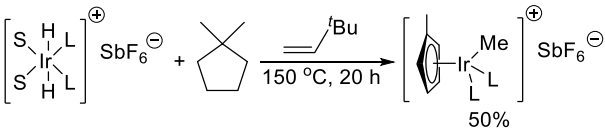
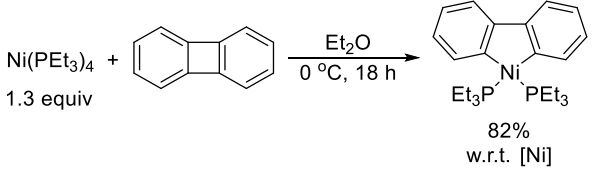
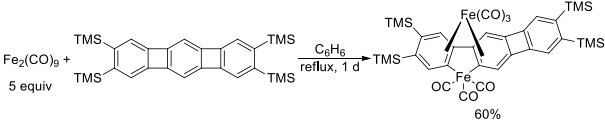
Table 1.4 Timeline of CCA of Hydrocarbons.

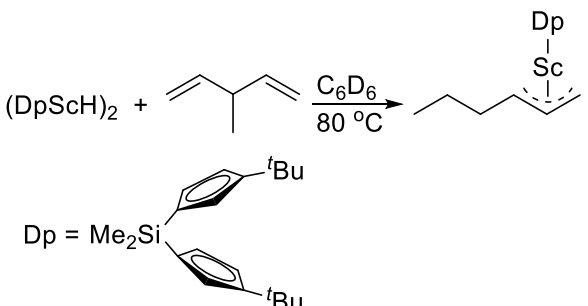
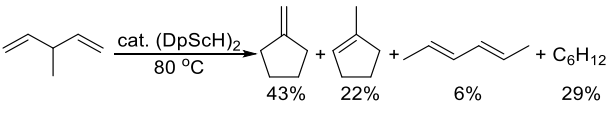
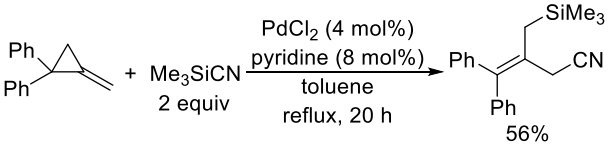
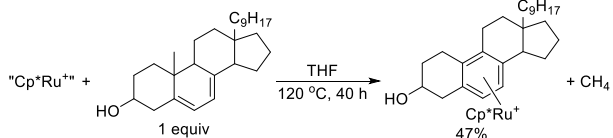
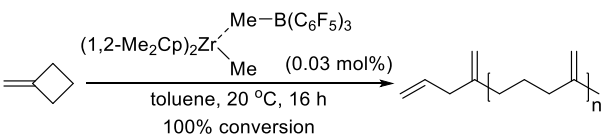
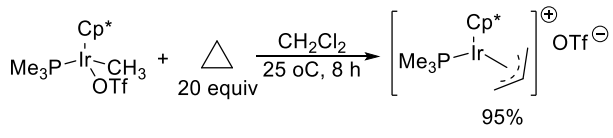
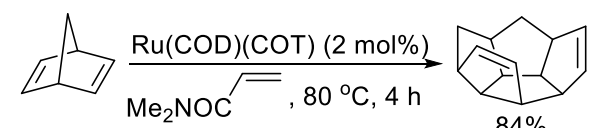
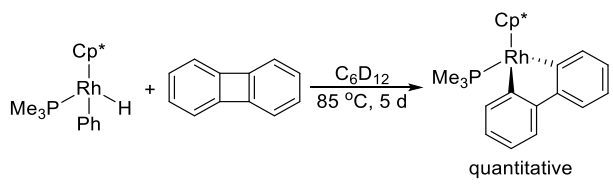
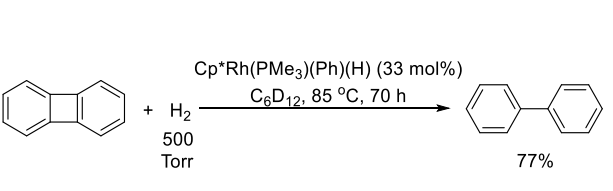
Stoichiometric	Catalytic
<p>Tipper 1955²¹</p> $\text{PtCl}_2 + \triangle \xrightarrow[\text{r.t., overnight}]{\text{acetic anhydride}} \left[\begin{array}{c} \text{Cl} \\ \\ \text{Pt} \\ \\ \text{Cl} \end{array} \text{---} \triangle \right]_n$	
	<p>Hogeveen 1967²²</p> <div style="text-align: center;">  <p>quantitative</p> </div> <div style="text-align: center;">  <p>quantitative</p> </div> <div style="text-align: center;">  <p>quantitative</p> </div>
	<p>Maitlis 1967²³</p> <div style="text-align: center;">  <p>quantitative</p> </div>
	<p>Hogeveen 1967²⁴</p> <div style="text-align: center;">  <p>20 : 1</p> <p>L = </p> </div>
	<p>Hogeveen 1969²⁵</p> <div style="text-align: center;">  <p>quantitative</p> </div> <div style="text-align: center;">  <p>quantitative</p> </div>

	<p>Katz 1969²⁶</p> 
	<p>Paquette 1970²⁷</p>  <p>quantitative</p>  <p>quantitative</p>
<p>Halpern 1970²⁸</p>  <p>90%</p>	<p>Halpern 1970²⁸</p>  <p>quantitative</p>
<p>Halpern 1970²⁹</p>  <p>80%</p>	
	<p>Eaton 1970³⁰</p>  <p>quantitative</p>  <p>quantitative</p> 

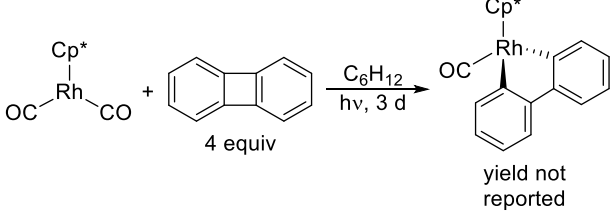
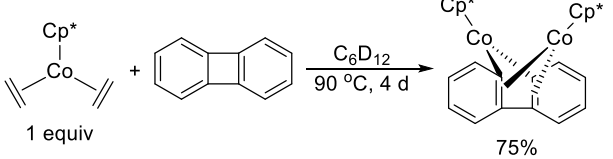
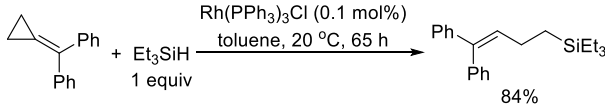
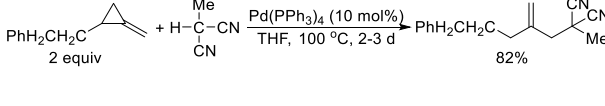
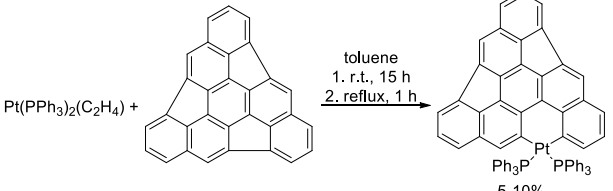
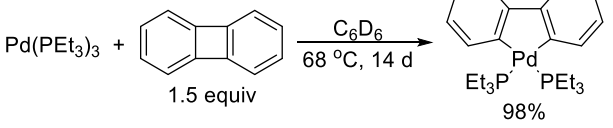
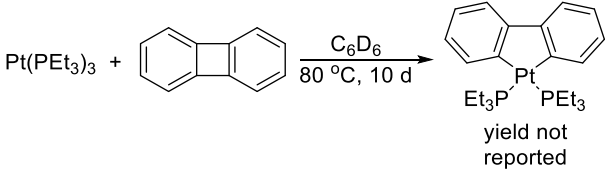
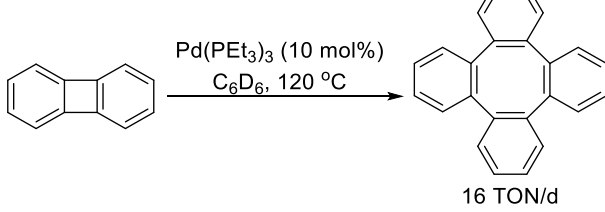
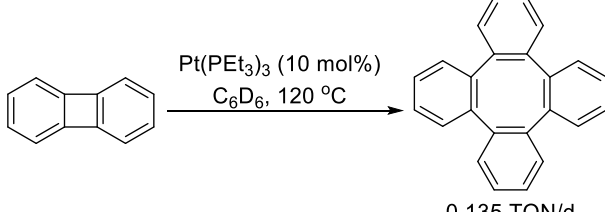


	<p>Gassman 1972³⁶</p> 
	<p>Furukawa 1974³⁷</p> 
	<p>Miller 1974³⁸</p> 
	<p>Weissberger 1975³⁹</p> 
<p>Ogoshi 1975⁴⁰</p> 	
<p>Eilbracht 1976⁴¹</p> 	

<p>Eilbracht 1976⁴²</p>  <p>$\text{Ni(CO)}_4 + 1 \text{ equiv}$ $\xrightarrow[\text{70 } ^\circ\text{C, 46 h}]{\text{hexane}}$ $(\text{CO})\text{Ni}$ (18%) + Ni_2 (19%)</p>	
<p>Halpern 1979⁴³</p>  <p>$[\text{Rh(CO)}_2\text{Cl}]_2 + 4 \text{ equiv}$ $\xrightarrow[\text{40 } ^\circ\text{C, 10 h}]{\text{CCl}_4}$ Rh (88%)</p> <p>$[\text{Rh(CO)}_2\text{Cl}]_2 + 2.4 \text{ equiv}$ $\xrightarrow[\text{5 } ^\circ\text{C, 1 d}]{\text{C}_6\text{H}_6}$ Rh (65%)</p>	<p>Halpern 1979⁴³</p>  <p>$\text{Diene} \xrightarrow[\text{C}_6\text{H}_6, 50 ^\circ\text{C, 4 h}]{[\text{Rh(NOR)Cl}]_2 (6 \text{ mol}\%)}$ Product (>90%)</p> <p>$\text{Diene} \xrightarrow[\text{C}_6\text{H}_6, 50 ^\circ\text{C, 3 h}]{[\text{Rh(NOR)Cl}]_2 (6 \text{ mol}\%)}$ Product 1 (67%) + Product 2 (12%)</p>
<p>Ogoshi 1980⁴⁴</p>  <p>$\text{Rh(oep)} + \text{Diene} \xrightarrow[\text{50 } ^\circ\text{C, 27 h}]{\text{EtOH}}$ Rh(oep) (24%)</p>	
<p>Crabtree 1984¹⁸</p>  <p>$[\text{Ir}] + \text{Diene} + \text{Alkene} \xrightarrow[\text{150 } ^\circ\text{C, 20 h}]{\text{SbF}_6^-}$ $[\text{Ir}]$ (50%)</p> <p>L = P(<i>p</i>-FC₆H₄)₃, S = acetone</p>	
<p>Eisch 1985⁴⁵</p>  <p>$\text{Ni(PEt}_3)_4 + 1.3 \text{ equiv}$ $\xrightarrow[\text{0 } ^\circ\text{C, 18 h}]{\text{Et}_2\text{O}}$ Ni (82% w.r.t. [Ni])</p>	
<p>Vollhardt 1985⁴⁶</p>  <p>$\text{Fe}_2(\text{CO})_9 + 5 \text{ equiv}$ $\xrightarrow[\text{reflux, 1 d}]{\text{C}_6\text{H}_6}$ Complex (60%)</p>	

<p>Bercaw 1988⁴⁷</p>  <p>$(DpScH)_2 + \text{2-methyl-2-butene} \xrightarrow[80\text{ }^\circ\text{C}]{C_6D_6}$ Sc complex</p> <p>$Dp = Me_2Si(2-tBu-5-methylphenyl)_2$</p>	<p>Bercaw 1988⁴⁷</p>  <p>$\text{2-methyl-2-butene} \xrightarrow[80\text{ }^\circ\text{C}]{\text{cat. } (DpScH)_2, C_6D_6}$ 43% + 22% + 6% + 29% C_6H_{12}</p>
	<p>Chatani 1988⁴⁸</p>  <p>$\text{Cyclopropane} + Me_3SiCN \xrightarrow[\text{toluene, reflux, 20 h}]{PdCl_2 (4\text{ mol}\%), \text{pyridine } (8\text{ mol}\%), 2\text{ equiv } Me_3SiCN}$ 56%</p>
<p>Chaudret 1993⁴⁹</p>  <p>$\text{Cp}^*Ru^{+} + \text{substrate} \xrightarrow[120\text{ }^\circ\text{C, 40 h}]{THF}$ 47% + CH_4</p>	
	<p>Marks 1993⁵⁰</p>  <p>$\text{Cycloolefin} \xrightarrow[\text{toluene, 20 }^\circ\text{C, 16 h}]{(1,2-Me_2Cp)_2Zr(Me)Me-B(C_6F_5)_3 (0.03\text{ mol}\%)}$ 100% conversion</p>
<p>Bergman 1993⁵¹</p>  <p>$Me_3P-Ir(CH_3)(OTf)(Cp^*) + 20\text{ equiv } \text{cyclopropane} \xrightarrow[25\text{ }^\circ\text{C, 8 h}]{CH_2Cl_2}$ 95%</p>	
	<p>Mitsudo, Watanabe 1994⁵²</p>  <p>$\text{Bicyclic olefin} \xrightarrow[80\text{ }^\circ\text{C, 4 h}]{Ru(COD)(COT) (2\text{ mol}\%), Me_2NOC}$ 84%</p>
<p>Jones 1994⁵³</p>  <p>$Me_3P-Rh(H)(Ph)(Cp^*) + \text{fluorene} \xrightarrow[85\text{ }^\circ\text{C, 5 d}]{C_6D_{12}}$ quantitative</p>	<p>Jones 1994⁵³</p>  <p>$\text{fluorene} + H_2 \xrightarrow[500\text{ Torr, } C_6D_{12}, 85\text{ }^\circ\text{C, 70 h}]{Cp^*Rh(PMe_3)(Ph)(H) (33\text{ mol}\%)}$ 77%</p>

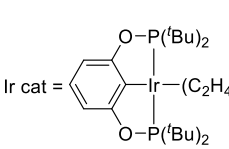
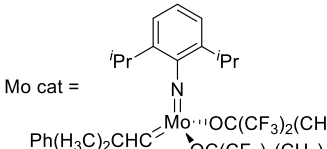

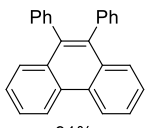
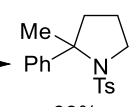
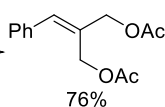
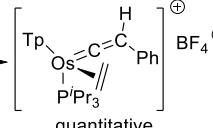
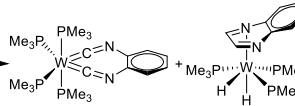
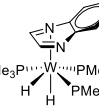
<p>Rosenthal, Burlakov 1994⁵⁴</p> <p>$\text{Cp}_2\text{Zr}(\text{THF})(\text{Me}_3\text{SiC}_2\text{SiMe}_3)_2 + \text{Me}_3\text{Si}-\text{C}\equiv\text{C}-\text{SiMe}_3 \xrightarrow{\text{THF, r.t., 8 h}} \text{Cp}_2\text{Zr}(\text{Me}_3\text{SiC}_2\text{SiMe}_3)_2$ (45%)</p>	
<p>Suzuki 1994⁵⁵</p> <p>$\text{Cp}^*\text{Ru}(\text{H})_3 + 5 \text{Cp} \xrightarrow{\text{THF, r.t., 12 h}} \text{Cp}^*\text{Ru}(\text{Cp})$ (quantitative)</p>	
<p>Crabtree 1995⁵⁶</p> <p>$[\text{Ir}(\text{COD})\text{Cl}]_2 + \text{Fluorene} \xrightarrow{\text{CH}_2\text{Cl}_2, 90^\circ\text{C, 2 h}} \text{COD-Ir-Cl-Ir-COD}(\text{Fluorenyl})_2$ (89%)</p>	
<p>Casey, Hallenbeck 1995⁵⁷</p> <p>$(\text{Cp}^*_2\text{YH})_2 + \text{Norbornene} \xrightarrow{\text{C}_6\text{D}_{11}\text{CD}_3, -78^\circ\text{C}} \text{Cp}^*\text{Y}(\text{Norbornene})$ (quantitative)</p>	
<p>Rubin 1996⁵⁸</p> <p>$\text{C}_{60} + \text{CpCo}(\text{CO})_2 \xrightarrow{\text{xylene, 135}^\circ\text{C}} \text{CpCo}(\text{C}_{60})$ (25%)</p>	
<p>Jones 1997⁵⁹</p> <p>$2 \text{Cp}^*\text{Rh}(\text{CO})_2 + \text{Fluorene} \xrightarrow{\text{C}_6\text{H}_{12}, 120^\circ\text{C, 2.5 d}} \text{Cp}^*\text{Rh}_2(\text{Fluorenyl})_2$ (83%)</p>	<p>Jones 1997⁵⁹</p> <p>$\text{Fluorene} + \text{CO} \xrightarrow{\text{Cp}^*\text{Rh}(\text{CO})_2 (22 \text{ mol\%}), \text{C}_6\text{D}_{12}, 160^\circ\text{C, 6 d, 500 Torr}} \text{Fluorenyl-Cp}^*\text{Rh}(\text{CO})$ (97%)</p> <p>$\text{Fluorene} + \text{CO} \xrightarrow{\text{Cp}^*\text{Co}(\text{CO})_2 (33 \text{ mol\%}), \text{C}_6\text{D}_{12}, 170^\circ\text{C, 45 h, 500 Torr}} \text{Fluorenyl-Cp}^*\text{Co}(\text{CO})$ (85%)</p>

 <p>yield not reported</p>  <p>75%</p>	
	<p>Beletskaya 1997⁶⁰</p>  <p>84%</p>
	<p>Yamamoto 1997⁶¹</p>  <p>82%</p>
<p>Stanley, Rabideau 1998⁶²</p>  <p>5-10%</p>	
<p>Jones 1998⁶³</p>  <p>98%</p>  <p>yield not reported</p>	<p>Jones 1998⁶³</p>  <p>16 TON/d</p>  <p>0.135 TON/d</p>

<p>Yeh 1998⁶⁴</p> <p> $\text{Fe}_3(\text{CO})_{12} + \text{1 equiv} \xrightarrow[n\text{-heptane reflux, 3 h}]{} \text{30\%}$ </p> <p> $\text{Fe}_2(\text{CO})_9 + \text{1 equiv} \xrightarrow[c\text{-hexane reflux, 5 h}]{} \text{36\%}$ </p> <p> $\text{Ru}_3(\text{CO})_{12} + \text{1 equiv} \xrightarrow[n\text{-octane reflux, 4 h}]{} \text{33\%}$ </p> <p> $\text{Os}_3(\text{CO})_{12} + \text{6 equiv} \xrightarrow[200^\circ\text{C, 15 h}]{n\text{-decane}} \text{23\%} + \text{30\%}$ </p> <p>33% recovery</p>	
<p>Yamamoto 1998⁶⁵</p> <p> $\text{Rh}(\text{PPh}_3)_3\text{Cl} + \text{5 equiv} \xrightarrow[50^\circ\text{C, 16 h}]{\text{toluene}} \text{95\%}$ </p>	
	<p>Jones 1998⁶⁶</p> <p> $\text{1} + \text{H}_2 \xrightarrow[0.92 \text{ atm}]{[\text{Ni}(\text{dippe})\text{H}]_2 (20 \text{ mol\%}), \text{toluene-}d_8, 50^\circ\text{C}} \text{16 TON/d}$ </p> <p> $\text{1} + \text{H}_2 \xrightarrow[0.92 \text{ atm}]{\text{Pd}(\text{PET}_3)_3 (20 \text{ mol\%}), \text{toluene-}d_8, 70^\circ\text{C}} \text{2.2 TON/d}$ </p> <p> $\text{1} + \text{H}_2 \xrightarrow[0.92 \text{ atm}]{\text{Pt}(\text{PET}_3)_3 (20 \text{ mol\%}), \text{toluene-}d_8, 120^\circ\text{C}} \text{1 TON/12 d}$ </p>
	<p>Yamamoto 1998⁶⁷</p> <p> $\text{2 equiv} \xrightarrow[2 \text{ equiv}]{c\text{-hex} + \text{Bn}_2\text{NH}} \text{72\%}$ </p> <p> $[(\eta^3\text{-C}_3\text{H}_5)\text{PdCl}]_2 (5 \text{ mol\%}), 12.5 \text{ mol\% dppp}, \text{DME}, 100^\circ\text{C}, 3 \text{ d}$ </p>
	<p>Yamamoto 1999⁶⁸</p> <p> $\text{Hept} + \text{Ph-CH}_2\text{-OH} \xrightarrow[\text{1 equiv}]{\text{Pd}(\text{PPh}_3)_4 (5 \text{ mol\%}), \text{P}(o\text{-tolyl})_3 (10 \text{ mol\%}), \text{toluene}, 100^\circ\text{C}, 3 \text{ d}} \text{69\%}$ </p>

	<p>Jones 1999⁶⁹</p>
	<p>Jones 1999⁷⁰</p>
<p>Sweigart 1999⁷¹</p>	
	<p>Yamamoto 2000⁷²</p>
	<p>Suginome, Ito 2000⁷³</p>
	<p>Jones 2001⁷⁴</p>

	<p> $\text{Indene} + \text{PhCHO} \xrightarrow[\text{C}_6\text{D}_6, 120\text{ }^\circ\text{C}, 7\text{ h}]{\text{Pd(PPh}_3)_4 (5\text{ mol\%)}, p\text{-cresol (10 mol\%)}}$ $\text{Indene-CH(Ph)-CH}_2\text{Ph}$ (84%) $\text{Indene} + \text{p-TolCN} \xrightarrow[\text{C}_6\text{D}_6, 120\text{ }^\circ\text{C}, 1\text{ d}]{\text{Pd(PPh}_3)_4 (5\text{ mol\%)}, p\text{-cresol (10 mol\%)}}$ $\text{Indene-CH(4-MePh)-CH}_2\text{Ph}$ (85%) </p>
<p>Jones 2001⁷⁵</p>	<p> $\text{Indene} + \text{Alkyne} \xrightarrow[\text{C}_6\text{D}_6, 85\text{ }^\circ\text{C}, 18\text{ h}]{[\text{Rh(dtbbp)Cl}]_2 (10\text{ mol\%})}$ $\text{Indene-1,2-dimethyl}$ (96%) $\text{Indene} + n\text{-PrAlkyne} \xrightarrow[\text{C}_6\text{D}_6/\text{CD}_2\text{Cl}_2, 125\text{ }^\circ\text{C}, 13\text{ h}]{\text{Rh(dtbbp)(BP)Cl (10 mol\%)}}$ Indene-n-Pr (61%) </p>
<p>Jones 2002⁷⁶</p>	<p> $\text{Indene} + \text{1,1-diphenylalkyne} \xrightarrow[\text{C}_6\text{D}_6, 70\text{ }^\circ\text{C}, 22.5\text{ h}]{\text{Ni(PN)(PhC}\equiv\text{CPh) (8 mol\%)}}$ $\text{Indene-1,2-diphenyl}$ (98%) </p>
<p>Chirik 2003⁷⁷</p>	<p> $\text{Cyclopropene-nBu} + \text{H}_2 \xrightarrow[\text{toluene, 130 }^\circ\text{C, 4 atm}]{\text{Rh(PPh}_3)_3\text{Cl (2 mol\%)}}$ nBu-2-butene (TOF = 0.25) $\text{Cyclopropene-nBu} \xrightarrow[\text{toluene, 130 }^\circ\text{C}]{\text{Rh(PPh}_3)_3\text{Cl (2 mol\%)}}$ nBu-1-butene (TOF = 0.05) </p>
	<p>Yamamoto 2004⁷⁸</p> <p> $\text{1,1-dibutylcyclopropene} + \text{Pyridine} \xrightarrow[120\text{ }^\circ\text{C, 42-48 h}]{\text{Pd(PPh}_3)_4 (5\text{ mol\%)}}$ $\text{1,1-dibutyl-2-pyridylcyclopropene}$ (38%) </p>

	<p>Goldman 2006²⁰ (dehydrogenation to olefin → metathesis → hydrogenation)</p> <p>$n\text{-C}_6\text{H}_{14} \xrightarrow[125\text{ }^\circ\text{C, 1 d}]{\text{Ir cat (0.14 mol\%)} \quad \text{Mo cat (0.22 mol\%)}} \text{linear C}_2 \text{ to C}_{15}$ 135 TON w.r.t. Ir</p> <p>Ir cat =  Mo cat = </p>
<p>Radius 2006⁷⁹</p> <p>$\text{Ni}(\text{Me}_2\text{Im})_3 + \text{indene} \xrightarrow[\text{r.t., overnight}]{\text{toluene}}$  84%</p>	<p>Radius 2006⁷⁹</p> <p>$\text{indene} + \text{Ph-CH=CH-Ph} \xrightarrow[\text{toluene, 80 }^\circ\text{C, overnight}]{\text{Ni}_2(\text{Pr}_2\text{Im})_4(\text{COD}) (1 \text{ mol\%})}$  91%</p>
	<p>Shi 2006⁸⁰</p> <p>$\text{cyclopropene} + \text{Ph} \xrightarrow[\text{1 equiv}]{\text{Au}(\text{PPh}_3)\text{Cl} (5 \text{ mol\%}) \quad \text{AgOTf} (5 \text{ mol\%})}$  68%</p>
<p>Eisch 2007⁸¹</p> <p>$\text{Zr}(\text{OEt})_2(\text{Bu})_2 + \text{Ph}_2\text{CH-CHPh}_2 \xrightarrow[\text{THF, 25 }^\circ\text{C, 3 d}]{75 \text{ W bulb } (> 300 \text{ nm}) \quad \text{Fe}(\text{acac})_3 (1 \text{ mol\%})}$ $\text{Zr}(\text{OEt})_2(\text{CHPh}_2)_2$ 2 equiv quantitative</p>	
	<p>Shi 2009⁸²</p> <p>$\text{cyclopropene} + \text{Ph} \xrightarrow[\text{3 equiv}]{\text{Pd}(\text{OAc})_2 (10 \text{ mol\%}) \quad \text{Bu}_4\text{NI} (1 \text{ equiv})}$  76%</p>
<p>Esteruelas, López, Mascareñas 2010⁸³</p> <p>$\left[\text{Tp-Os}(\text{O}^-\text{C}(\text{Me})_2) \right]^+ \text{BF}_4^- + \text{cyclopropene} \xrightarrow[\text{1.4 equiv}]{\text{C}_6\text{H}_5\text{F, r.t., 30 min}}$  quantitative</p>	
<p>Parkin 2010⁸⁴</p> <p>$\text{W}(\text{PMe}_3)_6 + \text{pyridine} \xrightarrow[90\text{ }^\circ\text{C, 18 h}]{\text{C}_6\text{D}_6}$  15% +  24%</p>	

	<p>Marek 2010⁸⁵</p> <p> $\text{Bu} \text{---} \text{C} \text{---} \text{C} \text{---} \text{C} \text{---} \text{C} \text{---} \text{C} \text{---} \text{C} + \text{HBpin} \xrightarrow[\text{CH}_2\text{Cl}_2, \text{ r.t., 12 h}]{\text{Rh(PPh}_3)_3\text{Cl (0.5 mol\%)}}$ 1.1 equiv PinB --- Bu --- Hex 90% </p> <p> $\text{Me}_2 \text{---} \text{C} \text{---} \text{C} \text{---} \text{C} \text{---} \text{C} \text{---} \text{C} + \text{PhMe}_2\text{SiH} \xrightarrow[\text{toluene, 80 }^\circ\text{C, 12 h}]{\text{Rh(PPh}_3)_3\text{Cl (0.5 mol\%)}}$ 1.5 equiv PhMe₂Si --- Me --- Et 90% (E/Z = 93:7) </p> <p> $\text{Me} \text{---} \text{C} \text{---} \text{C} \text{---} \text{C} \text{---} \text{C} \text{---} \text{C} + \text{Bu}_3\text{SnH} \xrightarrow[\text{THF, r.t., 30 min}]{\text{Pd(PPh}_3)_4 \text{ (3 mol\%)}}$ Bu₃Sn --- Me --- Et 88% (E/Z = 76:24) </p>
	<p>Marek 2010⁸⁶</p> <p> $\text{Bu} \text{---} \text{C} \text{---} \text{C} \text{---} \text{C} \text{---} \text{C} \text{---} \text{C} + \text{H}_2/\text{CO} \xrightarrow[\text{toluene, 70 }^\circ\text{C, 12 h}]{\text{Rh(acac)(CO)}_2 \text{ (0.04 mol\%)}}$ 1:1, 40 psi, bppf (0.08 mol%) H --- Bu --- Hex 93% </p>
<p>Chan 2010⁸⁷</p> <p> $\text{Rh(ttp)H} + \text{Cyclooctene} \xrightarrow[\text{solvent, 120 }^\circ\text{C, 15 h}]{\text{Rh}_2(\text{ttp})_2 \text{ (10 mol\%)}}$ Rh(ttp) --- --- --- --- --- --- --- --- 73% </p>	
<p>Chaplin 2010⁸⁸</p> <p> $[\text{Rh}(\text{P}'\text{Pr}_3)_2] \text{BF}_4^- + \text{Ligand} \xrightarrow[\text{40 }^\circ\text{C, 4 d}]{\text{toluene}}$ 10 equiv quantitative </p>	
	<p>Matsuda 2011⁸⁹</p> <p> $\text{Alkene} + \text{Et}_3\text{SiH} \xrightarrow[\text{toluene, 110 }^\circ\text{C, 2 h}]{\text{Pd(dba)}_2 \text{ (5 mol\%)}}$ 1.5 equiv, DavePhos (10 mol%) H --- SiEt₃ 95% </p> <p> $\text{Alkene} + \text{HBpin} \xrightarrow[\text{xylene, 140 }^\circ\text{C, 8 h}]{\text{Pd(dba)}_2 \text{ (5 mol\%)}}$ 2 equiv, MePhos (10 mol%) H --- Bpin 56% </p> <p> $\text{Alkene} + \text{Me}_3\text{Si-SiMe}_3 \xrightarrow[\text{toluene, 110 }^\circ\text{C, 3.5 h}]{\text{Pd(dba)}_2 \text{ (5 mol\%)}}$ 1.5 equiv, tBuDavePhos (10 mol%) Me₃Si --- SiMe₃ 77% </p> <p> $\text{Alkene} + \text{B}_2(\text{pin})_2 \xrightarrow[\text{xylene, 140 }^\circ\text{C, 5 h}]{\text{Pd(dba)}_2 \text{ (10 mol\%)}}$ 1.1 equiv, PBu₃ (20 mol%) pinB --- Bpin 57% </p> <p> $\text{Alkene} + \text{Me}_3\text{Ge-GeMe}_3 \xrightarrow[\text{toluene, 110 }^\circ\text{C, 4 h}]{\text{Pd(dba)}_2 \text{ (5 mol\%)}}$ 1.5 equiv, MePhos (10 mol%) Me₃Ge --- GeMe₃ 90% </p>

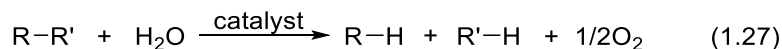
	<p>Shi 2011⁹⁰</p>
<p>Chan 2012⁹¹</p>	<p>Chan 2012⁹¹</p>
	<p>Tilley, Bergman 2013⁹²</p>
<p>Hou 2014⁹³</p>	

1.5 Water as Transfer Hydrogenating Agent

Water protonates carbanions readily due to its lower pKa value than most carbanions of hydrocarbon (Table 1.5).⁹⁴ This is why anhydrous solvents are used for Grignard type reactions. However, water seldom served as a hydrogen atom donor because of the strong O-H bond (Table 1.5).⁹⁵ Therefore, catalytic hydrogenation of C-C σ -bond using H₂O is a challenging research (eq 1.27).

Table 1.5 pKa and X-H BDE Values of H₂O and Selected Hydrocarbons.

Substrate	pKa (in H ₂ O)	X-H BDE / kcalmol ⁻¹
HO-H	15.7	118.8
H ₃ C-H	48	105.0
Bn-H	41	89.7
Ph ₃ C-H	31.5	81
PhC≡C-H	23	133

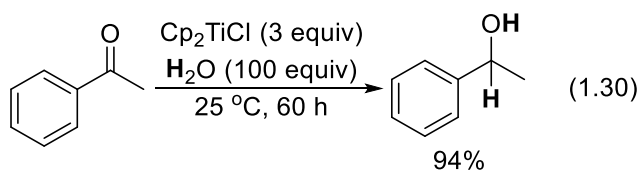
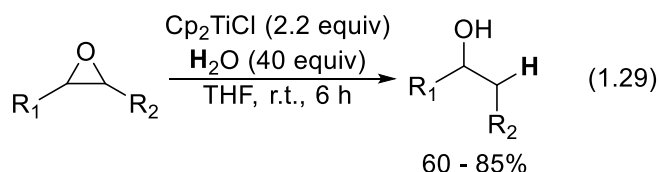
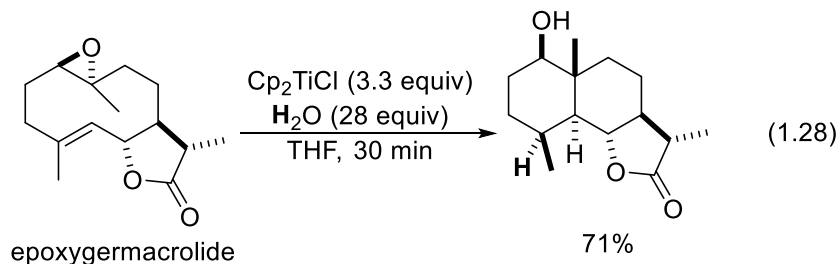


H₂ gas is a commonly employed hydrogenating agent nowadays because of its atom economical nature and much cheaper than most organic H atom donors like silane. However, H₂ exhibits poor solubility in most organic solvents under ambient conditions and low energy density. The storage and transfer via gas cylinder is inconvenient as well. In contrast, H₂O does not have the drawbacks mentioned above.

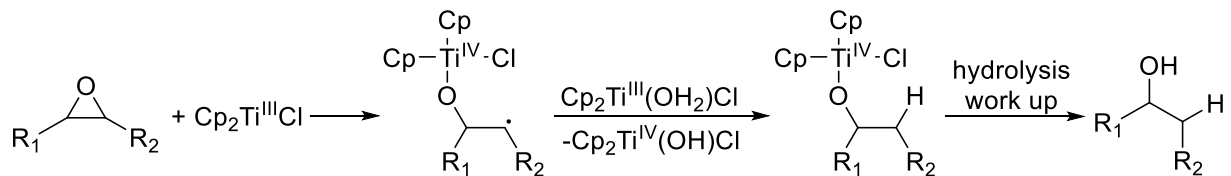
There are only three reported systems for the stoichiometric hydrogenation of carbon center using water via radical mechanism: (1) titanium/H₂O system; (2) cobalt/H₂O system; and (3) borane/H₂O system.

1.5.1 Titanium/H₂O System

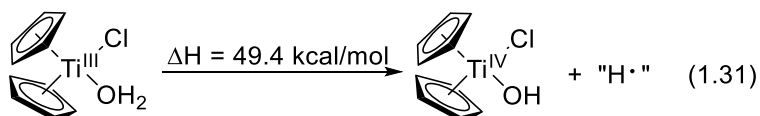
Barrero and Ultra probably observed the first H atom transfer from H₂O to carbon skeleton mediated by titanium complex in 2002. During their investigations on the Cp₂TiCl mediated transannular cyclization of epoxygermacrolide in the presence of H₂O, the unexpected reduction product was obtained in high yield (eq 1.28).^{96a} Labeling experiment using D₂O confirmed water as the hydrogen source. Later, the Cp₂TiCl/H₂O system has been utilized to reduce epoxides^{96b} and ketones^{96c} into alcohols (eqs 1.29 and 1.30).



The authors suggested that coordination of H₂O to Cp₂TiCl to form Cp₂Ti(OH₂)Cl^{96b,d} or Cp₂Ti(OH₂)₂^{96c} intermediates as the active hydrogen atom donor (Scheme 1.6). The coordination of H₂O to the titanium metal center weakens the O-H bond. Computational analysis shows that the reaction energy of eq 1.31 is endothermic by 49.4 kcal/mol, which is about 70 kcal/mol lesser than the BDE of O-H bond in water.^{96d} Replacing the water with more acidic phenol resulted in very low yield of reduction product, suggesting that protonation of carbon center is unlikely.

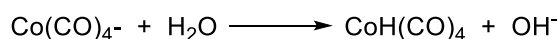
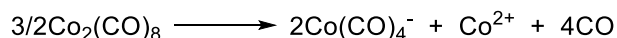
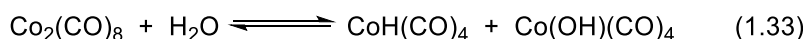
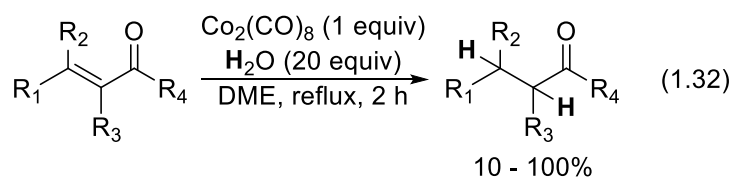


Scheme 1.6 Proposed Mechanism for the Epoxide Reduction



1.5.2 Cobalt/H₂O System

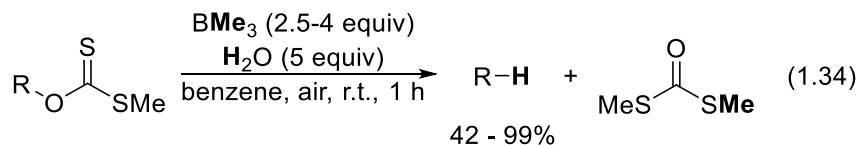
Selective reduction of α,β -unsaturated aldehydes and ketones to the corresponding saturated carbonyl compounds by $\text{Co}_2(\text{CO})_8/\text{H}_2\text{O}$ system has been reported (eq 1.32).⁹⁷ In situ formation of $\text{CoH}(\text{CO})_4$ was proposed to reduce the $\text{C}=\text{C}$ double bond. Since the author did not discuss how $\text{CoH}(\text{CO})_4$ was formed from $\text{Co}_2(\text{CO})_8$, these two mechanistic possibilities may be operating based on known cobalt chemistry: (1) oxidative addition of H_2O with $\text{Co}_2(\text{CO})_8$ (eq 1.33),⁹⁸ and (2) disproportionation of $\text{Co}_2(\text{CO})_8$ to form $\text{Co}(\text{CO})_4^-$ followed by protonation with H_2O (Scheme 1.7).⁹⁹



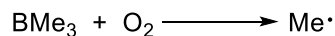
Scheme 1.7 Proposed $\text{CoH}(\text{CO})_4$ Formation from Disproportionation Channel.

1.5.3 Borane/H₂O System

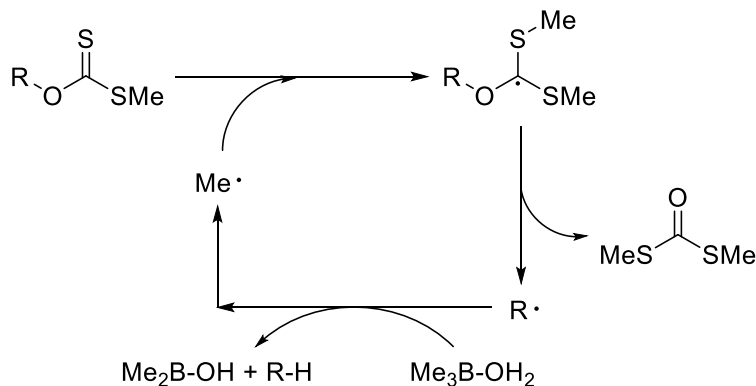
Hydrogenation of O-alkyl thiocarbonate ester to give alkane has been reported using $\text{BMe}_3/\text{H}_2\text{O}$ combination (eq 1.34 and scheme 1.5).¹⁰⁰ The role of BMe_3 is similar to Cp_2TiCl mentioned previously. Computational analysis suggested that coordination of H_2O to BMe_3 to form $\text{H}_2\text{O-BMe}_3$ intermediate weakened the O-H bond by 30 kcal/mol.



initiation



propagation



Scheme 1.7 Proposed Mechanism for Xanthate Reduction.

1.6 Porphyrins and Group 9 Metalloporphyrins

1.6.1 Porphyrin Ligands

Porphyrins are planar heterocyclic macrocycles with four pyrrole subunits interconnected by at their α carbons by methane bridges (Figure 1.1). They contain 22 π electrons with 18 of them in delocalization to contribute the aromaticity.¹⁰¹ Various *meso*- and β -substituted porphyrins can be prepared easily by condensation.¹⁰² Substituting four aryl groups at *meso*-positions gives tetraarylporphyrins which generally show better solubility in organic solvents. The first synthesis of porphyrin was reported by Rothmund in 1935.¹⁰³

Porphyrins commonly act as macrocyclic dianionic tetradentate ligands upon deprotonation of the two pyrrolic protons. The diagonal radii of the central cavity is 2.098 Å,

which allow the coordination of various metal of suitable sizes.¹⁰⁴ Metalloporphyrin is formed when metal is coordinated.

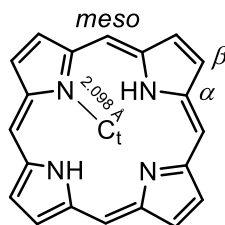


Figure 1.1 Structure of Porphyrin

1.6.2 Metalloporphyrins

Naturally occurring metalloporphyrins are the most common and best known metal complexes in nature. The universal coordination ability of porphyrin and the conformational flexibility allow diverse biological functions.¹⁰⁵ Hemoglobins (heme b) function as oxygen carrier by reversible oxygen binding (Figure 1.2a).¹⁰⁶ Coenzymes B₁₂ work as rearrangement catalyst due to its weak Co-C bond (Figure 1.2b).¹⁰⁷ Chlorophylls are green pigments that harvest light and transform light energy into chemical energy (Figure 1.2c).¹⁰⁸

Synthetic metalloporphyrins can be made by replacing the pyrrole protons with metal ions (eq 1.35).¹⁰⁹

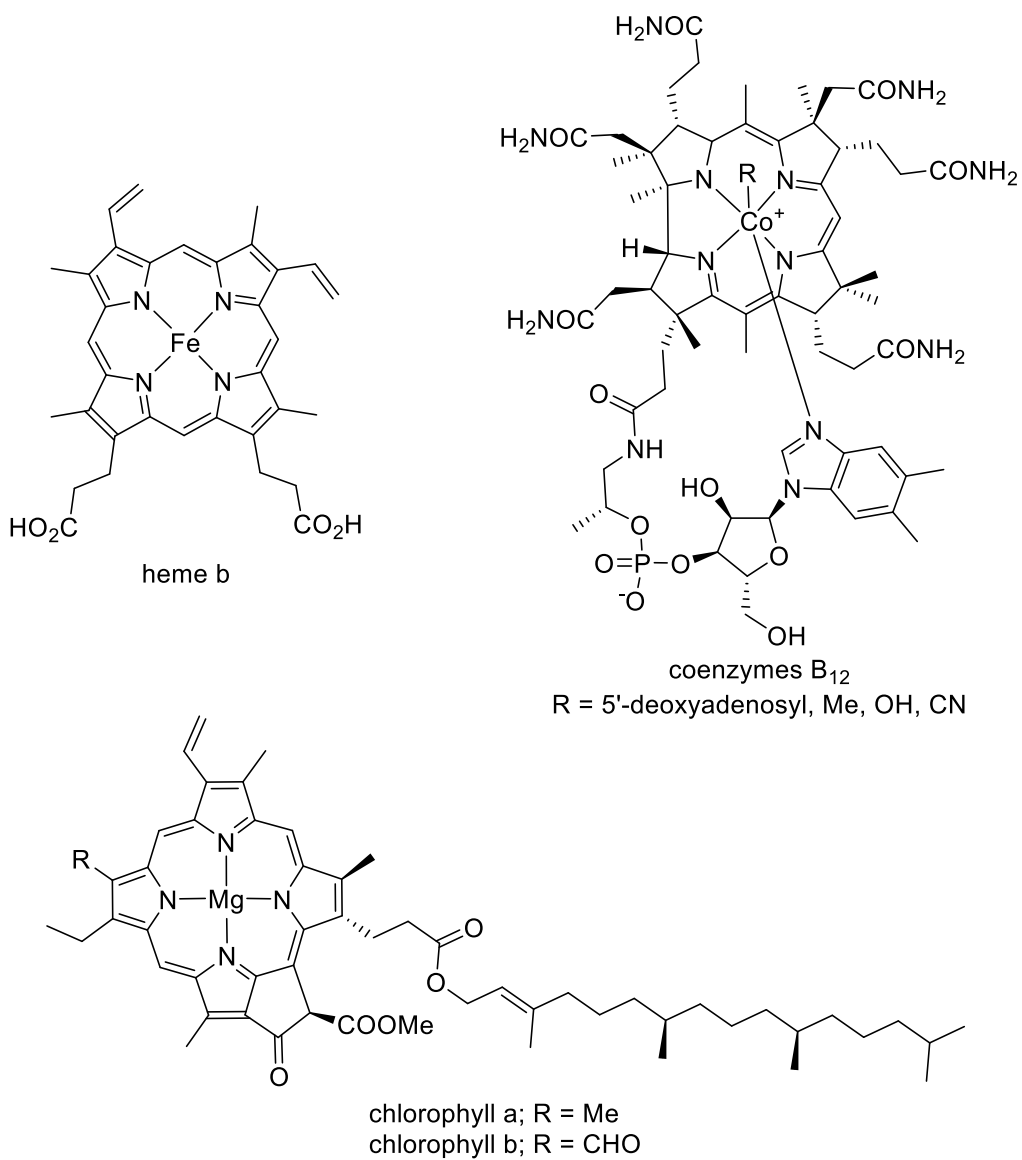
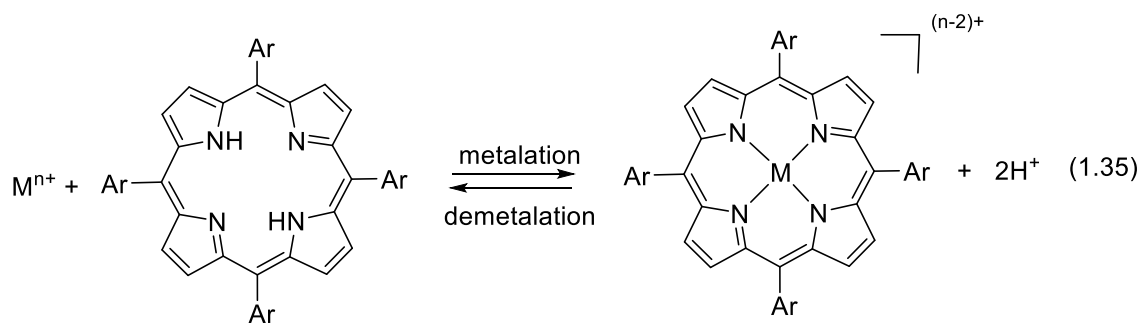


Figure 1.2(a) Structure of Heme b; (b) Structure of Coenzymes B₁₂; (c) Structure of Chlorophylls.



Porphyrin ligands are selective towards coordination of metal ions with ionic radii ranging from 60 to 70 pm. Therefore, 1st row transition metal ions usually fit into the central cavity to form in-plane square planar complexes.¹¹⁰ However, 2nd and 3rd row transition metal ions with larger ionic radii form complexes with slightly out-of-plane structures (Figure 1.3 and Table 1.6).

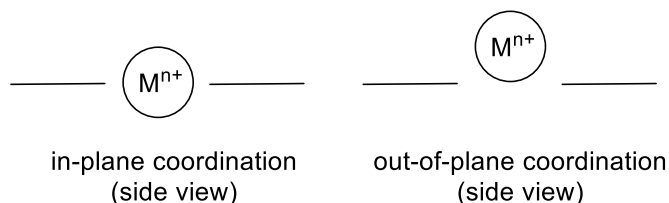


Figure 1.3 In-plane and out-of-plane coordination of metal ions with porphyrins

Table 1.6 Suitability of Various Transition Metal Ions with Porphyrin Coordination¹¹⁰

Metal ion	Ionic radius (pm)	Suitability of metal ion in complexes
Co ²⁺	82	Relatively large (out of plane)
Co ³⁺	64	Proper size
Rh ²⁺	86	Too large, out of plane
Rh ³⁺	75	Relatively large (out of plane)
Ir ²⁺	89	Too large, out of plane
Ir ³⁺	75	Relatively large (out of plane)

1.6.3 Chemistry of Group 9 Metalloporphyrins

Air stable cobalt, rhodium and iridium porphyrin complexes can be easily prepared by refluxing the porphyrin with corresponding metal salts (eqs 1.36 to 1.38). The common oxidation states of group 9 metalloporphyrins are +1 (d⁸), +2 (d⁷) and +3 (d⁶).^{110a} M^I(por), M^{II}(por) and M^{III}(por) (M = Co, Rh or Ir) behave like nucleophile, radical and electrophile, respectively, as

reflected from their energy level diagrams (Figure 1.4). The reactivities of rhodium and iridium porphyrin complexes, especially $M^I(\text{por})$ chemistry, will be discussed in details.

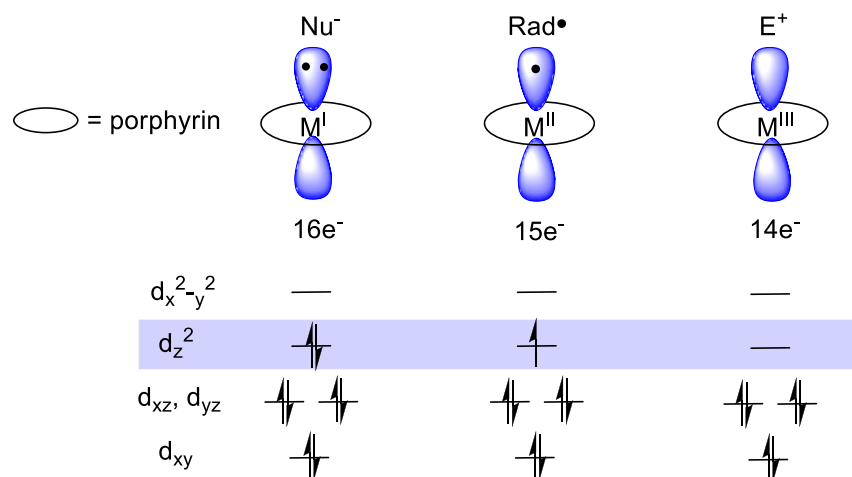
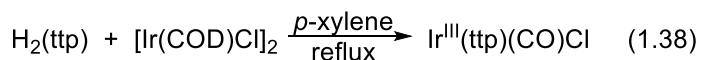
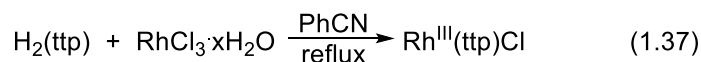
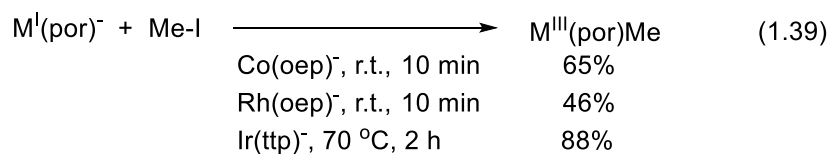


Figure 1.4 Energy Level Diagrams for Square Planar Group 9 Metalloporphyrins

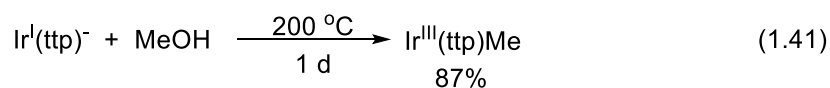
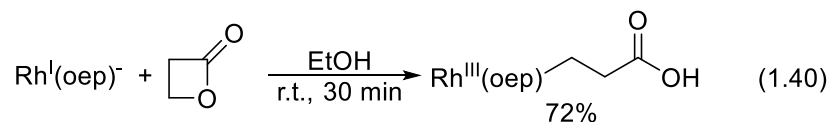
1.6.3.1 $M^I(\text{por})$ Chemistry

Both anionic $\text{Rh}^I(\text{por})^-$ and $\text{Ir}^I(\text{por})^-$ contains a pair of electron in the d_{z^2} orbital. Hence, they react like nucleophile. Examples of $M^I(\text{por})^-$ nucleophilic attack to alkyl halides (eq 1.39),¹¹¹ lactones (eq 1.40),¹¹² methanol (eq 1.41)¹¹³ and electron poor olefins (eq 1.42)^{111a,b} have been reported. Interestingly, Ogoshi demonstrated the nucleophilic substitution of non-polar C-C bond with $\text{Rh}^I(\text{oen})^-$ (eqs 1.43 and 1.44).^{40,44}

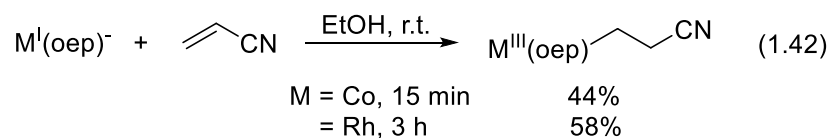
C-I Bond Cleavage



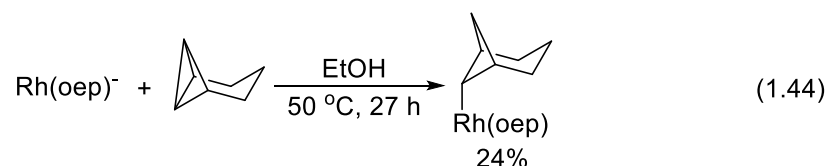
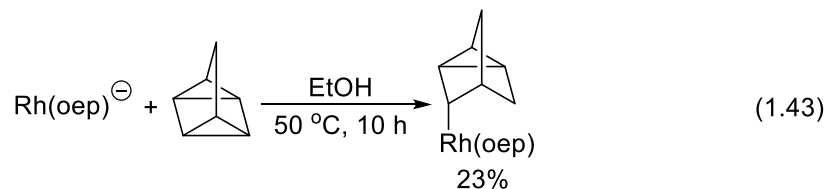
C-O Bond Cleavage



Nucleophilic Addition^{73a-b}



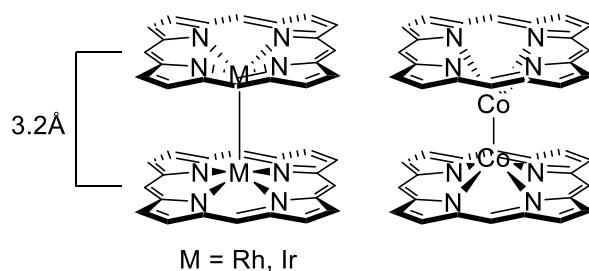
C-C Bond Cleavage



1.6.3.2 M^{II}(por) Chemistry

Monomeric M^{II}(por) has singly occupied dz² orbital. It is a metal-centered radical and often called metalloradical. Sterically non-bulky Rh^{II}(por) and Ir^{II}(por) dimerize to give M-M bonded Rh^{II}₂(por)₂ and Ir^{II}₂(por)₂ dimers, respectively.¹¹⁴ Sterically bulky Rh^{II}(tmp) and Ir^{II}(TTiPP) remain as monomer.¹¹⁴ Due to the weak and short Co-Co bond and inter-porphyrin π-π repulsion,^{115a} Co^{II}(por) does not form dimer (Table 1.7).

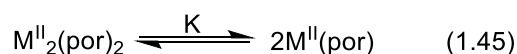
Table 1.7. Formation of $M^{II}(\text{por})$ Dimer.



M	Covalent Radii ^{115b} / Å	Theoretical M-M Bond Length in $M^{II}_2(\text{por})_2$ / Å
Co	1.26	2.52
Rh	1.42	2.84
Ir	1.41	2.82

Due to the weak Rh-Rh and Ir-Ir bonds in $M^{II}_2(\text{por})_2$ dimer, they equilibrate to give back monomeric $M^{II}(\text{por})$ when subjected to heating (Table 1.8 and eq 1.45).

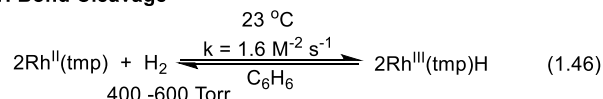
Table 1.8. Equilibrium between $M^{II}_2(\text{por})_2$ and $M^{II}(\text{por})$.^{114,116}



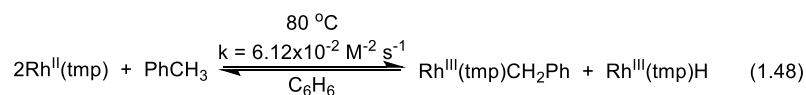
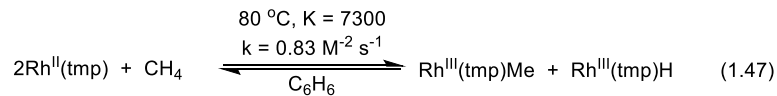
$M^{II}_2(\text{por})_2$	BDE / kcal mol ⁻¹	Estimated K	
		25 °C	200 °C
$\text{Rh}^{II}_2(\text{oep})_2$	16.5	5.3×10^{-6}	0.16
$\text{Rh}^{II}_2(\text{txp})_2$	12	0.011	19
$\text{Ir}^{II}_2(\text{oep})_2$	24	1.7×10^{-11}	5.5×10^{-5}
$\text{Ir}^{II}_2(\text{txp})_2$	20	1.4×10^{-8}	3.8×10^{-3}

The reactivity of $\text{Rh}^{II}(\text{por})$ has been extensively investigated. Various chemical transformations involving $\text{Rh}^{II}(\text{por})$ are summarized in eqs 1.46-1.59, including H-H activation (eq 1.46),¹¹⁷ C-H activation (eqs 1.47 and 1.48),¹¹⁸ C-N activation (eq 1.49),¹¹⁹ C-Si activation (eq 1.50),¹²⁰ C-X activation (X = Br, I) (eqs 1.51 and 1.52),¹²¹ CO reduction and coupling (eqs 1.53-1.55),¹²² oxidative addition with H_2O_2 (eq 1.56),¹²³ alkene insertion (eq 1.57),^{121a,124} reaction with diazo compounds (eq 1.58)¹²⁵ and ligand induced disproportionation (eq 1.59).¹²⁶

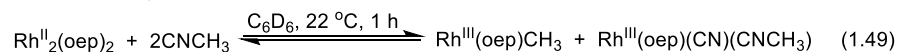
H-H Bond Cleavage



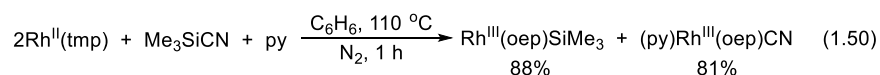
C-H Bond Cleavage



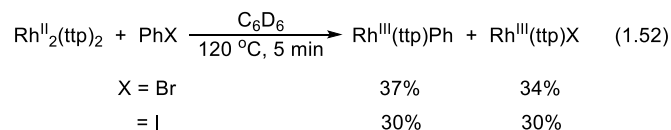
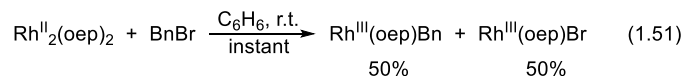
C-N Bond Cleavage



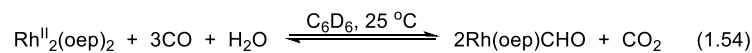
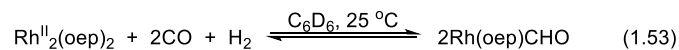
C-Si Bond Cleavage



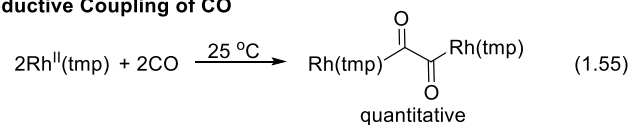
C-X Bond Cleavage (X = Br, I)



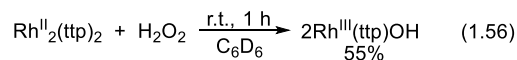
CO Activation



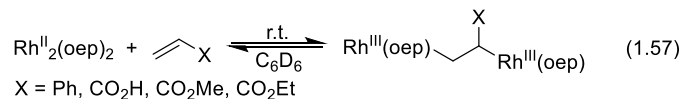
Reductive Coupling of CO



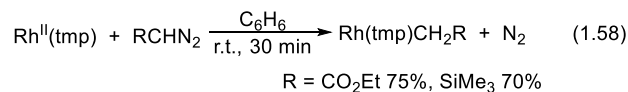
O-O Bond Cleavage



Alkene Insertion



Reaction with diazo compounds

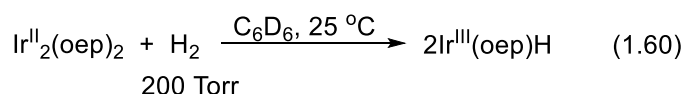


Disproportionation

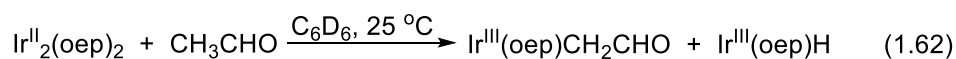
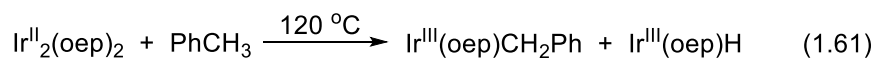


$\text{Ir}^{\text{II}}(\text{por})$ shares similar reactivities with $\text{Rh}^{\text{II}}(\text{por})$, but the scopes are limited to H-H bond (eq 1.60),¹²⁷ C-H bonds (eqs 1.61 and 1.62),¹²⁷ aryl C-X bonds (X = Cl, Br and I) bonds (eq 1.63),¹²⁸ alkene (eq 1.64)¹¹⁴ and CO (eqs 1.65 and 1.66).¹¹⁴ The temperature dependent spin density equilibrium between Ir metal center and porphyrin π orbital renders difficulties for detailed mechanistic studies.¹²⁹

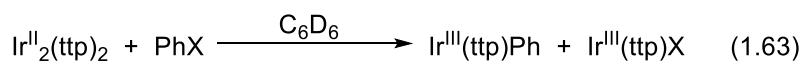
H-H Bond Cleavage



C-H Bond Cleavage

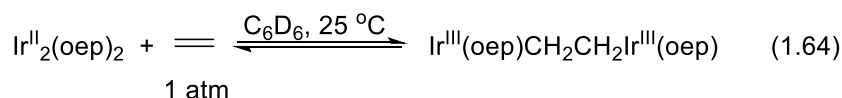


C-Br Bond Cleavage

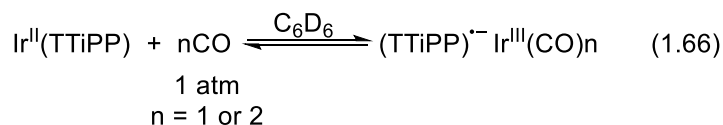
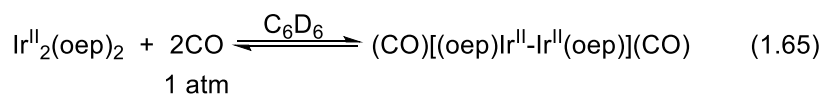


X = Cl	200 °C, 5 h	57%	4%
= Br	200 °C, 2 min	34%	32%
= I	200 °C, 1 min	37%	36%

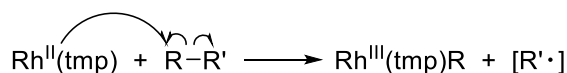
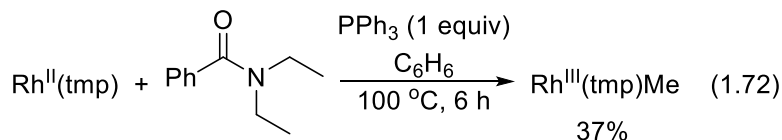
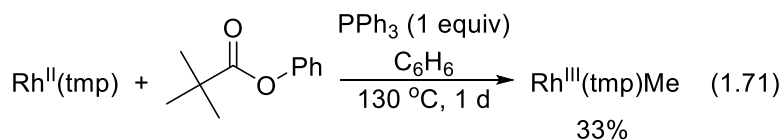
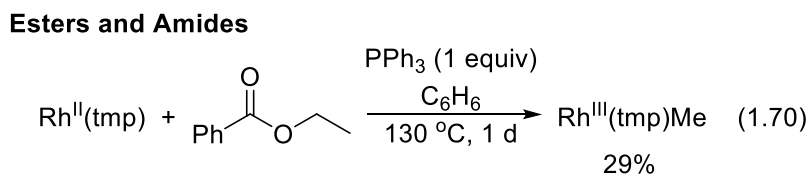
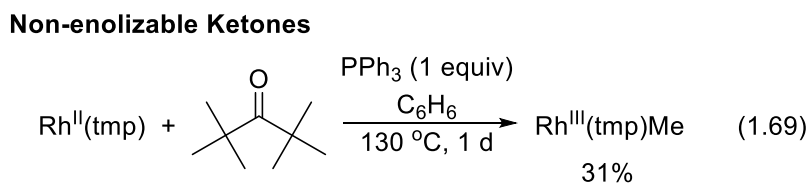
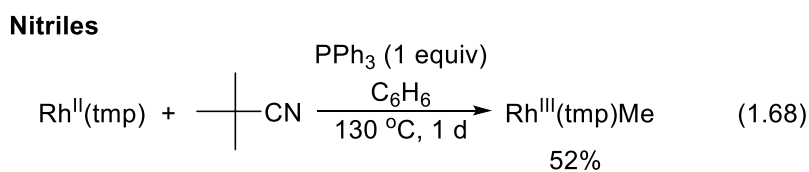
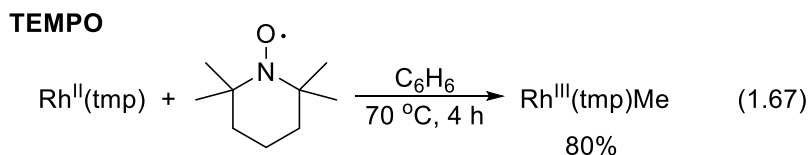
Alkene Insertion



Reaction with CO



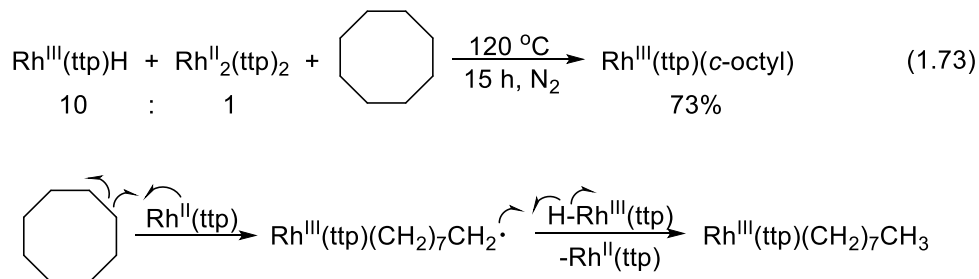
For CCA chemistry, Rh^{II}(tmp) is known to activate aliphatic C-C bonds in functionalized substrates such as TEMPO and its derivatives (eq 1.67),¹³⁰ nitriles (eq 1.68),¹³¹ non-enolizable ketones (eq 1.69),¹³² esters and amides (eqs 1.70-1.72).¹³³ A homolytic radical substitution mechanism (S_H2) was proposed (Scheme 1.8). The fate of organic co-product was not observed in most cases.



R = Me, Et, ⁿPr, Bn, (CH₂)₃Ph

Scheme 1.8 Homolytic Radical Substitution (S_H2) of C-C bond by Rh^{II}(tmp).

In 2010, the Chan group reported the aliphatic CCA in cyclooctane with $\text{Rh}^{\text{II}}_2(\text{ttp})_2/\text{Rh}^{\text{III}}(\text{ttp})\text{H}$ system (eq 1.73).¹³⁴ $\text{Rh}^{\text{II}}_2(\text{ttp})_2$, employed at lower concentration, cleaves the C-C bond efficiently at 120 °C via radical attack to first generate $\text{Rh}^{\text{III}}(\text{ttp})(\text{CH}_2)_7\text{CH}_2\cdot$ radical, followed by H atom transfer from $\text{Rh}^{\text{III}}(\text{ttp})\text{H}$ to yield $\text{Rh}^{\text{III}}(\text{ttp})(n\text{-octyl})$ in 73% yield (Scheme 1.9).



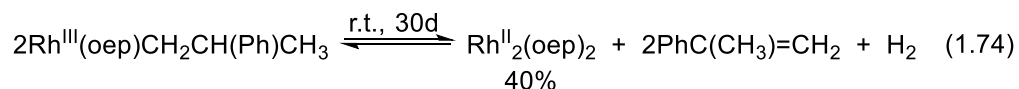
Scheme 1.9 $\text{Rh}^{\text{II}}(\text{ttp})$ Catalyzed CCA of Cyclooctane with $\text{Rh}^{\text{III}}(\text{ttp})\text{H}$.

Until now, the aliphatic CCA chemistry by $\text{Ir}^{\text{II}}(\text{por})$ is still unknown.

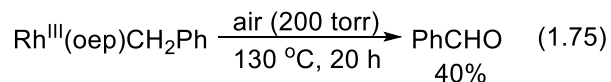
1.6.3.3 $\text{M}^{\text{III}}(\text{por})$ Chemistry

Most $\text{M}^{\text{III}}(\text{por})$ are air stable such as $\text{M}^{\text{III}}(\text{por})(\text{halide})$ and $\text{M}^{\text{III}}(\text{por})(\text{alkyl})$, which makes them common starting materials to generate reactive metalloporphyrin species like $\text{M}^{\text{II}}(\text{por})$ and $\text{M}^{\text{III}}(\text{por})\text{OH}$ for bond activation studies. Rhodium porphyrin examples are outlined, including thermal decomposition (eq 1.74),¹³⁵ oxidation (eq 1.75),¹³⁵ photolysis (eq 1.76),^{104b} intermolecular reductive elimination (eq 1.77),¹³⁶ alkyl 1,2-rearrangement (eq 1.78),¹³⁷ C-H bond activation (eqs 1.79-1.82)¹³⁸ and C-C bond activation (eq 1.83).¹³⁹

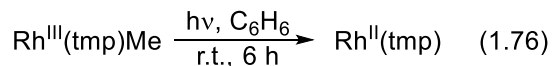
Thermal decomposition



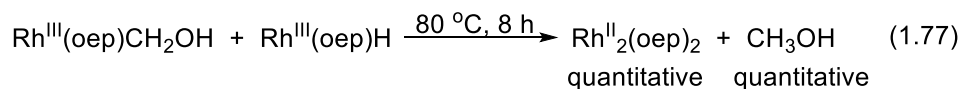
Oxidation



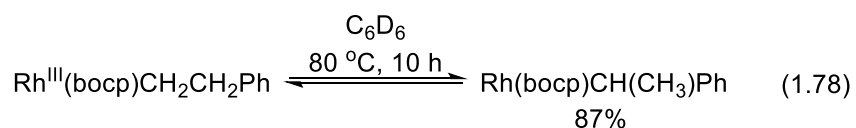
Photolysis



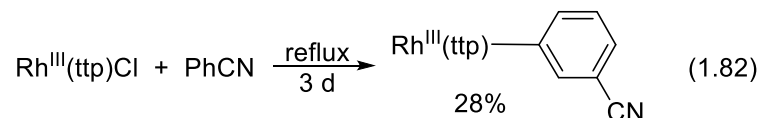
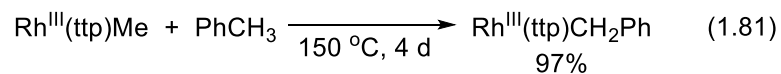
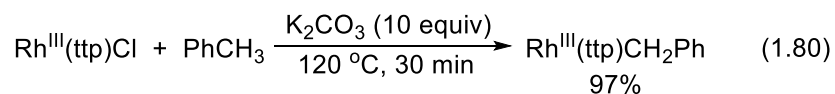
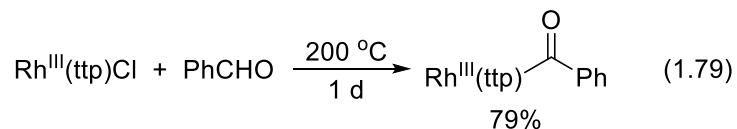
Intermolecular reductive elimination



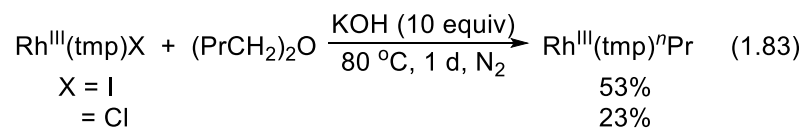
Alkyl 1,2-rearrangement



C-H Bond Cleavage

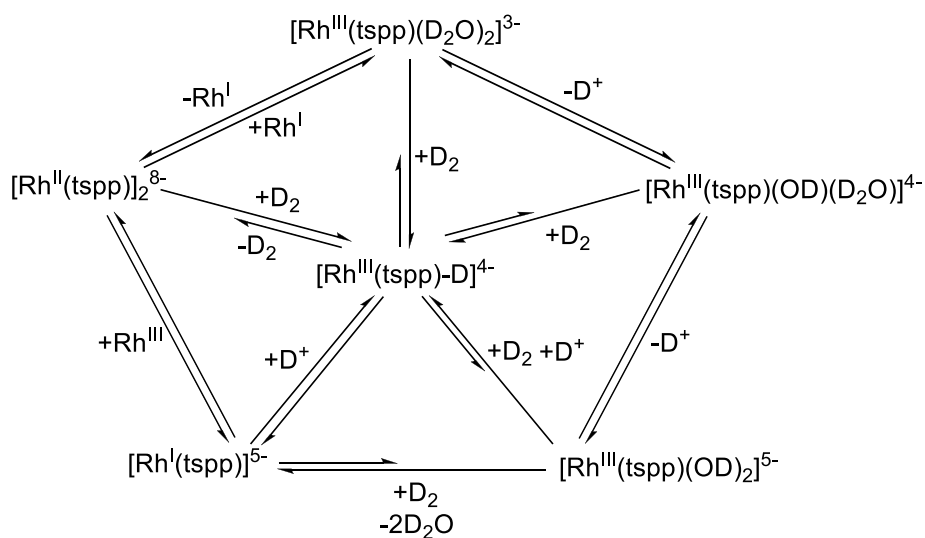


C-C Bond Cleavage

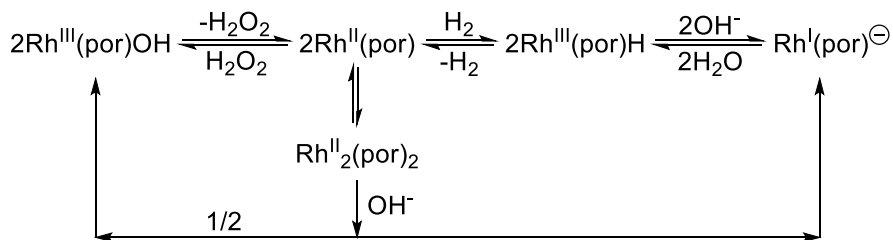


1.6.4 Equilibrium Between $M^I(\text{por})$, $M^{II}(\text{por})$ and $M^{III}(\text{por})$

Wayland has established the equilibria of water soluble Rh(I), Rh(II) and Rh(III) porphyrins in aqueous medium quantitatively (Scheme 1.10).¹⁴⁰ The distribution of these rhodium porphyrins depends on the pH of the medium. In analogy, the respective major species in organic solvent, for example benzene, will be $\text{Rh}^I(\text{por})^-$, $\text{Rh}^{II}(\text{por})$, $\text{Rh}^{III}(\text{por})\text{H}$ and $\text{Rh}^{III}(\text{por})\text{OH}$ (Scheme 1.11).



Scheme 1.10 Equilibrium of Rhodium Porphyrins in Water.



Scheme 1.11 Equilibrium of Rhodium Porphyrins in Organic Solvent.

1.7 Scope of Thesis

This thesis focuses on the catalytic carbon-carbon σ -bond hydrogenation of [2.2]paracyclophane (PCP) using water by group 9 metallocporphyrins. The thesis is outlined in the following sections:

- (i) mechanistic investigations on the stoichiometric and catalytic CCA of PCP with rhodium porphyrins;
- (ii) discovery on the reaction rate and yield enhancement with iridium porphyrins;
- (iii) preliminary results on catalytic hydrogenation of PCP with economical cobalt porphyrins.

References

1. Olah, G. A.; Molnár, Á. *Hydrocarbon Chemistry*, 2nd Ed., John Wiley & Sons, Inc., Hoboken, New Jersey, 2003.
2. Raseev, S. *Thermal and Catalytic Processes in Petroleum Refining*, Marcel Dekker, Inc.: New York, 2003.
3. (a) Hopf, H.; Gleiter, R. *Modern Cyclophane Chemistry*, WILEY-VCH Verlag GmbH & Co. KGaA, Weinheim, 2004. (b) Dodziuk, H. *Strained Hydrocarbons*, WILEY-VCH Verlag GmbH & Co. KGaA, Weinheim, 2009.
4. Brown, C. J.; Farthing, A. C. *Nature* **1949**, *164*, 915-916.
5. Boyd, R. H. *Tetrahedron* **1966**, *22*, 119-122.
6. Lonsdale, D. K.; Milledge, H. J.; Rao, K. V. K. *Proc. R. Soc. Lond. A* **1960**, *225*, 82-100.
7. Sato, T.; Torizuka, K. *J. Chem. Soc., Perkin Trans. 2* **1978**, 1199-1204.
8. Yamakita, Y.; Furukawa, Y.; Tasumi, M. *Chem. Lett.* **1993**, *2*, 311-314.
9. Reich, H. J.; Cram, D. J. *J. Am. Chem. Soc.* **1967**, *89*, 3078-3080.
10. Kaupp, G.; Teufel, E.; Hopf, H. *Angew. Chem.* **1979**, *91*, 232-234.
11. Adam, W.; Miranda, M. A.; Mojarrad, F.; Sheikh, H. *Chem. Ber.* **1994**, *127*, 875-879.
12. Sankararaman, S.; Hopf, H.; Dix, I.; Jones, P. G. *Eur. J. Org. Chem.* **2000**, 2711-2716.
13. Jun, C.-H. *Chem. Soc. Rev.* **2004**, *33*, 610-618.
14. (a) Jones, W. D. *Nature* **1993**, *364*, 676-677. (b) Rybtchinski, B.; Milstein, D. *Angew. Chem., Int. Ed.* **1999**, *38*, 870-883. (c) Sen, A. *Acc. Chem. Res.* **1998**, *31*, 550-557.
15. Halpern, J. *Acc. Chem. Res.* **1982**, *15*, 238-244.
16. Evans, J. A.; Everitt, G. F.; Kemmitt, R. D. W.; Russell, D. R. *J. Chem. Soc., Chem. Commun.* **1973**, 158-159.

17. Gozin, M.; Welsman, A.; Ben-David, Y.; Milstein, D. *Nature* **1993**, *364*, 699-701.
18. Crabtree, R. H.; Dion, R. P. *J. Chem. Soc., Chem. Commun.* **1984**, 1260-1261.
19. Hajela, S.; Bercaw, J. E. *Organometallics* **1994**, *13*, 1147-1154.
20. Goldman, A. S.; Roy, A. H.; Huang, Z.; Ahuja, R.; Schinski, W.; Brookhart, M. *Science* **2006**, *312*, 257-261.
21. Tipper, C. F. H. *J. Chem. Soc.* **1955**, 2045-2046.
22. Hogeveen, H.; Volger, H. C. *J. Am. Chem. Soc.* **1967**, *89*, 2486-2487.
23. Dietl, H.; Maitlis, P. M. *J. Chem. Soc., Chem. Commun.* **1967**, 759-760.
24. Hogeveen, H.; Volger, H. C. *J. Chem. Soc., Chem. Commun.* **1967**, 1133-1134.
25. Volger, H. C.; Hogeveen, H.; Gaasbeek, M. M. P. *J. Am. Chem. Soc.* **1969**, *91*, 2137-2138.
26. Katz, T. J.; Cerefice, S. *J. Am. Chem. Soc.* **1969**, *91*, 2405-2406.
27. Paquette, L. A.; Stowell, J. C. *J. Am. Chem. Soc.* **1970**, *92*, 2584-2586.
28. Cassar, L.; Eaton, P. E.; Halpern, J. *J. Am. Chem. Soc.* **1970**, *92*, 3515-3518.
29. Cassar, L.; Halpern, J. *J. Chem. Soc., Chem. Commun.* **1970**, 1082-1083.
30. Cassar, L.; Eaton, P. E.; Halpern, J. *J. Am. Chem. Soc.* **1970**, *92*, 6366-6368.
31. Wristers, J.; Brener, L.; Pettit, R. *J. Am. Chem. Soc.* **1970**, *92*, 7499-7501.
32. Gassman, P. G.; Atkins, T. J. *J. Am. Chem. Soc.* **1971**, *93*, 1042-1043.
33. Sakai, M.; Yamaguchi, H.; Westberg, H.; Masamune, S. *J. Am. Chem. Soc.* **1971**, *93*, 1043-1044.
34. Gassman, P. G.; Atkins, T. J. *J. Am. Chem. Soc.* **1971**, *93*, 4597-4599.
35. Roth, R. J.; Katz, T. J. *J. Am. Chem. Soc.* **1972**, *94*, 4770-4771.
36. Gassman, P. G.; Atkins, T. J.; Lumb, J. T. *J. Am. Chem. Soc.* **1972**, *94*, 7757-7761.
37. Yoshikawa, S.; Aoki, K.; Kiji, J.; Furukawa, J. *Tetrahedron Lett.* **1974**, *30*, 405-407.

38. Golden, H. J.; Baker, D. J.; Miller, R. G. *J. Am. Chem. Soc.* **1974**, *96*, 4235-4243.
39. Stockis, A.; Weissberger, E. *J. Am. Chem. Soc.* **1975**, *97*, 4288-4292.
40. Ogoshi, H.; Setsune, J.-I.; Yoshida, Z.-I. *J. Chem. Soc., Chem. Commun.* **1975**, 572-573.
41. Eilbracht, P. *Chem. Ber.* **1976**, *109*, 1429-1435.
42. Eilbracht, P. *Chem. Ber.* **1976**, *109*, 3136-3141.
43. Sohn, M.; Blum, J.; Halpern, J. *J. Am. Chem. Soc.* **1979**, *101*, 2694-2698.
44. Ogoshi, H.; Setsune, J.-I.; Yoshida, Z.-I. *J. Organomet. Chem.* **1980**, *185*, 95-104.
45. Eisch, J. J.; Piotrowski, A. M.; Han, K. I.; Krüger, C.; Tsay, Y. H. *Organometallics* **1985**, *4*, 224-231.
46. Berris, B. C.; Hovakeemian, G. H.; Lai, Y.-H.; Mestdagh, H.; Vollhardt, K. P. C. *J. Am. Chem. Soc.* **1985**, *107*, 5670-5687.
47. Bunel, E.; Burger, B. J.; Bercaw, J. E. *J. Am. Chem. Soc.* **1988**, *110*, 976-978.
48. Chatani N.; Takeyasu, T.; Hanafusa, T. *Tetrahedron Lett.* **1988**, *29*, 3979-3982.
49. Halcrow, M. A.; Urbanos, F.; Chaudret, B. *Organometallics* **1993**, *12*, 955-957.
50. Yang, X.; Jia, L.; Marks, T. J. *J. Am. Chem. Soc.* **1993**, *115*, 3392-3393.
51. Burger, P.; Bergman, R. G. *J. Am. Chem. Soc.* **1993**, *115*, 10462-10463.
52. Mitsudo, T.; Zhang, S.; Watanabe, Y. *J. Chem. Soc., Chem. Commun.* **1994**, 435-436.
53. Perthuisot, C.; Jones, W. D. *J. Am. Chem. Soc.* **1994**, *116*, 3647-3648.
54. Rosenthal, U.; Ohff, A.; Baumann, W.; Kempe, R.; Tillack, A.; Burlakov, V. V. *Organometallics* **1994**, *13*, 2903-2906.
55. Suzuki, H.; Takaya, Y.; Takemori, T. *J. Am. Chem. Soc.* **1994**, *116*, 10779-10780.
56. Lu, Z.; Jun, C.-H.; de Gala, S. R.; Sigalas, M. P.; Eisenstein, O.; Crabtree, R. H. *Organometallics* **1995**, *14*, 1168-1175.

57. Casey, C. P.; Hallenbeck, S. L.; Pollock, D. W.; Landis, C. R. *J. Am. Chem. Soc.* **1995**, *117*, 9770-9771.
58. Arce, M.-J.; Viado, A. L.; An, Y.-Z.; Khan, S. I.; Rubin, Y. *J. Am. Chem. Soc.* **1996**, *118*, 3775-3776.
59. Perthuisot, C.; Edelbach, B. L.; Zubris, D. L.; Jones, W. D. *Organometallics* **1997**, *16*, 2016-2023.
60. Bessmertnykh, A. G.; Blinov, K. A.; Grishin, Y. K.; Donskaya, N. A.; Tveritina, E. V.; Yur'eva, N. M.; Beletskaya, I. P. *J. Org. Chem.* **1997**, *62*, 6069-6076.
61. Tsukada, N.; Shibuya, A.; Nakamura, I.; Yamamoto, Y. *J. Am. Chem. Soc.* **1997**, *119*, 8123-8124.
62. Shaltout, R. M.; Sygula, R.; Sygula, A.; Fronczek, F. R.; Stanley, G. G.; Rabideau, P. W. *J. Am. Chem. Soc.* **1998**, *120*, 835-836.
63. Edelbach, B. L.; Lachicotte, R. J.; Jones, W. D. *J. Am. Chem. Soc.* **1998**, *120*, 2843-2853.
64. Yeh, W.-Y.; Hsu, S. C. N. *Organometallics* **1998**, *17*, 2477-2483.
65. Osakada, K.; Takimoto, H.; Yamamoto, T. *Organometallics* **1998**, *17*, 4532-4534.
66. Edelbach, B. L.; Vicic, D. A.; Lachicotte, R. J.; Jones, W. D. *Organometallics* **1998**, *17*, 4784-4794.
67. Nakamura, I.; Itagaki, H.; Yamamoto, Y. *J. Org. Chem.* **1998**, *63*, 6458-6459.
68. Camacho, D. H.; Nakamura, I.; Saito, S.; Yamamoto, Y. *Angew. Chem. Int. Ed.* **1999**, *38*, 3365-3367.
69. Edelbach, B. L.; Lachicotte, R. J.; Jones, W. D. *Organometallics* **1999**, *18*, 4040-4049.
70. Edelbach, B. L.; Lachicotte, R. J.; Jones, W. D. *Organometallics* **1999**, *18*, 4660-4668.
71. Zhang, X.; Carpenter, G. B.; Sweigart, D. A. *Organometallics* **1999**, *18*, 4887-4888.

72. Nakamura, I.; Saito, S.; Yamamoto, Y. *J. Am. Chem. Soc.* **2000**, *122*, 2661-2662.
73. Suginome, M.; Matsuda, T.; Ito, Y. *J. Am. Chem. Soc.* **2000**, *122*, 11015-11016.
74. Satoh, T.; Jones, W. D. *Organometallics* **2001**, *20*, 2916-2919.
75. Iverson, C. N.; Jones, W. D. *Organometallics* **2001**, *20*, 5745-5750.
76. Müller, C.; Lachicotte, R. J.; Jones, W. D. *Organometallics* **2002**, *21*, 1975-1981.
77. Bart, S. C.; Chirik, P. J. *J. Am. Chem. Soc.* **2003**, *125*, 886-887.
78. Siriwardana, A. I.; Nakamura, I.; Yamamoto, Y. *J. Org. Chem.* **2004**, *69*, 3202-3204.
79. Schaub, T.; Backes, M.; Radius, U. *Organometallics* **2006**, *25*, 4196-4206.
80. Shi, M.; Liu, L.-P.; Tang, J. *Org. Lett.* **2006**, *8*, 4043-4046.
81. Eisch, J. J.; Gitua, J. N. *Organometallics* **2007**, *26*, 778-779.
82. Jiang, M.; Shi, M. *Organometallics* **2009**, *28*, 5600-5602.
83. Castro-Rodrigo, R.; Esteruelas, M. A.; López, A. M.; López, F.; Mascareñas, J. L.; Oliván, M.; Oñate, E.; Saya, L.; Villarina, L. *J. Am. Chem. Soc.* **2010**, *132*, 454-455.
84. Sattler, A.; Parkin, G. *Nature* **2010**, *463*, 523-526.
85. Simaan, S.; Goldberg, A. F. G.; Rosset, S.; Marek, I. *Chem. Eur. J.* **2010**, *16*, 774-778.
86. Simaan, S.; Marek, I. *J. Am. Chem. Soc.* **2010**, *132*, 4066-4067.
87. Chan, Y. W.; Chan, K. S. *J. Am. Chem. Soc.* **2010**, *132*, 6920-6922.
88. Chaplin, A. B.; Tonner, R.; Weller, A. S. *Organometallics* **2010**, *29*, 2710-2714.
89. Matsuda, T.; Kirikae, H. *Organometallics* **2011**, *30*, 3923-3925.
90. Chen, K.; Jiang, M.; Zhang, Z.; Wei, Y.; Shi, M. *Eur. J. Org. Chem.* **2011**, 7189-7193.
91. To, C. T.; Choi, K. S.; Chan, K. S. *J. Am. Chem. Soc.* **2012**, *134*, 11388-11391.
92. Bowring, M. A.; Bergman, R. G.; Tilley, T. D. *J. Am. Chem. Soc.* **2013**, *135*, 13121-13128.
93. Hu, S.; Shima, T.; Hou, Z. *Nature*, **2014**, *512*, 413-415.

94. Evans pKa Table, Harvard University.
95. Luo, Y. R. *Comprehensive Handbook of Chemical Bond Energies*, CRC Press, Boca Raton, FL, 2007.
96. (a) Barrero, A. F.; Oltra, J. E.; Cuerva, J. M.; Rosales, A. *J. Org. Chem.* **2002**, *67*, 2566-2571. (b) Cuerva, J. E.; Campana, A. G.; Justicia, J.; Rosales, A.; Oller-López, J. L.; Robles, R.; Cárdenas, D. J.; Bunuel, E.; Oltra, J. E. *Angew. Chem. Int. Ed.* **2006**, *45*, 5522-5526. (c) Rosale, A.; Munoz-Bascón, J.; Roldan-Molina, E.; Castaneda, M. A.; Padial, N. M.; Gansäuer, A.; Rodríguez-García, I.; Oltra, J. E. *J. Org. Chem.* **2014**, *79*, 7672-7676. (d) Paradas, M.; Campana, A. G.; Jiménez, T.; Robles, R.; Oltra, J. E.; Bunuel, E.; Justicia, J.; Cárdenas, D. J.; Cuerva, J. M. *J. Am. Chem. Soc.* **2010**, *132*, 12748-12756.
97. Lee, H.-Y.; An, M. *Tetrahedron Lett.* **2003**, *44*, 2775-2778.
98. Halpern, J. *Acc. Chem. Res.* **1970**, *3*, 386-392.
99. Fachinetti, G.; Del Cima, F. *J. Organomet. Chem.* **1984**, *275*, C25-C29.
100. Spiegel, D. A.; Wilberg, K. B.; Schacherer, L. N.; Medeiros, M. R.; Wood, J. L. *J. Am. Chem. Soc.* **2005**, *127*, 12513-12515.
101. (a) Fleischer, E. B. *Acc. Chem. Res.* **1970**, *3*, 105-112. (b) Ogoshi, H.; Mizutani, A. *Acc. Chem. Res.* **1998**, *31*, 81-89.
102. Shanumgathasan, S.; Edwards, C.; Boyle, R. W. *Tetrahedron* **2000**, *56*, 1025-1046.
103. Rothmund, P. *J. Am. Chem. Soc.* **1935**, *57*, 2010-2011.
104. Smith, K. M. *Porphyrins and Metalloporphyrins*, Ed.; Elsevier Scientific Pub. Co.; New York, 1975.

105. (a) Shelnut, J. A.; Song, X.-Z.; Ma, J.-G.; Jia, S.-L.; Jentzen, W.; Medforth, J. C. *Chem. Soc. Rev.* **1998**, *27*, 31-41. (b) Ravikanth, M.; Chandrashedar, T. K. *Struct. & Bonding (Berlin)* **1995**, *82*, 105-188.
106. Warburton, P. R.; Busch, D. H. *Perspectives on Bioinorganic Chemistry Vol. 2*, Jai Press Ltd., Greenwich, 1993.
107. Banerjee, R. *Chemistry and Biochemistry of B₁₂*, Ed. John Wiley, New York, 1999.
108. Ort, D. R.; Yocum, C. F. *Oxygenic Photosynthesis: The Light Reactions*, Ed., Kluwer Academic Publishers, Dordrecht, 1996.
109. Adler, A. D.; Longo, F. R.; Kampas, F.; Kim, J. J. *Inorg. Nucl. Chem.* **1970**, *32*, 2445-2448.
110. (a) Kadish, K. M.; Smith, K. M.; Guilard, R. *The Porphyrin Handbook Vol. 3*, Eds., Academic Press, Boston, 2000. (b) Kaim, W.; Schwederski, B. *Bioinorganic Chemistry: Inorganic Elements In The Chemistry of Life: An Introduction and Guide*, Ed., John Wiley, New York, 1994. (c) Emsley, J. *The Elements*, 3rd Ed. Clarendon Press, Oxford, 1998.
111. (a) Ogoshi, H.; Watanabe, E.; Koketsu, N.; Yoshida, Z. *Bull. Chem. Soc. Jpn.* **1976**, *49*, 2529-2536. (b) Ogoshi, H.; Setsune, J.; Omura, T.; Yoshida, Z. *J. Am. Chem. Soc.* **1975**, *97*, 6461-6466. (c) Yeung, S. K.; Chan, K. S. *Organometallics* **2005**, *24*, 6426-6430.
112. Mizutani, T.; Uesaka, T.; Ogoshi, H. *Organometallics* **1995**, *14*, 341-346.
113. Cheung, C. W.; Fung, H. S.; Lee, S. Y.; Qian, Y. Y.; Chan, Y. W.; Chan, K. S. *Organometallics* **2010**, *29*, 1343-1354.
114. Cui, W.; Li, S.; Wayland, B. B. *J. Organomet. Chem.* **2007**, *692*, 3198-3206.

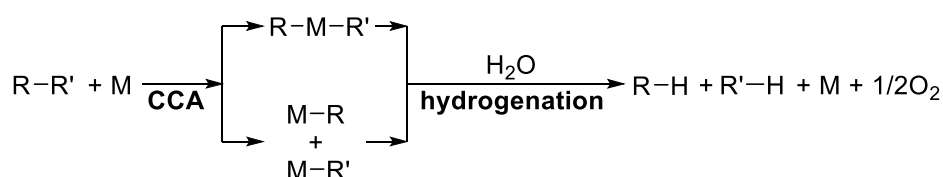
115. (a) Sun, D.; Tam, F. S.; Reed, C. A.; Chaker, L.; Boyd, P. D. W. *J. Am. Chem. Soc.* **2011**, *124*, 6604-6612. (b) Cordero, B.; Gómez, V.; Platero-Prats, A. E.; Revés, M.; Echeverría, J.; Cremades, E.; Barragan, F.; Alvarez, S. *Dalton Trans.* **2008**, 2832-2838.
116. (a) Wayland, B. B. *Polyhedron*, **1988**, *7*, 1545-1558. (b) Wayland, B. B.; Ba, S.; Sherry, A. E. *J. Am. Chem. Soc.* **1991**, *113*, 5305-5311.
117. Wayland, B. B.; Ba, S.; Sherry, A. E. *Inorg. Chem.* **1992**, *31*, 148-150.
118. (a) Wayland, B. B.; Sherry, A. E. *J. Am. Chem. Soc.* **1990**, *112*, 1259-1261. (b) Wayland, B. B.; Ba, S.; Sherry, A. E. *J. Am. Chem. Soc.* **1991**, *113*, 5305-5311.
119. Poszmik, G.; Carroll, P. J.; Wayland, B. B. *Organometallics* **1993**, *12*, 3410-3417.
120. Chan, K. S.; Zhang, L. R.; Fung, C. W. *Organometallics* **2004**, *23*, 6097-6098.
121. (a) Paonessa, R. S.; Thomas, N. C.; Halpern, J. *J. Am. Chem. Soc.* **1985**, *107*, 4333-4335. (b) Qian, Y. Y.; Chan, K. S. *Organometallics* **2012**, *31*, 5452-5462.
122. (a) Wayland, B. B.; Woods, B. A.; Pierce, R. *J. Am. Chem. Soc.* **1982**, *104*, 302-303. (b) Wayland, B. B.; Sherry, A. E.; Poszmik, G.; Bunn, A. G. *J. Am. Chem. Soc.* **1992**, *114*, 1673-1681.
123. Choi, K. S.; Lai, T. H.; Lee, S. Y.; Chan, K. S. *Organometallics* **2011**, *30*, 2633-2635.
124. Wayland, B. B.; Poszmik, G. *Organometallics* **1992**, *11*, 3534-3542.
125. Zhang, L. R.; Chan, K. S. *Organometallics* **2007**, *26*, 679-684.
126. Wayland, B. B.; Balkus, K. J., Jr.; Farnos, M. D. *Organometallics* **1989**, *8*, 950-955.
127. Del Rossi, K. J.; Wayland, B. B. *J. Chem. Soc., Chem. Commun.* **1986**, 1963-1965.
128. (a) Cheung, C. W.; Chan, K. S. *Organometallics* **2011**, *30*, 4999-5009. (b) Cheung, C. W.; Chan, K. S. *Organometallics* **2011**, *30*, 4269-4283.
129. Zhai, H.; Bunn, A.; Wayland, B. B. *Chem. Commun.* **2001**, 1294-1295.

130. (a) Tse, M. K.; Chan, K. S. *J. Chem. Soc., Dalton Trans.* **2001**, 510-511. (b) Chan, K. S.; Li, X. Z.; Dzik, W. I.; de Bruin, B. *J. Am. Chem. Soc.* **2008**, *130*, 2051-2061. (c) Chan, K. S.; Li, X. Z.; Lee, S. Y. *Organometallics* **2010**, *29*, 2850-2856.
131. (a) Chan, K. S.; Li, X. Z.; Fung, C. W.; Zhang, L. *Organometallics* **2007**, *26*, 20-21. (b) Chan, K. S.; Li, X. Z.; Zhang, L.; Fung, C. W. *Organometallics* **2007**, *26*, 2679-2687.
132. Zhang, L.; Chan, K. S. *J. Organomet. Chem.* **2006**, *691*, 3782-3787.
133. Zhang, L.; Chan, K. S. *J. Organomet. Chem.* **2007**, *692*, 2021-2027.
134. Chan, Y. W.; Chan, K. S. *J. Am. Chem. Soc.* **2010**, *132*, 6920-6922.
135. De Rossi, K. J.; Wayland, B. B. *J. Am. Chem. Soc.* **1985**, *107*, 7941-7944.
136. Van Voorhees, S. L.; Wayland, B. B. *Organometallics* **1985**, *4*, 1887-1888.
137. Mak, K. W.; Chan, K. S. *J. Am. Chem. Soc.* **1998**, *120*, 9689-9687.
138. (a) Chan, K. S.; Lau, C. M. *Organometallics* **2006**, *25*, 260-265. (b) Chan, K. S.; Chiu, P. F.; Choi, K. S. *Organometallics* **2007**, *26*, 1117-1119. (c) Choi, K. S.; Chiu, P. F.; Chan, K. S. *Organometallics* **2010**, *29*, 624-629. (d) Zhou, X.; Li, Q.; Mak, T. C. W.; Chan, K. S. *Inorg. Chim. Acta* **1998**, *270*, 551-554. (e) Zhou, X.; Tse, M. K.; Wu, D.-D.; Mak, T. C. W.; Chan, K. S. *J. Organomet. Chem.* **2000**, *598*, 80-86.
139. Lai, T. H.; Chan, K. S. *Organometallics* **2009**, *28*, 6845-6846.
140. Fu, X.; Wayland, B. B. *J. Am. Chem. Soc.* **2004**, *126*, 2623-2631.

Chapter 2 Catalytic Carbon-Carbon Bond Hydrogenation of [2.2]Paracyclophane with Water by Rhodium Porphyrin Complexes

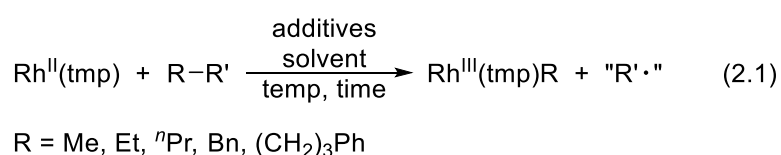
2.1 Introduction

Catalytic carbon-carbon σ -bond hydrogenation using water involves two fundamental steps: (1) carbon-carbon bond activation (CCA) and (2) hydrogenation using water (Scheme 2.1).

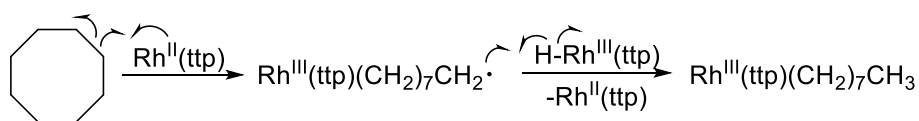
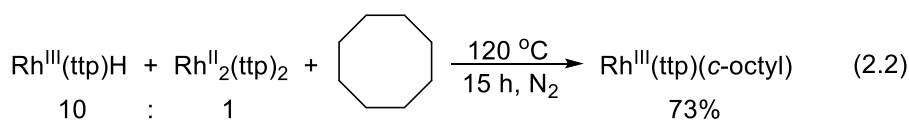


Scheme 2.1 Catalytic Carbon-Carbon σ -Bond Hydrogenation using Water

The Chan group has reported the stoichiometric intermolecular aliphatic CCA in TEMPO and derivatives,¹ nitriles,² non-enolizable ketones,³ ester⁴ and amides⁴ by monomeric $\text{Rh}^{\text{II}}(\text{tmp})$ metalloradical. $\text{Rh}^{\text{II}}(\text{tmp})$ undergoes homolytic substitution ($\text{S}_{\text{H}2}$) at the carbon center which leads to carbon-carbon bond cleavage and rhodium-carbon bond formation (eq 2.1).

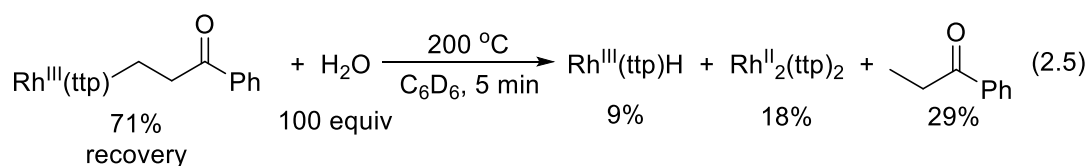
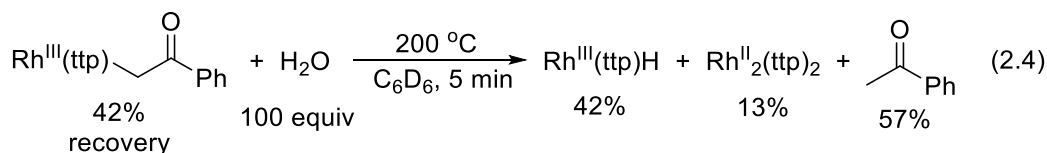
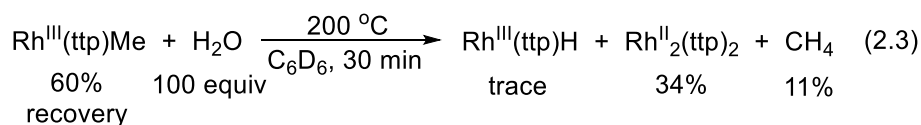


The Chan group also discovered the $\text{Rh}^{\text{II}}(\text{ttp})$ catalyzed 1,2-insertion of $\text{Rh}^{\text{III}}(\text{ttp})\text{H}$ into the carbon-carbon bond of cyclooctane (eq 2.2 and Scheme 2.2).⁵ This ascertained the potency of rhodium(II) porphyrins for CCA of hydrocarbon substrates.



Scheme 2.2 CCA of Cyclooctane by $\text{Rh}^{\text{II}}(\text{ttp})$ Catalyzed 1,2-Insertion of $\text{Rh}^{\text{III}}(\text{ttp})\text{H}$.

Rhodium(III) porphyrin alkyls undergo hydrolysis at elevated temperature. This allows the hydrogenation of alkyl fragment using H_2O . $\text{Rh}^{\text{III}}(\text{ttp})\text{Me}$, $\text{Rh}^{\text{III}}(\text{ttp})\text{CH}_2\text{COPh}$ and $\text{Rh}^{\text{III}}(\text{ttp})\text{CH}_2\text{CH}_2\text{COPh}$ have been shown to undergo hydrolysis in C_6D_6 at $200 \text{ }^\circ\text{C}$ to produce CH_4 , PhCOMe and PhCOEt , respectively (eqs 2.3-2.5).⁶ At the same time, $\text{Rh}^{\text{II}}_2(\text{ttp})_2$ is generated and capable for CCA.



Therefore, by combining the reactivity of $\text{Rh}^{\text{II}}(\text{por})$ towards CCA and hydrolysis of $\text{Rh}^{\text{III}}(\text{por})\text{R}$, catalytic carbon-carbon σ -bond hydrogenation using H_2O by rhodium porphyrins is achievable.

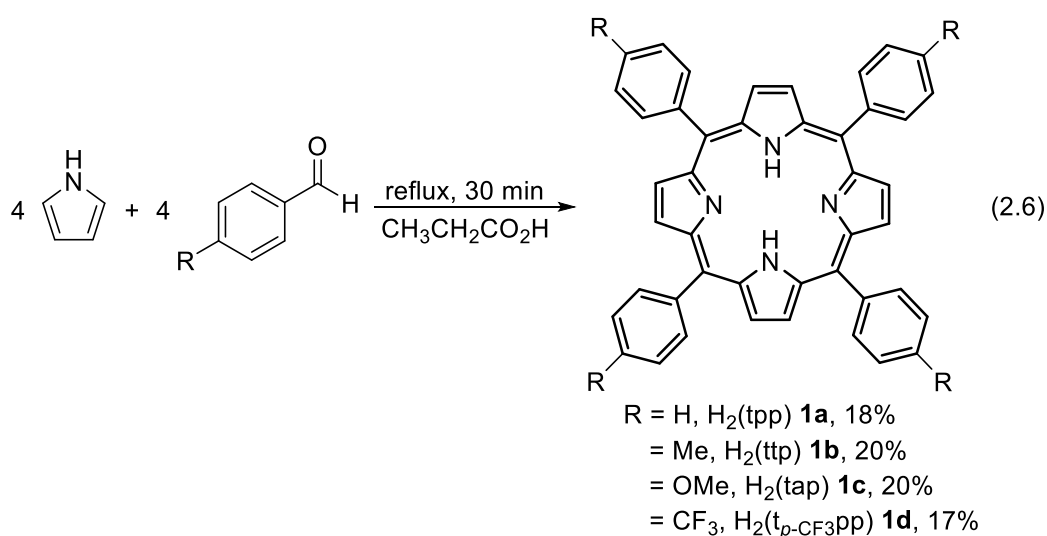
2.2 Objectives of the Work

We aim to achieve catalytic carbon-carbon σ -bond hydrogenation of hydrocarbons using H_2O by rhodium porphyrins.

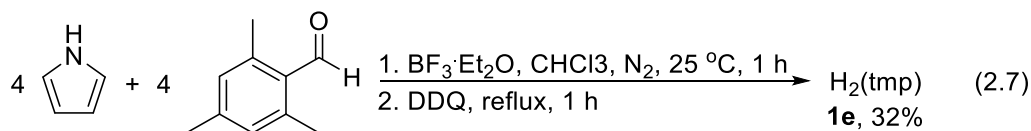
2.3 Preparation of Starting Materials

2.3.1 Synthesis of Porphyrins

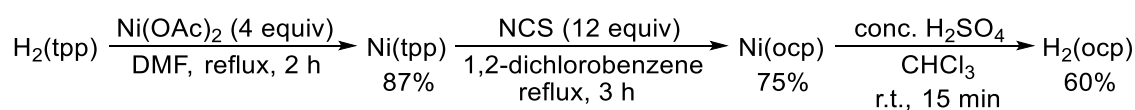
Various *meso*-aryl substituted free base porphyrins $\text{H}_2(\text{tpp})$, $\text{H}_2(\text{ttp})$, $\text{H}_2(\text{tap})$ and $\text{H}_2(\text{t}_p\text{-CF}_3\text{pp})$) were prepared by the condensation of corresponding aldehydes and pyrrole in refluxing propionic acid for 30 min in 18%, 20%, 20% and 17% yields, respectively, according to the literature procedures (eq 2.6).⁷



$\text{H}_2(\text{tmp})$ **1e** was prepared in 32% yield from mesitaldehyde and pyrrole according to literature procedures (eq 2.7).⁸



The electron deficient porphyrin H₂(ocp) was prepared in three steps from H₂(tpp) (Scheme 2.3).^{9,10}

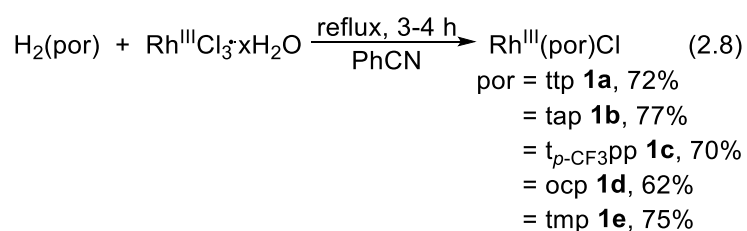


Scheme 2.3 Preparation of H₂(ocp) from H₂(tpp)

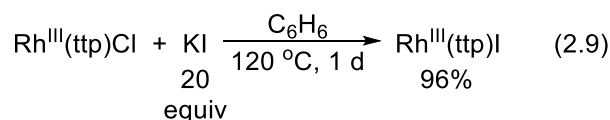
2.3.2 Synthesis of Metalloporphyrins

2.3.2.1 Synthesis of Rhodium(III) Porphyrin Halides

Rh^{III}(ttp)Cl, Rh^{III}(tap)Cl, Rh^{III}(*t*_p-CF₃pp)Cl, Rh^{III}(ocp)Cl and Rh^{III}(tmp)Cl were synthesized by refluxing the corresponding free base porphyrin with Rh^{III}Cl₃·xH₂O in PhCN in 72%, 77%, 70%, 62% and 75% yields, respectively, according to literature procedures (eq 2.8).¹¹

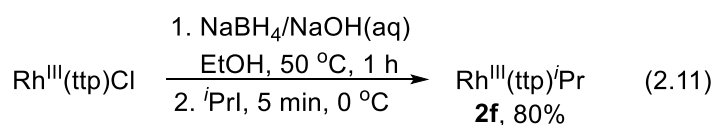
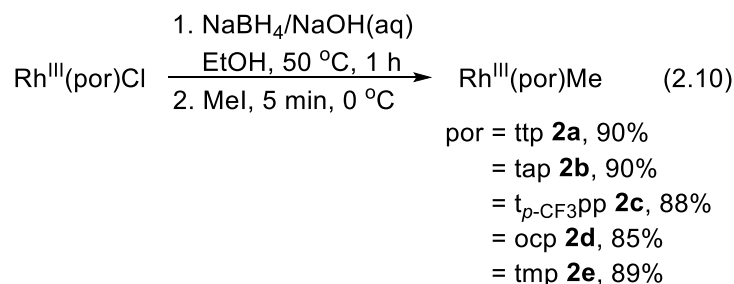


Rh^{III}(ttp)I¹² was prepared from modified procedures by reacting Rh^{III}(ttp)Cl with KI in C₆H₆ at 120 °C in 96% yield (eq 2.9).

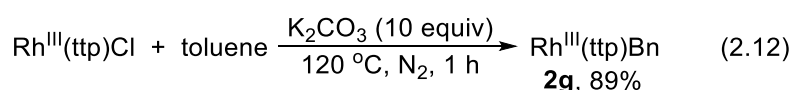


2.3.2.2 Synthesis of Rhodium(III) Porphyrin Alkyls

$\text{Rh}^{\text{III}}(\text{ttp})\text{Me}$, $\text{Rh}^{\text{III}}(\text{tap})\text{Me}$, $\text{Rh}^{\text{III}}(\text{t}_p\text{-CF}_3\text{pp})\text{Me}$, $\text{Rh}^{\text{III}}(\text{ocp})\text{Me}$, $\text{Rh}^{\text{III}}(\text{tmp})\text{Me}$ and $\text{Rh}^{\text{III}}(\text{ttp})^i\text{Pr}$ were synthesized by reductive alkylation of the corresponding $\text{Rh}^{\text{III}}(\text{por})\text{Cl}$ with alkyl iodide in 90%, 90%, 88%, 85%, 89% and 80% yields, respectively (eqs 2.10 and 2.11).¹³

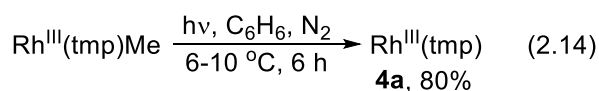


$\text{Rh}^{\text{III}}(\text{ttp})\text{Bn}$ was prepared by the base promoted BnCHA of toluene with $\text{Rh}^{\text{III}}(\text{ttp})\text{Cl}$ (eq 2.12).¹⁴



2.3.2.3 Synthesis of $\text{Rh}^{\text{II}}(\text{tmp})$

$\text{Rh}^{\text{II}}(\text{tmp})$ was prepared by the photolysis of $\text{Rh}^{\text{III}}(\text{tmp})\text{Me}$ at 6-10 °C in C_6H_6 (eq 2.14).¹⁵

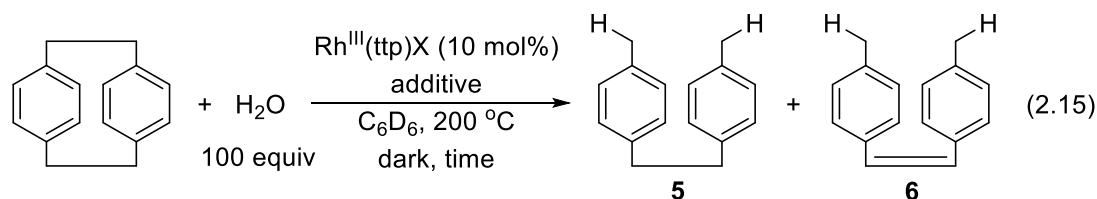


2.4 Optimization of Catalytic PCP Hydrogenation with H₂O

2.4.1 Initial Screenings

Initially, PCP with KOH (1 equiv) and H₂O (100 equiv) heated at 200 °C in the presence of 10 mol% Rh^{III}(ttp)I in C₆D₆ for 25 h yielded 83% of 4,4'-dimethylbibenzyl **5** (Table 2.1, eq 2.15, entry 1). The saturated [NaOH] in toluene at 25 °C has been reported to be ~9 mM.¹⁶ It is assumed that KOH has the same solubility in C₆D₆ at 25 °C. Therefore, KOH was completely dissolved in the catalysis to give [KOH] = 9.6 mM. In addition, the saturated [H₂O] in C₆H₆ at 200 °C has been reported to be ~2 M. It is assumed that H₂O/C₆D₆ system would behave similarly.¹⁷ Therefore, H₂O was completely dissolved in the catalysis to give [H₂O] = 0.96 M. Hence, the reaction mixture was homogeneous at 200 °C.

Table 2.1 Catalytic PCP Hydrogenation using H₂O.



entry	X	additive	time	yield / %				
				PCP recovery	5	6	X-H ^a	Rh ^{III} (ttp)H ^a
1	I	KOH (1 equiv)	25 h	0	83	12	--	29
2 ^b	I	KOH (1 equiv)	5 d	9	52	4	--	0
3	Me	--	54 h	0	78	9	79	55
4	ⁱ Pr	--	50 h	0	68	10	20 ^c	41
5	none	none	4.5 d	100	0	0	--	--

^a w.r.t. Rh^{III}(ttp)X

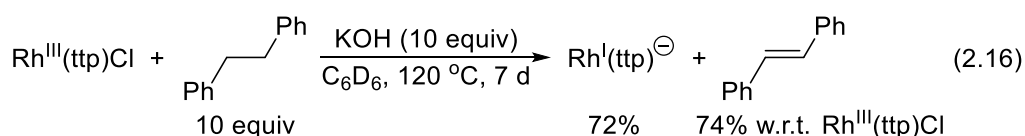
^b carried out under room light, see experimental for details

^c propene was formed in 18% yield

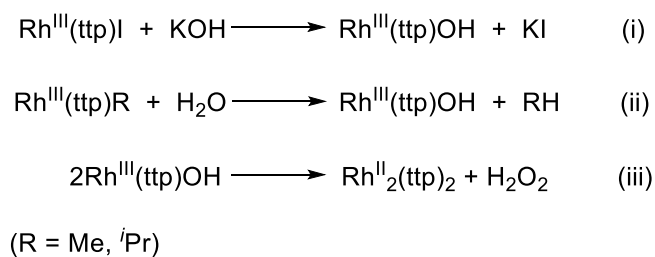
In the presence of room light, the catalysis was greatly retarded (Table 2.1, eq 2.15, entry 2). The rhodium porphyrin complexes might be photochemically decomposed at elevated temperature as formation of dark purple precipitate was observed. The catalytic hydrogenation proceeded smoothly under neutral conditions using Rh^{III}(ttp)Me pre-catalyst to produce **5** in 78% yield after 54 h (Table 2.1, eq 2.15, entry 3). Rh^{III}(ttp)ⁱPr was a good pre-

catalyst and **5** was formed in 68% yield after 50 h (Table 2.1, eq 2.15, entry 4). Control experiment showed that PCP was stable at 200 °C in the presence of H₂O up to 4.5 d with quantitative recovery (Table 2.1, eq 2.15, entry 5).

All pre-catalysts produced small amounts of 4,4'-dimethylstilbene **6** (Table 2.1, eq 2.15, entries 1-4). The stoichiometric dehydrogenation of bibenzyl to trans-stilbene promoted by rhodium porphyrin complex has been studied by the Chan group (eq 2.16).¹⁸ Hence, two possible pathways can lead to product **6**: (1) dehydrogenation of PCP to [2.2]paracyclophane-1-ene followed by CCA and hydrogenation; or (2) direct dehydrogenation of **5** to **6**. The former pathway is less likely because dehydrogenation of PCP to give more strained [2.2]paracyclophane-1-ene is energetically uphill by 4.6 kcal/mol based on their corresponding strain energies.¹⁹

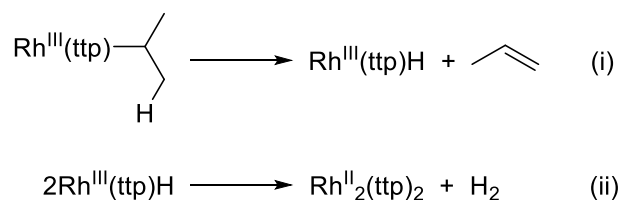


We reasoned that the CCA of PCP is associated with the Rh^{II}(ttp) metalloradical attack at the benzylic C-C bond. Indeed, Rh^{III}(ttp)I, Rh^{III}(ttp)Me and Rh^{III}(ttp)ⁱPr are readily available precursors of Rh^{II}₂(ttp)₂, via a common intermediate Rh^{III}(ttp)OH. Rh^{III}(ttp)I undergoes fast ligand substitution with KOH to give Rh^{III}(ttp)OH, followed by thermal rapid reduction to give Rh^{II}₂(ttp)₂ (Scheme 2.4, and further explained in details in mechanistic discussion part below).²⁰ Similarly, hydrolysis of Rh^{III}(ttp)Me and Rh^{III}(ttp)ⁱPr first generate Rh^{III}(ttp)OH and then converted to Rh^{II}₂(ttp)₂ under neutral conditions (Scheme 2.4).⁶ The detection of CH₄ and propane further supports the hydrolysis step.



Scheme 2.4 Conversion of Pre-Catalysts to Rh^{II}₂(ttp)₂.

In addition, the propene co-formation from Rh^{III}(ttp)ⁱPr pre-catalyst suggests a parallel β-H elimination process to first give Rh^{III}(ttp)H intermediate.²¹ Rh^{III}(ttp)H then undergoes bi-molecular thermal dehydrogenation to give Rh^{II}₂(ttp)₂ and H₂ (Scheme 2.5).²²

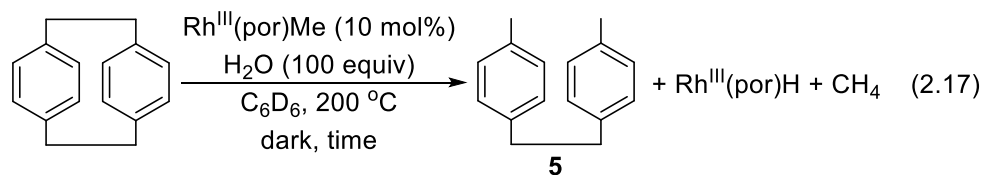


Scheme 2.5 Alternative Conversion Pathway from Rh^{III}(ttp)ⁱPr to Rh^{II}₂(ttp)₂.

2.4.2 Porphyrin Ligand Electronic Effects

The electronic effects of the porphyrin ligand on catalytic PCP hydrogenation were then examined with both electron rich and poor Rh^{III}(por)Me (Table 2.2, eq 2.16). The rate of PCP consumption increased with electron deficiency of the porphyrin, e.g. t₄-CF₃pp > ttp > tap (Table 2.2, eq 2.17, entries 1-3). CCA of PCP would be more favorable with electron rich rhodium porphyrin since the oxidation of Rh^{II} to Rh^{III} in the CCA step is better stabilized. Electron rich ligand usually gives complex with stronger Rh-C bond than electron poor one.²³ The reverse reactivity trend observed probably reflects that CCA of PCP is not the rate determining step in the catalysis.

Table 2.2 Catalytic PCP Hydrogenation by Various Rh^{III}(por)Me.



entry	por	time / h	yield / %			
			5	6	Rh ^{III} (por)H ^a	CH ₄ ^a
1	tap	84	62	7	30	33
2	ttp	54	78	9	55	79
3 ^b	t ₄ -CF ₃ pp	40	59	14	4	13
4	ocp	4 d	54	15	not observed	58
5 ^c	tmp	7 d	39	14	Rh ^{III} (tmp)D, 16	--

^a w.r.t. Rh^{III}(por)Me

^b Rh^{III}(t₄-CF₃pp)H was observed after 24 h

^c D₂O was used

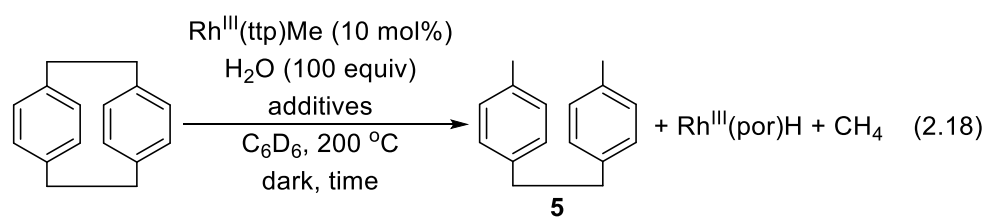
Alternatively, the formation of electron richer Rh^{II}₂(por)₂ for CCA is slower. In the base-promoted reduction of Rh^{III}(por)I to Rh^{II}₂(por)₂ via Rh^{III}(por)OH intermediate, the reaction with Rh^{III}(tap)I is about 4 times slower than Rh^{III}(ttp)I.²⁰ Since hydrolysis of Rh^{III}(por)Me is proposed to go through Rh^{III}(por)OH intermediate, which is reduced to Rh^{II}₂(por)₂ and favored by electron poor porphyrin ligand. However, the half-life of Rh^{III}(ttp)OH reduction to Rh^{II}₂(ttp)₂ is estimated to be 15 min at 120 °C (assume 4 half-lives for complete reaction).²⁰ This suggests a short half-life of about 4 s at 200 °C. Despite the carry over effect in the catalysis, the rate of conversion of Rh^{III}(por)Me pre-catalyst to Rh^{II}₂(por)₂ is unlikely to affect the catalysis time in hour scale.

The hydrogenation catalyzed by very electron deficient Rh^{III}(ocp)Me required 4 d to give 54% yield of **5** (Table 2.2, eq 2.16, entry 4). The saddle-shaped ocp ligand may induce steric hindrance on CCA and slowed down the catalysis.²⁴ Similarly, the sterically bulky Rh^{III}(tmp)Me catalyzed the PCP hydrogenation very slowly to give only 39% yield of **5** after 7 d (Table 2.2, eq 2.16, entry 5). After the completion of catalytic PCP hydrogenation, Rh^{III}(por)H was the organometallic end product obtained in low to moderate yields.

2.4.3 Additive Effects

In order to promote the hydrolysis by enhancing the mixing of H₂O in non-polar benzene solvent, various polar additives were introduced to the catalytic system. ^tBuOH, BnEt₃NCl and PPh₄Br at various loadings did not give significant improvements (Table 2.3, eq 2.17). Extensive decomposition of phase transfer catalyst PPh₄Br to PPh₃ and O=PPh₃ was observed (Table 2.3, eq 2.18, entry 6). PPh₄Br was hydrolyzed to first give O=PPh₃, followed by reduction to produce PPh₃ (Scheme 2.6).²⁵ Higher additive loadings were not examined because rhodium porphyrins are known to cleave the C-N bond in amine²⁶ or reacts with alcohol.^{3b,27}

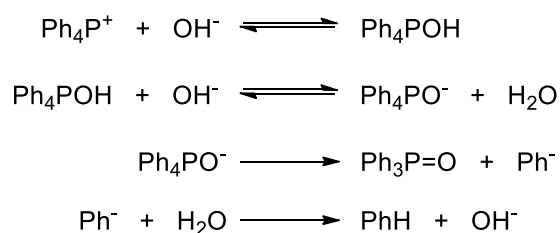
Table 2.3 Polar Additive Effects on Catalytic PCP Hydrogenation.



entry	additives	equiv	time / h	yield / %	
				5	Rh ^{III} (por)H ^a
1	--	--	54	78	55
2	^t BuOH	2	54	68	0
3	^t BuOH	10	47	74	0
4	BnEt ₃ NCl	0.1	50	56	9
5	BnEt ₃ NCl	1	41	75	0
6 ^b	PPh ₄ Br	0.1	61	70	9

^a w.r.t. Rh^{III}(tp)Me

^b 73% PPh₃ and 21% O=PPh₃ were formed w.r.t. PPh₄Br

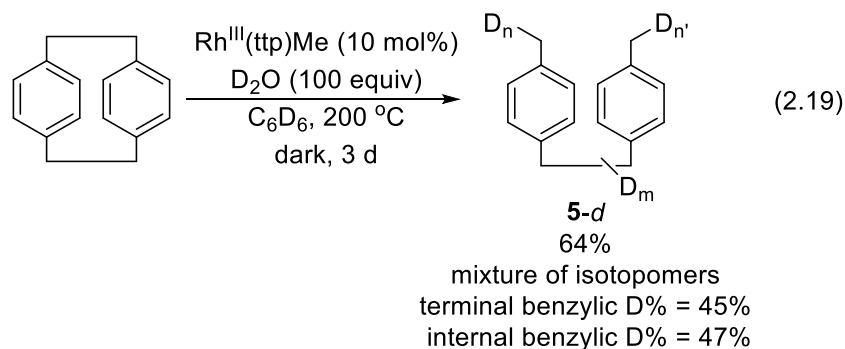


Scheme 2.6 Hydrolysis of PPh₄⁺ to O=PPh₃.

2.5 Mechanistic Investigations

2.5.1 Deuterium Labeling Experiments

To test whether water was the hydrogen source to enrich PCP to give **5**, a series of deuterium labeling experiments using D₂O were performed. Under the standard catalytic PCP hydrogenation conditions with H₂O replaced with D₂O, PCP was converted to deuterium-enriched **5-d** in 64% yield (eq 2.18).²⁸ ¹H NMR analysis of the isolated **5-d** gave proton integration ratio with aromatic : internal benzylic : terminal benzylic = 8.00 : 2.12 : 3.3, assuming no aromatic H/D exchange (Figure 2.1). Hence, the terminal benzylic positions are $((6 - 3.31) / 6) \times 100\% = 45\%$ deuterated, while the internal benzylic positions are $((4 - 2.12) / 4) \times 100\% = 47\%$ deuterated. Attempted detection of 4-*d*₁,4'-*d*₁-dimethylbibenzyl upon its initial formation by ¹H NMR spectroscopy was unsuccessful because the benzylic ¹H signal of PCP ($\delta = 2.81$ ppm) partially overlapped with the internal benzylic ¹H signal of deuterated **5** ($\delta = 2.79$ ppm), giving non-conclusive ¹H integration. Nevertheless, no deuterated PCP was observed during the catalysis.



Since H/D exchange at the internal benzylic positions was observed, we independently examined the H/D exchange activity of **5** under identical conditions (eq 2.19). The isolated **5-d'** was analyzed by ¹H NMR spectroscopy to give proton integration ratio with aromatic : internal benzylic : terminal benzylic = 8.00 : 1.15 : 5.51 (Figure 2.1). Hence, the terminal benzylic positions are $((6 - 5.51) / 6) \times 100\% = 8\%$ deuterated, while the internal

benzylic positions are $((4 - 1.15) / 4) \times 100\% = 71\%$ deuterated. This suggested that the post-exchange activity at the terminal benzylic positions was minor within the catalysis time scale. The more extensive internal benzylic H/D exchange was due to the more rapid benzylic CHA with ethylbenzene than toluene, governed by the weaker C-H bond.²⁹ These observations, in addition to the control experiment in Table 2.1, eq 2.21, further support that water is the hydrogen source.

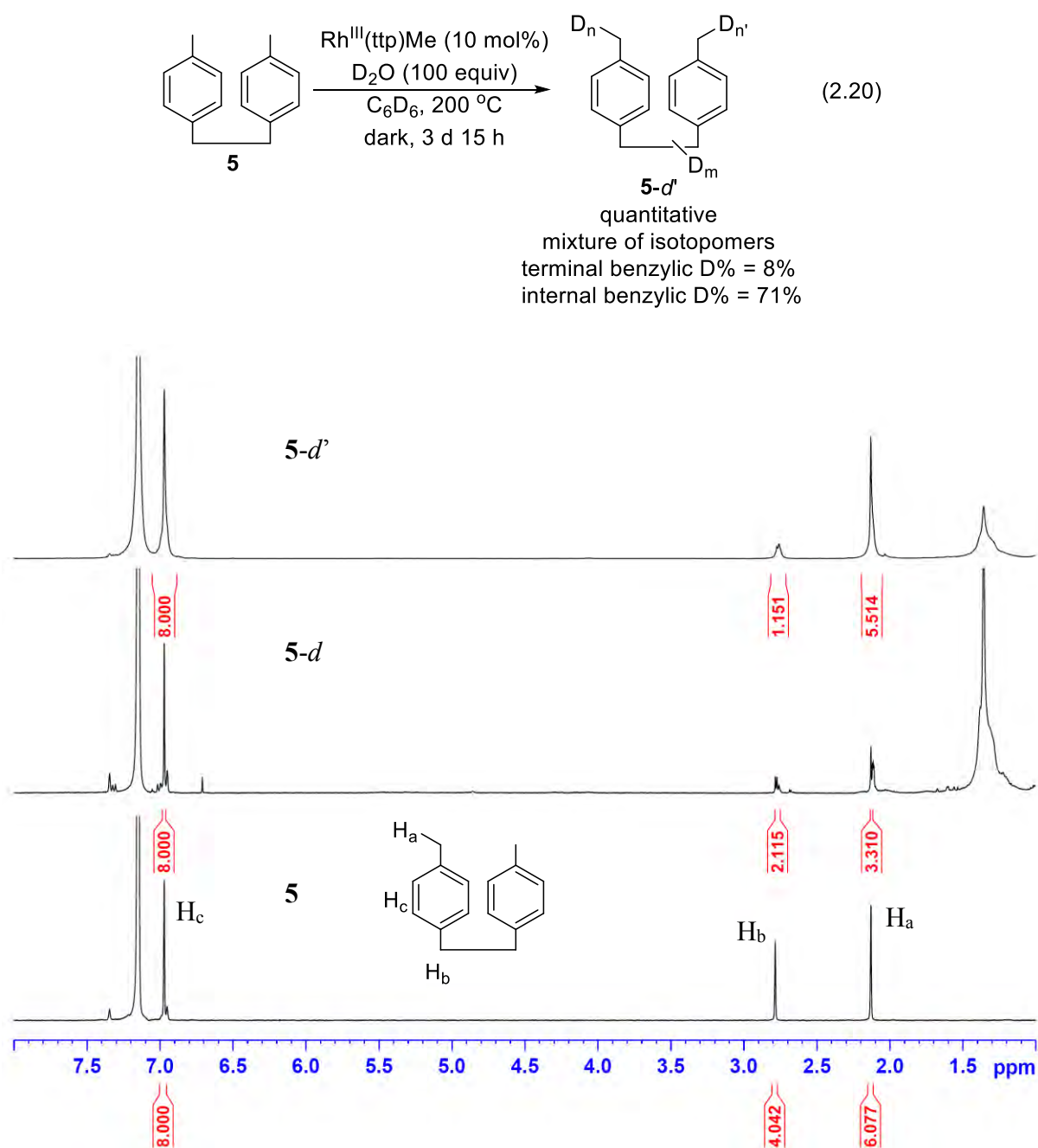
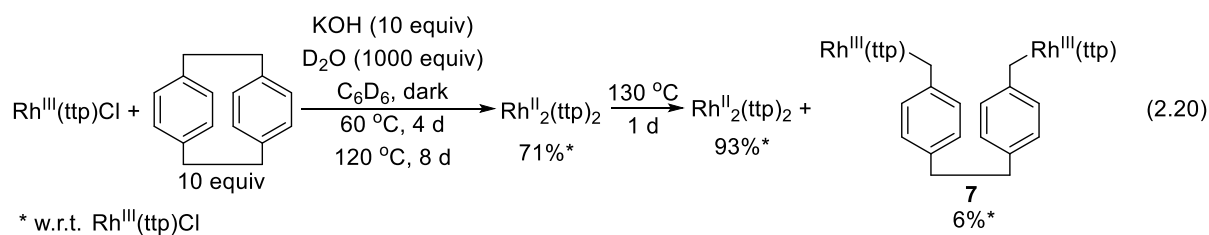


Figure 2.1 ^1H NMR Spectra of Product **5**, **5-d** and **5-d'**.

2.5.2 CCA via CHA Intermediate

As Milstein and Jones have shown CHA is a prior step to the CCA in α,α' -diphosphino-*m*-xylenes³⁰ and biphenylene,³¹ respectively, we investigated whether benzylic CHA would also take place for the CCA of PCP. The stoichiometric reaction of Rh^{III}(ttp)Cl with PCP (10 equiv) in the presence of KOH (10 equiv) and D₂O (1000 equiv) was closely monitored by ¹H NMR spectroscopy (Table 2.4, eq 2.20, Figure 1). After 12 d of heating at 60 °C and then at 120 °C, PCP remained unreacted and undeuterated. At the same time, Rh^{III}(ttp)Cl was completely consumed to give Rh^{II}₂(ttp)₂ in 71% yield. The poor mass balance for rhodium porphyrin complexes, especially at 60 °C, was due to the poor solubility of Rh^{II}₂(ttp)₂. No benzylic CHA of PCP with Rh^{II}₂(ttp)₂ to give Rh^{III}(ttp)(cyclophanyl) was observed.^{14,29,32b} The rigid structure of PCP may induces steric repulsion between the benzene rings and Rh^{II}(ttp), such that the four-centered transition state for benzylic CHA is not accessible (Scheme 2.7).³² Upon further heating at 130 °C for 1 d the reaction mixture yielded 6% of di-rhodium benzyl intermediate 7. Therefore, CCA of PCP occurred directly without any observable CHA process.

Table 2.4 Reaction Time Profile of Rh^{III}(ttp)Cl with PCP under Basic Conditions.



entry	temp / °C	time / h	yield / %				
			Rh ^{III} (ttp)Cl	Rh ^{II} ₂ (ttp) ₂	Rh ^{III} (ttp)H	7	Total [Rh]
1	r.t.	0	100	0	0	0	100
2	60	1	35	8	2	0	45
3	60	18	0	22	14	0	36
4	60	72	0	24	4	0	28
5	60	96	0	30	4	0	34
6	120	104	0	53	7	0	60
7	120	120	0	60	9	0	69
8	120	144	0	55	9	0	64
9	120	216	0	56	5	0	61
10	120	288	0	71	7	0	78
11	130	312	0	93	0	6	99

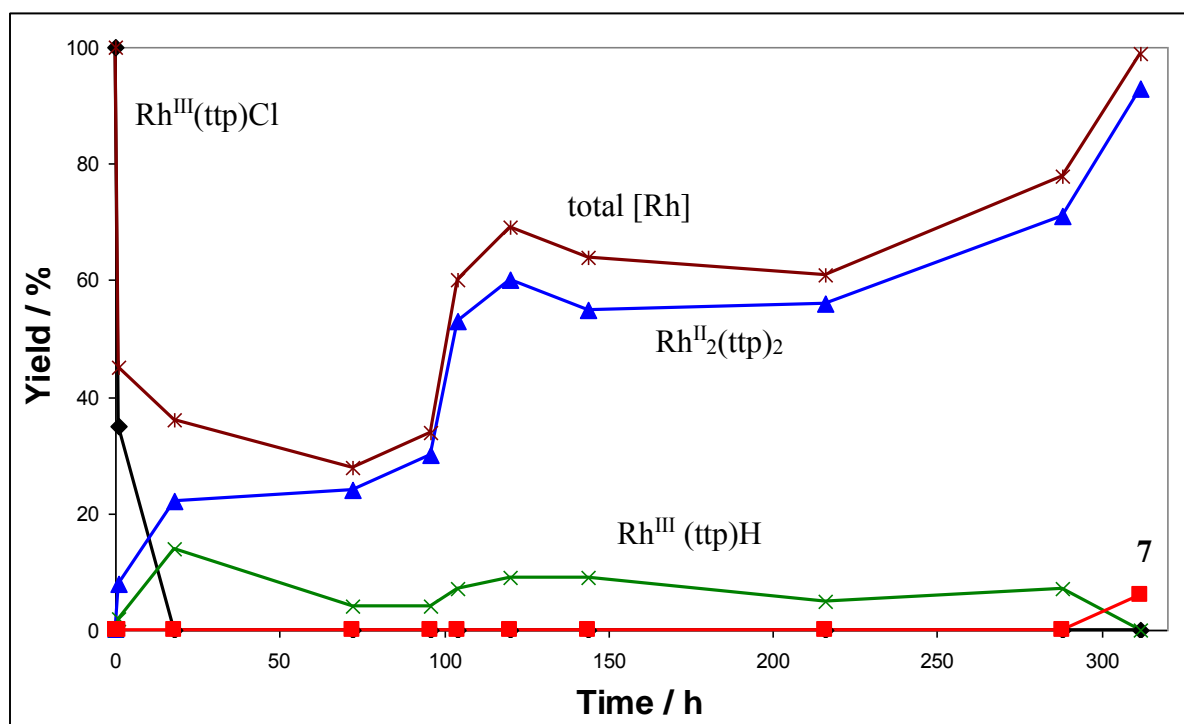
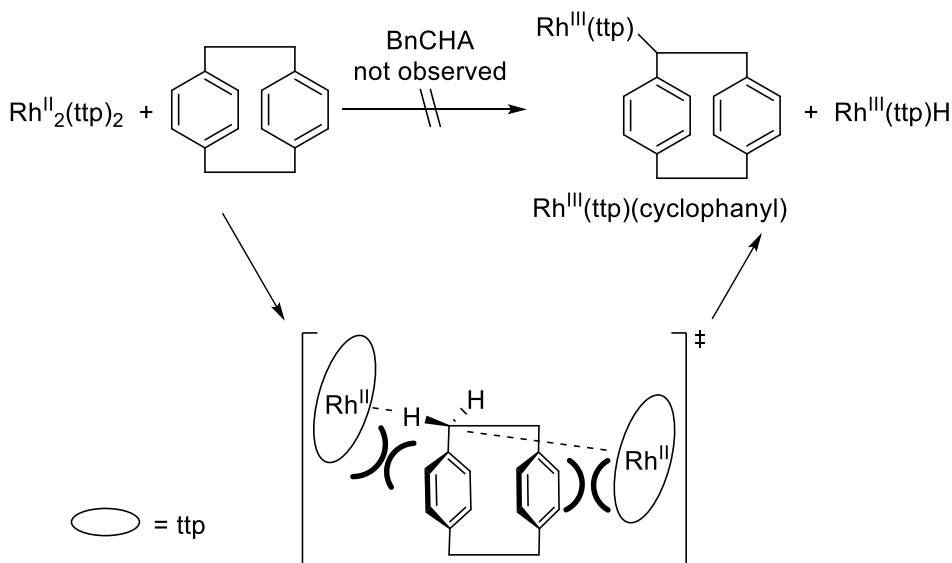


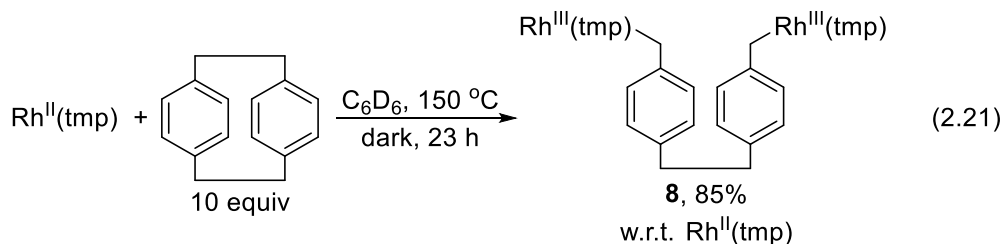
Figure 2.1 Reaction Time Profile of Reaction of Rh^{III}(ttp)Cl with [2.2]Paracyclophane in the presence of KOH and D₂O



Scheme 2.7 Absence of BnCHA of PCP with $\text{Rh}^{\text{II}}_2(\text{ttp})_2$.

2.5.3 ^1H NMR Kinetics of Stoichiometric CCA

In order to gain a deeper understanding on the CCA step of PCP with rhodium(II) porphyrins, the reaction kinetics of stoichiometric CCA of PCP with monomeric $\text{Rh}^{\text{II}}(\text{tmp})$ were monitored by ^1H NMR spectroscopy. $\text{Rh}^{\text{II}}(\text{tmp})$, pioneered by Wayland et al, is an ideal candidate since it exists as a persistent metalloradical.³³ $\text{Rh}^{\text{II}}(\text{tmp})$ reacted smoothly with PCP at 150 °C in C_6D_6 for 23 h to yield 85% of di-rhodium benzyl CCA product **8** without any intermediates observed, establishing the high yielding stoichiometric reaction (eq 2.21).



Attempt to search for any pre-coordination between PCP and $\text{Rh}^{\text{II}}(\text{tmp})$ by ^1H NMR spectroscopy was not fruitful. No change in chemical shift was observed both for $\text{Rh}^{\text{II}}(\text{tmp})$ ($\delta = 18.38$ ppm for pyrrole proton) and PCP ($\delta = 6.33$ ppm for aromatic proton and $\delta = 2.81$

ppm for benzylic proton). The kinetic runs were then conducted with $[\text{Rh}^{\text{II}}(\text{tmp})] = 0.24\text{-}0.48$ mM, $[\text{PCP}] = 4.8\text{-}14.4$ mM in at least 10 fold excess and temperature of 140-170 °C till the disappearance of $\text{Rh}^{\text{II}}(\text{tmp})$ for at least 4 half-lives.

2.5.3.1 Determination of Reaction Orders

The rate equation can be expressed as eq 2.22. Since PCP was employed in excess, eq 2.22 is simplified to eq 2.23 where $k_{\text{obs}} = k[\text{PCP}]^n$.

$$\text{rate} = k[\text{Rh}^{\text{II}}(\text{tmp})]^m[\text{PCP}]^n \quad (2.22)$$

$$= k_{\text{obs}}[\text{Rh}^{\text{II}}(\text{tmp})]^m \quad (2.23)$$

First, the value of m was evaluated with typical conditions $[\text{Rh}^{\text{II}}(\text{tmp})] = 0.24\text{-}0.48$ mM and $[\text{PCP}] = 9.6$ mM at 150 °C. The disappearance of $\text{Rh}^{\text{II}}(\text{tmp})$ fitted best with pseudo second order kinetics (Figure 2.2 and Appendix II for other plots). The kinetic order of $\text{Rh}^{\text{II}}(\text{tmp})$ was measured to be two and hence $m = 2$. The corresponding derivation of the second order integrated rate equation is as follow:

$$\text{rate} = -d[\text{Rh}^{\text{II}}]/dt = k_{\text{obs}}[\text{Rh}^{\text{II}}]^2$$

$$-d[\text{Rh}^{\text{II}}]/[\text{Rh}^{\text{II}}]^2 = k_{\text{obs}}dt$$

Integrate both sides of the equation from time = 0 to time = t.

$$1/[\text{Rh}^{\text{II}}]_t - 1/[\text{Rh}^{\text{II}}]_0 = k_{\text{obs}}t$$

$$1/[\text{Rh}^{\text{II}}]_t = 1/[\text{Rh}^{\text{II}}]_0 + k_{\text{obs}}t$$

Where $1/[\text{Rh}^{\text{II}}]_t$ and t are the y-axis and x-axis, respectively.

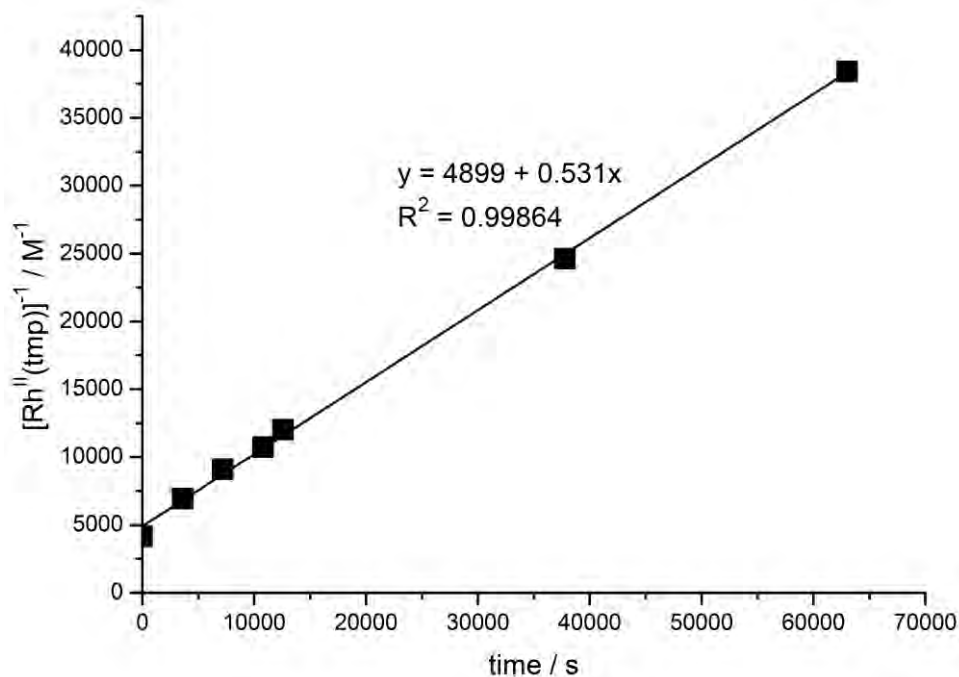


Figure 2.2 A Typical Pseudo 2nd Order Kinetic Plot with $[\text{Rh}^{\text{II}}(\text{tmp})] = 0.24 \text{ mM}$ and $[\text{PCP}] = 9.6 \text{ mM}$ at $150 \text{ }^\circ\text{C}$.

The value of n was then evaluated with typical conditions $[\text{Rh}^{\text{II}}(\text{tmp})] = 0.24 \text{ mM}$ and $[\text{PCP}] = 4.8\text{-}14.4 \text{ mM}$ at $150 \text{ }^\circ\text{C}$. The results also fitted best with pseudo second order kinetic plot (Appendix II). The rate of disappearance of $\text{Rh}^{\text{II}}(\text{tmp})$ increases linearly with increasing $[\text{PCP}]$ from 4.8 mM to 14.4 mM , giving a pseudo first order kinetic plot (Figure 2.3). The kinetic order of PCP was measured to be one and hence $n = 1$.

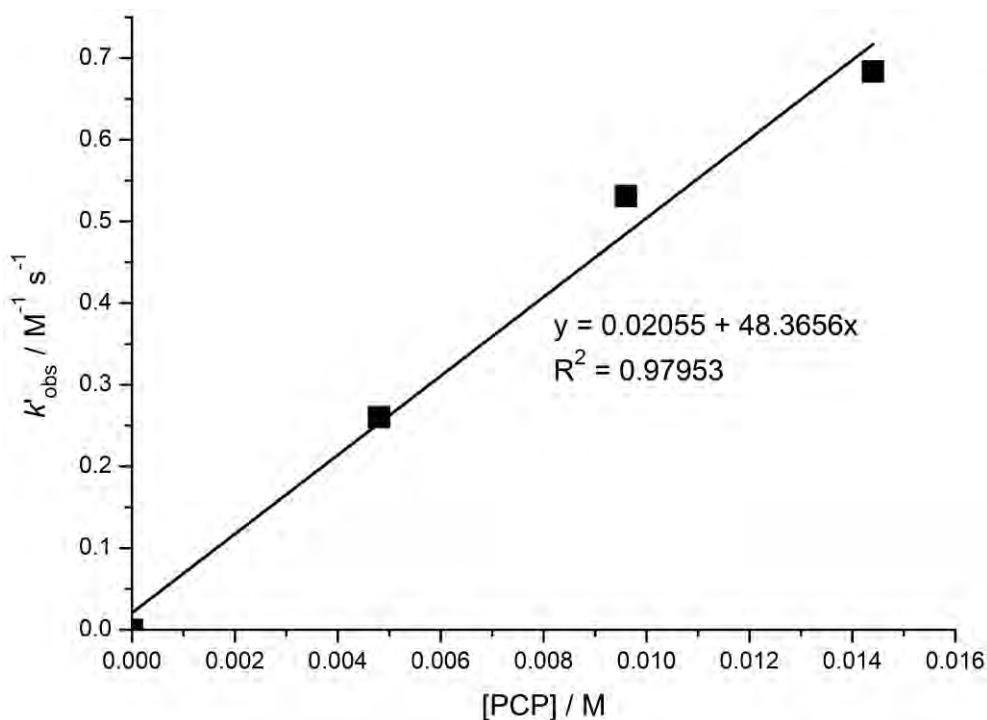


Figure 2.3 Plot of k_{obs} against [PCP] with $[\text{Rh}^{\text{II}}(\text{tmp})] = 0.24 \text{ mM}$ and $[\text{PCP}] = 4.8\text{-}14.4 \text{ mM}$.

Table 2.5 summarizes the k_{obs} measured at various conditions. The kinetic orders of $\text{Rh}^{\text{II}}(\text{tmp})$ and PCP were fitted to be two and one, respectively. The rate equation can be expressed as $\text{rate} = k[\text{Rh}^{\text{II}}(\text{tmp})]^2[\text{PCP}]$.

Table 2.5 k_{obs} Measured at Various Conditions.

entry	$[\text{Rh}^{\text{II}}(\text{tmp})] / \text{mM}$	$[\text{PCP}] / \text{mM}$	$k_{\text{obs}} / \text{M}^{-1} \text{s}^{-1}$
1	0.24	9.6	0.53 ± 0.01
2	0.24	9.6	0.56 ± 0.03
3	0.48	9.6	0.55 ± 0.03
4	0.24	4.8	0.26 ± 0.02
5	0.24	14.4	0.68 ± 0.04

2.5.3.2 Activation Parameters

The rates were measured at typical conditions $[\text{Rh}^{\text{II}}(\text{tmp})] = 0.24 \text{ mM}$ and $[\text{PCP}] = 9.6 \text{ mM}$ at $140 \text{ }^\circ\text{C}$ to $170 \text{ }^\circ\text{C}$. Table 2.6 summarized the temperature dependent rate constants (Appendix II for kinetic plots). These data were used to evaluate the activation parameters.

Table 2.6 k_{obs} Measured at Various Conditions.

entry	$[\text{Rh}^{\text{II}}(\text{tmp})] / \text{mM}$	$[\text{PCP}] / \text{mM}$	$T / ^\circ\text{C}$	$k_{\text{obs}} / \text{M}^{-1} \text{s}^{-1}$	$k / \text{M}^{-2} \text{s}^{-1}$
1	0.24	9.6	140	0.152 ± 0.007	15.8
2	0.24	9.6	150	0.53 ± 0.01	55.3
3	0.48	9.6	160	2.0 ± 0.2	205
4	0.24	4.8	170	3.1 ± 0.3	319

where $k = k_{\text{obs}}/[\text{PCP}]$

The Eyring equation describes the relationships between the temperature dependent rate constants and activation parameters (eq 2.24).³⁴

$$\ln(k/T) = -\Delta H^\ddagger/(RT) + \ln(\kappa/h) + \Delta S^\ddagger/R \quad (2.24)$$

(κ is the Boltzmann constant, R is the ideal gas constant and h is the Planck's constant.)

Therefore, a plot of $\ln(k/T)$ against $1/T$ gives a linear Eyring plot with a slope of $-\Delta H^\ddagger/R$ and a y-intercept of $\ln(\kappa/h) + \Delta S^\ddagger/R$ (Table 2.7 and Figure 2.4).

Table 2.7 $\ln(k_{\text{obs}}/T)$ at Various $1/T$.

entry	$T / ^\circ\text{C}$	$1/T / \text{K}^{-1}$	$k / \text{M}^{-2} \text{s}^{-1}$	$\ln(k/T)$
1	140	0.00242	15.8	-3.262
2	150	0.00236	55.3	-2.036
3	160	0.00231	205	-0.746
4	170	0.00226	319	-0.328

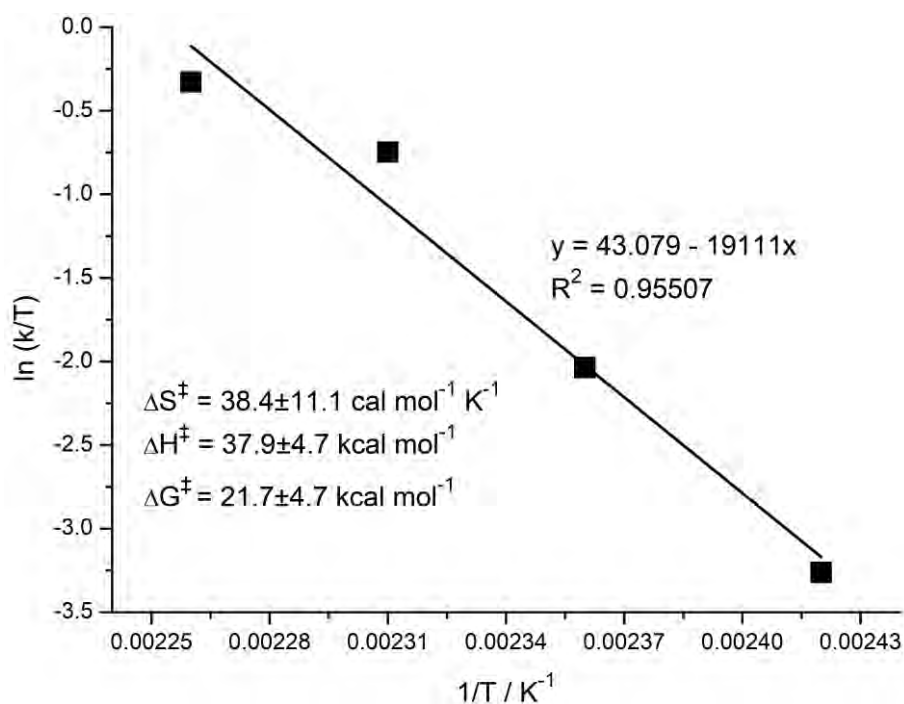


Figure 2.4 Eyring Plot of the CCA of PCP with Rh^{II}(tmp) at 140 °C to 170 °C.

Since $y\text{-intercept} = \ln(\kappa/h) + \Delta S^\ddagger/R$

$$43.079 = \ln(1.3807 \times 10^{-23} / 6.6261 \times 10^{-34}) + \Delta S^\ddagger / 1.9859$$

$$\Delta S^\ddagger = 38.4 \pm 11.1 \text{ cal mol}^{-1} \text{ K}^{-1}$$

And $\text{slope} = \Delta H^\ddagger/R$

$$-19111 = \Delta H^\ddagger / 1.9859$$

$$\Delta H^\ddagger = 37.9 \pm 4.7 \text{ kcal mol}^{-1}$$

Then $\Delta G^\ddagger = \Delta H^\ddagger - T\Delta S^\ddagger$

$$\Delta G^\ddagger = 21.7 \pm 4.7 \text{ kcal mol}^{-1} (150 \text{ }^\circ\text{C})$$

Roth has reported the computed activation parameters of PCP thermolysis at 188 °C (eq 2.25).³⁵ These values were compared with the current experimental results in Table 2.8. The activation enthalpies were very similar, agreeing the cleavage of benzylic C-C bond. The activation entropy ΔS^\ddagger of $38.4 \pm 11.1 \text{ cal mol}^{-1} \text{ K}^{-1}$ is much greater than the computed value of

$2.7 \pm 1.1 \text{ cal mol}^{-1} \text{ K}^{-1}$.³⁵ This positive value suggests a dissociative nature of the transition state, however, does not simply resembles a simple thermal PCP ring-opening situation.

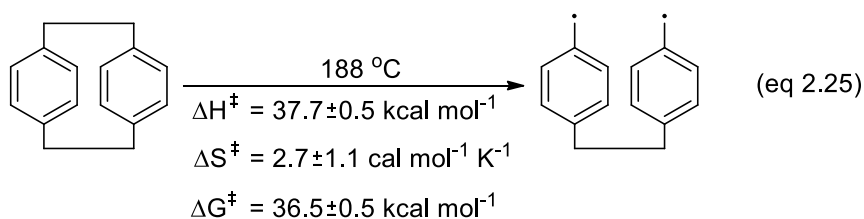


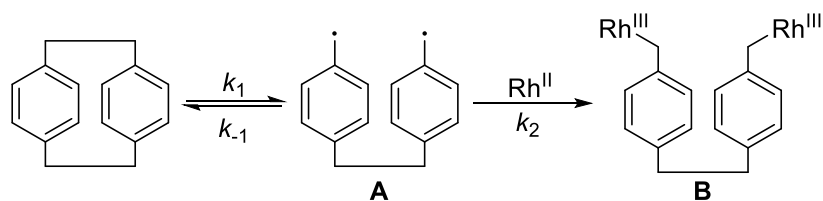
Table 2.8 Comparison of Activation Parameters

	reaction 2.21 (this work)	reaction 2.25
$\Delta H^\ddagger / \text{kcal mol}^{-1}$	37.9 ± 4.7	37.7 ± 0.5
$\Delta S^\ddagger / \text{cal mol}^{-1} \text{ K}^{-1}$	38.4 ± 11.1	2.7 ± 1.1
$\Delta G^\ddagger / \text{kcal mol}^{-1}$	$21.7 \pm 4.7 (150 \text{ }^\circ\text{C})$	$36.5 \pm 0.5 (188 \text{ }^\circ\text{C})$

2.5.4 Mechanistic Implications

2.5.4.1 $\text{Rh}^{\text{II}}(\text{tmp})$ as a Trap

$\text{Rh}^{\text{II}}(\text{tmp})$ can be a reagent for CCA or a radical trap. If it is a trap, the kinetic scheme would follow the one illustrated in Scheme 2.8, such that the consumption of PCP, i.e. the reaction rate, is independent of $[\text{Rh}^{\text{II}}(\text{tmp})]$. The current experimental results show that the reaction rates are $[\text{Rh}^{\text{II}}(\text{tmp})]$ dependent. Saturation kinetics is unable to determine since data points are limited at this moment.



with steady state approximation on diradical intermediate **A**

$$d[\mathbf{A}]/dt = k_1[\text{PCP}] - k_{-1}[\mathbf{A}] - k_2[\text{Rh}^{\text{II}}]^2[\mathbf{A}] = 0$$

$$[\mathbf{A}] = k_1[\text{PCP}]/(k_{-1} + k_2[\text{Rh}^{\text{II}}]^2)$$

$$\begin{aligned} -d[\text{PCP}]/dt = d[\mathbf{B}]/dt &= k_2[\text{Rh}^{\text{II}}]^2[\mathbf{A}] \\ &= k_1k_2[\text{Rh}^{\text{II}}]^2[\text{PCP}]/(k_{-1} + k_2[\text{Rh}^{\text{II}}]^2) \end{aligned}$$

case 1: $k_2[\text{Rh}^{\text{II}}]^2 \gg k_{-1}$, i.e. Rh^{II} is a fast trap

$$\text{then } -d[\text{PCP}]/dt = k_1[\text{PCP}]$$

case 2: $k_2[\text{Rh}^{\text{II}}]^2 \ll k_{-1}$, i.e. Rh^{II} is a slow trap

$$\text{then } -d[\text{PCP}]/dt = (k_1k_2/k_{-1})[\text{Rh}^{\text{II}}]^2[\text{PCP}]$$

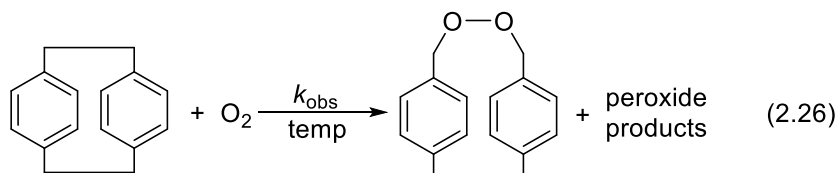
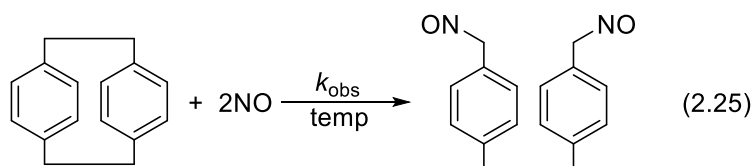
case 3: $k_2[\text{Rh}^{\text{II}}]^2 \sim k_{-1}$

$$\begin{aligned} \text{then } -d[\text{PCP}]/dt &= k_1k_2[\text{Rh}^{\text{II}}]^2[\text{PCP}]/(2k_2[\text{Rh}^{\text{II}}]^2) \\ &= (k_1/2)[\text{PCP}] \end{aligned}$$

Scheme 2.8 Kinetic Scheme of Trapping by Rh^{II} .

The kinetics of PCP thermolysis in the presence of NO or O_2 as radical trap have been investigated by Roth (Table 2.8, eqs. 2.25 and 2.26).³⁵ The trapping rate constants are in the range of 10^{-6} to 10^{-3} s^{-1} with saturation rate constants at about 10^{-3} s^{-1} . In contrast, the rate constants of CCA of PCP with $\text{Rh}^{\text{II}}(\text{tmp})$ are in the range of 10 to $10^2 \text{ M}^{-2} \text{ s}^{-1}$, which is greater than the saturation rate constants by at least four orders of magnitude. The superior performance of $\text{Rh}^{\text{II}}(\text{tmp})$ suggests that it is unlikely a radical trap.

Table 2.8 Trapping Rate Constants of PCP with NO and O₂.

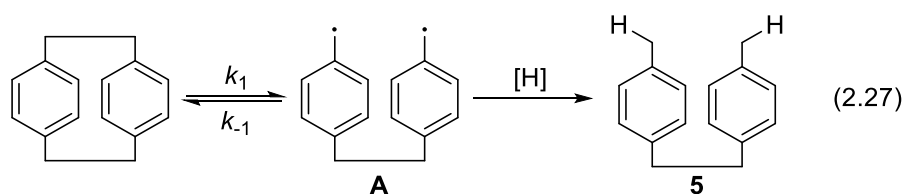


$$\text{rate} = k_{\text{obs}}[\text{PCP}]$$

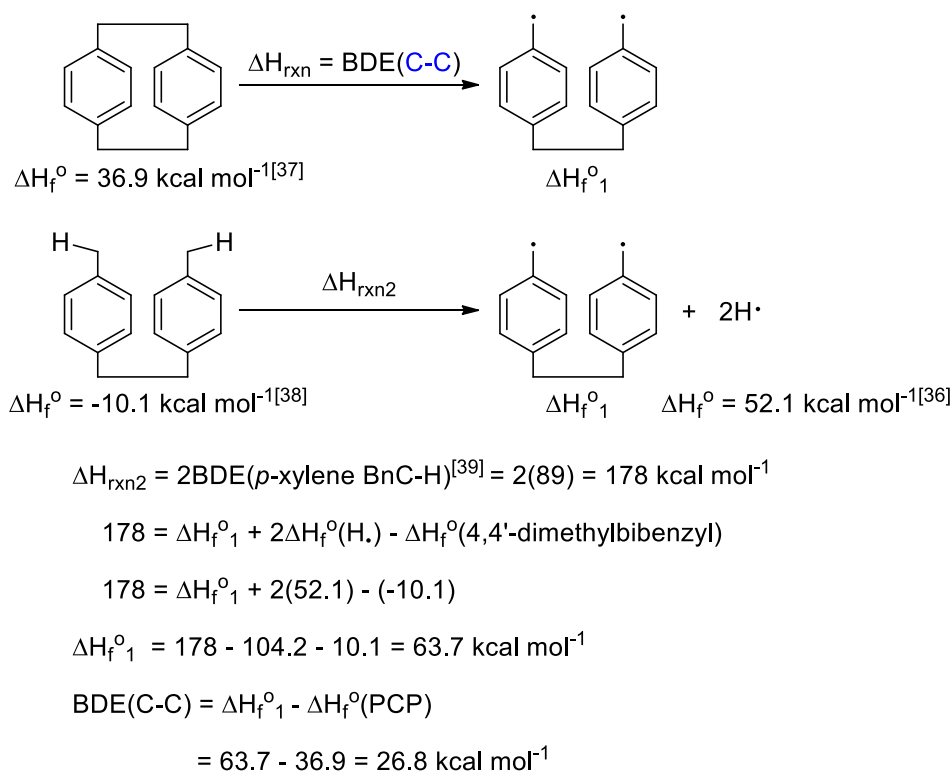
entry	trap (pressure)	temperature range / °C	k_{obs} range / s ⁻¹
1	NO (51.5 to 448.31 mbar)	168.90 to 208.40	5.43x10 ⁻⁶ to 2.34x10 ⁻³
2	O ₂ (300.5 to 931.1 mbar)	178.90 to 218.29	2.16x10 ⁻⁵ to 5.57x10 ⁻⁴

2.5.4.2 PCP Homolysis Rate at 200 °C

Even though Rh^{II}(tmp) is not a trap, the benzylic C-C bond of PCP may undergo homolysis with sufficient rate upon heating when the bond is weak. In the presence of H atom donor, e.g. Rh^{III}(por)H, the bis-benzylic radical intermediate **A** will be trapped to yield the hydrogenation product **5** (eq 2.27).



The benzylic C-C BDE of PCP is estimated to be 26.8 kcal mol⁻¹ based on the method employed by Jones, which the C-C BDE of biphenylene was estimated (Scheme 2.7).³⁶



Scheme 2.7 Estimation of Benzylic C-C BDE of PCP.

Assume the ΔG^\ddagger of homolysis in eq 2.27 equals the benzylic C-C BDE of PCP, i.e. $26.8 \text{ kcal mol}^{-1}$, it yields $k_1 = 4.1 \text{ s}^{-1}$ at $200 \text{ }^\circ\text{C}$ calculated from the eq 2.28. This is equivalent to a fast half-life of 0.17 s . In other words, the reaction in eq 2.27 can reach completion in about 1 s in the presence of sufficient H atom donor as trap.

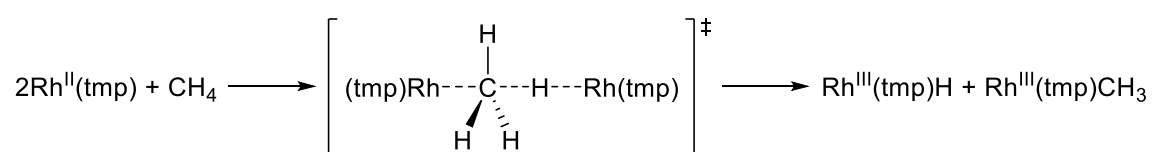
$$\ln k = \ln(k_B T/h) - (\Delta G^\ddagger/RT) \quad (2.28)$$

(k_B is the Boltzman constant, h is the Plank constant, R is the ideal gas constant)

The present experimental results on catalytic PCP hydrogenation contradict with this fast homolysis rate. This probably implies (1) the intramolecular radical recombination of **A** is very fast such that trapping is impossible; or (2) H atom donor is very limited in the reaction and most **A** is converted back to PCP.

2.5.4.3 Possible CCA Transition State

The second order dependence of $\text{Rh}^{\text{II}}(\text{tmp})$ and first order dependence of PCP suggest a termolecular CCA process which have been proposed by Wayland for the $\text{Rh}^{\text{II}}(\text{tmp})$ bi-metalloradical CHA process (Scheme 2.8).³² The simultaneous breaking of one bond and formation of two bonds provide a synergistic effect to lower down the activation barrier. However, with the best understanding at this stage, we are unclear about the dissociative nature of the transition state based on the positive ΔS^\ddagger .



Scheme 2.8 Termolecular Reaction in CHA of CH_4 with $\text{Rh}^{\text{II}}(\text{tmp})$.

2.5.4.4 Computational Study

To better understand the interaction between $\text{Rh}^{\text{II}}(\text{tmp})$ and PCP in the CCA process, transition state geometry analysis by Spartan '10 software at PM3 level has been performed, as limited by our theoretical capability. The *meso*-aryl groups omitted rhodium porphyrins were used to shorten the calculation steps without over simplify the system. The transition state geometry was optimized under the following two constrains: (1) the $\text{Rh}_1\text{-C}_1$ and $\text{Rh}_2\text{-C}_2$ distance does not exceed 3.100 Å, which is about 1.5 times of the $\text{Rh-C}(\text{benzylic})$ bond length in $\text{Rh}^{\text{III}}(\text{ttp})\text{Bn}(p\text{-}^t\text{Bu})$ (2.085 Å) and $\text{Rh}^{\text{III}}(\text{ttp})\text{Bn}(p\text{-F})$ (2.064 Å);⁴⁰ (2) the $\text{C}_1\text{-C}_2$ distance does not exceed 2.350 Å, which is 1.5 times of a intact benzylic C-C bond length in PCP.

From the optimized transition state geometry shown in Figure 2.5, the $\text{C}_1\text{-C}_2$ bond is lengthened from 1.556 Å ($\text{C}_3\text{-C}_4$) to 1.793 Å. Rh_1 interacts with C_1 at an angle of 33° to the $\text{C}_1\text{-C}_2$ bond and a distance of 2.349 Å away. Rh_2 interacts with C_2 at an angle of 49° to the $\text{C}_1\text{-C}_2$ bond and a distance of 2.239 Å away. Distortion of rhodium porphyrin from planarity

is observed, probably due to steric congestion. A zig-zag Rh-C-C-Rh interaction is observed (Figure 2.6).

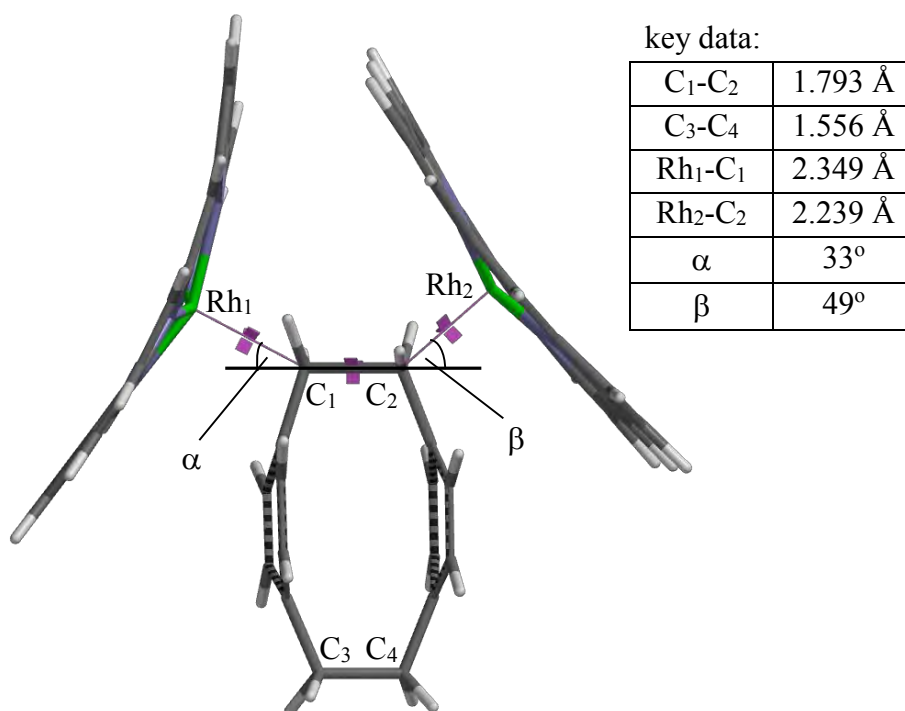


Figure 2.5 Computed Transition State Geometry of CCA of PCP with Rh(por) (side view).

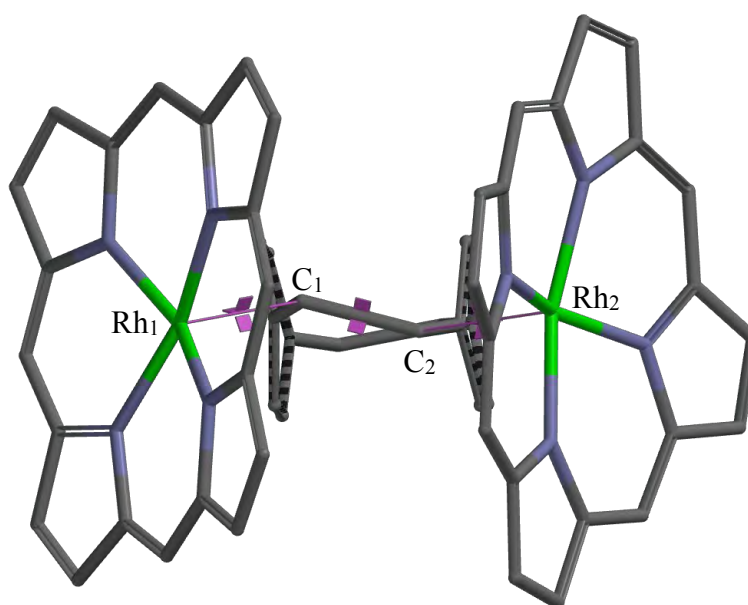
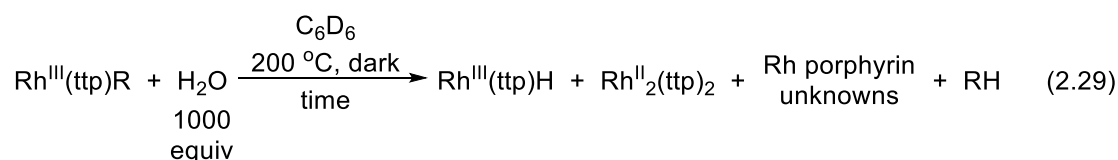


Figure 2.6 Computed Transition State Geometry of CCA of PCP with Rh(por) (top view, hydrogen omitted for clarity).

2.5.5 Hydrolysis of Rh^{III}(ttp)R

To further confirm that hydrolysis of Rh^{III}(ttp)R indeed releases alkane from the rhodium porphyrin, Rh^{III}(ttp)R (R = Me, Bn and ⁱPr) was subjected to hydrolysis study. The 1° alkyls Rh^{III}(ttp)Me and Rh^{III}(ttp)Bn were hydrolyzed to give good yields of CH₄ and toluene, respectively (Table 2.9, eq 2.29, entries 1 and 2). The hydrolysis of Rh^{III}(ttp)Bn serves as a mimic of the hydrolysis of CCA product di-rhodium benzyl **7** to give 4,4'-dimethylbibenzyl **5**. The 2° alkyl Rh^{III}(ttp)ⁱPr underwent competitive hydrolysis and β-H elimination to give a mixture of propane and propene (Table 2.9, eq 2.29, entry 3).

Table 2.9 Hydrolysis of Rh^{III}(ttp)R.

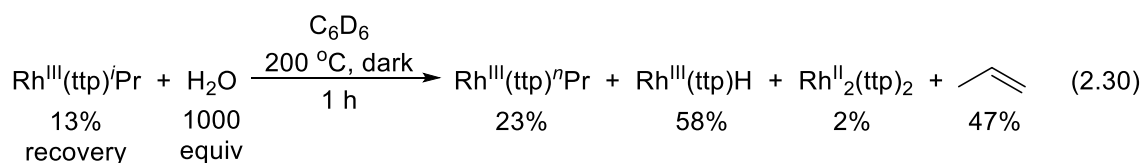


entry	R	time	yield / %					
			Rh ^{III} (ttp)R	Rh ^{III} (ttp)H	Rh ^{II} ₂ (ttp) ₂	Rh porphyrin unknowns	Total [Rh]	RH
1 ^a	Me	1 d	13	6	11	20	50	87
2	Bn	3.5 d	2	15	0	41	58	66
3	ⁱ Pr	50 h	2	36	2	20	60	45 ^b

^a conducted at 150 °C, Fung, H. S. *Unpublished Results*, CUHK, 2011

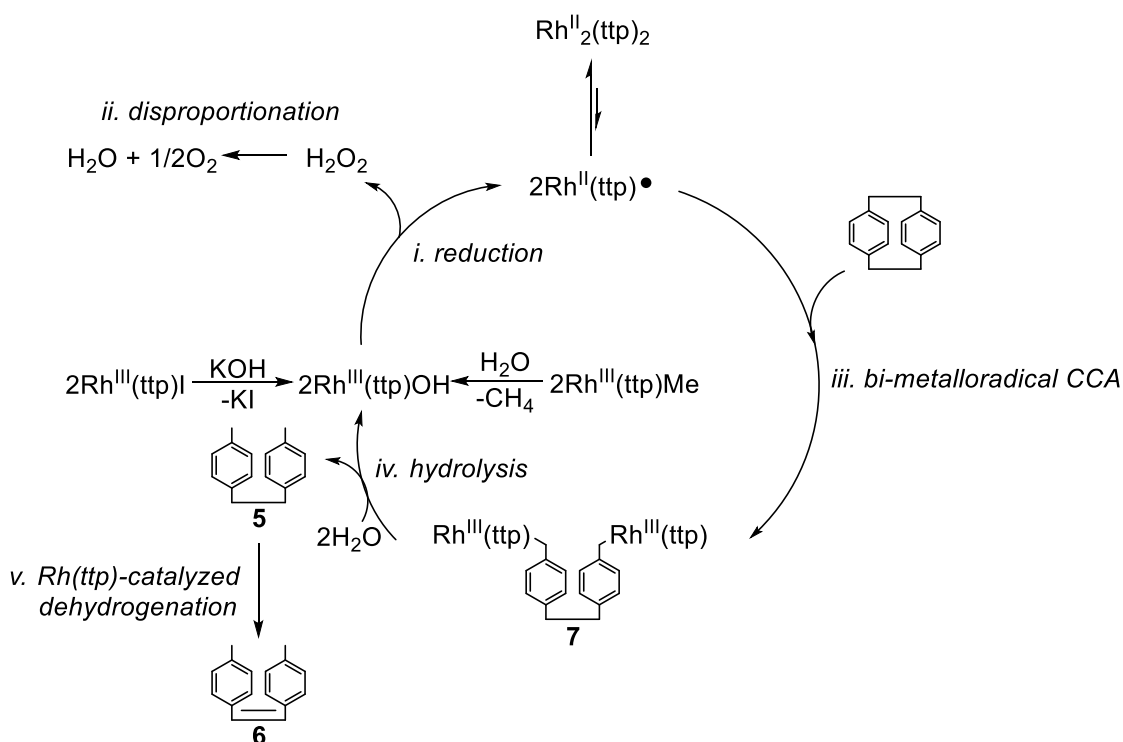
^b 35% yield of propene was formed

During the hydrolysis of Rh^{III}(ttp)ⁱPr, rapid alkyl 1,2-rearrangement of Rh^{III}(ttp)ⁱPr was observed and attained equilibrium after 1 h to give a mixture of Rh^{III}(ttp)ⁱPr, Rh^{III}(ttp)ⁿPr and Rh^{III}(ttp)H in 13%, 23% and 58% yields, respectively, together with 47% yield of propene (eq 2.30).²¹ The secondary : primary ratio of 0.57 agrees with the previous reported ratio of 0.70 measured at 120 °C.^{21b} Rh^{III}(ttp)H is the dominant product since elimination is favored by high temperature.



2.6 Proposed Mechanism

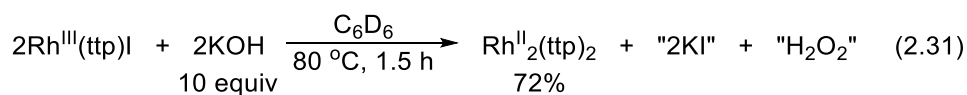
Based on the previous studies and current findings, Scheme 2.9 illustrates the proposed catalytic cycle for the catalytic PCP hydrogenation using H₂O.



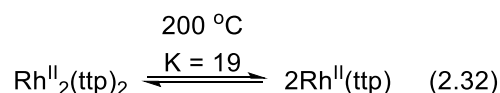
Scheme 2.9 Proposed Catalytic Cycle for the Catalytic Hydrogenation of PCP using H₂O.

Rh^{III}(ttp)I pre-catalyst undergoes rapid ligand substitution with KOH to first give Rh^{III}(ttp)OH.²⁰ The hydroxide then donates one electron to the ligated Rh^{III} metal center and reduces it to Rh^{II}, with itself oxidized to hydroxyl radical (step i).⁴¹ Electron poor porphyrin ligand may further favor this reduction process to Rh(II). Hydroxyl radicals combine to form H₂O₂. In the presence of OH⁻, I⁻ or transition metals, they catalyze the disproportionation of

H₂O₂ to H₂O and O₂ (step ii).⁴² Previous study by Chan group shows that Rh^{III}(ttp)I reacted with 10 equiv of KOH at 80 °C in C₆D₆ for 1.5 h to yield 72% of Rh^{II}₂(ttp)₂ (eq 2.31).²⁰ Alternatively, Rh^{III}(ttp)Me pre-catalyst is hydrolyzed by H₂O to give CH₄ and Rh^{III}(ttp)OH, which is converted to Rh^{II}₂(ttp)₂ accordingly.⁶



Under thermal conditions, Rh^{II}₂(ttp)₂ dissociates to form Rh^{II}(ttp) with equilibrium constant estimated to be 19 at 200 °C (eq 2.32 and Scheme 2.10).⁴³ Rh^{II}(ttp) cleaves the benzylic carbon-carbon bond of PCP, in a termolecular manner similar to Rh^{II}(tmp), to yield the di-rhodium benzyl **7** (step iii).



$$\Delta G = \Delta H - T\Delta S$$

$$\Delta H = \text{Rh-Rh BDE in Rh}^{\text{II}}_2(\text{txp})_2 = 12 \text{ kcal mol}^{-1}$$

$$\text{assume } S = S(\text{H}_2) = 31.2 \text{ cal mol}^{-1} \text{ K}^{-1}$$

$$\Delta G = 12 - (473)(0.0312) = -2.8 \text{ kcal mol}^{-1}$$

$$\Delta G = -RT\ln K$$

$$-2.8 = -(1.9872 \times 10^{-3})(473)\ln K$$

$$K = 19$$

Scheme 2.10 Equilibrium Estimation for Rh^{II}₂(ttp)₂.

Subsequently, hydrolysis of **7** produces the hydrogenation product 4,4'-dimethylbibenzyl **5** and regenerates Rh^{III}(ttp)OH to complete the catalytic cycle (step iv), which is supported by the hydrolysis of Rh^{III}(ttp)Bn to give toluene. Rhodium porphyrin catalyzes dehydrogenation of **5** occurs to give **6** (step v).

2.7 Conclusions

We have discovered the rhodium porphyrin catalyzed carbon-carbon σ -bond hydrogenation of PCP using H₂O as the convenient hydrogen source. This demonstrates that H₂O is a transfer hydrogenating agent. Kinetic studies suggest a Rh^{II}(tmp) bi-metalloradical CCA process. Hydrogenation via hydrolysis of rhodium porphyrin alkyls is a general process to produce hydrocarbons.

References

1. (a) Tse, M. K.; Chan, K. S. *J. Chem. Soc., Dalton Trans.* **2001**, 510-511. (b) Chan, K. S.; Li, X. Z.; Dzik, W. I.; de Bruin, B. *J. Am. Chem. Soc.* **2008**, *130*, 2051-2061. (c) Chan, K. S.; Li, X. Z.; Lee, S. Y. *Organometallics* **2010**, *29*, 2850-2856.
2. (a) Chan, K. S.; Li, X. Z.; Fung, C. W.; Zhang, L. *Organometallics* **2007**, *26*, 20-21. (b) Chan, K. S.; Li, X. Z.; Zhang, L.; Fung, C. W. *Organometallics* **2007**, *26*, 2679-2687.
3. Zhang, L.; Chan, K. S. *J. Organomet. Chem.* **2006**, *691*, 3782-3787.
4. Zhang, L.; Chan, K. S. *J. Organomet. Chem.* **2007**, *692*, 2021-2027.
5. Chan, Y. W.; Chan, K. S. *J. Am. Chem. Soc.* **2010**, *132*, 6920-6922.
6. Fung, H. S.; Li, B. Z.; Chan, K. S. *Organometallics* **2012**, *31*, 570-579.
7. Alder, A. D.; Longo, F. R.; Finarelli, J. D.; Goldmacher, J.; Assour, J.; Korsakoff, L. *J. Org. Chem.* **1967**, *32*, 476-477.
8. Wagner, R. W.; Lawrence, D. S.; Lindsey, J. S. *Tetrahedron Lett.* **1987**, *28*, 3069-3070.
9. Adler, A. D.; Longo, F. R.; Kampas, F.; Kim, J. *J. Inorg. Nucl. Chem.* **1970**, *32*, 2445-2448.
10. Spyroulias, G. A.; Despotopoulos, A. P.; Raptopoulou, C. P.; Terzis, A.; de Montauzon, D.; Poilblanc, R.; Coutsolelos, A. G. *Inorg. Chem.* **2002**, *41*, 2648-2659.
11. (a) Zhou, Z.; Li, Q.; Mak, T. C. W.; Chan, K. S. *Inorg. Chim. Acta.* **1998**, *270*, 551-554. (b) Zhou, X.; Wang, R. J.; Xue, F.; Mak, T. C. W.; Chan, K. S. *J. Organomet. Chem.* **1999**, *580*, 22-25.
12. Wayland, B. B.; Van Voorhees, S. L.; Wilker, C. *Inorg. Chem.* **1986**, *25*, 4039-4042.
13. (a) Chan, K. S.; Mak, K. W.; Tse, M. K.; Yeung, S. K.; Li, B. Z.; Chan, Y. W. *J. Organomet. Chem.* **2008**, *693*, 399-407. (b) Fung, H. S.; Chan, Y. W.; Cheung, C. W.; Choi, K. S.; Lee, S. Y.; Qian, Y. Y.; Chan, K. S. *Organometallics* **2009**, *28*, 3981-3989.
14. Chan, K. S.; Chiu, P. F.; Choi, K. S. *Organometallics* **2007**, *26*, 1117-1119.

15. Wayland, B. B.; Sherry, A. E.; Poszmik, G.; Bunn, A. G.; *J. Am. Chem. Soc.* **1992**, *114*, 1673-1681.
16. Hradil, J.; Švec, F. *Polym. Bull.* **1983**, *10*, 14-20.
17. For the solubility of H₂O in C₆H₆ from 0 to 250 °C, see: Góral, M.; Wiśniewska-Gocłowska, B.; Mączyński, A. *J. Phys. Chem. Ref. Data* **2004**, *33*, 1159-1188.
18. Choi, K. S. *Ph.D. Thesis* **2011**, CUHK.
19. de Meijere, A. Kozhushkov, S. I.; Rauch, K.; Schill, H.; Verevkin, S. P.; Kümmerlin, M.; Beckhaus, H.-D.; Rüchardt, C.; Yufit, D. S. *J. Am. Chem. Soc.* **2003**, *125*, 15110-15113.
20. Choi, K. S.; Lai, T. H.; Lee, S. Y.; Chan, K. S. *Organometallics* **2011**, *30*, 2633-2635.
21. The β -H elimination of Rh^{III}(por)R has been demonstrated in the alkyl 1,2-rearrangement.
(a) Mak, K. W.; Chan, K. S. *J. Am. Chem. Soc.* **1998**, *120*, 9686-9687. (b) Mak, K. W.; Xue, F.; Mak, T. C. W.; Chan, K. S. *J. Chem. Soc., Dalton Trans.* **1999**, 3333-3334.
22. Ogoshi, H.; Setsune, J.; Yoshida, Z. *J. Am. Chem. Soc.* **1977**, *99*, 3869-3870.
23. Martinho Simões, J. A.; Beauchamp, J. L. *Chem. Rev.* **1990**, *90*, 629-688.
24. Gruden, M.; Grubišić, S.; Coutsolelos, A. G.; Niketić, S. R. *J. Mol. Struct.* **2001**, *595*, 209-224.
25. Aldridge, S.; Warwick, P.; Evans, N.; Vines, S. *Chemosphere* **2007**, *66*, 672-676.
26. Au, C. C.; Lai, T. H.; Chan, K. S. *J. Organomet. Chem.* **2010**, *695*, 1370-1374.
27. Sarkar, S.; Li, S.; Wayland, B. B. *J. Am. Chem. Soc.* **2010**, *132*, 13569-13571.
28. D₂O has been reported to be slightly less soluble than H₂O in C₆H₆ at milder temperatures, see: Moule, D. C. *Can. J. Chem.* **1966**, *44*, 3009-3015.
29. Del Rossi, K. J.; Wayland, B. B. *J. Am. Chem. Soc.* **1985**, *107*, 7941-7944.
30. Gozin, M.; Welsman, A.; Ben-David, Y.; Milstein, D. *Nature* **1993**, *364*, 699-701.
31. Perthuisot, C.; Jones, W. D. *J. Am. Chem. Soc.* **1994**, *116*, 3647-3648.

32. For examples of four-centered transition state, see: (a) Sherry, A. E.; Wayland, B. B. *J. Am. Chem. Soc.* **1990**, *112*, 1259-1261. (b) Wayland, B. B.; Ba, S.; Sherry, A. E. *J. Am. Chem. Soc.* **1991**, *113*, 5305-5311. (c) Wayland, B. B.; Ba, S.; Sherry, A. E. *Inorg. Chem.* **1992**, *31*, 148-150. (d) Cui, W.; Zhang, X. P.; Wayland, B. B. *J. Am. Chem. Soc.* **2003**, *125*, 4994-4995. (e) Cui, W.; Wayland, B. B. *J. Am. Chem. Soc.* **2004**, *126*, 8266-8274.
33. Sherry, A. E.; Wayland, B. B. *J. Am. Chem. Soc.* **1989**, *111*, 5010-5012.
34. Espenson, J. *Chemical Kinetics and Reaction Mechanisms*, 2nd Ed., McGraw-Hill Companies, Inc., USA, 2002.
35. Roth, W. R.; Hopf, H.; de Meijere, A.; Hunold, F.; Börner, S.; Neumann, M.; Wasser, T.; Szurowski, J.; Mlynek, C. *Liebigs Ann.* **1996**, 2141-2154.
36. Perthuisot, C. P.; Edelbach, B. L.; Zubris, D. L.; Simhai, N.; Iverson, C. N.; Müller, C.; Satoh, T.; Jones, W. D. *J. Mol. Catal. A: Chem.*, **2002**, *189*, 157-168.
37. Boyd, R. H. *Tetrahedron*, **1966**, *22*, 119-122.
38. NIST Chemistry Webbook, <http://webbook.nist.gov/cgi/cbook.cgi?Name=4%2C4%27-dimethylbibenzyl&Units=SI&cTG=on&cTC=on&cTP=on&cTR=on&cIE=on&cIC=on>
39. Luo, Y. R. *Comprehensive Handbook of Chemical Bond Energies*, CRC Press, Boca Raton, FL, 2007.
40. Choi, K. S.; Chiu, P. F.; Chan, K. S. *Organometallics* **2010**, *29*, 624-629.
41. Sawyer, D. T.; Roberts, J. L. Jr. *Acc. Chem. Res.* **1988**, *21*, 469-476.
42. (a) Harned, H. S. *J. Am. Chem. Soc.* **1918**, *40*, 1461-1481. (b) Walling, C. *Acc. Chem. Res.* **1975**, *8*, 125-131. (c) Kumar, A.; McCluskey, R. J. *Ind. Eng. Chem. Res.* **1987**, *26*, 1323-1329. (d) Kato, S.; Ueno, T.; Fukuzumi, S.; Watanabe, Y. *J. Bio. Chem.* **2004**, *279*, 52376-52381. (e) Zhang, J.; Li, S.; Fu, X.; Wayland, B. B. *Dalton Trans.* **2009**, *19*, 3661-3663.

43. Estimated from the Rh-Rh BDE of 12 kcal mol⁻¹ in sterically similar Rh^{II}₂(txp)₂. Wayland, B. B.; Ba, S.; Sherry, A. E. *J. Am. Chem. Soc.* **1991**, 113, 5305-5311.

Experimental Section

General Procedures

Unless otherwise specified, all reagents were purchased from commercial suppliers and directly used without further purification. [2.2]paracyclophane was further tested by melting point (m.p. = 288.6-289.4 °C, lit. = 285-287.2 °C).¹ Hexane for chromatography was distilled from anhydrous CaCl₂. Benzene-*d*₆ was distilled from sodium under N₂, degassed with three freeze-pump-thaw cycles and stored in a Teflon screw head stoppered flask. Benzonitrile was distilled from anhydrous P₂O₅. Thin layer chromatography was performed on pre-coated silica gel 60 F₂₅₄ plates. Silica gel (Merck, 70-230 mesh) was used for column chromatography under air.

Melting points were recorded on an MPA100 Automated Melting Point System. ¹H NMR spectra were recorded on a Bruker AV-400 MHz at 400 MHz. Chemical shifts were referenced internally to the residual solvent proton resonance in C₆D₆ (δ = 7.15 ppm), CDCl₃ (δ = 7.26 ppm) or with tetramethylsilane (δ = 0.00 ppm) as the internal standard. Chemical shifts (δ) are reported in parts per million (ppm). Coupling constants (*J*) are reported in hertz (Hz). High resolution mass spectra (HRMS) were recorded on a Thermofinnigan MAT 95 XL mass spectrometer. Fast atom bombardment was performed with 3-nitrobenzyl alcohol (NBA) as the matrix.

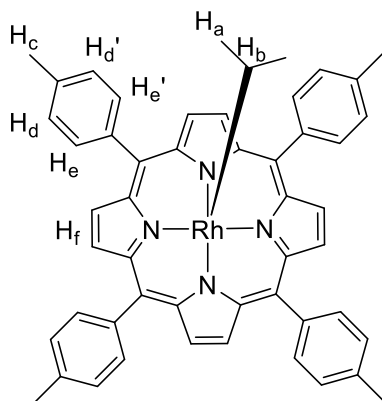
All reactions in 0.5 mL benzene-*d*₆ were carried out in a flame-sealed NMR tube in vacuum with the reaction mixture degassed with three freeze(77 K)-pump(0.005 mmHg)-thaw cycles, then heated in oven in dark and wrapped with aluminum foil to protect from exposure to room light before ¹H NMR measurements. The NMR yields were with benzene residue as the internal standard. Aqueous stock solution of KOH was prepared separately, transferred to the reaction vessel and dried under vacuum at r.t. to obtain anhydrous starting materials. Benzene stock solutions of Rh^{III}(ttp)X (X = Cl, I, Me, Bn and ^{*i*}Pr) were prepared

separately, transferred to the reaction vessel and dried under vacuum at r.t. to obtain anhydrous starting materials. Benzene-*d*₆ stock solution of [2.2]paracyclophane was prepared separately and transferred to the reaction vessel.

All free base porphyrins,² Rh^{III}(ttp)X (X = Cl, I, Me, Bn, *i*Pr),^{3,4} Rh^{III}(tap)X (X = Cl and Me),⁴ Rh^{III}(t₄-CF₃pp)X (X = Cl and Me),⁴ Rh^{III}(tmp)X (X = Cl and Me),^{3,5} Rh^{II}(tmp)⁵ were prepared according to the literature procedures.

Rh^{III}(ttp)*i*Pr has been reported earlier but spectroscopic characterization was not provided.⁶ Its ¹H and ¹³C{¹H} NMR spectra are now attached.

¹H NMR (C₆D₆, 400 MHz) δ -4.00 (d, ³J_{H-H} = 6.2 Hz, 6 H, H_a), -3.89 (br, 1 H, H_b), 2.41 (s, 12 H, H_c), 7.27 (d, ³J_{H-H} = 7.6 Hz, 4 H, H_d), 7.34 (d, ³J_{H-H} = 7.5 Hz, 4 H, H_{d'}), 8.07 (d, ³J_{H-H} = 7.5 Hz, 4 H, H_e), 8.19 (d, ³J_{H-H} = 7.5 Hz, 4 H, H_{e'}), 8.97 (s, 8 H, H_f). ¹³C{¹H} NMR (CDCl₃, 175 MHz) δ 21.7, 22.6, 27.7 (d, ¹J_{Rh-C} = 27.5 Hz), 122.8, 127.4, 127.5, 131.5, 133.7, 134.2, 137.2, 139.5, 143.4.

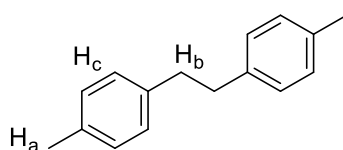


Experimental Procedures

Catalytic PCP Hydrogenation with H₂O Catalyzed by 10 mol% of Rh^{III}(ttp)X.

With Rh^{III}(ttp)I and KOH (1 equiv). Rh^{III}(ttp)I (0.43 mg, 0.00048 mmol), KOH (0.27 mg, 0.0048 mmol) and H₂O (8.6 μL, 0.48 mmol) were added into benzene-*d*₆ stock solution (500 μL) of [2.2]paracyclophane (1.0 mg, 0.0048 mmol) in a NMR tube. The orange mixture was

degassed for three freeze-pump-thaw cycles and the NMR tube was flame-sealed under vacuum. It was heated at 200 °C in the dark for 25 h. It was monitored with ^1H NMR spectroscopy at particular time intervals and the NMR yields were taken. 4,4'-dimethylbibenzyl **5** was isolated by column chromatography on silica gel eluting with hexane. $R_f = 0.31$ (hexane). m.p. = 81.8-83.1 °C, lit. = 81-82 °C.⁷ ^1H NMR (CDCl_3 , 400 MHz) δ 2.32 (s, 6 H, H_a), 2.86 (s, 4 H, H_b), 7.09 (s, 8 H, H_c).



With $\text{Rh}^{\text{III}}(\text{ttp})\text{I}$, KOH (1 equiv) and Under Light. $\text{Rh}^{\text{III}}(\text{ttp})\text{I}$ (0.43 mg, 0.00048 mmol), KOH (0.27 mg, 0.0048 mmol) and H_2O (8.6 μL , 0.48 mmol) were added into benzene- d_6 stock solution (500 μL) of [2.2]paracyclophane (1.0 mg, 0.0048 mmol) in a NMR tube. The orange mixture was degassed for three freeze-pump-thaw cycles and the NMR tube was flame-sealed under vacuum. It was heated in an oil bath at 200 °C under the light conditions (Philips Master TL5 HE 21W/835, 21 W, approx. 1 m above) for 5 d. It was monitored with ^1H NMR spectroscopy at particular time intervals and the NMR yields were taken. **1** was formed in 52% yield and 9% of [2.2]paracyclophane was remained. Therefore light did not catalyze the hydrogenation of PCP.

With $\text{Rh}^{\text{III}}(\text{ttp})\text{Me}$. $\text{Rh}^{\text{III}}(\text{ttp})\text{Me}$ (0.38 mg, 0.00048 mmol) and H_2O (8.6 μL , 0.48 mmol) were added into benzene- d_6 stock solution (500 μL) of [2.2]paracyclophane (1.0 mg, 0.0048 mmol) in a NMR tube. The orange mixture was degassed for three freeze-pump-thaw cycles and the NMR tube was flame-sealed under vacuum. It was heated at 200 °C in the dark for 54 h. It was monitored with ^1H NMR spectroscopy at particular time intervals and the NMR yields were taken.

With Rh^{III}(ttp)ⁱPr. Rh^{III}(ttp)ⁱPr (0.39 mg, 0.00048 mmol) and H₂O (8.6 μL, 0.48 mmol) were added into benzene-*d*₆ stock solution (500 μL) of [2.2]paracyclophane (1.0 mg, 0.0048 mmol) in a NMR tube. The orange mixture was degassed for three freeze-pump-thaw cycles and the NMR tube was flame-sealed under vacuum. It was heated at 200 °C in the dark for 50 h. It was monitored with ¹H NMR spectroscopy at particular time intervals and the NMR yields were taken.

Without Rh^{III}(ttp)X. H₂O (8.6 μL, 0.48 mmol) was added into benzene-*d*₆ stock solution (500 μL) of [2.2]paracyclophane (1.0 mg, 0.0048 mmol) in a NMR tube. The colorless mixture was degassed for three freeze-pump-thaw cycles and the NMR tube was flame-sealed under vacuum. It was heated at 200 °C in the dark for 4.5 d. It was monitored with ¹H NMR spectroscopy at particular time intervals and the NMR yields were taken. [2.2]Paracyclophane remained quantitative.

Porphyrin Ligand Electronic Effects.

With Rh^{III}(tap)Me. Rh^{III}(tap)Me (0.41 mg, 0.00048 mmol) and H₂O (8.6 μL, 0.48 mmol) were added into benzene-*d*₆ stock solution (500 μL) of [2.2]paracyclophane (1.0 mg, 0.0048 mmol) in a NMR tube. The orange mixture was degassed for three freeze-pump-thaw cycles and the NMR tube was flame-sealed under vacuum. It was heated at 200 °C in the dark for 84 h. It was monitored with ¹H NMR spectroscopy at particular time intervals and the NMR yields were taken.

With Rh^{III}(t₄-CF₃pp)Me. Rh^{III}(t₄-CF₃pp)Me (0.48 mg, 0.00048 mmol) and H₂O (8.6 μL, 0.48 mmol) were added into benzene-*d*₆ stock solution (500 μL) of [2.2]paracyclophane (1.0 mg, 0.0048 mmol) in a NMR tube. The orange mixture was degassed for three freeze-pump-thaw cycles and the NMR tube was flame-sealed under vacuum. It was heated at 200 °C in the dark

for 40 h. It was monitored with ^1H NMR spectroscopy at particular time intervals and the NMR yields were taken.

With $\text{Rh}^{\text{III}}(\text{ocp})\text{Me}$. $\text{Rh}^{\text{III}}(\text{ocp})\text{Me}$ (0.49 mg, 0.00048 mmol) and H_2O (8.6 μL , 0.48 mmol) were added into benzene- d_6 stock solution (500 μL) of [2.2]paracyclophane (1.0 mg, 0.0048 mmol) in a NMR tube. The red mixture was degassed for three freeze-pump-thaw cycles and the NMR tube was flame-sealed under vacuum. It was heated at 200 $^\circ\text{C}$ in the dark for 4 d. It was monitored with ^1H NMR spectroscopy at particular time intervals and the NMR yields were taken.

With $\text{Rh}^{\text{III}}(\text{tmp})\text{Me}$. $\text{Rh}^{\text{III}}(\text{tmp})\text{Me}$ (0.43 mg, 0.00048 mmol) and D_2O (8.7 μL , 0.48 mmol) were added into benzene- d_6 stock solution (500 μL) of [2.2]paracyclophane (1.0 mg, 0.0048 mmol) in a NMR tube. The red mixture was degassed for three freeze-pump-thaw cycles and the NMR tube was flame-sealed under vacuum. It was heated at 200 $^\circ\text{C}$ in the dark for 7 d. It was monitored with ^1H NMR spectroscopy at particular time intervals and the NMR yields were taken.

Additive Effects.

With $^t\text{BuOH}$ (2 equiv). $\text{Rh}^{\text{III}}(\text{ttp})\text{Me}$ (0.38 mg, 0.00048 mmol), $^t\text{BuOH}$ (0.9 μL , 0.0096 mmol) and H_2O (8.6 μL , 0.48 mmol) were added into benzene- d_6 stock solution (500 μL) of [2.2]paracyclophane (1.0 mg, 0.0048 mmol) in a NMR tube. The orange mixture was degassed for three freeze-pump-thaw cycles and the NMR tube was flame-sealed under vacuum. It was heated at 200 $^\circ\text{C}$ in the dark for 54 h. It was monitored with ^1H NMR spectroscopy at particular time intervals and the NMR yields were taken.

With $^t\text{BuOH}$ (10 equiv). $\text{Rh}^{\text{III}}(\text{ttp})\text{Me}$ (0.38 mg, 0.00048 mmol), $^t\text{BuOH}$ (4.6 μL , 0.048 mmol) and H_2O (8.6 μL , 0.48 mmol) were added into benzene- d_6 stock solution (500 μL) of [2.2]paracyclophane (1.0 mg, 0.0048 mmol) in a NMR tube. The orange mixture was

degassed for three freeze-pump-thaw cycles and the NMR tube was flame-sealed under vacuum. It was heated at 200 °C in the dark for 47 h. It was monitored with ^1H NMR spectroscopy at particular time intervals and the NMR yields were taken.

With BnEt_3NCl (0.1 equiv). $\text{Rh}^{\text{III}}(\text{ttp})\text{Me}$ (0.38 mg, 0.00048 mmol), BnEt_3NCl (0.11 mg, 0.00048 mmol) and H_2O (8.6 μL , 0.48 mmol) were added into benzene- d_6 stock solution (500 μL) of [2.2]paracyclophane (1.0 mg, 0.0048 mmol) in a NMR tube. The orange mixture was degassed for three freeze-pump-thaw cycles and the NMR tube was flame-sealed under vacuum. It was heated at 200 °C in the dark for 50 h. It was monitored with ^1H NMR spectroscopy at particular time intervals and the NMR yields were taken.

With BnEt_3NCl (1 equiv). $\text{Rh}^{\text{III}}(\text{ttp})\text{Me}$ (0.38 mg, 0.00048 mmol), BnEt_3NCl (1.1 mg, 0.0048 mmol) and H_2O (8.6 μL , 0.48 mmol) were added into benzene- d_6 stock solution (500 μL) of [2.2]paracyclophane (1.0 mg, 0.0048 mmol) in a NMR tube. The orange mixture was degassed for three freeze-pump-thaw cycles and the NMR tube was flame-sealed under vacuum. It was heated at 200 °C in the dark for 41 h. It was monitored with ^1H NMR spectroscopy at particular time intervals and the NMR yields were taken.

With PPh_4Br (0.1 equiv). $\text{Rh}^{\text{III}}(\text{ttp})\text{Me}$ (0.38 mg, 0.00048 mmol), PPh_4Br (0.2 mg, 0.00048 mmol) and H_2O (8.6 μL , 0.48 mmol) were added into benzene- d_6 stock solution (500 μL) of [2.2]paracyclophane (1.0 mg, 0.0048 mmol) in a NMR tube. The orange mixture was degassed for three freeze-pump-thaw cycles and the NMR tube was flame-sealed under vacuum. It was heated at 200 °C in the dark for 61 h. It was monitored with ^1H NMR spectroscopy at particular time intervals and the NMR yields were taken.

Deuterium Labeling Experiments.

Catalytic Deuteration of [2.2]Paracyclophane with $\text{Rh}^{\text{III}}(\text{ttp})\text{Me}$. $\text{Rh}^{\text{III}}(\text{ttp})\text{Me}$ (0.38 mg, 0.00048 mmol) and D_2O (8.7 μL , 0.48 mmol) were added into benzene- d_6 stock solution (500

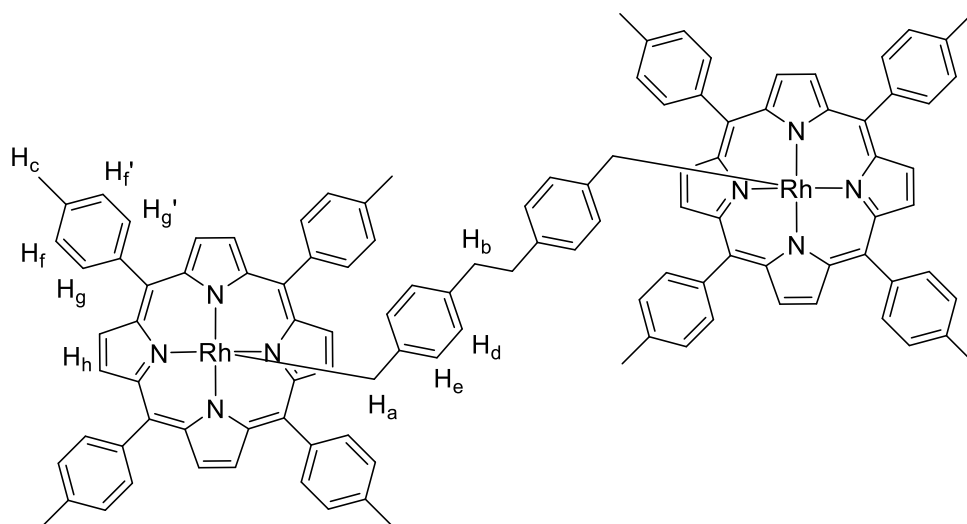
μL) of [2.2]paracyclophane (1.0 mg, 0.0048 mmol) in a NMR tube. The orange mixture was degassed for three freeze-pump-thaw cycles and the NMR tube was flame-sealed under vacuum. It was heated at 200 °C in the dark for 3 d. It was monitored with ^1H NMR spectroscopy at particular time intervals and the NMR yields were taken. **5-d** was isolated by column chromatography on silica gel eluting with hexane. ^1H NMR (C_6D_6 , 400 MHz) δ 2.11-2.13 (m), 2.76-2.79 (m), 6.97 (s, 8 H).

Benzylic H/D Exchange of 4,4'-Dimethylbibenzyl 5. $\text{Rh}^{\text{III}}(\text{ttp})\text{Me}$ (0.38 mg, 0.00048 mmol) and D_2O (8.7 μL , 0.48 mmol) were added into benzene- d_6 stock solution (500 μL) of 4,4'-dimethylbibenzyl (1.0 mg, 0.0048 mmol) in a NMR tube. The orange mixture was degassed for three freeze-pump-thaw cycles and the NMR tube was flame-sealed under vacuum. It was heated at 200 °C in the dark for 3 d 15 h. It was monitored with ^1H NMR spectroscopy at particular time intervals and the NMR yields were taken. **5-d'** was isolated by column chromatography on silica gel eluting with hexane. ^1H NMR (C_6D_6 , 400 MHz) δ 2.13 (s), 2.76-2.77 (m), 6.97 (s, 8 H).

Reaction of $\text{Rh}^{\text{III}}(\text{ttp})\text{Cl}$ with [2.2]Paracyclophane at Lower Temperature. $\text{Rh}^{\text{III}}(\text{ttp})\text{Cl}$ (0.39 mg, 0.00048 mmol), KOH (0.27 mg, 0.0048 mmol) and D_2O (8.7 μL , 0.48 mmol) were added into benzene- d_6 stock solution (500 μL) of [2.2]paracyclophane (1.0 mg, 0.0048 mmol) in a NMR tube. The orange mixture was degassed for three freeze-pump-thaw cycles and the NMR tube was flame-sealed under vacuum. It was heated in the dark at 60 °C for 4 d, 120 °C for 8 d and 130 °C for 1 d. It was monitored with ^1H NMR spectroscopy at particular time intervals and the NMR yields were taken.

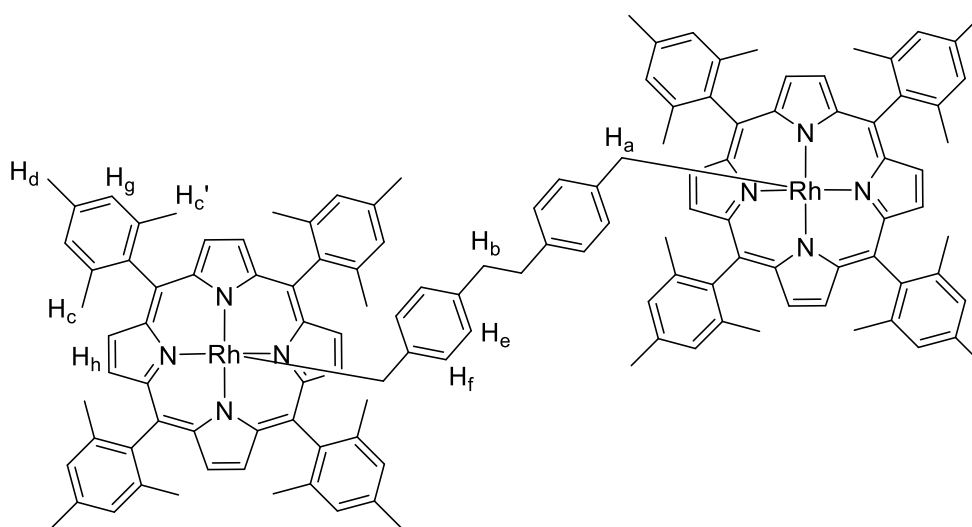
Independent Synthesis of Di-rhodium Benzyl 7. $\text{Rh}^{\text{III}}(\text{ttp})\text{I}$ (0.43 mg, 0.00048 mmol) and KOH (0.27 mg, 0.0048 mmol) were added into benzene- d_6 stock solution (500 μL) of

[2.2]paracyclophane (1.0 mg, 0.0048 mmol) in a NMR tube. The orange mixture was degassed for three freeze-pump-thaw cycles and the NMR tube was flame-sealed under vacuum. It was heated at 150 °C in the dark for 15 h to give 82% yield of **7**. Attempted isolation of **7** by column chromatography led to decomposition to intractable products. ¹H NMR (C₆D₆, 400 MHz) δ -3.42 (d, ²J_{Rh-H} = 3.3 Hz, 4 H, H_a), 1.96 (s, 4 H, H_b), 2.42 (s, 24 H, H_c), 3.16 (d, ³J_{H-H} = 7.7 Hz, 4 H, H_d), 5.61 (d, ³J_{H-H} = 8.0 Hz, 4 H, H_e), 7.31 (d, ³J_{H-H} = 7.8 Hz, 8 H, H_f), 7.35 (d, ³J_{H-H} = 6.8 Hz, 8 H, H_f'), 8.04 (d, ³J_{H-H} = 7.6 Hz, 8 H, H_g), 8.21 (d, ³J_{H-H} = 7.4 Hz, 8 H, H_g'), 8.93 (s, 16H, H_h). HRMS calcd. for (C₁₁₂H₈₈N₈Rh₂)⁺: m/z 1751.5269. Found: m/z 1751.5269.



Reaction of Rh^{II}(tmp) with [2.2]Paracyclophane. Rh^{II}(tmp) (0.42 mg, 0.00048 mmol) was added into benzene-*d*₆ stock solution (500 μL) of [2.2]paracyclophane (1.0 mg, 0.0048 mmol) in a NMR tube. The orange mixture was degassed for three freeze-pump-thaw cycles and the NMR tube was flame-sealed under vacuum. It was heated at 150 °C in the dark for 23 h to give **8** in 85% yield. ¹H NMR (C₆D₆, 400 MHz) δ -3.20 (d, ²J_{Rh-H} = 2.8 Hz, 4 H, H_a), 1.62 (s, 4 H, H_b), 1.89 (s, 24 H, H_c), 1.97 (s, 24 H, H_c'), 2.43 (s, 24 H, H_d), 3.50 (d, ³J_{H-H} = 7.4 Hz, 4

H, H_e), 5.38 (d, ³J_{H-H} = 8.0 Hz, 4 H, H_f), 7.12 (*meso*-aryl *meta* protons overlapped with solvent residual C₆H₆, H_g), 8.66 (s, 16H, H_h).



General Procedures for Kinetic Experiments.

Rh^{II}(tmp) was added into benzene-*d*₆ stock solution (500 μL) of [2.2]paracyclophane in a NMR tube. The orange mixture was degassed for three freeze-pump-thaw cycles and the NMR tube was flame-sealed under vacuum. It was heated at designated temperature in the dark. The reaction was monitored with ¹H NMR spectroscopy at particular time intervals and the NMR yields were taken. The collected kinetic data were analyzed and plotted into graphs using OriginPro 7.5 software.

Hydrolysis of Rh^{III}(ttp)R.

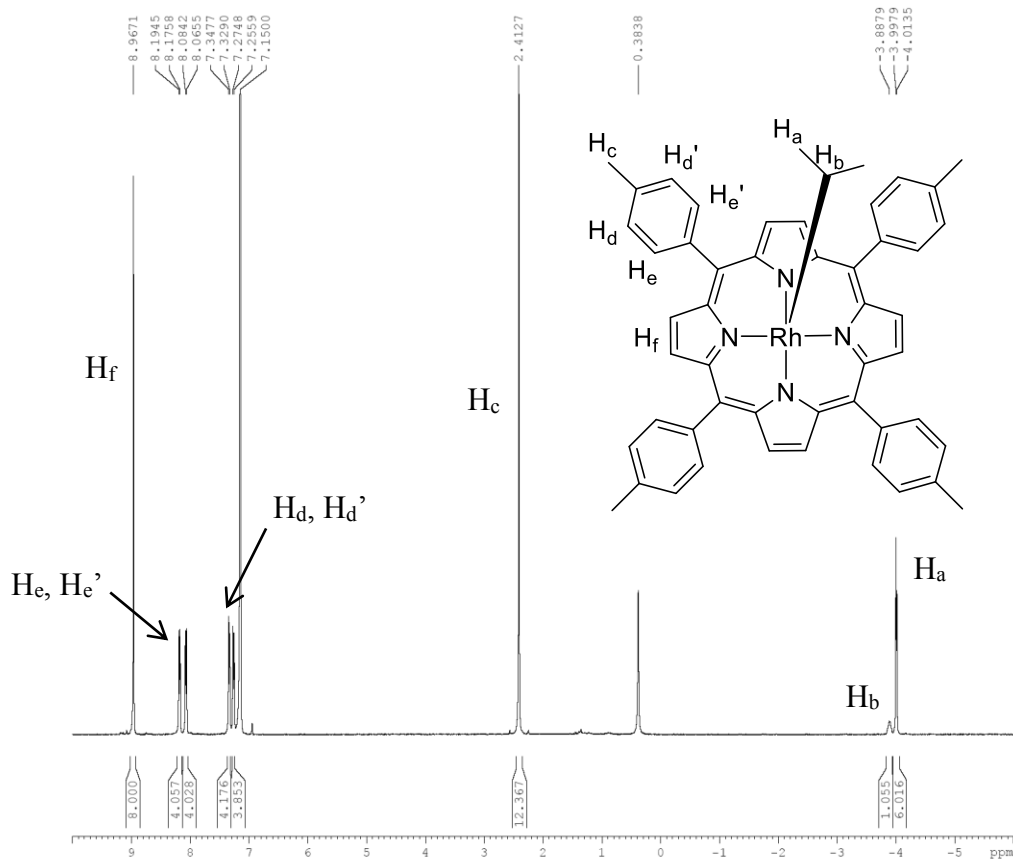
Rh^{III}(ttp)Bn. Rh^{III}(ttp)Bn (0.41 mg, 0.00048 mmol) and H₂O (8.6 μL, 0.48 mmol) were added into benzene-*d*₆ (500 μL) in a NMR tube. The orange mixture was degassed for three freeze-pump-thaw cycles and the NMR tube was flame-sealed under vacuum. It was heated at 200 °C in the dark for 3.5 d. It was monitored with ¹H NMR spectroscopy at particular time intervals and the NMR yields were taken.

Rh^{III}(ttp)ⁱPr. Rh^{III}(ttp)ⁱPr (0.39 mg, 0.00048 mmol) and H₂O (8.6 μL, 0.48 mmol) were added into benzene-*d*₆ (500 μL) in a NMR tube. The orange mixture was degassed for three freeze-pump-thaw cycles and the NMR tube was flame-sealed under vacuum. It was heated at 200 °C in the dark for 50 h. It was monitored with ¹H NMR spectroscopy at particular time intervals and the NMR yields were taken.

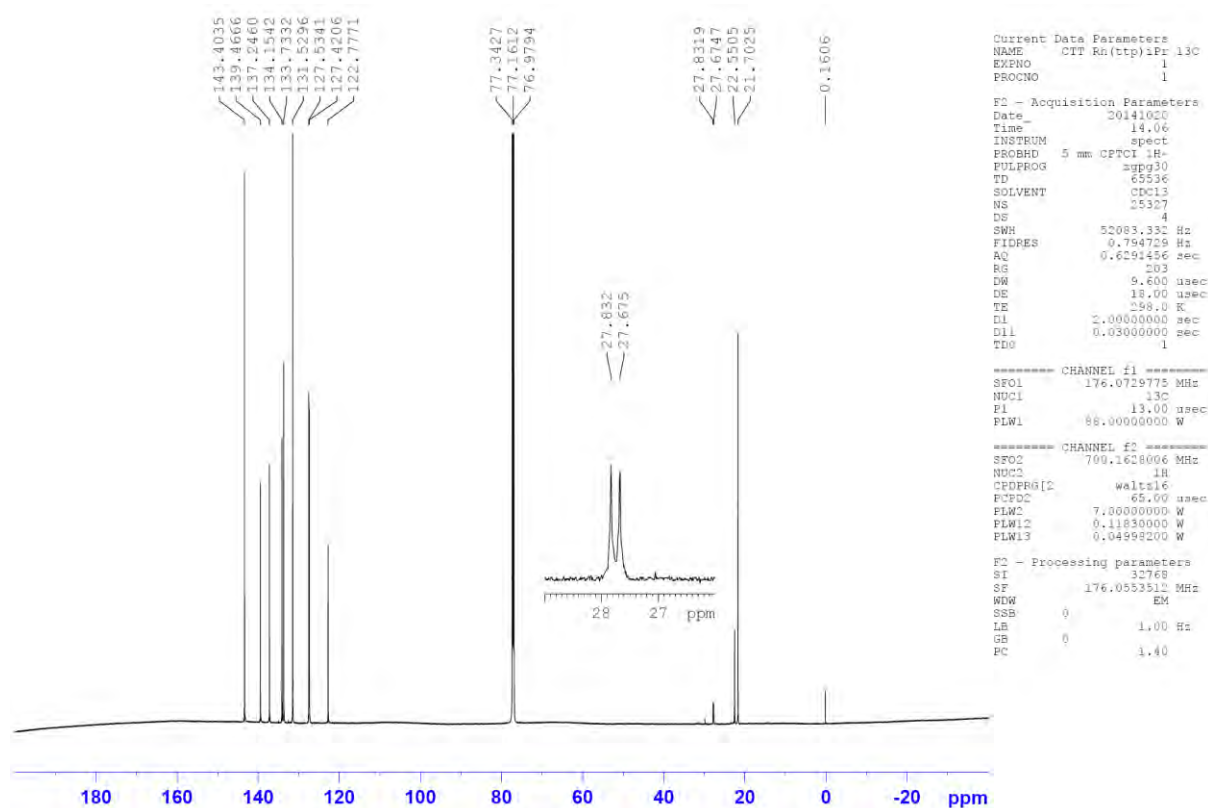
Appendix I List of Spectra

No.	Spectra	Page
1	^1H NMR spectrum of $\text{Rh}^{\text{III}}(\text{ttp})^i\text{Pr}$	98
2	$^{13}\text{C}\{^1\text{H}\}$ NMR spectrum of $\text{Rh}^{\text{III}}(\text{ttp})^i\text{Pr}$	98
3	^1H NMR spectrum of 4,4'-dimethylbibenzyl 5	99
4	^1H NMR spectrum of deuterated 5-d	99
5	^1H NMR spectrum of deuterated 5-d'	100
6	^1H NMR spectrum of di-rhodium benzyl 7	101
7	^1H NMR spectrum of di-rhodium benzyl 8	102
8	HRMS spectrum of di-rhodium benzyl 7	103

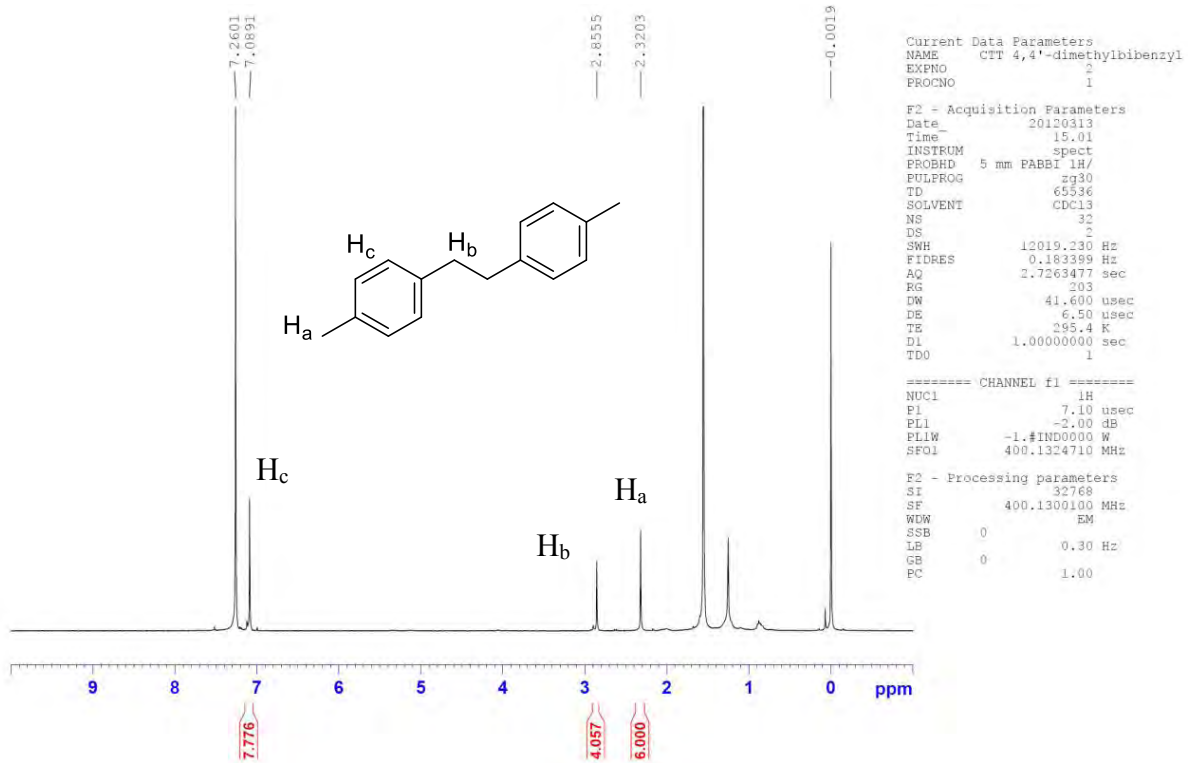
Rh^{III}(ttp)ⁱPr (¹H)



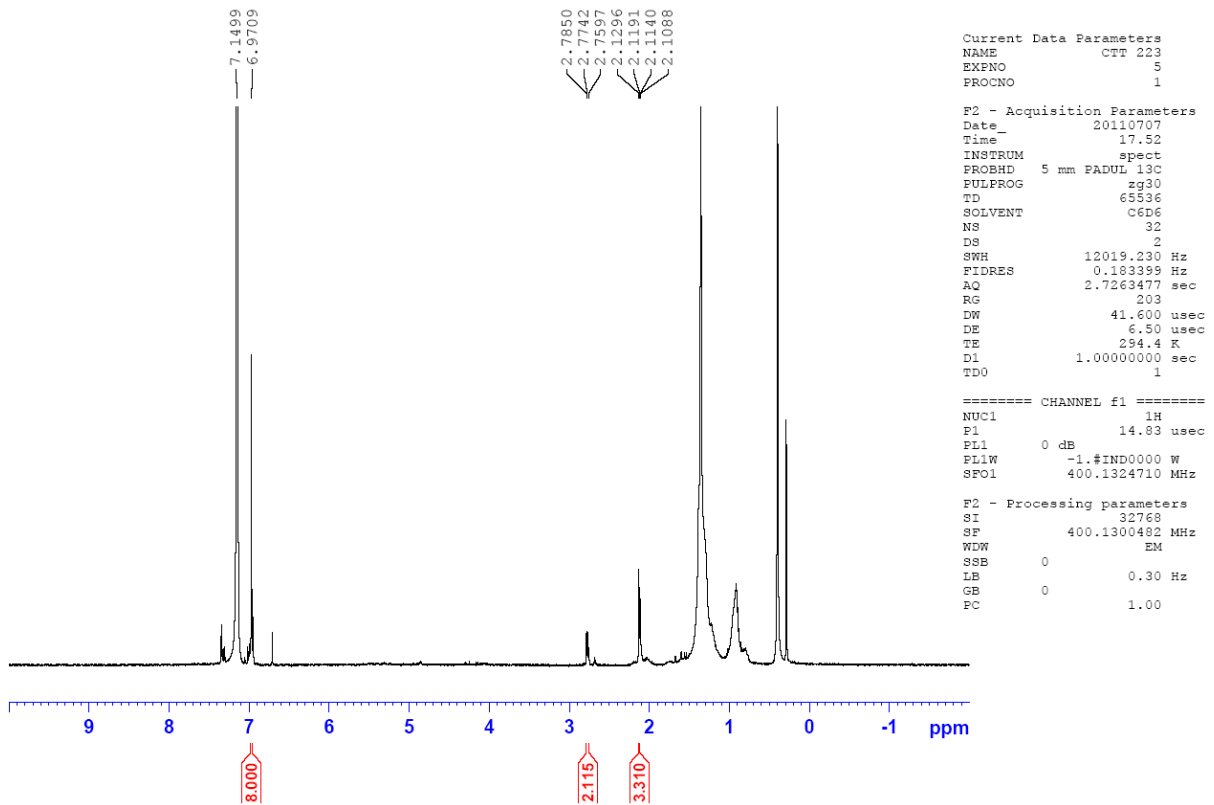
Rh^{III}(ttp)ⁱPr (¹³C{¹H})



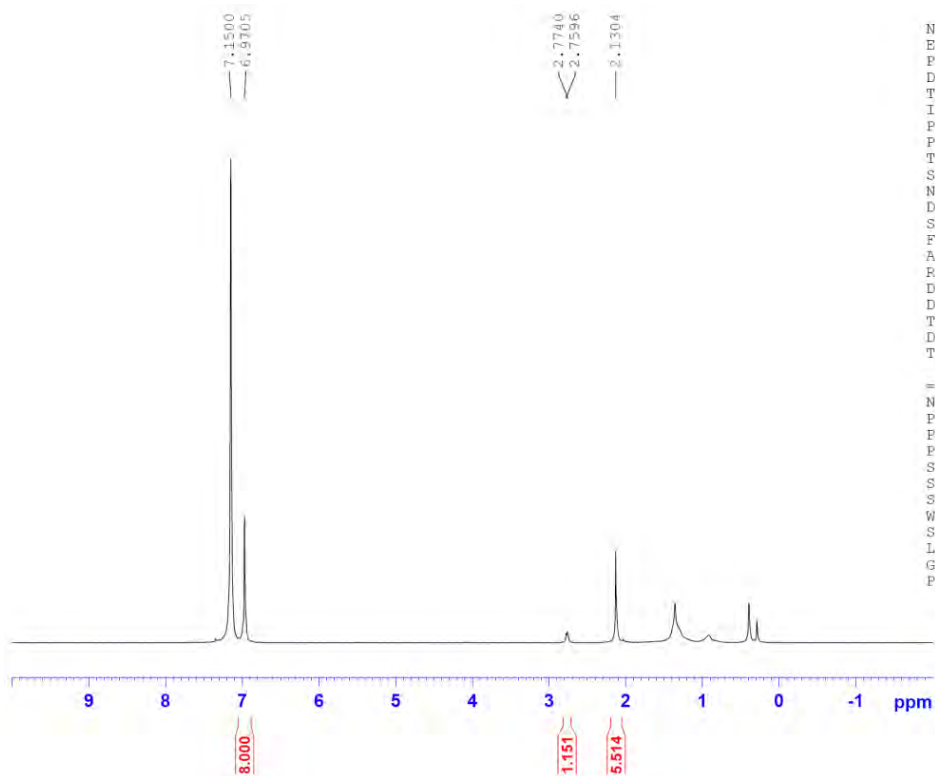
4,4'-Dimethylbibenzyl 5 (¹H)



5-d (¹H)



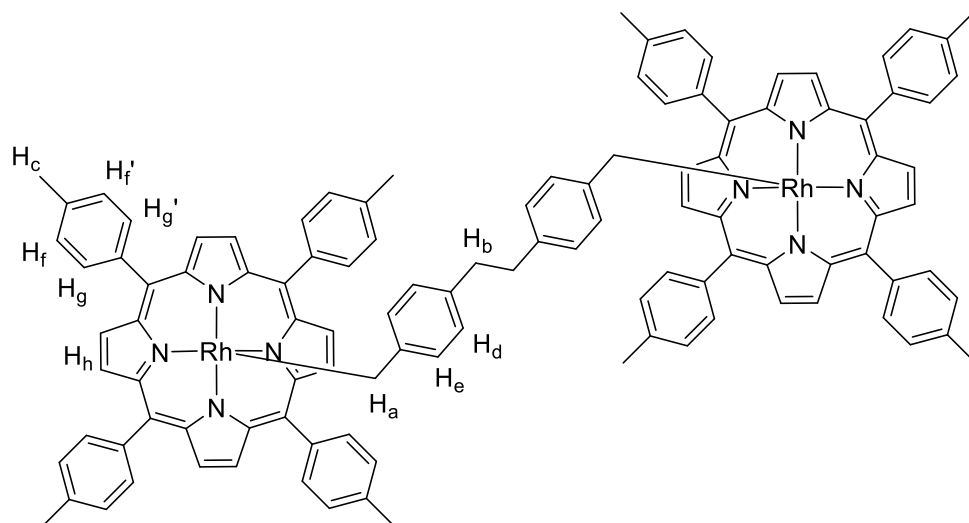
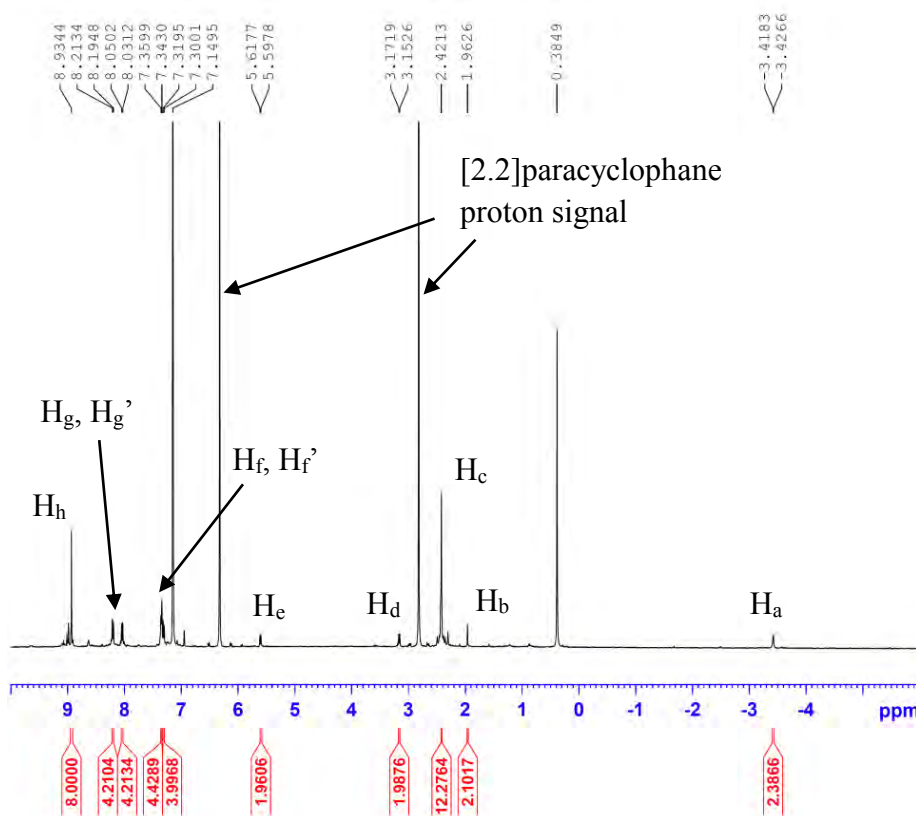
5-d' (¹H)



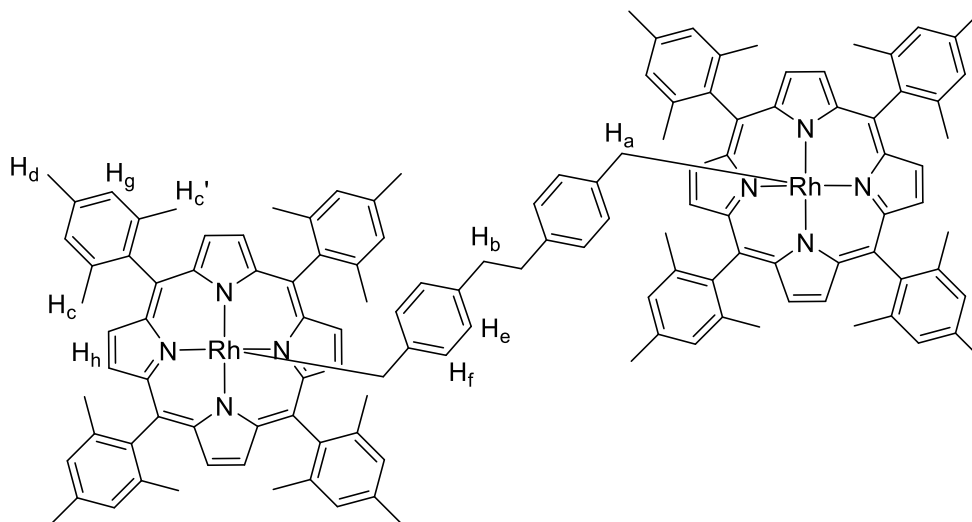
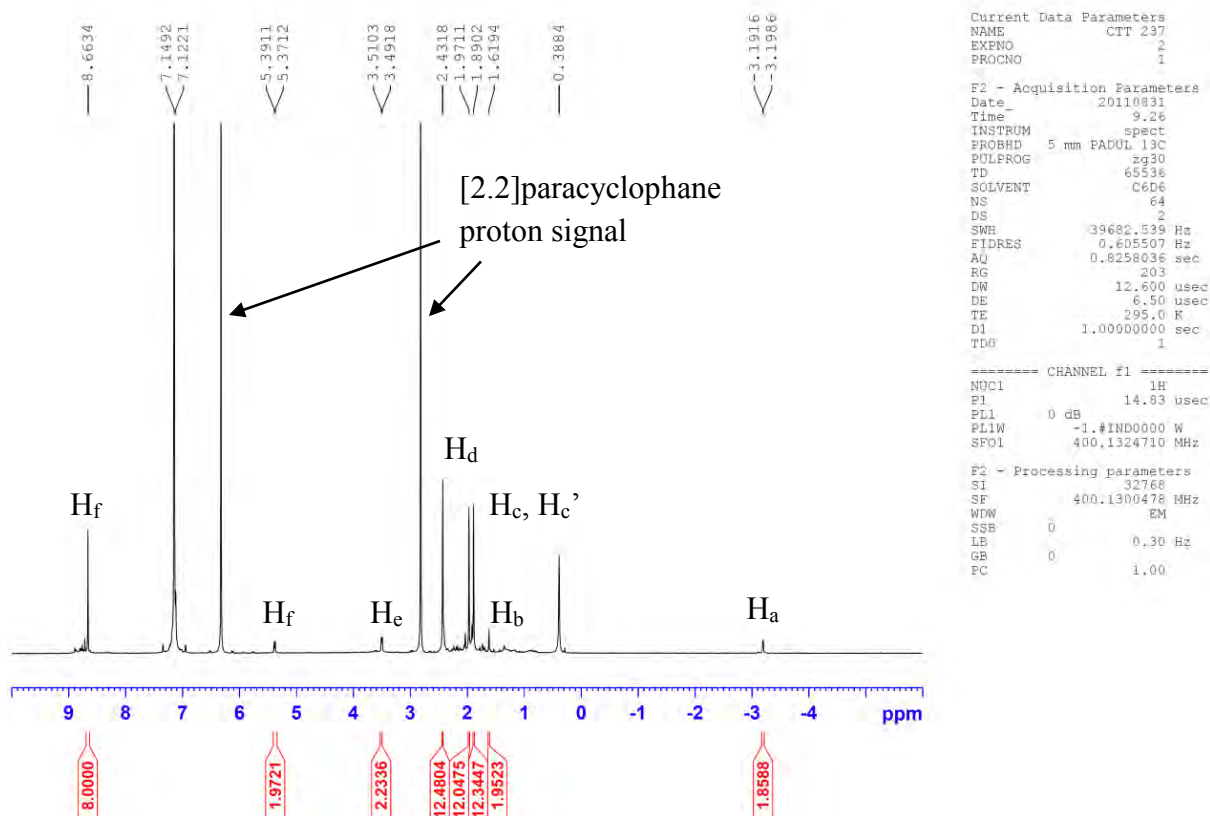
NAME CTT 265
EXPNO 10
PROCNO 1
Date 20120116
Time 12.52
INSTRUM spect
PROBHD 5 mm PABBI 1H/
PULPROG zg30
TD 65536
SOLVENT C6D6
NS 32
DS 2
SWH 12019.230 Hz
FIDRES 0.183399 Hz
AQ 2.7263477 sec
RG 203
DW 41.600 usec
DE 6.50 usec
TE 295.5 K
D1 1.00000000 sec
TD0 1

===== CHANNEL f1 =====
NUC1 1H
P1 7.10 usec
PL1 -2.00 dB
PL1W 13.17734718 W
SFO1 400.1324710 MHz
SI 32768
SF 400.1300480 MHz
WDW EM
SSB 0
LB 0.30 Hz
GB 0
PC 1.00

Di-rhodium benzyl 7 (¹H)

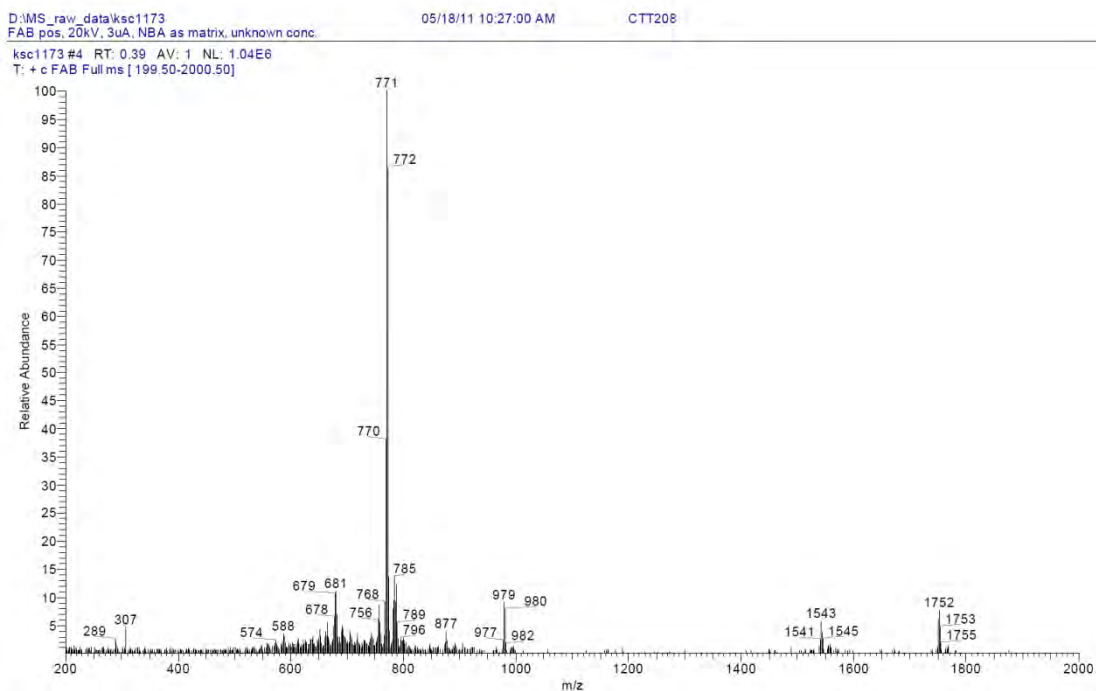


Di-rhodium benzyl 8 (¹H)

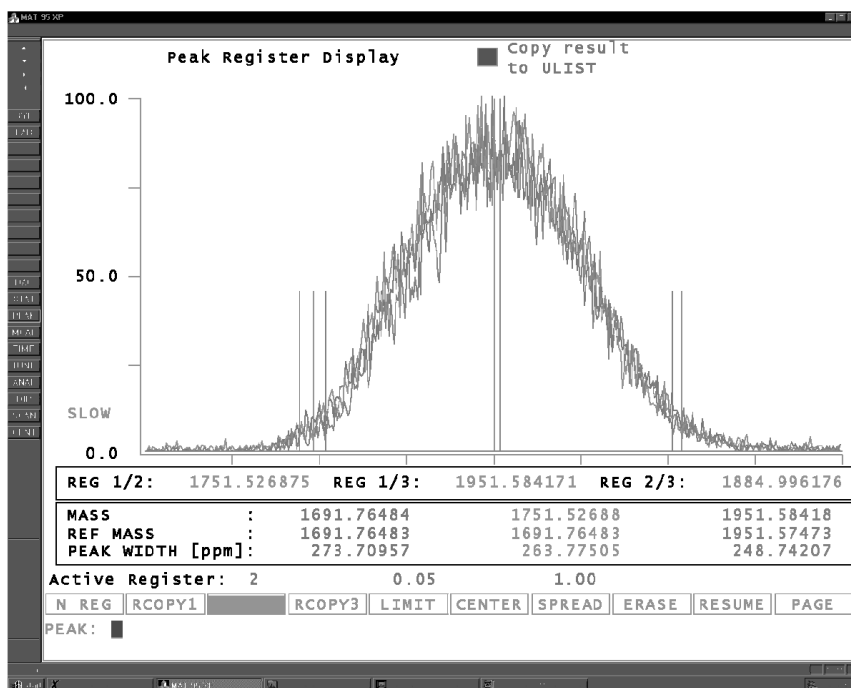


HRMS Spectra

Di-rhodium benzyl 7 (FAB)



Accurate Mass Measurement



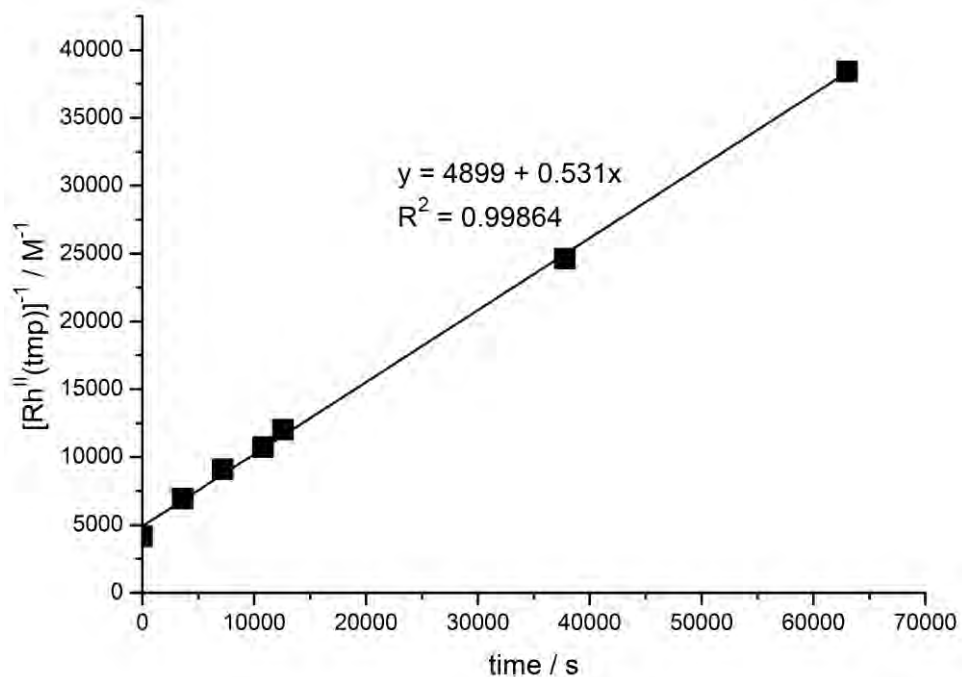
Molecular formula
 $C_{112}H_{88}N_8Rh_2$
 $[M]^+$ (theoretical)
= 1751.5269

Appendix II ¹H NMR Kinetic Data

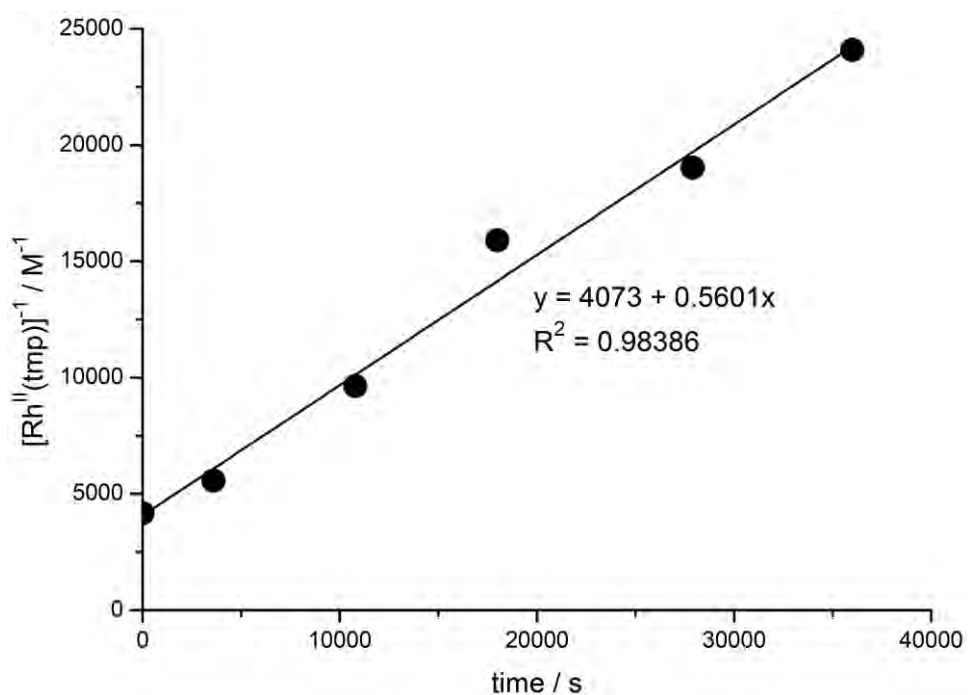
[PCP] = 9.6 mM, 150 °C					
[Rh ^{II} (tmp)] = 0.24 mM			[Rh ^{II} (tmp)] = 0.48 mM		
Trial 1		Trial 2			
time / s	[Rh ^{II} (tmp)] / mM	time / s	[Rh ^{II} (tmp)] / mM	time / s	[Rh ^{II} (tmp)] / mM
0	0.240	0	0.240	0	0.480
3600	0.144	3600	0.147	1800	0.377
7200	0.110	10800	0.104	12600	0.134
10800	0.093	18000	0.063	23400	0.112
12600	0.083	27900	0.053	28800	0.094
37800	0.041	36000	0.042	32400	0.075
63000	0.026			39600	0.064

[Rh ^{II} (tmp)] = 0.24 mM, 150 °C			
[PCP] = 4.8 mM		[PCP] = 14.4 mM	
time / s	[Rh ^{II} (tmp)] / mM	time / s	[Rh ^{II} (tmp)] / mM
0	0.240	0	0.240
1800	0.174	1800	0.156
3600	0.168	3600	0.139
7200	0.140	7200	0.096
11700	0.109	11700	0.085
18900	0.103	18900	0.052
33300	0.079	33300	0.037
52000	0.053		

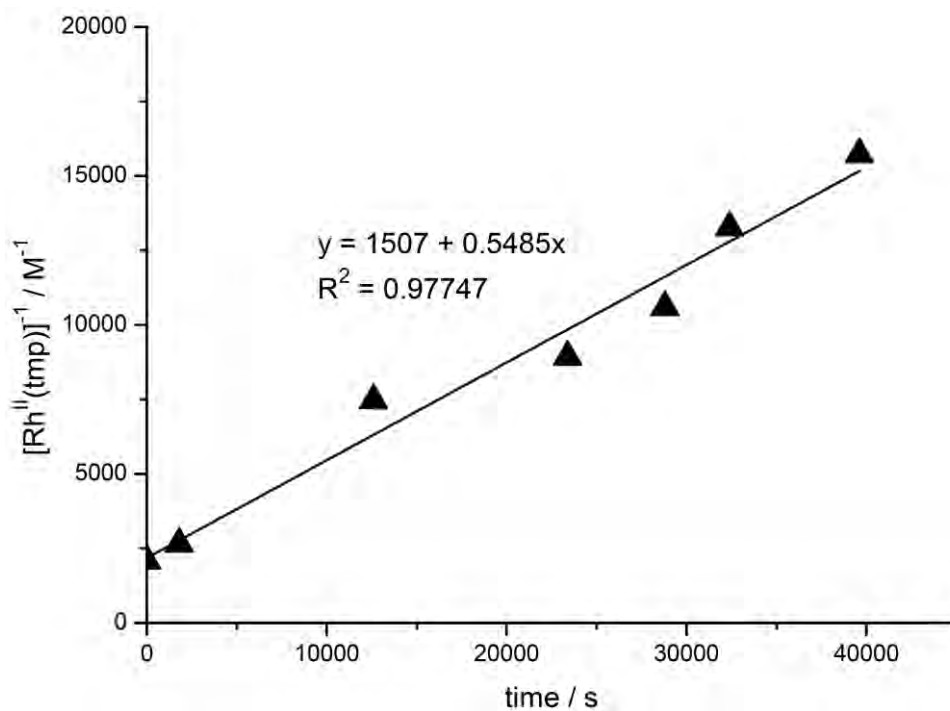
[Rh ^{II} (tmp)] = 0.24 mM, [PCP] = 9.6 mM					
140 °C		160 °C		170 °C	
time / s	[Rh ^{II} (tmp)] / mM	time / s	[Rh ^{II} (tmp)] / mM	time / s	[Rh ^{II} (tmp)] / mM
0	0.240	0	0.240	0	0.240
18000	0.158	3600	0.081	3600	0.080
28200	0.119	5400	0.062	5400	0.053
46800	0.092	6300	0.058	6300	0.047
52000	0.083	8100	0.056	8100	0.034
		9900	0.042		
		10800	0.037		



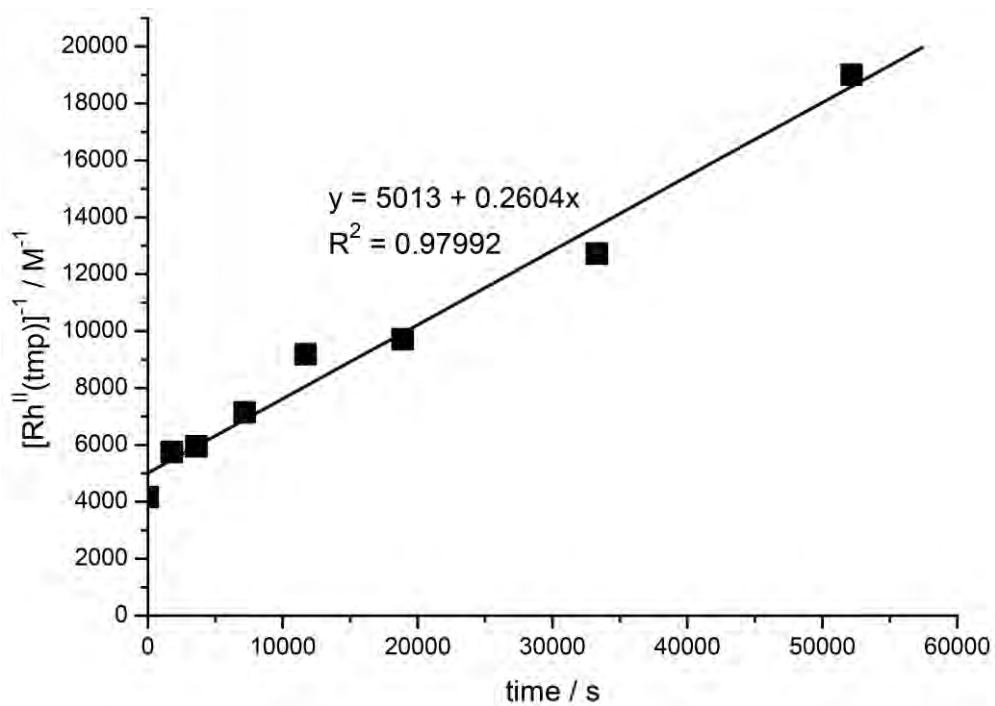
Pseudo 2nd Order Kinetic Plot with $[\text{Rh}^{\text{II}}(\text{tmp})] = 0.24 \text{ mM}$ and $[\text{PCP}] = 9.6 \text{ mM}$ at $150 \text{ }^\circ\text{C}$.



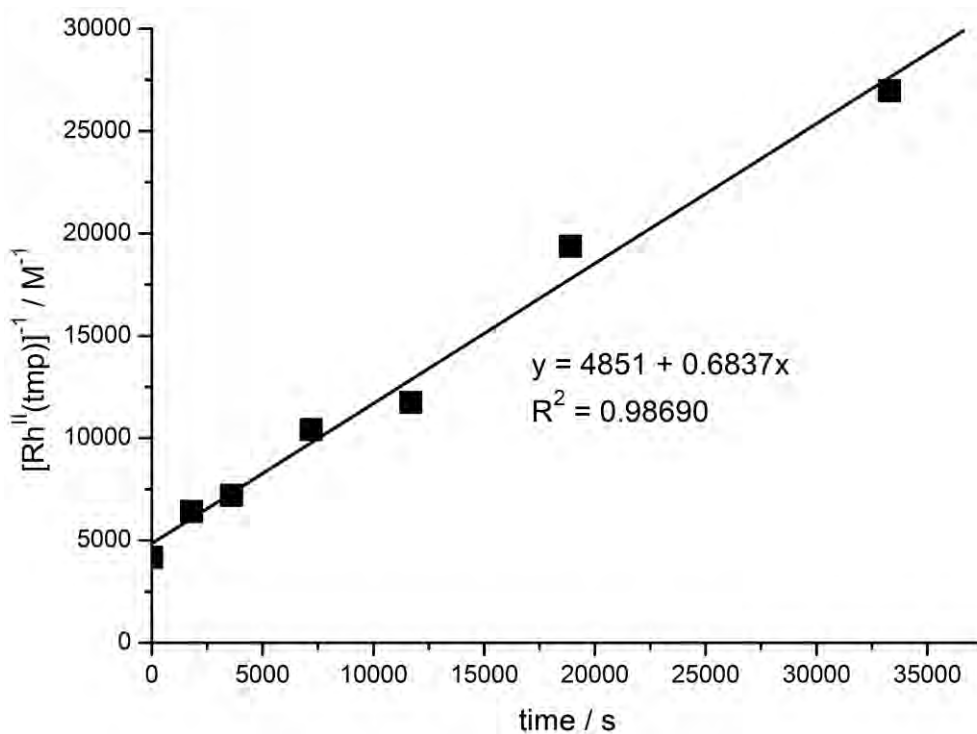
Pseudo 2nd Order Kinetic Plot with $[\text{Rh}^{\text{II}}(\text{tmp})] = 0.24 \text{ mM}$ and $[\text{PCP}] = 9.6 \text{ mM}$ at $150 \text{ }^\circ\text{C}$.



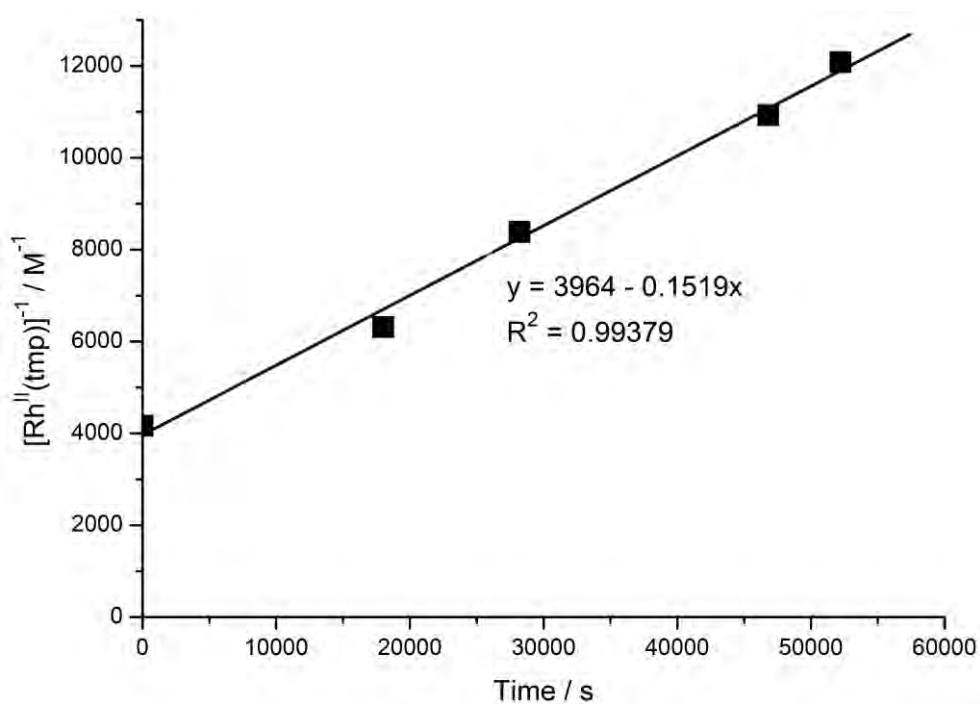
Pseudo 2nd Order Kinetic Plot with $[Rh^{II}(tmp)] = 0.48$ mM and $[PCP] = 9.6$ mM at 150 °C.



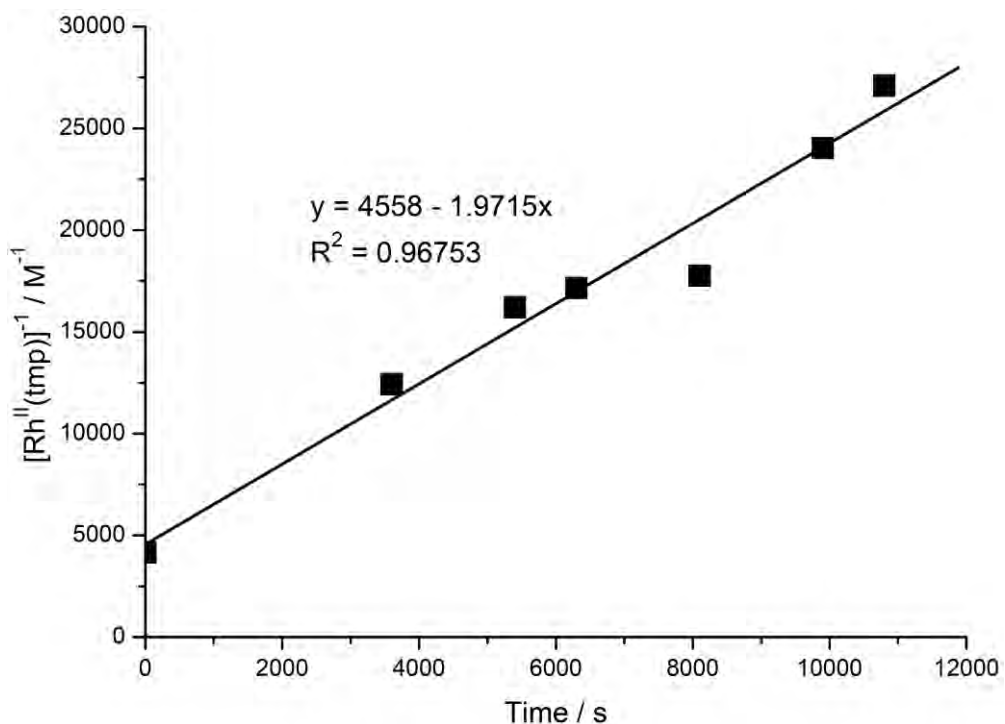
Pseudo 2nd Order Kinetic Plot with $[Rh^{II}(tmp)] = 0.24$ mM and $[PCP] = 4.8$ mM at 150 °C.



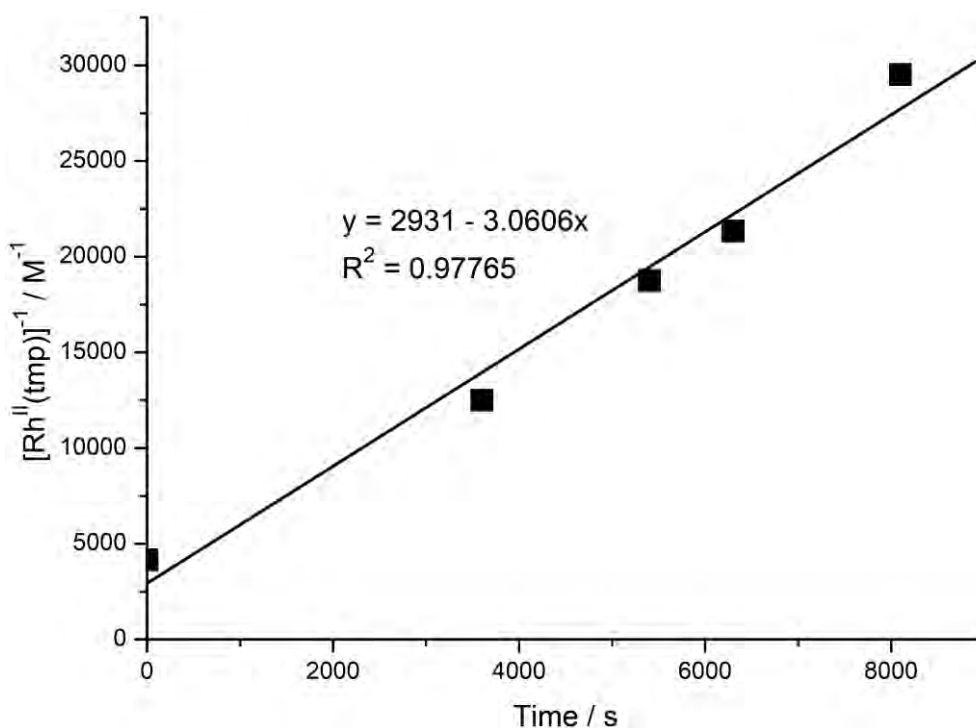
Pseudo 2nd Order Kinetic Plot with $[Rh^{II}(tmp)] = 0.24 \text{ mM}$ and $[PCP] = 14.4 \text{ mM}$ at $150 \text{ }^\circ\text{C}$.



Pseudo 2nd Order Kinetic Plot with $[Rh^{II}(tmp)] = 0.24 \text{ mM}$ and $[PCP] = 9.6 \text{ mM}$ at $140 \text{ }^\circ\text{C}$.



Pseudo 2nd Order Kinetic Plot with $[Rh^{II}(tmp)] = 0.24 \text{ mM}$ and $[PCP] = 9.6 \text{ mM}$ at $160 \text{ }^\circ\text{C}$.



Pseudo 2nd Order Kinetic Plot with $[Rh^{II}(tmp)] = 0.24 \text{ mM}$ and $[PCP] = 9.6 \text{ mM}$ at $170 \text{ }^\circ\text{C}$.

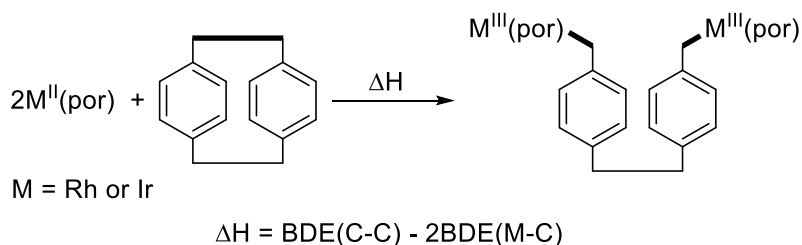
References

1. Cram, D. J.; Steinberg, H. *J. Am. Chem. Soc.* **1951**, *73*, 5691-5703.
2. Alder, A. D.; Longo, F. R.; Finarelli, J. D.; Goldmacher, J.; Assour, J.; Korsakoff, L. *J. Org. Chem.* **1967**, *32*, 476-477.
3. (a) Zhou, X.; Li, Q.; Mak, T. C. W.; Chan, K. S. *Inorg Chim. Acta.* **1998**, *270*, 551-554.
(b) Zhou, X.; Wang, R. J.; Xue, F.; Mak, T. C. W.; Chan, K. S. *J. Organomet. Chem.* **1999**, *580*, 22-25.
4. (a) Chan, K. S.; Mak, K. W.; Tse, M. K.; Yeung, S. K.; Li, B. Z.; Chan, Y. W. *J. Organomet. Chem.* **2008**, *693*, 399-407. (b) Fung, H. S.; Chan, Y. W.; Cheung, C. W.; Choi, K. S.; Lee, S. Y.; Qian, Y. Y.; Chan, K. S. *Organometallics* **2009**, *28*, 3981-3989.
5. Wayland, B. B.; Sherry, A. E.; Poszmik, G.; Bunn, A. G. *J. Am. Chem. Soc.* **1992**, *114*, 1673-1681.
6. Mak, K. W.; Xue, F.; Mak, T. C. W.; Chan, K. S. *J. Chem. Soc., Dalton Trans.* **1999**, 3333-3334.
7. Reich, H. J.; Cram, D. J. *J. Am. Chem. Soc.* **1967**, *89*, 3078-3080.

Chapter 3 Catalytic Carbon-Carbon Bond Hydrogenation of [2.2]Paracyclophane with Water by Iridium Porphyrin Complexes

3.1 Introduction

Chapter 2 describes the rhodium porphyrin catalyzed hydrogenation of PCP using water. The CCA of PCP with rhodium(II) porphyrin metalloradical is proposed with the cleavage of benzylic C-C bond of PCP and the formation of two Rh-C bonds (Scheme 3.1). Since the reaction enthalpy is solely governed by the BDE of M-C bond being formed, the CCA step can be made more exothermic by forming a M-C bond that is stronger than Rh-C bond.



Scheme 3.1 CCA of PCP with $M^{II}(\text{por})$.

Table 3.1 lists the M-CH₃ BDEs for group 9 metalloporphyrin complexes as examples. The strengths of the M-CH₃ bonds follow the trend: Ir > Rh >> Co. Hence, the CCA of PCP with iridium(II) porphyrin should be thermodynamically more favorable. Without the resting state or rate determining step well defined at this stage, we hope that better efficiency for the catalytic hydrogenation of PCP with H₂O can be achieved using iridium porphyrin catalyst. The iridium porphyrin catalyzed hydrogenation protocol is thus examined.

Table 3.1 M-CH₃ BDE in $M^{III}(\text{por})\text{-CH}_3$ Complexes.

M	$M^{III}(\text{por})\text{-CH}_3$ BDE / kcal mol ⁻¹
Co	18.7 ¹
Rh	56.9 ²
Ir	62 ³

3.2 Objectives of the Work

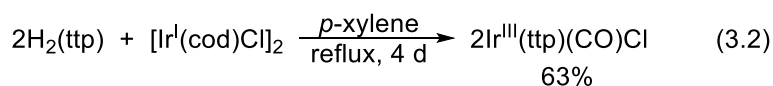
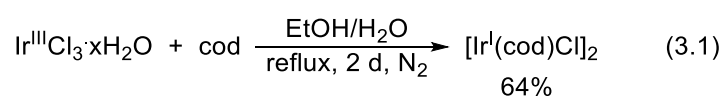
We aim to develop a more facile iridium porphyrin catalyzed C-C σ -bond hydrogenation protocol using H₂O.

3.3 Preparation of Starting Materials

3.3.1 Synthesis of Metalloporphyrins

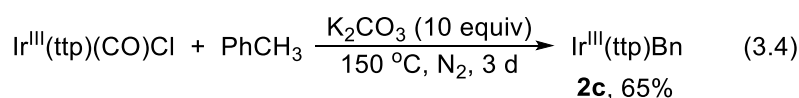
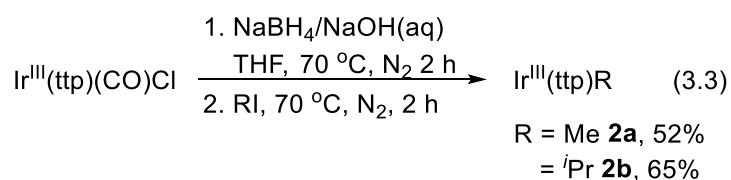
3.3.1.1 Synthesis of Iridium(III) Porphyrin Halides

Ir^{III}(ttp)(CO)Cl, the starting material for other iridium porphyrin complexes, can be prepared from H₂(ttp) using [Ir^I(cod)Cl]₂ complex as the iridium source. [Ir^I(cod)Cl]₂ was first prepared by refluxing Ir^{III}Cl₃·xH₂O with 1,5-cyclooctadiene in EtOH/H₂O mixed solvent for 2 d in 64% yield according to the literature method (eq 3.1).⁴ Ir^{III}(ttp)(CO)Cl was then prepared by refluxing H₂(ttp) with [Ir^I(cod)Cl]₂ in *p*-xylene for 4 d in 63% yield (eq 3.2).⁵



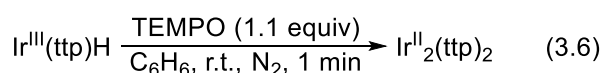
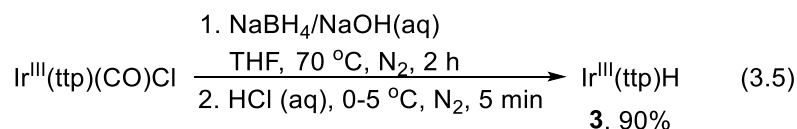
3.3.1.2 Synthesis of Iridium(III) Porphyrin Alkyls

Ir^{III}(ttp)Me and Ir^{III}(ttp)^{*i*}Pr, were synthesized by reductive alkylation of Ir^{III}(ttp)(CO)Cl with alkyl iodide in 52% and 65% yields, respectively (eq 3.3).^{5b,6} Ir^{III}(ttp)Bn was prepared by base-promoted benzylic CHA of toluene with Ir^{III}(ttp)(CO)Cl (eq 3.4).⁷



3.3.1.3 Synthesis of Ir^{III}(ttp)H and Ir^{II}₂(ttp)₂

Ir^{III}(ttp)H was prepared by the reductive protonation of Ir^{III}(ttp)(CO)Cl (eq 3.5).^{5a,7} Ir^{II}₂(ttp)₂ was then prepared by reacting Ir^{III}(ttp)H with TEMPO followed by removal of TEMPO-H (eq 3.6).^{7,8}



3.4 Optimization of Catalytic PCP Hydrogenation with H₂O

3.4.1 With Ir^{III}(ttp)R Pre-catalysts

Based on the successful catalytic hydrogenation of PCP with H₂O using Rh^{III}(ttp)Me pre-catalyst, we first examined the reaction with Ir^{III}(ttp)R pre-catalysts (R = Me, Bn and ^{*i*}Pr). To our delight, PCP was catalytically hydrogenated to give **5** in over 90% yields. (Table 3.2, eq 3.8, entries 1-3). The dehydrogenation product of **5**, 4,4'-dimethylstilbene, was not observed. This accounts for the neat and high yielding conversion from PCP to **5**.

Ir^{III}(ttp)SiEt₃ was a poor pre-catalyst (Table 3.2, eq 3.8, entry 4). It underwent very slow hydrolysis with 81% recovery yield after 48 h. In contrast, hydrolysis of Rh^{III}(ttp)SiEt₃ occurred readily at 150 °C in C₆D₆ to give Rh^{III}(ttp)H and organic co-product HOSiEt₃ (eq 3.9).⁹ H₂O undergoes S_N2 at the Si center of Rh^{III}(ttp)SiEt₃ and Rh^I(ttp)⁻ is the leaving group (pK_a of Rh^{III}(ttp)H ≈ 11).¹⁰ However, Ir^I(ttp)⁻ is a poorer leaving group because Ir^{III}(ttp)H is less acidic.¹¹ Hence, Ir^{III}(ttp)SiEt₃ is less reactive towards hydrolysis.

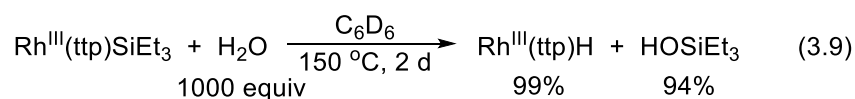
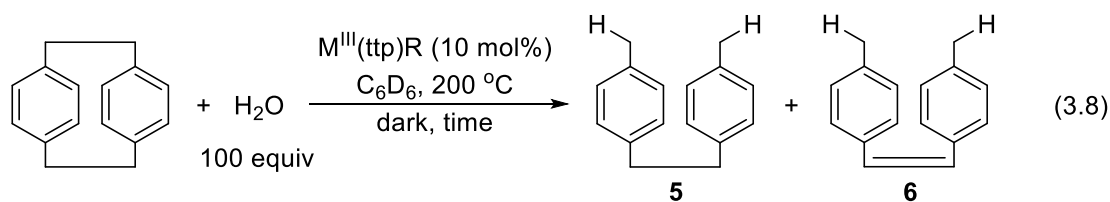


Table 3.2 Catalytic Hydrogenation of PCP using H₂O.



entry	M	R	time / h	yield / %			
				PCP recovery	5	6	R-H ^a
1	Ir	Me	53	0	94	0	0
2	Ir	Bn	48	0	95	0	42
3	Ir	ⁱ Pr	41	0	98	0	24 ^b
4 ^c	Ir	SiEt ₃	48	70	10	0	0 ^d
5	Ir	H	35	0	96	0	0
6	Rh	Me	54	0	78	9	79
7	Rh	ⁱ Pr	50	0	68	10	20 ^e

^a w.r.t. M^{III}(tpp)R

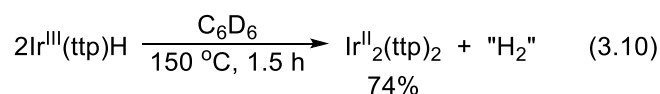
^b 29% propene

^c 81% recovery of Ir^{III}(tpp)SiEt₃

^d HOSiEt₃ was not observed

^e 18% propene

The use of Ir^{III}(tpp)H pre-catalyst resulted in the shortest reaction time (Table 3.2, eq 3.8, entry 5), suggesting a facile conversion of Ir^{III}(tpp)H to Ir^{II}₂(tpp)₂ for CCA. Previous investigations showed that Ir^{II}₂(tpp)₂ was formed from the thermal dehydrogenation of Ir^{III}(tpp)H (eq 3.10).⁷

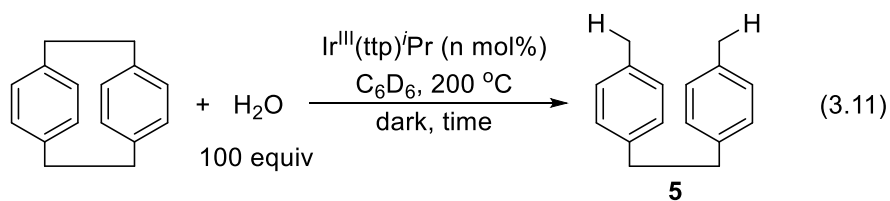


The catalytic efficiency using Ir^{III}(tpp)R pre-catalysts (R = Me, Bn and ⁱPr) followed the order: Ir^{III}(tpp)ⁱPr > Ir^{III}(tpp)Bn > Ir^{III}(tpp)Me. The improved catalytic efficiency from Ir^{III}(tpp)Me to Ir^{III}(tpp)ⁱPr was unique since similar improvement was not observed for Rh^{III}(tpp)Me and Rh^{III}(tpp)ⁱPr (Table 3.2, eq 3.8, entries 6 and 7).

3.4.2 Ir^{III}(ttp)ⁱPr Pre-Catalyst Loading

With Ir^{III}(ttp)ⁱPr as the best and convenient pre-catalyst chosen, we then examined the catalytic hydrogenation of PCP at various Ir^{III}(ttp)ⁱPr loadings. The reaction was very slow with 2.5 mol% of Ir^{III}(ttp)ⁱPr and did not reach completion after 3 d (Table 3.3, eq 3.11, entry 1). Increasing the loading to 5, 10 and 20 mol% gave almost quantitative conversion of PCP to **5** with shortened reaction time, respectively (Table 3.3, eq 3.11, entries 2-4).

Table 3.3 Catalytic PCP Hydrogenation at Various Ir^{III}(ttp)ⁱPr Loadings.



entry	Ir ^{III} (ttp) ⁱ Pr / mol%	time / h	yield / %		TOF / h ⁻¹
			PCP recovery	5	
1	2.5	76	10	74	0.39
2	5	58	0	97	0.33
3	10	41	0	98	0.24
4	20	33	0	95	0.14

Interestingly, the catalytic efficiency in terms of turnover frequency (TOF) decreased with increasing Ir^{III}(ttp)ⁱPr loadings in a slightly concave manner (Figure 3.1). This probably implies that there were non-productive resting states in the catalysis and became dominant at high concentration of iridium porphyrin complexes.

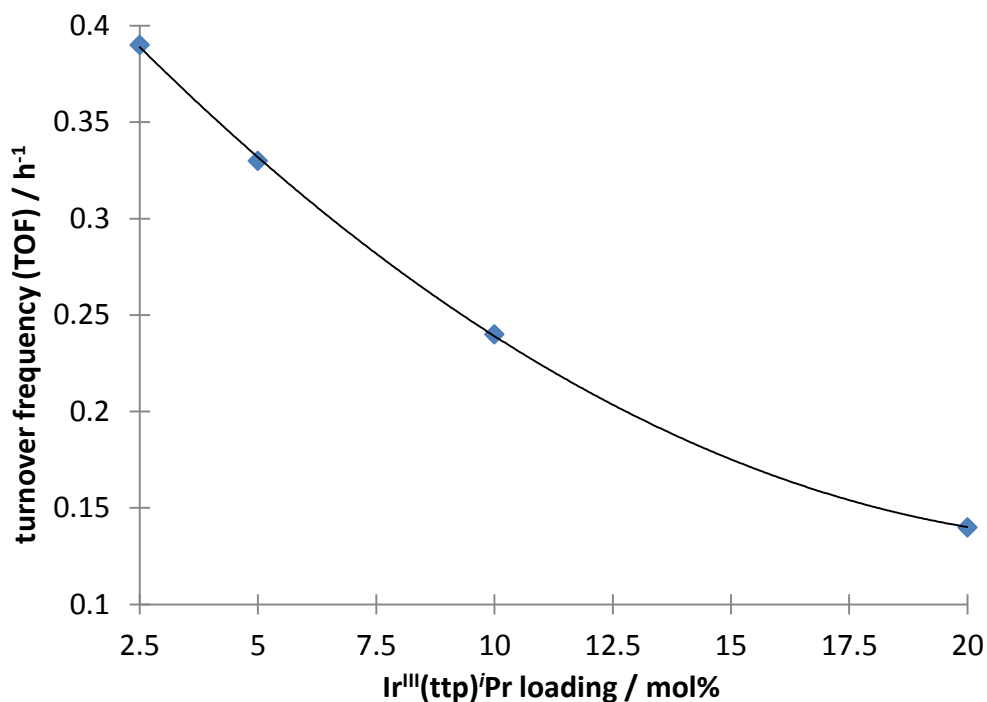
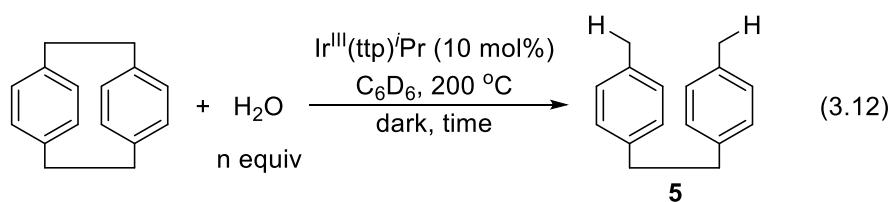


Figure 3.1 Plot of Turnover Frequency Against Ir^{III}(ttp)Pr Loadings.

3.4.3 Water loading Effects

Since H₂O is proposed to be the hydrogenating agent, its loadings were examined. Without any H₂O added, the catalytic hydrogenation of PCP still proceeded to afford **5** in 97% yield after 55 h (Table 3.4, eq. 3.12, entry 1). The C₆D₆ solvent was found to contain ~3 equiv of residual H₂O, it was already excess to PCP. Adding 2.3 equiv of H₂O to the catalytic system yielded 98% of **5** in 59 h (Table 3.3, eq 3.12, entry 2). Since it was difficult to maintain an absolute anhydrous reaction conditions even from using Na metal purified C₆D₆, it was unable to examine whether the hydrogenation would be stopped or not without any H₂O.

Table 3.4 Water Loading Effects.



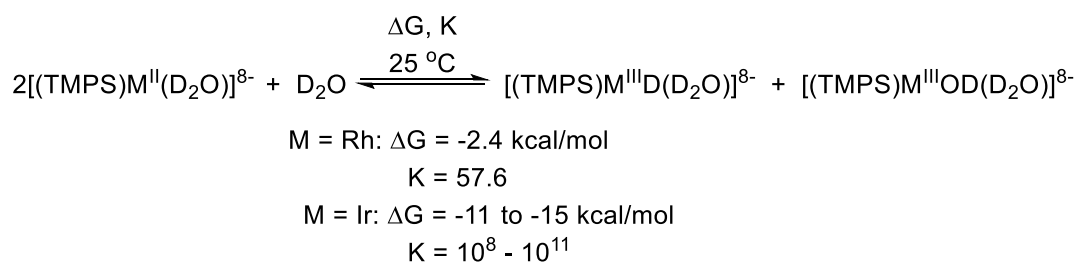
entry	H ₂ O loading ^a / equiv	time / h	yield 5 / %
1	0 ^b	55	97
2	2.3 ^b	59	98
3	100	41	98

^a refer to external H₂O added

^b ~3 equiv of solvent residual H₂O estimated from ¹H NMR

Comparing entries 1 and 3 in Table 3.4, it was surprising that the H₂O loading affected minimally on the reaction rate. The [H₂O] in C₆D₆ at 200 °C reached ~1 M when 100 equiv of H₂O was added, which was 33 times higher than without H₂O added.¹² Hence, direct uncatalyzed hydrogenation using H₂O is unlikely. An alternative hydrogen source may be generated in situ and derived from H₂O.

Wayland has estimated that the oxidative addition of D₂O with water soluble rhodium porphyrin [(TMPS)Rh^{II}(D₂O)]⁸⁻ to form [(TMPS)Rh^{III}D(D₂O)]⁸⁻ and [(TMPS)Rh^{III}OD(D₂O)]⁸⁻ was exergonic by -2.4 kcal/mol at 25 °C (Scheme 3.2).¹³ Analogous oxidative addition with [(TMPS)Ir^{II}(D₂O)]⁸⁻ has been suggested to be more exergonic due to the stronger (TMPS)Ir-D bond than (TMPS)Rh-D bond by 4-6 kcal/mol, and (TMPS)Ir-OD bond than (TMPS)Rh-OD bond by 7-9 kcal/mol (Scheme 3.3).¹⁴



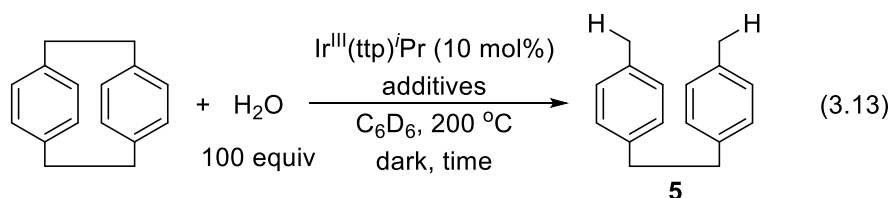
Scheme 3.2 Oxidative Addition of H₂O with Rhodium and Iridium Porphyrin Complexes.

Similarly, Ir^{II}(ttp) may react with H₂O to give Ir^{III}(ttp)H and Ir^{III}(ttp)OH. Ir^{III}(ttp)H is a better hydrogen atom donor than H₂O because of the much weaker Ir-H bond (70 kcal/mol)³ than the HO-H bond (118.8 kcal/mol).¹⁵

3.4.4 Additive Effects

Despite insignificant effects were observed for adding polar additives in the rhodium catalyzed system, we examined two more active benzene/water emulsifying agents in the iridium catalyzed protocol. Dioctyl sodium sulfosuccinate (DSS) and benzyldimethylhexadecylammonium chloride (BDHA) help to solubilize H₂O in non-polar organic solvents by forming reverse micelles.¹⁵ However, no significant enhancement on reaction rate was observed with added DSS and BDHA (Table 3.5, eq 3.13, entries 2-3). The reverse micelles might not survive at 200 °C and hence addition of DSS and BDHA showed no effects. Alternatively, H₂O was already sufficiently soluble in C₆D₆ at 200 °C.

Table 3.5 Polar Additive Effects on Catalytic PCP Hydrogenation.



entry	additives	mol%	time / h	yield / %	
				PCP recovery	5
1	--	--	41	0	98
2	DSS ^a	2.3	45	0	97
3	BDHA ^b	13	41	0	86
4	DMF- <i>d</i> ₇ solvent	--	53	51	30

^a DSS = Dioctyl sodium sulfosuccinate

^b BDHA = benzyldimethylhexadecylammonium chloride

Changing the solvent from C₆D₆ to DMF-*d*₇ was attempted to provide a homogeneous reaction conditions. However, the catalytic hydrogenation was greatly retarded and the reaction was stopped after 53 h (Table 3.5, eq 3.13, entry 4). Ir^{III}(ttp)H and (L)Ir^{III}(ttp)H,

where L might be DMF-*d*₇, CO or (CD₃)₂ND, were found to be the major resting species. The three characteristic Ir-H ¹H signals observed at $\delta = -32.2$, -37.2 and -41.6 ppm supported the coordination of ligands (Figure 3.2). At this stage it was unable to differentiate which ligands were coordinated due to their deuterated nature or lack of ¹H NMR signals.

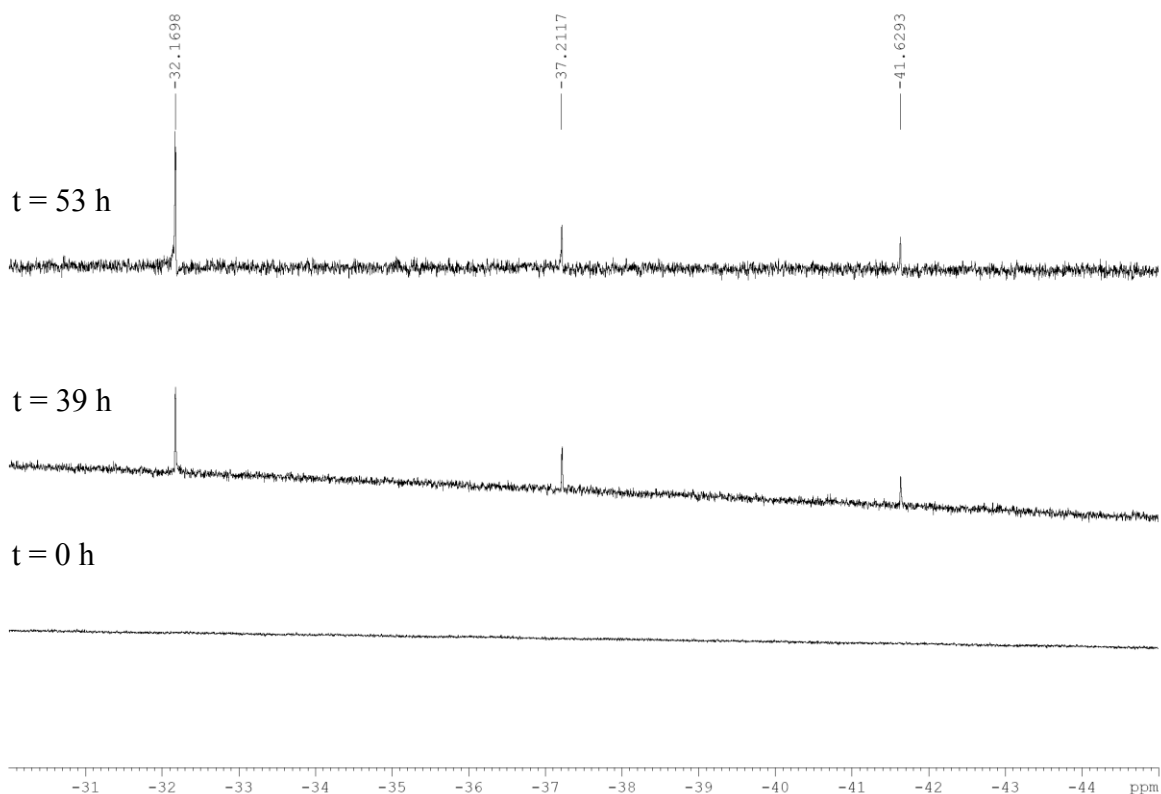
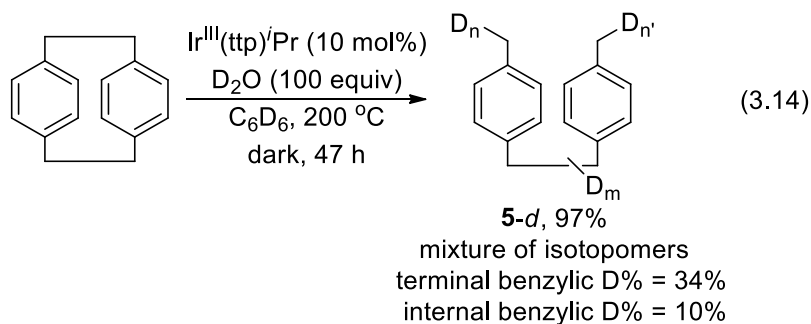


Figure 3.2 Expanded ¹H NMR Spectra Showing Upfield Ir-H Signals in DMF-*d*₇.

3.5 Mechanistic Investigations

3.5.1 Deuterium Labeling Experiments

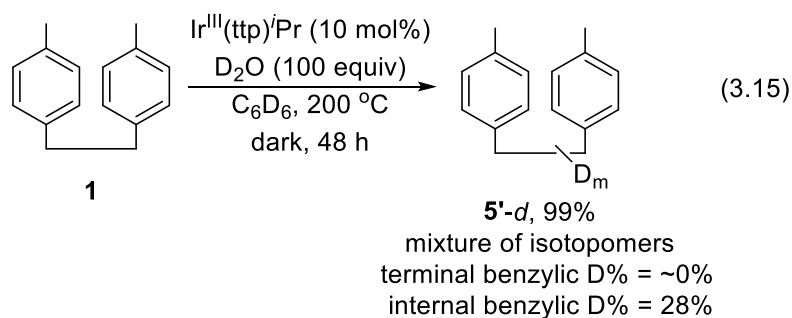
To verify whether water also acted as the hydrogen source in the iridium catalyzed hydrogenation of PCP, D₂O was employed and the deuterium content of the resultant product was analyzed. Under the standard conditions for catalytic hydrogenation of PCP using D₂O, a high yielding conversion from PCP was obtained to yield 97% of deuterium enriched **5-d** (eq 3.14).²⁴ No deuterated PCP was observed during the catalysis.



^1H NMR analysis of the isolated **5-d** gave proton integration ratio with aromatic : internal benzylic : terminal benzylic = 8.00 : 3.60 : 3.95. Hence, the terminal benzylic positions were $((6-3.95)/6)\times 100\% = 34\%$ deuterated. This suggested that there were in average two deuterium atoms incorporated at the terminal benzylic positions. The internal benzylic positions were $((4-3.60)/4)\times 100\% = 10\%$ deuterated.

The degree of internal benzylic H/D exchange was minor when comparing with the rhodium catalyzed H/D exchange. The reduced metalloradical character of iridium(II) porphyrin may lead to less extensive benzylic C-H activation. Indeed, the K_2CO_3 -promoted benzylic C-H activation of toluene in solvent free conditions required higher temperature (200 °C vs 120 °C) and base loading (20 equiv vs 10 equiv) for iridium than rhodium porphyrin complexes.^{7,16}

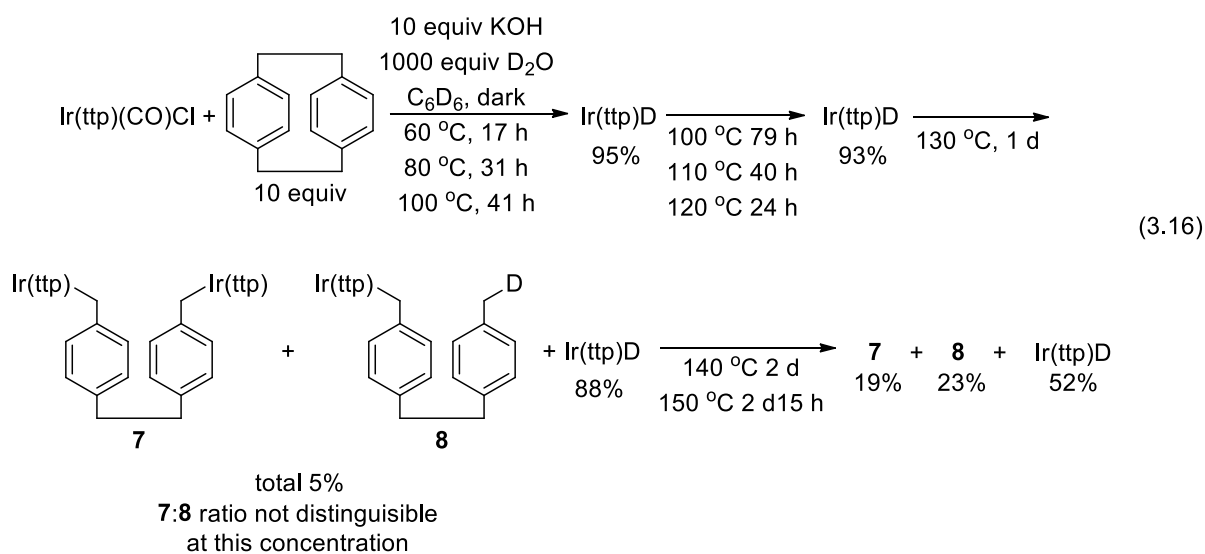
To further verify this hypothesis, we then examined the H/D exchange activity of **5** under identical conditions (eq 3.15). ^1H NMR analysis of the isolated **5'-d** gave proton integration ratio with aromatic : internal benzylic : terminal benzylic = 8.00 : 2.87 : 6.04. Hence, the terminal benzylic positions were $((6-6.04)/6)\times 100\% \approx 0\%$ deuterated, while the internal benzylic positions were $((4-2.87)/4)\times 100\% = 28\%$ deuterated. The absence of terminal benzylic H/D exchange strongly supported that the deuterium incorporation via post-exchange of **5-d** in reaction 3.14 is unlikely. Hence, water was the hydrogenating agent.



3.5.2 CCA via CHA Intermediate

It has been demonstrated that PCP was inert towards benzylic CHA with rhodium porphyrin complexes. To examine whether this is general to iridium porphyrin complexes, we attempted to observe any benzylic C-H activation intermediates $\text{Ir}^{\text{III}}(\text{ttp})(\text{cyclophanyl})$ or catalyzed H/D exchanged product deuterated PCP using analogous strategy. $\text{Ir}^{\text{III}}(\text{ttp})(\text{CO})\text{Cl}$, a convenient precursor of $\text{Ir}^{\text{II}}_2(\text{ttp})_2$ upon reaction with base, was allowed to react with PCP (10 equiv) in the presence of KOH (10 equiv) and D_2O (1000 equiv) in C_6D_6 with gradual heating from 60 °C to 150 °C (Table 3.6, eq 3.16). The reaction progress was closely monitored by ^1H NMR spectroscopy. After 9 d of heating from 60 °C to 120 °C, $\text{Ir}^{\text{III}}(\text{ttp})(\text{CO})\text{Cl}$ was completely consumed to give 93% yield of $\text{Ir}^{\text{III}}(\text{ttp})\text{D}$, without any $\text{Ir}^{\text{III}}(\text{ttp})(\text{cyclophanyl})$ formed. PCP remained unreacted and undeuterated. Upon further heating at 130 °C for 1 d the reaction mixture produced two CCA products di-Ir **7** and mono-Ir **8** in 5% total yield, with 88% recovery of $\text{Ir}^{\text{III}}(\text{ttp})\text{D}$. Finally, **7** and **8** were formed in 19% and 23% yields, with 52% recovery of $\text{Ir}^{\text{III}}(\text{ttp})\text{D}$. Therefore, CCA of PCP occurred directly without prior benzylic CHA process. The rigid structure of PCP discussed in Chapter 2 should be the conclusive reason for the absence of benzylic CHA of PCP.

Table 3.6 Reaction Time Profile of Ir^{III}(ttp)(CO)Cl with PCP under Basic Conditions.

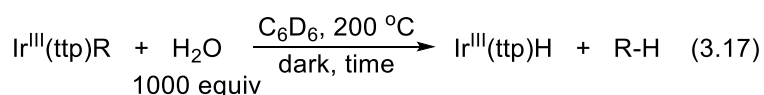


Time / h	Temp / °C	Yield / %				
		Ir ^{III} (ttp)(CO)Cl	Ir ^{III} (ttp)D	7	8	total [Ir]
0	--	100	0	0	0	100
1.5	60	91	7	0	0	98
17	80	66	29	0	0	95
21	80	52	37	0	0	89
24	80	43	50	0	0	93
40	80	33	54	0	0	87
48	100	27	63	0	0	90
64	100	14	80	0	0	94
88	100	0	95	0	0	95
167	110	0	93	0	0	93
191	110	0	83	0	0	83
207	120	0	95	0	0	95
215	120	0	89	0	0	89
231	130	0	94	0	0	94
238	130	0	93	0	0	93
255	140	0	88	5% in total		93
263	140	0	90	3% in total		93
279	140	0	83	6% in total		89
294	140	0	88	8% in total		96
303	150	0	87	9% in total		96
318	150	0	76	7	11	94
342	150	0	62	14	20	96
366	150	0	52	19	23	94

3.5.3 Hydrolysis of Ir^{III}(ttp)R

After figuring out the hydrogenating agent, we examined the reasons behind the pre-catalyst effect on shortening the catalysis time. Based on the proposed catalytic cycle for rhodium catalyzed hydrogenation of PCP, we suggested that the iridium catalyzed protocol operated similarly and the hydrolysis of Ir^{III}(ttp)R pre-catalyst to Ir^{II}(ttp) for CCA (the induction period) was the only factor that differentiated the catalysis time. Therefore we investigated the hydrolysis of Ir^{III}(ttp)R (R = Me, Bn and ⁱPr).¹⁷

Table 3.7. Hydrolysis of Ir^{III}(ttp)R



entry	R	time / h	yield / %		
			Ir ^{III} (ttp)R recovery	Ir ^{III} (ttp)H	R-H
1	Me	75	81	8	0 ^a
2	Bn	43	3	56	72
3	ⁱ Pr	44	0	76	26 ^b

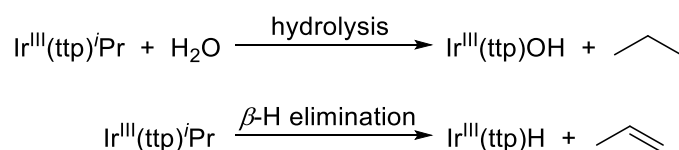
^a the [CH₄] in C₆D₆ might be too low to be observed

^b 68% yield of propene was formed

Unexpectedly, Ir^{III}(ttp)Me was quite stable towards hydrolysis (Table 3.7, eq 3.17, entry 1). 81% of Ir^{III}(ttp)Me was recovered after 75 h of heating at 200 °C with 8% yield of Ir^{III}(ttp)H. The organic co-product CH₄ was not observed. It might be formed in little amount due to the partial hydrolysis of Ir^{III}(ttp)Me. Hence CH₄ was too diluted in C₆D₆ to be detected by ¹H NMR spectroscopy.

Ir^{III}(ttp)Bn and Ir^{III}(ttp)ⁱPr were hydrolyzed in similar reaction time of 44 h to give 56% and 76% yields of Ir^{III}(ttp)H, respectively (Table 3.7, eq 3.17, entries 2 and 3). Toluene was formed exclusively in 72% yield in the hydrolysis of Ir^{III}(ttp)Bn. Ir^{III}(ttp)ⁱPr underwent competitive hydrolysis and β-H elimination to give the organic co-products propane and

propene in 26% and 68% yields, respectively. The propane : propene ratio of about 1 : 2.5 reflected that β -H elimination is a more facile process (Scheme 3.3).

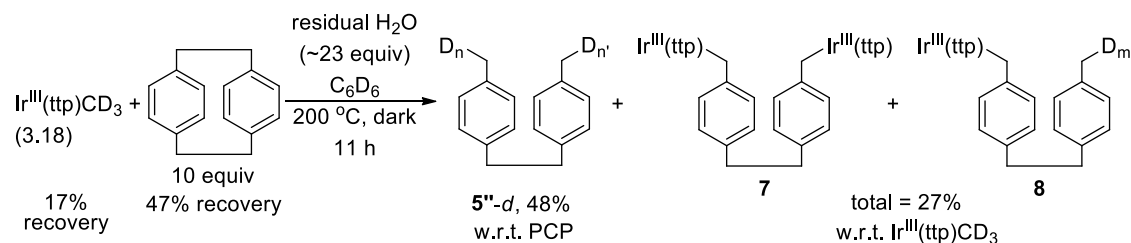


Scheme 3.3 Competitive Hydrolysis and β -H Elimination of $\text{Ir}^{\text{III}}(\text{ttp})^i\text{Pr}$.

The generally slow hydrolysis of $\text{Ir}^{\text{III}}(\text{ttp})\text{R}$ were unable to account for the fast turnovers in catalytic hydrogenation of PCP. The hydrolytic stable $\text{Ir}^{\text{III}}(\text{ttp})\text{Me}$ requires amendments in the initial mechanistic assumption. The parallel decomposition of $\text{Ir}^{\text{III}}(\text{ttp})^i\text{Pr}$ was mechanistic interesting. Therefore, we pursued further investigations on $\text{Ir}^{\text{III}}(\text{ttp})\text{Me}$ and $\text{Ir}^{\text{III}}(\text{ttp})^i\text{Pr}$.

3.5.3.1 Investigation with $\text{Ir}^{\text{III}}(\text{ttp})\text{CD}_3$

To investigate how $\text{Ir}^{\text{III}}(\text{ttp})\text{Me}$ pre-catalyst was consumed in the catalytic hydrogenation of PCP, we traced the fate of deuterium by reacting $\text{Ir}^{\text{III}}(\text{ttp})\text{CD}_3$ with PCP in C_6D_6 . $\text{Ir}^{\text{III}}(\text{ttp})\text{CD}_3$ reacted with PCP at 200 °C for 11 h to yield the CCA products di-Ir **7** and mono-Ir **8** in 27% total yields w.r.t. $\text{Ir}^{\text{III}}(\text{ttp})\text{CD}_3$, with 17% recovery of $\text{Ir}^{\text{III}}(\text{ttp})\text{CD}_3$ (eq 3.18). PCP was catalytically converted to 48% of **5''-d**, with 47% recovery of PCP. The solvent residual H_2O was in excess to PCP and therefore catalytic conversion was occurred.



The ^2H NMR spectrum of this reaction mixture at $t = 11$ h showed characteristic resonances at $\delta = -5.95$ ppm and 2.02 ppm, which were assigned as $\text{Ir}^{\text{III}}(\text{ttp})\text{-CD}_3$ and terminal benzylic D of $\mathbf{5}''\text{-}d$, respectively (Figure 3.3). A ^2H signal at $\delta = 1.28$ ppm was also observed, which its identity was unclear. Based on its chemical shift, it might be deuterated alkane. At this stage, it could be concluded that the D atoms in $\text{Ir}^{\text{III}}(\text{ttp})\text{CD}_3$ were transferred to the terminal benzylic positions of $\mathbf{5}''\text{-}d$.

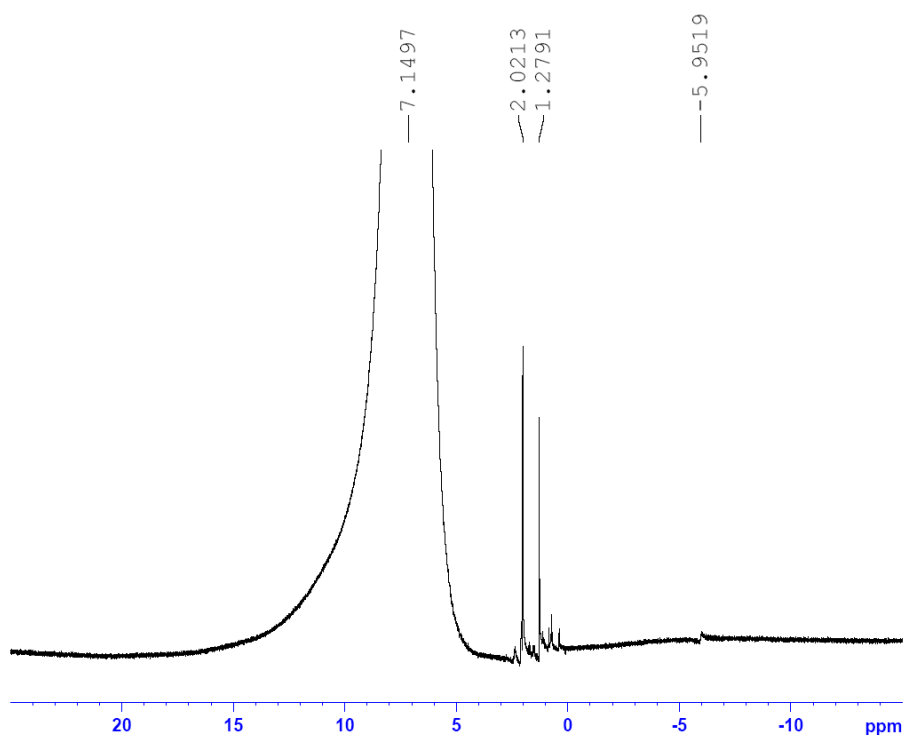
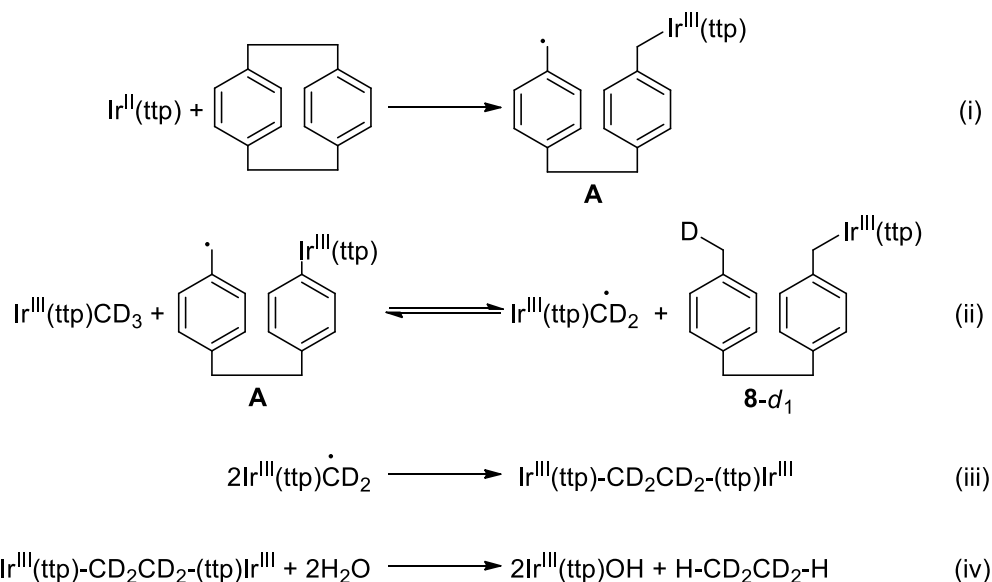


Figure 3.3 ^2H NMR Spectrum of Reaction 3.18 at $t = 11$ h.

To account for this observation, a possible reaction mechanism was proposed in Scheme 3.4. Initially, trace amount of $\text{Ir}^{\text{II}}(\text{ttp})$, formed from the slow hydrolysis of $\text{Ir}^{\text{III}}(\text{ttp})\text{CD}_3$, undergoes homolytic radical substitution at the benzylic carbon of PCP to give the iridium benzylic radical intermediate **A** (step i), analogous to the $\text{Rh}^{\text{II}}(\text{ttp})$ -catalyzed ring-opening of *c*-octane with $\text{Rh}^{\text{III}}(\text{ttp})\text{H}$.¹⁸ It then abstracts a deuterium atom from the abundant $\text{Ir}^{\text{III}}(\text{ttp})\text{CD}_3$ to give mono-Ir **8-d**₁ and $\text{Ir}^{\text{III}}(\text{ttp})\text{CD}_2$ carbon-centered radical, which was estimated to be 16.6 kcal/mol uphill (step ii).¹⁹ Two $\text{Ir}^{\text{III}}(\text{ttp})\text{CD}_2$ carbon-centered radicals

combine to form $\text{Ir}^{\text{III}}(\text{ttp})\text{CD}_2\text{CD}_2(\text{ttp})\text{Ir}^{\text{III}}$ (step iii). It might be formed in very little amount such that the characteristic very up-field Ir- CD_2CD_2 -Ir signal at around -10 ppm was not observed in the ^2H NMR spectrum.²¹ Hydrolysis of $\text{Ir}^{\text{III}}(\text{ttp})\text{CD}_2\text{CD}_2(\text{ttp})\text{Ir}^{\text{III}}$ yields partial deuterated ethane which accounted for the ^2H NMR signal observed at $\delta = 1.28$ ppm (step iv).

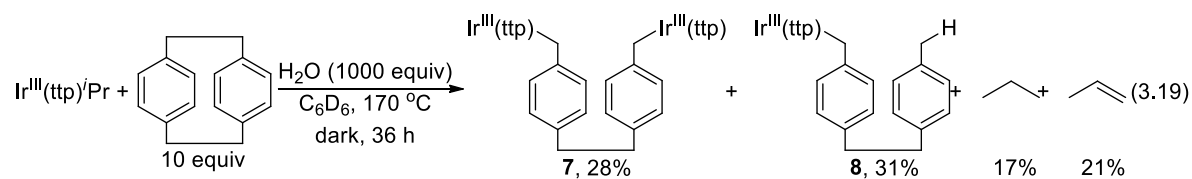


Scheme 3.4 Proposed Mechanism for the Reaction between $\text{Ir}^{\text{III}}(\text{ttp})\text{CD}_3$ and PCP.

3.5.3.2 Investigation with $\text{Ir}^{\text{III}}(\text{ttp})^i\text{Pr}$

$\text{Ir}^{\text{III}}(\text{ttp})^i\text{Pr}$ underwent parallel hydrolysis and β -H elimination in its hydrolysis study and in catalytic hydrogenation of PCP both supported by the formation of propane and propene. To investigate whether these parallel processes aided $\text{Ir}^{\text{III}}(\text{ttp})^i\text{Pr}$ as the most active pre-catalyst, the initial stage of the catalytic hydrogenation of PCP was closely monitored by ^1H NMR spectroscopy. In order to slow down any fast transformations or to observe unstable intermediates, the reaction was carried out at 170 °C instead of 200 °C.

Table 3.8 Initial Stage of Catalytic Hydrogenation of PCP using Ir^{III}(ttp)ⁱPr at 170 °C



*all yields w.r.t. Ir^{III}(ttp)ⁱPr

Time / h	Yield / %						
	Ir ^{III} (ttp) ⁱ Pr	7	8	total Ir complexes	propane	propene	total gases
0	100	0	0	100	0	0	0
3	85	10	0	95	0	6	6
6	61	16	8	85	5	10	15
8	46	19	10	75	7	12	19
10.5	39	24	14	77	8	16	24
14	30	32	25	87	15	18	33
18	14	29	25	68	20	23	43
21	7	30	32	69	15	24	39
36	0	28	31	59	17	21	38

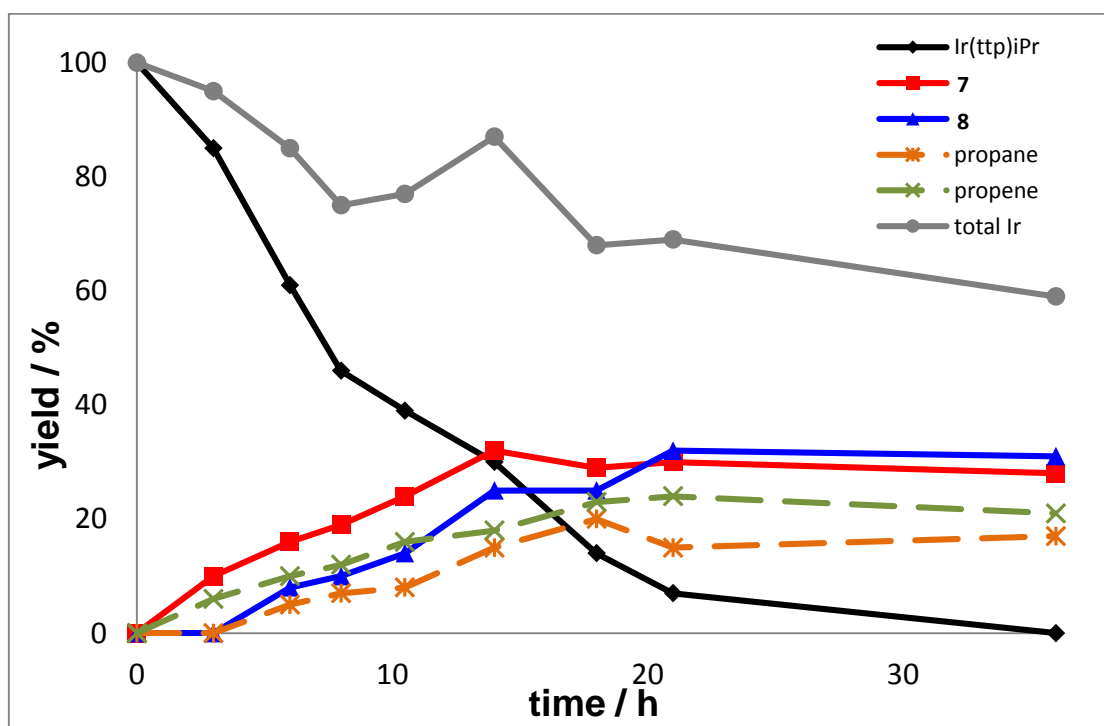
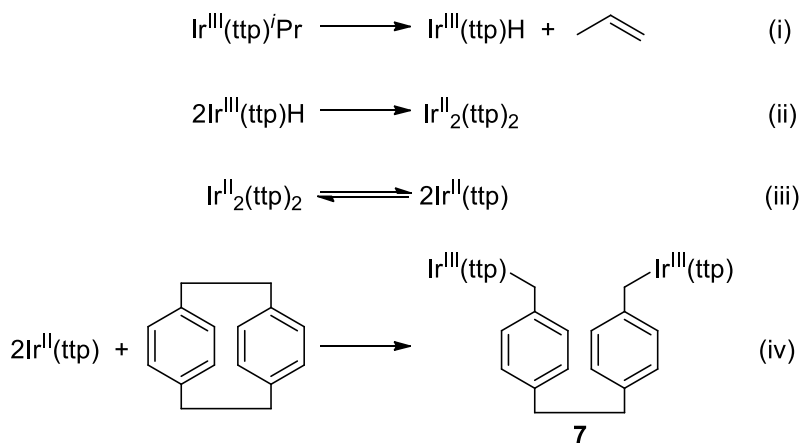


Figure 3.3 Reaction Profile of Reaction 3.19.

Initially, 15% of $\text{Ir}^{\text{III}}(\text{ttp})^i\text{Pr}$ was consumed to produce 10% of CCA product di-Ir **7** and 6% of propene after 3 h (Table 3.8, eq 3.19, Figure 3.3). $\text{Ir}^{\text{III}}(\text{ttp})^i\text{Pr}$ first reacted via β -H elimination to give propene (Scheme 3.5, step i).²¹ $\text{Ir}^{\text{III}}(\text{ttp})\text{H}$ underwent facile dehydrogenation to give $\text{Ir}^{\text{II}}_2(\text{ttp})_2$ rapidly (step ii).⁷ $\text{Ir}^{\text{II}}_2(\text{ttp})_2$ then dissociated to give $\text{Ir}^{\text{II}}(\text{ttp})$ for CCA to give **7** (steps iii and iv).



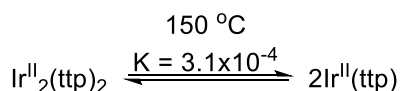
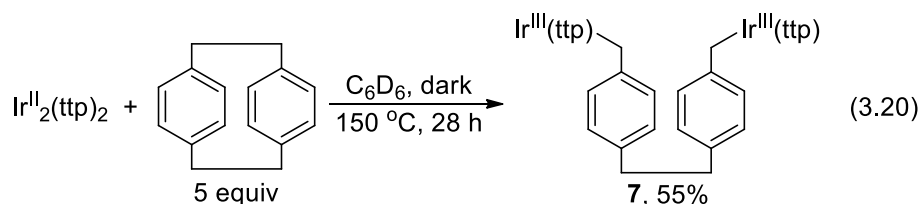
Scheme 3.5 Initial Reaction Pathway of $\text{Ir}^{\text{III}}(\text{ttp})^i\text{Pr}$ via β -H Elimination.

Further heating to 6 h produced both CCA products di-Ir **7** and mono-Ir **8** in 16% and 8% yields, respectively. Hydrolysis of $\text{Ir}^{\text{III}}(\text{ttp})^i\text{Pr}$ was now observed to yield 5% of propane and $\text{Ir}^{\text{III}}(\text{ttp})\text{OH}$, which was quickly reduced to $\text{Ir}^{\text{II}}_2(\text{ttp})_2$.²³ $\text{Ir}^{\text{II}}_2(\text{ttp})_2$ reacted rapidly with PCP to yield **7** (Scheme 3.5, steps iii and iv, and see eq 3.20). After 36 h, $\text{Ir}^{\text{III}}(\text{ttp})^i\text{Pr}$ was completely consumed to yield 28% of **7**, 31% of **8**, 17% of propane and 21 % of propene. No benzylic C-H activation of PCP was observed to form any $\text{Ir}^{\text{III}}(\text{ttp})(\text{cyclophanyl})$ intermediates.⁷

Hence, β -H elimination of $\text{Ir}^{\text{III}}(\text{ttp})^i\text{Pr}$ followed by thermal dehydrogenation was a faster pathway than hydrolysis to provide $\text{Ir}^{\text{II}}_2(\text{ttp})_2$ for CCA. Alternatively, $\text{Ir}^{\text{III}}(\text{ttp})\text{H}$ reacted with PCP directly to afford the CCA product mono-Ir **8**. $\text{Ir}^{\text{III}}(\text{ttp})\text{H}$ and $\text{Ir}^{\text{II}}_2(\text{ttp})_2$ were the possible intermediates for the CCA of PCP. Their stoichiometric reactions with PCP were then examined independently.

3.5.4 Reaction of Ir^{II}₂(ttp)₂ with PCP

At 150 °C, Ir^{II}₂(ttp)₂ was completely reacted with PCP to give 55% yield of CCA product di-Ir **7** after 28 h (eq 3.20). Under thermal conditions, Ir^{II}₂(ttp)₂ equilibrates with Ir^{II}(ttp) due to the weak Ir-Ir bond.²⁴ The Ir-Ir BDE in Ir^{II}₂(ttp)₂ was estimated 20 kcal/mol using the sterically similar Ir^{II}₂(txp)₂ as reference.³ The equilibrium constant for Ir^{II}₂(ttp)₂ dissociation at 150 °C was evaluated to be 3.1 x 10⁻⁴ (Scheme 3.6). This closely resembled the bi-metalloradical CCA of PCP with Rh^{II}(tmp).



$$\Delta G = \Delta H - T\Delta S$$

$$\Delta H = \text{Ir-Ir BDE in Ir}^{\text{II}}_2(\text{txp})_2 = 20 \text{ kcal mol}^{-1}$$

$$\text{assume } S = \text{entropy of H}_2 = 31.2 \text{ cal mol}^{-1} \text{ K}^{-1} \text{ [25]}$$

$$\Delta G = 20 - (423)(0.0312) = 6.8 \text{ kcal mol}^{-1}$$

$$\Delta G = -RT \ln K$$

$$6.8 = -(1.9872 \times 10^{-3})(423) \ln K$$

$$K = 3.1 \times 10^{-4}$$

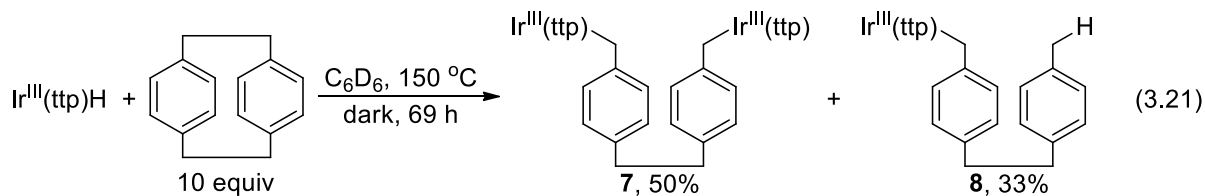
Scheme 3.6 Equilibrium Estimation for the Ir^{II}₂(ttp)₂ Dissociation.

3.5.5 Reaction of Ir^{III}(ttp)H with PCP

Ir^{III}(ttp)H reacted with PCP at 150 °C in 35 h to give di-Ir **7** and mono-Ir **8** in 12% and 21% yields, respectively, with 37% recovery yield of Ir^{III}(ttp)H (Table 3.9, eq 3.21 and Figure 3.4). Interestingly, the mono-Ir **8** was the major CCA product throughout the first 35 h

of the reaction. Then, di-Ir **7** took the lead as the major product upon further heating from 35 h to 69 h, yielding 50% of **7** and 33% of **8** as the minor product, with complete consumption of Ir^{III}(ttp)H.

Table 3.9 Reaction of Ir^{III}(ttp)H with PCP at 150 °C.



Time / h	Yield / %			total Ir complexes
	Ir ^{III} (ttp)H	7	8	
0	100	0	0	100
2	100	0	0	100
5.5	92	3	7	102
9.5	80	4	9	93
28.5	53	11	19	83
35	37	12	21	70
52	22	29	24	75
69	0	50	33	83

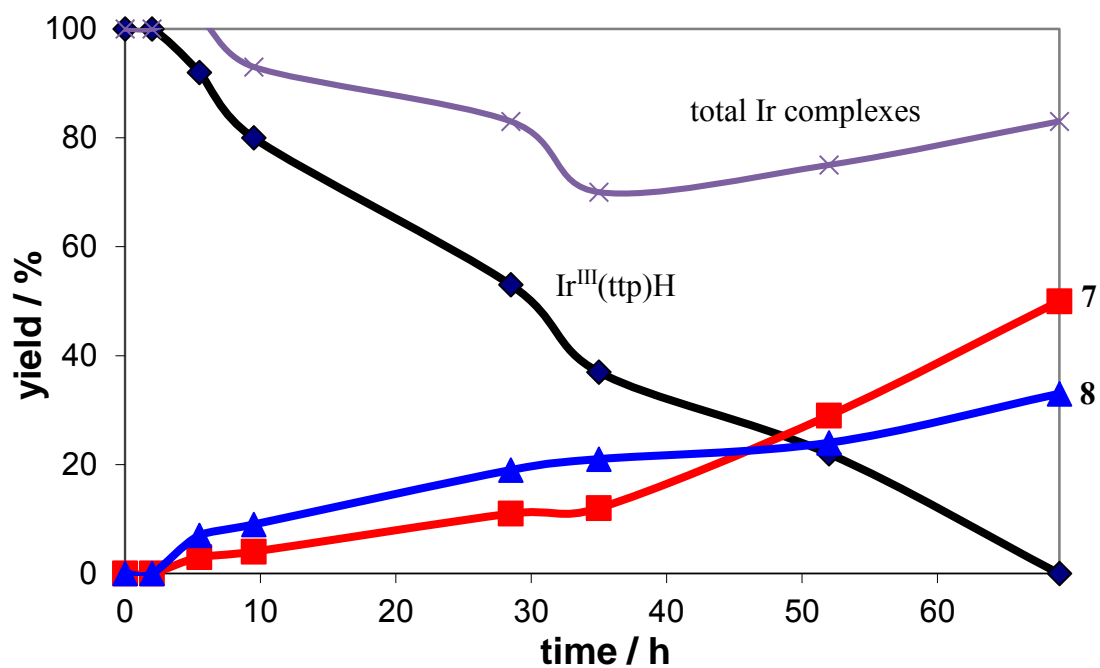
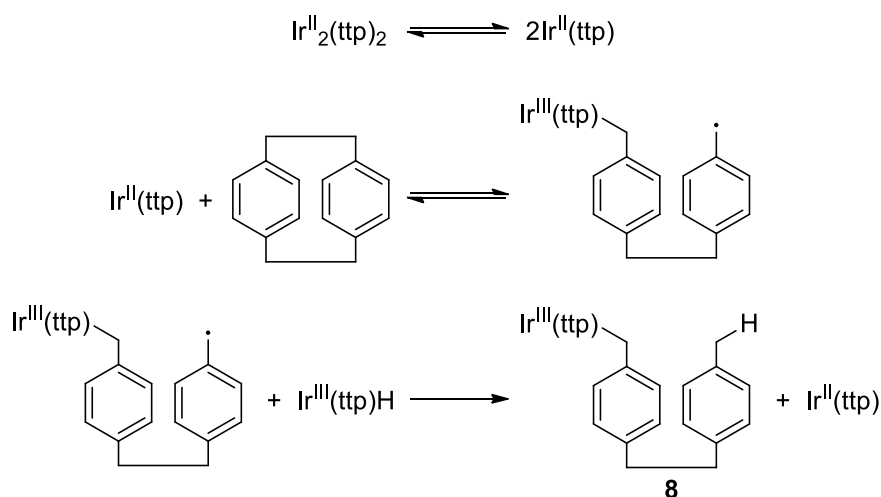
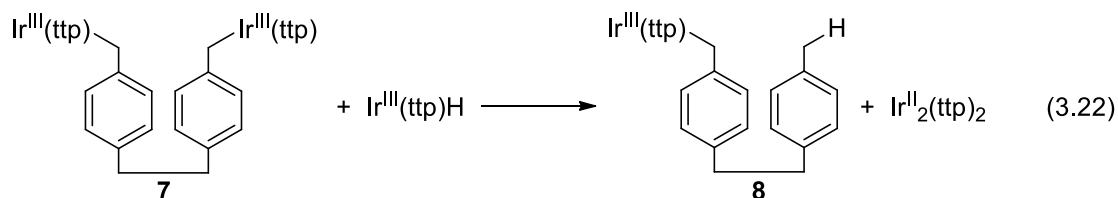


Figure 3.4 Reaction Profile of Reaction 3.21.

The formation of di-Ir **7** can be well accounted by the in situ formation of Ir^{II}(ttp) from Ir^{III}(ttp)H followed by CCA with PCP as discussed previously. However, the preferential formation of mono-Ir **8** at the initial stage of reaction contradicted with the bi-metalloradical CCA proposal. Since the hydrolysis of Ir^{III}(ttp)Bn, as a simplified structural model of **7**, was slow at 200 °C, the hydrolysis of **7** by the solvent residual water at 150 °C was unlikely a source of **8**. We suspected that the abundant Ir^{III}(ttp)H present in the reaction mixture has promoted two reaction channels to form **8** in a much faster manner. The two pathways are: (1) Ir^{II}(ttp)-catalyzed 1,2-addition of Ir^{III}(ttp)H across the benzylic C-C bond of PCP to form **8**, bypassing the formation of **7** (Scheme 3.7)¹⁸ and (2) bi-molecular reductive elimination from Ir^{III}(ttp)H and **7** to give **8** and Ir^{II}₂(ttp)₂ (eq 3.22).²⁶ These two possibilities were then investigated.



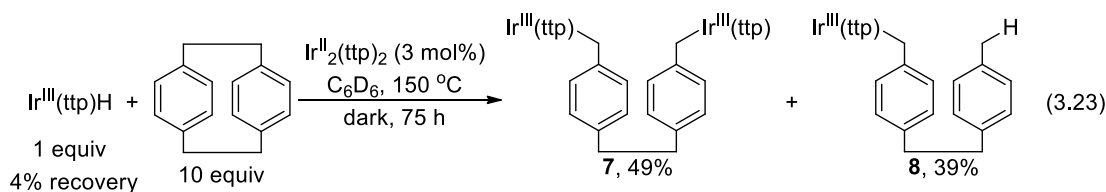
Scheme 3.7 Ir^{II}(ttp)-Catalyzed 1,2-Addition of Ir^{III}(ttp)H.



3.5.5.1 Ir^{II}(ttp)-Catalyzed 1,2-Addition of Ir^{III}(ttp)H

With catalytic amount of Ir^{II}₂(ttp)₂ (3 mol%), Ir^{III}(ttp)H reacted with PCP at 150 °C in C₆D₆ to yield 49% of **7** and 39% of **8** in 75 h (Table 3.10, eq 3.23, Figure 3.5). The reaction profile was very similar to reaction 3.21 without Ir^{II}₂(ttp)₂ added. The mono-Ir **8** was the major CCA product at initial and then shifted to di-Ir **7** as the major product. In addition, the rate of formation of **8** was not enhanced in the presence of Ir^{II}₂(ttp)₂ (Figure 3.6). Therefore, the Ir^{II}(ttp)-catalyzed 1,2-addition of Ir^{III}(ttp)H pathway does not operate at 150 °C. Kinetically, the much lower equilibrium concentration of Ir^{II}(ttp) than that of Rh^{II}(ttp) at same temperature should be a key reason.

Table 3.10. Reaction Ir^{III}(ttp)H with PCP with 3 mol% of Ir^{II}₂(ttp)₂ at 150 °C.



Time / h	Yield / %			
	Ir ^{III} (ttp)H	6	7	total Ir complexes
0	100	0	0	100
6	95	1	3	99
12	87	3	9	99
27	67	11	15	93
36	53	17	21	91
51	30	36	32	98
75	4	49	39	92

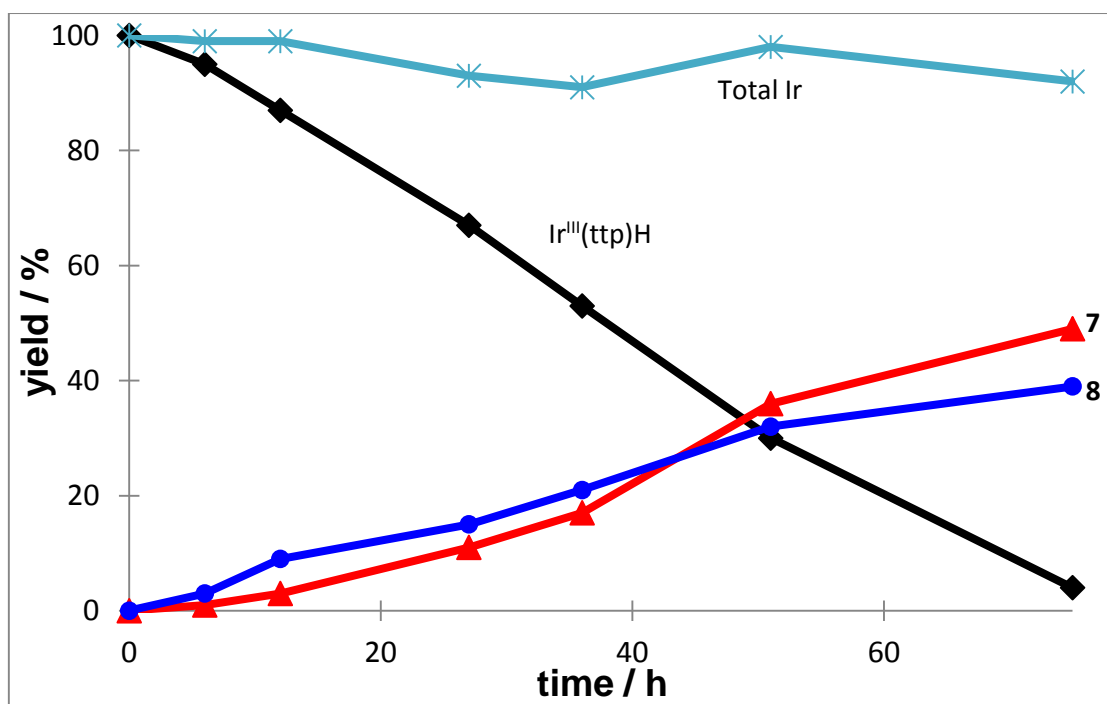


Figure 3.5 Reaction Time Profile of Reaction 3.23.

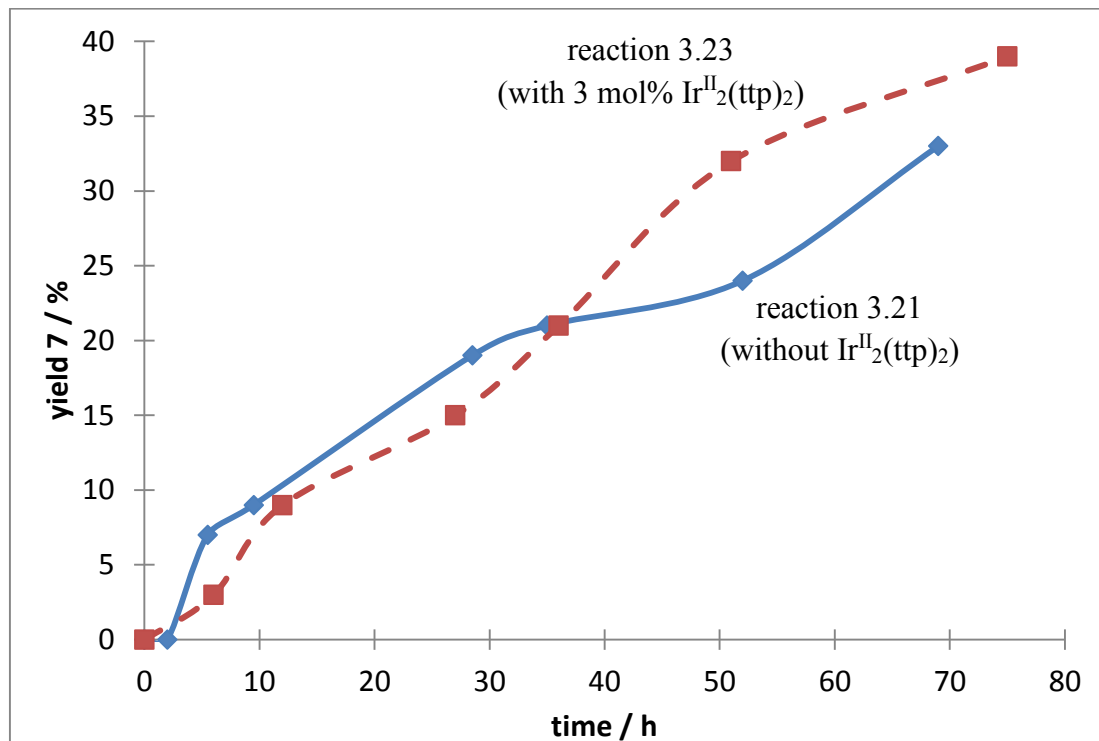
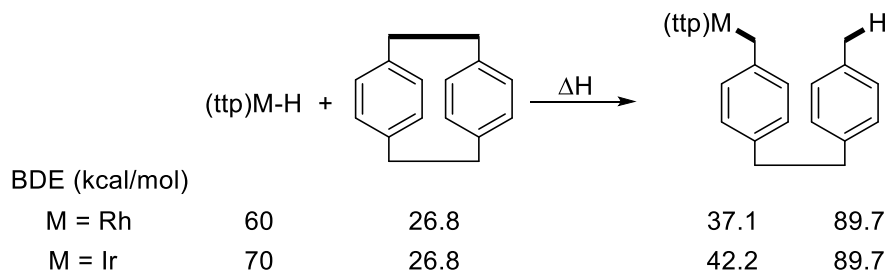


Figure 3.6 Comparison of the Formation of Mono-Ir 8 from Reactions 3.21 and 3.23.

To better understand why the Ir^{II}(ttp)-catalyzed 1,2-addition of Ir^{III}(ttp)H pathway was not operating, the reaction thermodynamics of this pathway and bi-metalloradical CCA with rhodium and iridium scenarios were estimated (Scheme 3.8).

In the M^{II}(ttp)-catalyzed 1,2-addition of M^{III}(ttp)H pathway, the breaking of stronger Ir-H bond is 10 kcal/mol uphill than the breaking of Rh-H bond.²⁷ This energetically uphill demand cannot be compensated by forming the Ir-C bond since it is only 5.1 kcal/mol stronger than the Rh-C bond.²⁸ On the contrary, the bi-metalloradical activation of PCP with Ir^{II}₂(ttp)₂ is more favored than with Rh^{II}₂(ttp)₂. Although the breaking of stronger Ir-Ir bond is 8 kcal/mol uphill than the breaking of Rh-Rh bond, it can be compensated by forming of two Ir-C bonds which is 10.2 kcal/mol downhill than forming two Rh-C bonds.

M^{II}(ttp)-catalyzed 1,2-addition of M^{III}(ttp)H

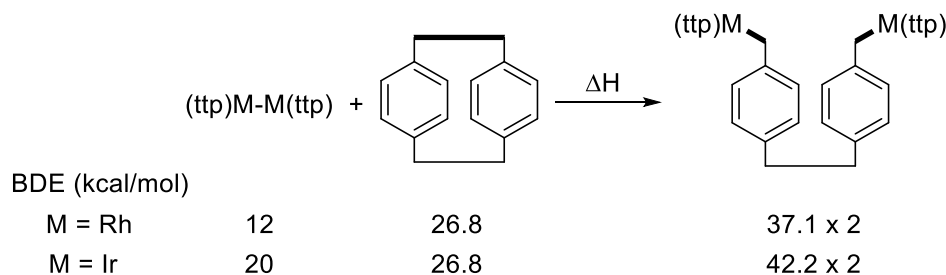


For Rh: $\Delta H = 60 + 26.8 - 37.1 - 89.7 = -40.0$ kcal/mol

For Ir: $\Delta H = 70 + 26.8 - 42.2 - 89.7 = -35.1$ kcal/mol

Ir is **less favorable** than Rh in this process by 4.9 kcal/mol.

CCA with M^{II}₂(ttp)₂



For Rh: $\Delta H = 12 + 26.8 - (37.1 \times 2) = -35.4$ kcal/mol

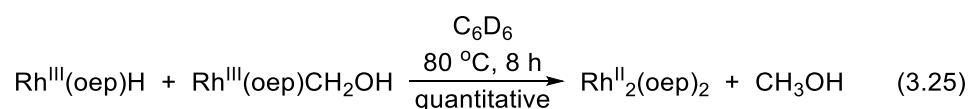
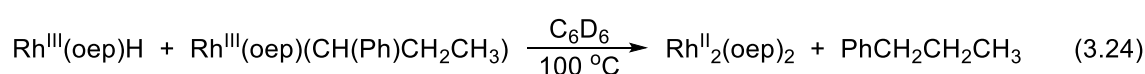
For Ir: $\Delta H = 20 + 26.8 - (42.2 \times 2) = -37.6$ kcal/mol

Ir is **more favorable** than Rh in this process by 2.2 kcal/mol.

Scheme 3.8 Thermodynamic Comparison on Two CCA Pathways.

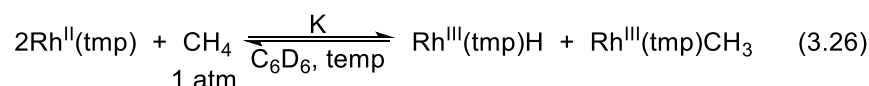
3.5.5.2 Bi-molecular Reductive Elimination with Ir^{III}(ttp)H

Wayland has reported various examples of intermolecular reductive elimination from Rh^{III}(por)H and Rh^{III}(por)R to give Rh^{II}(por) and alkanes,²⁹ alkylaromatics²⁶ and MeOH.³⁰ The bi-molecular reductive elimination from Rh^{III}(oep)H and Rh^{III}(oep)(CH(Ph)CH₂CH₃) at 100 °C in C₆D₆ gave *n*-propylbenzene (eq 3.24).²⁶ Similarly, quantitative bi-molecular reductive elimination of MeOH from Rh^{III}(oep)CH₂OH and Rh^{III}(oep)H has been reported (eq 3.25).³⁰



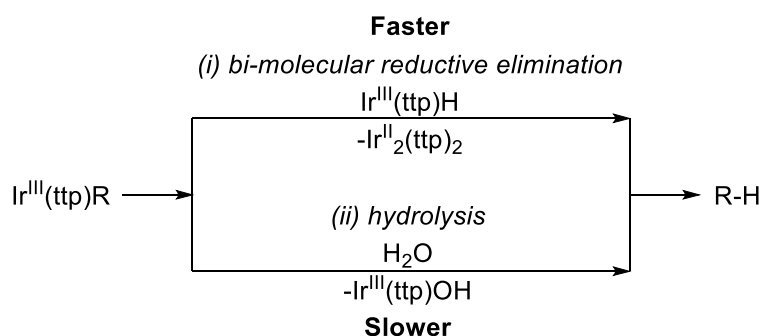
In the reversible C-H bond activation of CH₄ with Rh^{II}(tmp) to give Rh^{III}(tmp)CH₃ and Rh^{III}(tmp)H, the bi-molecular reductive elimination of CH₄ proceeded favorably at elevated temperatures (Table 3.11, eq 3.26).²⁹

Table 3.11 Reversible C-H Activation of CH₄ with Rh^{II}(tmp).



entry	Temp / °C	K
1	80	7300±700
2	100	3300±400
3	120	1100±200

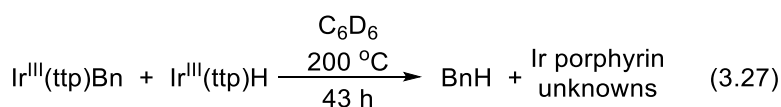
We propose that this kind of bi-molecular reductive elimination is general to iridium porphyrin system. If the formation of R-H from Ir^{III}(ttp)H and Ir^{III}(ttp)R (Scheme 3.9, pathway i) is faster than the hydrolysis of Ir^{III}(ttp)R (Scheme 3.9, pathway ii), this will provide an additional and faster pathway for C-H bond formation.



Scheme 3.9 Parallel Pathway for the Formation of R-H.

To our delight, $\text{Ir}^{\text{III}}(\text{ttp})\text{H}$ reacted with $\text{Ir}^{\text{III}}(\text{ttp})\text{Bn}$ at 200 °C to give 78% yield of toluene in 43 h (Table 3.12, eq 3.27, Figures 3.7). The initial rates of $\text{Ir}^{\text{III}}(\text{ttp})\text{Bn}$ consumption and toluene formation were both 3 times faster than that of $\text{Ir}^{\text{III}}(\text{ttp})\text{Bn}$ hydrolysis, estimated from the initial 3 h of the two reactions (Figures 3.8 and 3.9), supporting the promoting effect of $\text{Ir}^{\text{III}}(\text{ttp})\text{H}$ towards faster hydrogenation.

Table 3.12 Reaction Time Profile of Bi-molecular Reductive Elimination between $\text{Ir}^{\text{III}}(\text{ttp})\text{Bn}$ and $\text{Ir}^{\text{III}}(\text{ttp})\text{H}$



Time / h	Yield / %			
	$\text{Ir}^{\text{III}}(\text{ttp})\text{Bn}^{\text{a}}$	$\text{Ir}^{\text{III}}(\text{ttp})\text{H}^{\text{b}}$	BnH ^a	Ir por unknowns ^c
0	100	100	0	0
1	74	117	25	11
2	64	95	32	10
6	53	116	48	17
21	27	117	66	22
28	19	120	73	26
43	11	107	78	30

^a w.r.t. $\text{Ir}^{\text{III}}(\text{ttp})\text{Bn}$

^b w.r.t. $\text{Ir}^{\text{III}}(\text{ttp})\text{H}$

^c w.r.t. total [Ir] at initial

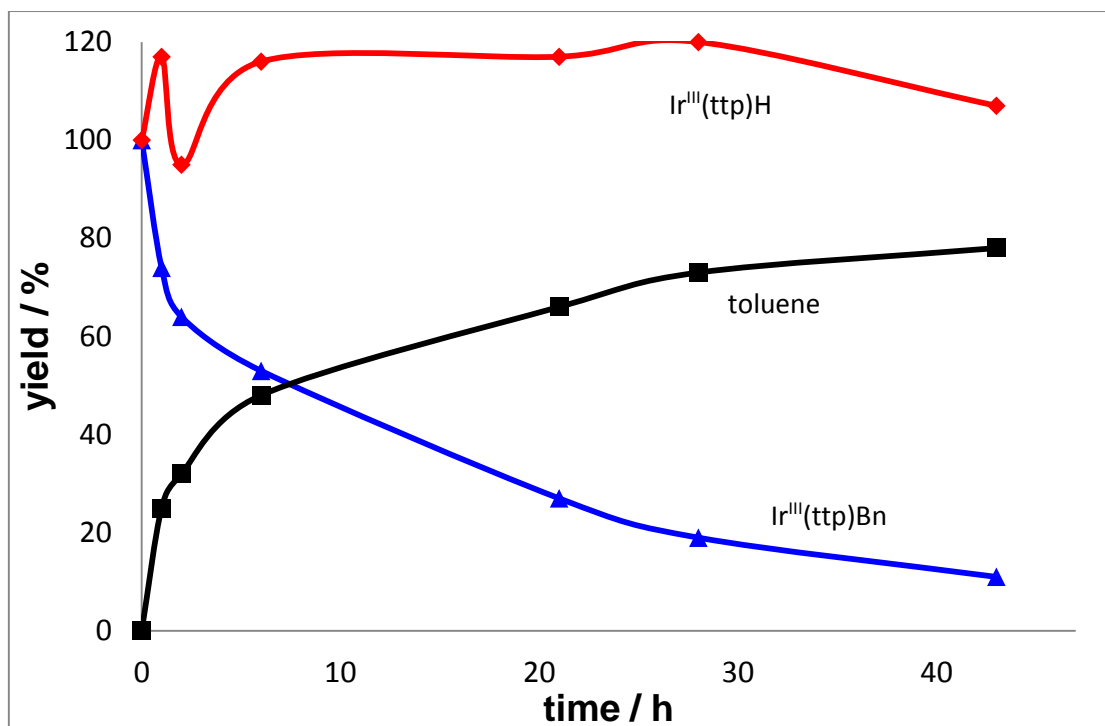


Figure 3.7 Reaction Time Profile of Reaction 3.27.

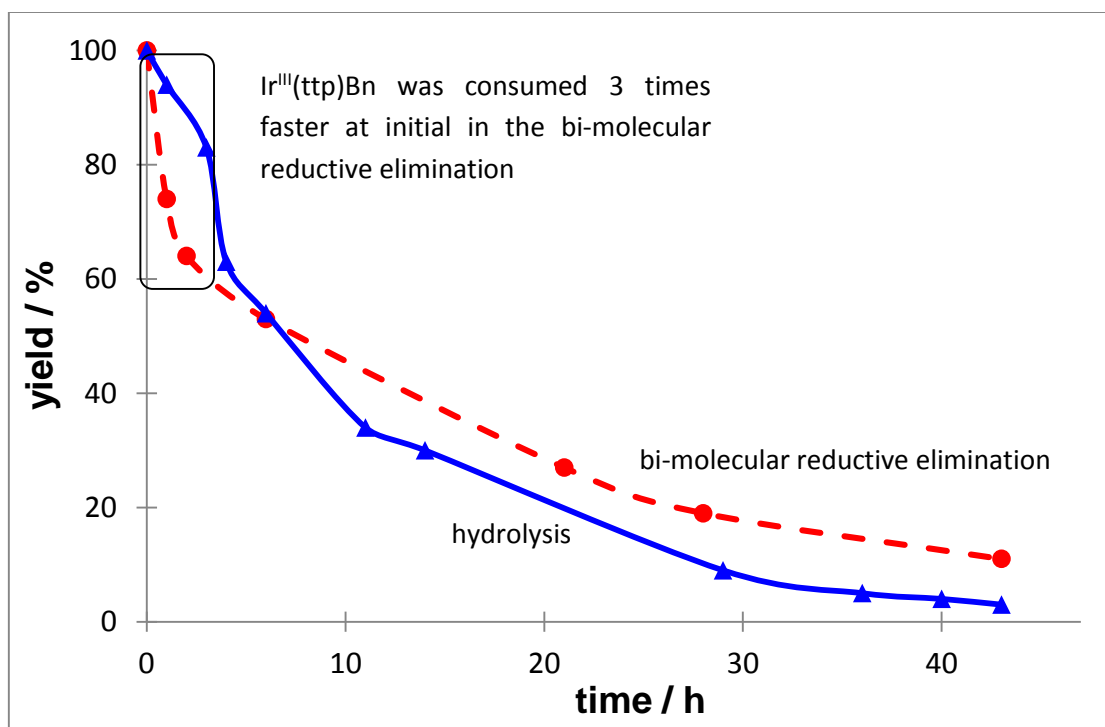


Figure 3.8 Comparison on Ir^{III}(ttp)Bn Consumption between Bi-molecular Reductive Elimination and Hydrolysis.

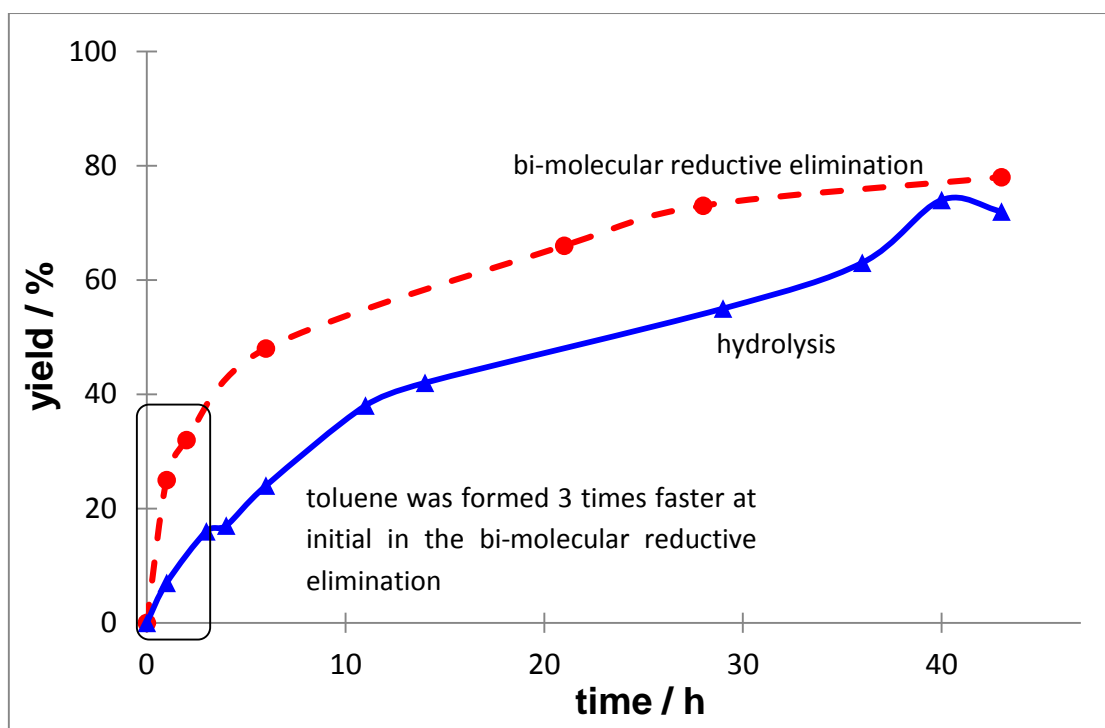
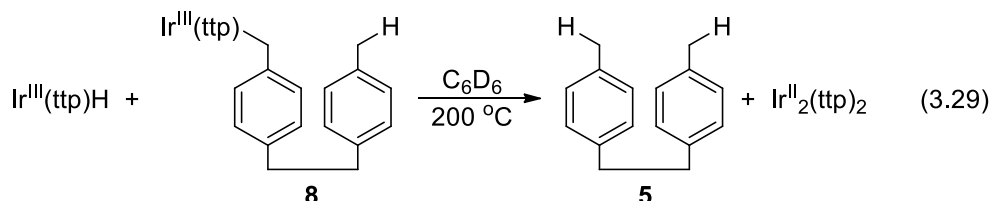
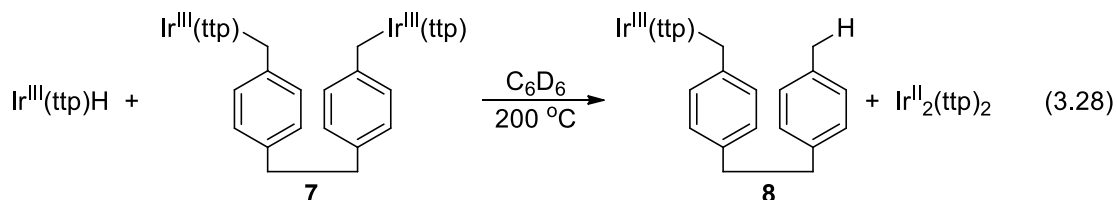


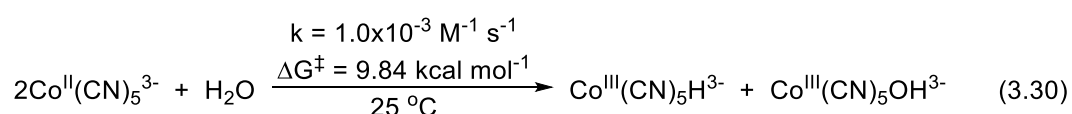
Figure 3.9 Comparison on Toluene Formation between Bi-molecular reductive elimination and Hydrolysis.

Therefore, in the reaction of $\text{Ir}^{\text{III}}(\text{ttp})\text{H}$ with PCP (Table 3.9, eq 3.21, Figure 3.4), the intermolecular elimination of mono-Ir **8** from $\text{Ir}^{\text{III}}(\text{ttp})\text{H}$ and di-Ir **7** occurred rapidly right after **7** was formed provided that the $[\text{Ir}^{\text{III}}(\text{ttp})\text{H}]$ was still high at the initial stage of reaction (eq 3.28). In analogy, $\text{Ir}^{\text{III}}(\text{ttp})\text{H}$ can react with **8** to yield the hydrogenation product **5** (eq 3.29). These two sequential reaction pathways can operate in the catalytic hydrogenation of PCP to achieve a faster hydrogenation process, bypassing the slower hydrolysis.

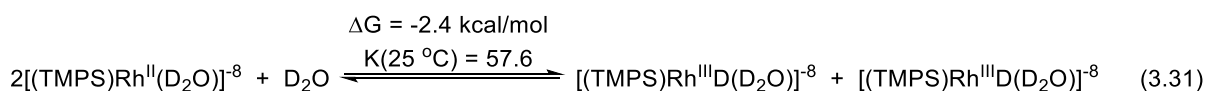


3.5.6 Reaction of Ir^{II}₂(ttp)₂ with H₂O

A continuous generation of Ir^{III}(ttp)H in the catalytic hydrogenation of PCP is essential to sustain the fast intermolecular elimination reaction. β -H elimination of Ir^{III}(ttp)ⁱPr pre-catalyst only provides Ir^{III}(ttp)H at the beginning of the catalysis. Oxidative addition of H₂O with group 9 metalloradical is another channel. The reaction of Co^{II}(CN)₅³⁻ with H₂O to give Co^{III}(CN)₅H³⁻ and Co^{III}(CN)₅OH³⁻ occurs readily at 25 °C in aqueous medium (eq 3.30).³¹



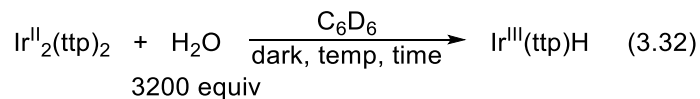
Wayland has reported the thermodynamic favorable oxidative addition of D₂O with water soluble rhodium porphyrin [(TMPS)Rh^{II}(D₂O)]⁻⁸ (eq 3.31).¹³ The analogous reaction with [(TMPS)Ir^{II}(D₂O)]⁻⁸ has been suggested to be more exergonic by -11 to -15 kcal/mol due to the stronger Ir-D and Ir-OD bonds than the corresponding Rh-D and Rh-OD bonds.³²



Similarly, the lipophilic Ir^{II}(ttp) may undergo oxidative addition with H₂O to generate Ir^{III}(ttp)H and Ir^{III}(ttp)OH. The Ir^{III}(ttp)OH once formed, quickly reverts back to Ir^{II}₂(ttp)₂ with elimination of H₂O₂.²² Indeed, Ir^{II}₂(ttp)₂ reacted readily with excess H₂O in C₆D₆ at 27 °C to 50 °C to give 55% yield of Ir^{III}(ttp)H, with 8% recovery of Ir^{II}₂(ttp)₂ after 110 h (Table 3.13, eq 3.32, Figure 3.10). Prolonged heating at 50 °C gave no further conversions. The saturated [H₂O] in C₆D₆ at 27 °C and 50 °C were estimated to be 35 mM and 78 mM, respectively.¹¹ Deep brown precipitates were formed gradually during the reaction and led to

the decreased total yield. The H₂O₂ formed, if not decomposed quickly to less oxidizing O₂ and H₂O, probably induced the oxidative decomposition of iridium porphyrin complexes.

Table 3.13 Reaction of Ir^{II}₂(ttp)₂ with H₂O.



Time / h	Temp / °C	Yield / %		
		Ir ^{II} ₂ (ttp) ₂	Ir ^{III} (ttp)H	total Ir complexes
0	27	100	0	100
1.5	27	82	0	82
16.5	27	60	6	66
24	27	60	10	70
41	27	43	10	53
44	50	34	16	50
48	50	29	21	50
63	50	22	35	57
91	50	10	44	54
110	50	8	55	63
134	50	7	60	67
209	50	8	58	66

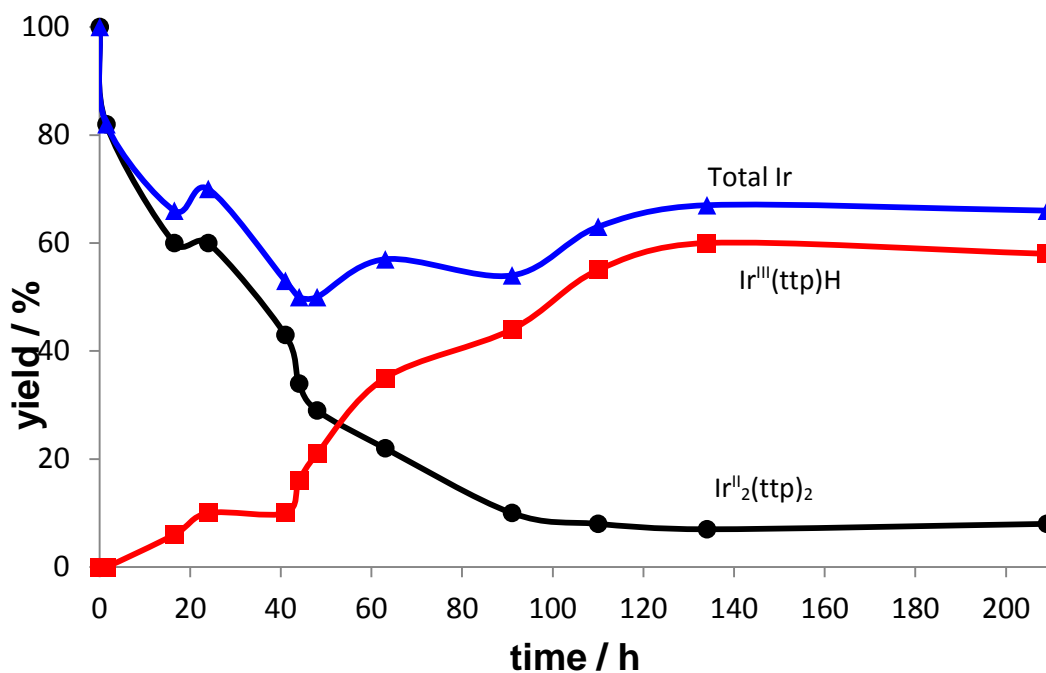


Figure 3.10 Reaction Time Profile of Reaction of Ir^{II}₂(ttp)₂ with H₂O.

(H₂O)Ir^{III}(ttp)-O-Ir^{III}(ttp)(H₂O), the condensation product of Ir^{III}(ttp)OH, was not observed based on reported characteristic pyrrole ¹H signal at δ = 8.36 ppm in C₆D₆ (Figure 3.11).²² Rapid hydrolysis of (H₂O)Ir^{III}(ttp)-O-Ir^{III}(ttp)(H₂O) to give back Ir^{III}(ttp)OH and then Ir^{II}₂(ttp)₂ at 27 °C or 50 °C was unlikely, since it was prepared in good yields by heating Ir^{III}(ttp)CH₂CH₂OH at 120 °C in C₆D₆ for 23 d (eq 3.33). In addition, stability test showed that the μ-oxo complex decomposed very slowly to Ir^{III}(ttp)H at 200 °C under basic conditions (eq 3.34). This suggested that (H₂O)Ir^{III}(ttp)-O-Ir^{III}(ttp)(H₂O) should be reasonably stable to be observed at 27 °C or 50 °C, if it had been present.

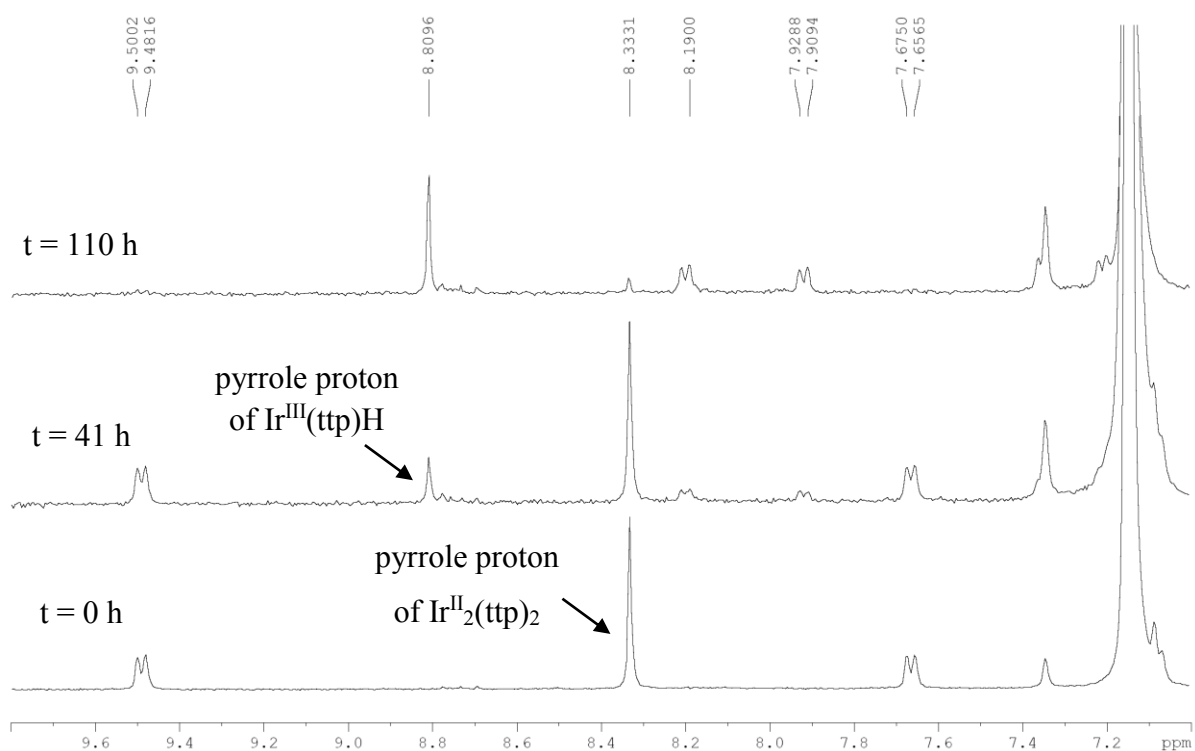
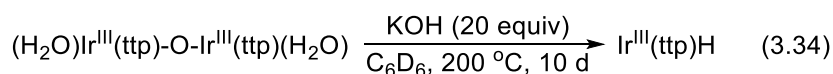
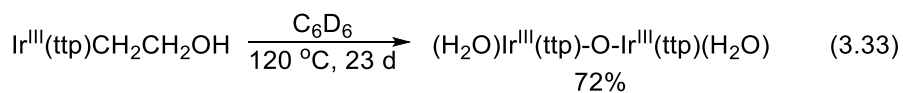
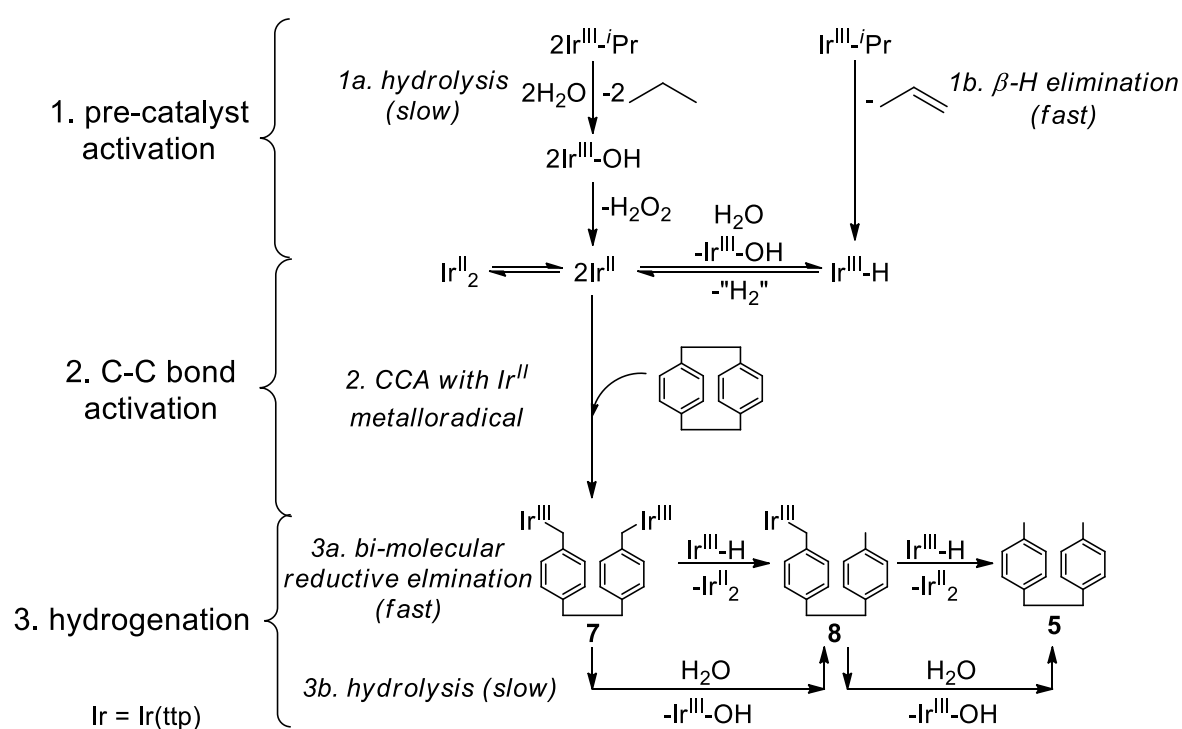


Figure 3.11 Expanded ¹H NMR Spectra at Selected Time Intervals from Reaction 3.32.



3.6 Proposed Mechanism

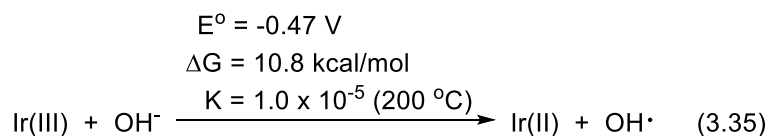
Based on the previous understandings of rhodium porphyrin catalyzed hydrogenation of PCP and current findings on the reactivity of iridium porphyrin complexes, Scheme 3.10 illustrates the proposed mechanism for the iridium catalyzed hydrogenation of PCP with H₂O. Using Ir^{III}(ttp)ⁱPr pre-catalyst as example, the proposed mechanism contains three major steps: (1) pre-catalyst activation; (2) C-C bond activation and (3) hydrogenation.



Scheme 3.10 Proposed Mechanism for the Iridium Catalyzed Hydrogenation of PCP with H₂O.

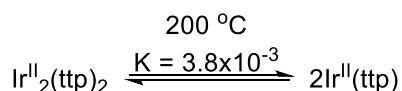
(1) Pre-catalyst activation: Ir^{III}(ttp)ⁱPr undergoes slow hydrolysis to generate Ir^{III}(ttp)OH and propane (step 1a). In aprotic solvent, the hydroxide ligand in Ir^{III}(ttp)OH acts as an efficient single electron reductant to reduce the Ir(III) metal center to Ir(II), forming Ir^{II}(ttp) and H₂O₂ as co-product. The oxidation potentials of OH⁻ in MeCH and H₂O have been reported to be +0.68 V and +1.65V, respectively (vs SCE).³³ Therefore OH⁻ is more reducing in non-polar C₆D₆ due to the even poorer solvation. The 1st reduction potential of

$\text{Ir}^{\text{III}}(\text{ttp})(\text{CO})\text{Cl}$ in PhCN has been reported to be -1.15 V (vs SCE).³⁴ This yields the reaction potential of $(-1.15) + (+0.68) = -0.47$ V (vs SCE) in aprotic solvent (eq 3.35). It is equivalent to $\Delta G = 10.8$ kcal/mol using $\Delta G = nFE^\circ$ relationships ($n = 1$ and $F = 23.0$ kcal/mol) and has equilibrium constant $K = 1.0 \times 10^{-5}$ at 200 °C.



Concurrently, fast β -H elimination of $\text{Ir}^{\text{III}}(\text{ttp})^i\text{Pr}$ occurs to give $\text{Ir}^{\text{III}}(\text{ttp})\text{H}$ and propene (step 1b). $\text{Ir}^{\text{II}}(\text{ttp})$ and $\text{Ir}^{\text{III}}(\text{ttp})\text{H}$ can be interconverted via oxidative addition with H_2O or dehydrogenation, respectively.

(2) C-C bond activation: $\text{Ir}^{\text{II}}_2(\text{ttp})_2$ dissociates to give $\text{Ir}^{\text{II}}(\text{ttp})$ upon heating. The equilibrium constant at 200 °C is estimated to be 3.8×10^{-3} (Scheme 3.11). $\text{Ir}^{\text{II}}(\text{ttp})$ then cleaves the benzylic carbon-carbon bond of PCP to yield the CCA product **7**.



$$\Delta G = \Delta H - T\Delta S$$

$$\Delta H = \text{Ir-Ir BDE in } \text{Ir}^{\text{II}}_2(\text{ttp})_2 = 20 \text{ kcal mol}^{-1}$$

$$\text{assume } S = \text{entropy of } \text{H}_2 = 31.2 \text{ cal mol}^{-1} \text{ K}^{-1} \text{ [25]}$$

$$\Delta G = 20 - (473)(0.0312) = 5.2 \text{ kcal mol}^{-1}$$

$$\Delta G = -RT \ln K$$

$$5.2 = -(1.9872 \times 10^{-3})(473) \ln K$$

$$K = 3.8 \times 10^{-3}$$

Scheme 3.11 Equilibrium Constant Estimation for $\text{Ir}^{\text{II}}_2(\text{ttp})_2$ Dissociation.

(3) Hydrogenation: With continuous production of $\text{Ir}^{\text{III}}(\text{ttp})\text{H}$ via the oxidative addition of H_2O with $\text{Ir}^{\text{II}}(\text{ttp})$, the CCA products **7** and **8** undergo fast bi-molecular reductive

elimination with Ir^{III}(ttp)H to yield **5** as the final hydrogenation product (step 3a). The slow hydrolysis of **7** and **8** acts as the minor hydrogenation process.

3.7 Conclusions

We have discovered the fast and high yielding catalytic hydrogenation of PCP with H₂O by iridium porphyrin complexes. Ir^{II}₂(ttp)₂ undergoes oxidative addition with H₂O readily to produce Ir^{III}(ttp)H for bi-molecular reductive elimination of alkyl-H with Ir^{III}(ttp)(alkyl), which can furnish concurrent hydrogenation much faster than hydrolysis. This provides a new insight towards designing new catalytic hydrogenation using H₂O with iridium porphyrin system by enhancing the rate of in situ formation of Ir^{III}(ttp)H.

References

1. Fukuzumi, S.; Miyamoto, K.; Suenobu, T.; Caemelbecke, E. V.; Kadish, K. M. *J. Am. Chem. Soc.* **1998**, *120*, 2880-2889.
2. Wayland, B. B., In *Energetics of Organometallic Species*, Marinho, J. A., Ed., NATO Ser. C: 367, Kluwer Academic Publisher, Dordrecht, The Netherlands, pp. 69-74, 1992.
3. Wayland, B. B. *Personal Communication*, Temple University, Philadelphia, PA, 2008.
4. Van der Ent, A.; Onderdelinden, A. L. *Inorg. Synth.* **1973**, *14*, 92-95.
5. (a) Ogoshi, H.; Setsune, J.-I.; Yoshida, Z.-I. *J. Organomet. Chem.* **1978**, *159*, 317-328. (b) Yeung, S. K.; Chan, K. S. *Organometallics* **2005**, *24*, 6426-6430.
6. Ogoshi, H.; Setsune, J.-I.; Omura, T.; Yoshida, Z.-I. *J. Am. Chem. Soc.* **1975**, *97*, 6461-6466.
7. Cheung, C. W.; Chan, K. S. *Organometallics* **2008**, *27*, 3043-3055.
8. Chan, K. S.; Leung, Y.-B. *Inorg. Chem.* **1994**, *33*, 3187.
9. Qian, Y. Y. *Unpublished Results*, CUHK, **2011**.
10. Nelson, A. P.; Dimagno, S. G. *J. Am. Chem. Soc.* **2000**, *22*, 8569-8570.
11. The pK_a values of Ir-H complexes have been reported to be higher than that of Rh-H complexes by about 10. Qi, X.-J.; Liu, L.; Fu, Y.; Guo, Q.-X. *Organometallics* **2006**, *25*, 5879-5886.
12. The solubility of H₂O in C₆D₆ from 0 to 250 °C has been discussed in Chapter 2. See: Góral, M.; Wiśniewska-Gocłowska, B.; Mączyński, A. *J. Phys. Chem. Ref. Data* **2004**, *33*, 1159-1188.
13. Fu, X.; Li, S.; Wayland, B. B. *Inorg. Chem.* **2006**, *45*, 9884-9889.
14. Bhagan, S.; Wayland, B. B. *Inorg. Chem.* **2011**, *50*, 11011-11020.
15. Luo, Y. R. *Comprehensive Handbook of Chemical Bond Energies*, CRC Press, Boca Raton, FL, 2007.

16. (a) Fendler, J. H. *Acc. Chem. Res.* **1976**, *9*, 153-161. (b) Tamura, K.; Schelly, Z. A. *J. Am. Chem. Soc.* **1981**, *103*, 1013-1018. (c) Goto, A.; Yoshioka, H.; Kishimoto, H.; Fujita, T. *Langmuir* **1992**, *8*, 441-445. (d) Correa, N. M.; Biasutti, M. A.; Silber, J. J. *J. Colloid Interface Sci.* **1996**, *184*, 570-578. (e) Baptista, M. S.; Tran, C. D. *J. Phys. Chem. B* **1997**, *101*, 4209-4217.
17. Chan, K. S.; Chiu, P. F.; Choi, K. S. *Organometallics* **2007**, *26*, 1117-1119.
18. The Chan group has reported the hydrolysis of Ir^{III}(ttp)CH₂COPh. See: Li, B. Z.; Fung, H. S.; Song, S.; Chan, K. S. *Organometallics*, **2011**, *30*, 1984-1990.
19. Chan, Y. W.; Chan, K. S. *J. Am. Chem. Soc.* **2010**, *132*, 6920-6922.
20. Due to the limited data on α -C-H BDE in iridium porphyrin alkyls, we assumed that the Ir^{III}(ttp)CD₂-D BDE is the same as CD₃-D with 107.3 kcal/mol. We also assumed PhCH₂-D bond was 1 kcal/mol stronger than PhCH₂-H bond (89.7 kcal/mol) based on the difference between CH₃-H (105.0 kcal/mol) and CH₃-D (106.0 kcal/mol). Hence the BDE of PhCH₂-D was estimated to be 90.7 kcal/mol. The difference between 107.3 and 90.7 kcal/mol yielded the ΔH for step ii in Scheme 3.4. See ref 14 for the BDE values.
21. Rh^{III}(ttp)CH₂CH₂(ttp)Ir^{III} gave characteristic Rh-CH₂CH₂-Rh signal at -10.6 ppm in CDCl₃. Yeung, S. K. *PhD. Thesis* **2005**, CUHK.
22. β -H abstraction of Ir^{III}(ttp*)'Pr by Ir^{II}(ttp) to give Ir^{II}(ttp*), Ir^{III}(ttp)H and propene maybe operating. β -H abstraction of Ir^{III}(ttp)(alkyl) by TEMPO has been reported, see: Yeung, S. K.; Chan, K. S. *Organometallics* **2005**, *24*, 6426-6430.
23. Cheung, C. W.; Chan, K. S. *Organometallics* **2011**, *30*, 4269-4283.
24. Cui, W.; Li, S.; Wayland, B. B. *J. Organomet. Chem.* **2007**, *692*, 3198-3206.
25. Chase, M. W., Jr. *J. Phys. Chem. Ref. Data, Monograph 9* **1998**, 1-1951.

26. The thermal bi-molecular reductive elimination of *n*-propylbenzene from $\text{Rh}^{\text{III}}(\text{oep})(\text{CH}(\text{Ph})\text{CH}_2\text{CH}_3)$ and $\text{Rh}^{\text{III}}(\text{oep})\text{H}$ in C_6D_6 has been reported. See: Del Rossi, K. J.; Wayland, B. B. *J. Am. Chem. Soc.* **1985**, *107*, 7941-7944.
27. Using $\text{Rh}^{\text{III}}(\text{txp})\text{-H}$ and $\text{Ir}^{\text{III}}(\text{txp})\text{-H}$ BDEs as the references, see ref 3 and Wayland, B. B.; Ba, S.; Sherry, A. E. *J. Am. Chem. Soc.* **1991**, *113*, 5305-5311.
28. This has been discussed in Section 3.1, Table 3.1.
29. Wayland, B. B.; Ba, S.; Sherry, A. E. *J. Am. Chem. Soc.* **1991**, *113*, 5305-5311.
30. Van Voorhees, S. L.; Wayland, B. B. *Organometallics* **1985**, *4*, 1887-1888.
31. Sokol, C. S.; Brubaker, Jr. C. H. *J. Inorg. Nucl. Chem.* **1968**, *30*, 3267-3271.
32. This has been explained in details in Section 3.4.3, Scheme 3.2.
33. Sawyer, D. T.; Roberts Jr., J. L. *Acc. Chem. Res.* **1988**, *21*, 469-476.
34. Swistak, C.; Cornillon, J.-L.; Anderson, J. E.; Kadish, K. M. *Organometallics* **1987**, *6*, 2146-2150.

Experimental Section

General Procedures

Unless otherwise specified, all reagents were purchased from commercial suppliers and directly used without further purification. The purity of [2.2]paracyclophane was further tested by melting point (m.p. = 288.6-289.4 °C, lit. = 285-287.2 °C).¹ Hexane for chromatography was distilled from anhydrous CaCl₂. Benzene-*d*₆ was distilled from sodium under vacuum, degassed with three freeze-pump-thaw cycles and stored in a Teflon screw head stoppered flask under N₂. Thin layer chromatography was performed on pre-coated silica gel 60 F₂₅₄ plates. Silica gel (Merck, 70-230 mesh) was used for column chromatography under air.

Melting points were recorded on an MPA100 Automated Melting Point System. ¹H NMR spectra were recorded on a Bruker AV-400 MHz at 400 MHz. Chemical shifts were referenced internally to the residual solvent proton resonance in C₆D₆ (δ = 7.15 ppm), CDCl₃ (δ = 7.26 ppm) or with tetramethylsilane (δ = 0.00 ppm) as the internal standard. Chemical shifts (δ) are reported in parts per million (ppm). Coupling constants (*J*) are reported in hertz (Hz). High resolution mass spectra (HRMS) were recorded on a Thermofinnigan MAT 95 XL mass spectrometer. Fast atom bombardment was performed with 3-nitrobenzyl alcohol (NBA) as the matrix.

All reactions in 0.5 mL benzene-*d*₆ were carried out in a flame-sealed NMR tube in vacuum with the reaction mixture degassed with three freeze(77 K)-pump(0.005 mmHg)-thaw(r.t.) cycles, then heated in oven in dark and wrapped with aluminum foil to protect from exposure to room light before ¹H NMR measurements. The NMR yields were with benzene residue as the internal standard. Aqueous stock solution of KOH was prepared separately, transferred to the reaction vessel and dried under vacuum at r.t. to obtain anhydrous starting materials. Benzene stock solutions of Ir(tp)*X* (*X* = Me, Bn, ^{*i*}Pr, H and Ir(tp)) were prepared separately, transferred to the reaction vessel and dried under vacuum at r.t. to obtain

anhydrous starting materials. Benzene-*d*₆ stock solution of [2.2]paracyclophane was prepared separately, degassed and stored under N₂ before transferred to the reaction vessel.

[Ir(cod)Cl]₂,² Ir^{III}(ttp)(CO)Cl,³ Ir^{III}(ttp)Me,^{3b,4} Ir^{III}(ttp)Bn,⁵ Ir^{III}(ttp)H^{3a,5} and Ir^{II}₂(ttp)₂^{5,6} were prepared according to the literature procedures. Ir^{III}(ttp)SiEt₃ and Ir^{III}(ttp)CD₃ were borrowed from group members.

Experimental Procedures

Preparation of Ir^{III}(ttp)^{*i*}Pr. The reductive alkylation of Ir^{III}(ttp)(CO)Cl is described as a typical example for the preparation of Ir^{III}(ttp)-alkyl complexes, adapting the literature procedure.^{3b,4} A suspension of Ir^{III}(ttp)(CO)Cl (20 mg, 0.022 mmol) in 2 mL THF in a Teflon screw head stoppered tube and a solution of NaBH₄ (8.2 mg, 0.22 mmol) in aqueous NaOH (1 M, 1 mL) in a Schlenk tube were purged with N₂ for 15 min separately. The NaBH₄ solution was added slowly to the suspension of Ir^{III}(ttp)(CO)Cl via a cannula. The mixture was heated at 70 °C under N₂ for 2 h to give a brown suspension. The reaction was then cooled to r.t. and 2-iodopropane (4.4 μL, 0.044 mmol) was added under N₂. The reaction mixture was further heated at 70 °C for 2 h to give a reddish brown suspension. It was worked up by extraction with CH₂Cl₂/H₂O. The organic layer was rotary evaporated. The crude solid was purified by column chromatography on silica gel eluting with CH₂Cl₂/hexane = 1:1. The major red fraction was collected and dried to give reddish purple solid Ir^{III}(ttp)^{*i*}Pr (13 mg, 0.014 mmol, 65%). R_f = 0.84 (CH₂Cl₂/hexane = 1:1). ¹H NMR (CDCl₃, 400 MHz) δ -5.09 (septet, ³J_{H-H} = 6.6 Hz, 1 H), -4.45 (d, ³J_{H-H} = 6.6 Hz, 6 H), 2.68 (s, 12 H), 7.51 (two d overlapped, 8 H), 7.98 (d, ³J_{H-H} = 7.4 Hz, 4 H), 8.03 (d, ³J_{H-H} = 7.4 Hz, 4 H), 8.49 (s, 8 H). ¹H NMR (C₆D₆, 400 MHz) δ -4.74 (h, ³J_{H-H} = 6.6 Hz, 1 H), -4.06 (d, ³J_{H-H} = 6.6 Hz, 6 H), 2.40 (s, 12 H), 7.24 (d, ³J_{H-H} = 7.8 Hz, 4 H), 7.35 (d, ³J_{H-H} = 6.1 Hz, 4 H), 8.03 (dd, ⁴J_{H-H} = 1.5, ³J_{H-H} = 7.6 Hz, 4 H), 8.18 (dd, ⁴J_{H-H} = 1.5, ³J_{H-H} = 7.6 Hz, 4 H), 8.75 (s, 8 H). ¹³C NMR (CDCl₃,

100 MHz) δ -3.0, 21.6, 21.7, 124.8, 127.6, 127.7, 131.5, 133.6, 134.0, 137.3, 138.9, 143.7.

HRMS calcd. for $(C_{51}H_{43}N_4Ir)^+$: m/z 904.3115. Found: m/z 904.3119.

Catalytic Hydrogenation of [2.2]Paracyclophane with Water by Ir^{III}(ttp)R Pre-Catalyst.

With Ir^{III}(ttp)Me. Ir^{III}(ttp)Me (0.42 mg, 0.00048 mmol), H₂O (8.6 μ L, 0.48 mmol) and benzene-*d*₆ stock solution (500 μ L) of [2.2]paracyclophane (1.0 mg, 0.0048 mmol) were added successively to a NMR tube. The orange mixture was degassed for three freeze-pump-thaw cycles and the NMR tube was flame-sealed under vacuum. It was heated at 200 °C in the dark for 53 h. It was monitored with ¹H NMR spectroscopy at particular time intervals and the NMR yields were taken. 4,4'-Dimethylbibenzyl **5** was formed in 94% yield.

With Ir^{III}(ttp)Bn. Ir^{III}(ttp)Bn (0.46 mg, 0.00048 mmol), H₂O (8.6 μ L, 0.48 mmol) and benzene-*d*₆ stock solution (500 μ L) of [2.2]paracyclophane (1.0 mg, 0.0048 mmol) were added successively to a NMR tube. The orange mixture was degassed for three freeze-pump-thaw cycles and the NMR tube was flame-sealed under vacuum. It was heated at 200 °C in the dark for 48 h. It was monitored with ¹H NMR spectroscopy at particular time intervals and the NMR yields were taken. 4,4'-Dimethylbibenzyl **5** was formed in 95% yield.

With Ir^{III}(ttp)ⁱPr. Ir^{III}(ttp)ⁱPr (0.43 mg, 0.00048 mmol), H₂O (8.6 μ L, 0.48 mmol) and benzene-*d*₆ stock solution (500 μ L) of [2.2]paracyclophane (1.0 mg, 0.0048 mmol) were added successively to a NMR tube. The orange mixture was degassed for three freeze-pump-thaw cycles and the NMR tube was flame-sealed under vacuum. It was heated at 200 °C in the dark for 41 h. It was monitored with ¹H NMR spectroscopy at particular time intervals and the NMR yields were taken. 4,4'-Dimethylbibenzyl **5** was formed in 98% yield.

With Ir^{III}(ttp)SiEt₃. Ir^{III}(ttp)SiEt₃ (0.47 mg, 0.00048 mmol), H₂O (8.6 μ L, 0.48 mmol) and benzene-*d*₆ stock solution (500 μ L) of [2.2]paracyclophane (1.0 mg, 0.0048 mmol) were added successively to a NMR tube. The orange mixture was degassed for three freeze-pump-

thaw cycles and the NMR tube was flame-sealed under vacuum. It was heated at 200 °C in the dark for 48 h. It was monitored with ^1H NMR spectroscopy at particular time intervals and the NMR yields were taken. 4,4'-Dimethylbibenzyl **5** was formed in 10% yield. PCP was recovered in 70% yield.

With $\text{Ir}^{\text{III}}(\text{ttp})\text{H}$. $\text{Ir}^{\text{III}}(\text{ttp})\text{H}$ (0.41 mg, 0.00048 mmol), H_2O (8.6 μL , 0.48 mmol) and benzene- d_6 stock solution (500 μL) of [2.2]paracyclophane (1.0 mg, 0.0048 mmol) were added successively to a NMR tube. The orange mixture was degassed for three freeze-pump-thaw cycles and the NMR tube was flame-sealed under vacuum. It was heated at 200 °C in the dark for 35 h. It was monitored with ^1H NMR spectroscopy at particular time intervals and the NMR yields were taken. 4,4'-Dimethylbibenzyl **5** was formed in 96% yield.

$\text{Ir}^{\text{III}}(\text{ttp})^i\text{Pr}$ Pre-Catalyst Loading.

With 2.5 mol%. $\text{Ir}^{\text{III}}(\text{ttp})^i\text{Pr}$ (0.11 mg, 0.00012 mmol) and H_2O (8.6 μL , 0.48 mmol) and benzene- d_6 stock solution (500 μL) of [2.2]paracyclophane (1.0 mg, 0.0048 mmol) were added successively to a NMR tube. The orange mixture was degassed for three freeze-pump-thaw cycles and the NMR tube was flame-sealed under vacuum. It was heated at 200 °C in the dark for 76 h. It was monitored with ^1H NMR spectroscopy at particular time intervals and the NMR yields were taken. 4,4'-Dimethylbibenzyl **5** was formed in 74% yield. PCP was recovered in 10% yield.

With 5 mol%. $\text{Ir}^{\text{III}}(\text{ttp})^i\text{Pr}$ (0.22 mg, 0.00024 mmol) and H_2O (8.6 μL , 0.48 mmol) and benzene- d_6 stock solution (500 μL) of [2.2]paracyclophane (1.0 mg, 0.0048 mmol) were added successively to a NMR tube. The orange mixture was degassed for three freeze-pump-thaw cycles and the NMR tube was flame-sealed under vacuum. It was heated at 200 °C in the dark for 58 h. It was monitored with ^1H NMR spectroscopy at particular time intervals and the NMR yields were taken. 4,4'-Dimethylbibenzyl **5** was formed in 97% yield.

With 20 mol%. Ir^{III}(ttp)ⁱPr (0.86 mg, 0.00096 mmol) and H₂O (8.6 μL, 0.48 mmol) and benzene-*d*₆ stock solution (500 μL) of [2.2]paracyclophane (1.0 mg, 0.0048 mmol) were added successively to a NMR tube. The orange mixture was degassed for three freeze-pump-thaw cycles and the NMR tube was flame-sealed under vacuum. It was heated at 200 °C in the dark for 33 h. It was monitored with ¹H NMR spectroscopy at particular time intervals and the NMR yields were taken. 4,4'-Dimethylbibenzyl **5** was formed in 95% yield.

Water loading Effects.

Without H₂O added. Ir^{III}(ttp)ⁱPr (0.43 mg, 0.00048 mmol) and benzene-*d*₆ stock solution (500 μL) of [2.2]paracyclophane (1.0 mg, 0.0048 mmol) were added successively to a NMR tube. The orange mixture was degassed for three freeze-pump-thaw cycles and the NMR tube was flame-sealed under vacuum. ¹H NMR analysis at t = 0 showed that the reaction mixture already contained ~3 equiv of H₂O. It was heated at 200 °C in the dark for 55 h. It was monitored with ¹H NMR spectroscopy at particular time intervals and the NMR yields were taken. 4,4'-Dimethylbibenzyl **5** was formed in 97% yield.

With 2.3 equiv of H₂O added. Ir^{III}(ttp)ⁱPr (0.43 mg, 0.00048 mmol), H₂O (0.2 μL, 0.011 mmol) and benzene-*d*₆ stock solution (500 μL) of [2.2]paracyclophane (1.0 mg, 0.0048 mmol) were added successively to a NMR tube. The orange mixture was degassed for three freeze-pump-thaw cycles and the NMR tube was flame-sealed under vacuum. It was heated at 200 °C in the dark for 59 h. It was monitored with ¹H NMR spectroscopy at particular time intervals and the NMR yields were taken. 4,4'-Dimethylbibenzyl **5** was formed in 98% yield.

Additive Effects.

With DSS added. Ir^{III}(ttp)ⁱPr (0.43 mg, 0.00048 mmol), H₂O (0.2 μL, 0.011 mmol), DSS (0.049 mg, 0.11 μmol) and benzene-*d*₆ stock solution (500 μL) of [2.2]paracyclophane (1.0

mg, 0.0048 mmol) were added successively to a NMR tube. The orange mixture was degassed for three freeze-pump-thaw cycles and the NMR tube was flame-sealed under vacuum. It was heated at 200 °C in the dark for 45 h. It was monitored with ¹H NMR spectroscopy at particular time intervals and the NMR yields were taken. 4,4'-Dimethylbibenzyl **5** was formed in 97% yield.

With BDHA added. Ir^{III}(ttp)ⁱPr (0.43 mg, 0.00048 mmol), H₂O (0.2 μL, 0.011 mmol), BDHA (0.25 mg, 0.11 μmol) and benzene-*d*₆ stock solution (500 μL) of [2.2]paracyclophane (1.0 mg, 0.62 μmol) were added successively to a NMR tube. The orange mixture was degassed for three freeze-pump-thaw cycles and the NMR tube was flame-sealed under vacuum. It was heated at 200 °C in the dark for 41 h. It was monitored with ¹H NMR spectroscopy at particular time intervals and the NMR yields were taken. 4,4'-Dimethylbibenzyl **5** was formed in 86% yield.

With DMF-*d*₇ solvent. Ir^{III}(ttp)ⁱPr (0.43 mg, 0.00048 mmol), H₂O (0.2 μL, 0.011 mmol) and DMF-*d*₇ stock solution (500 μL) of [2.2]paracyclophane (1.0 mg, 0.0048 mmol) were added successively to a NMR tube. The orange mixture was degassed for three freeze-pump-thaw cycles and the NMR tube was flame-sealed under vacuum. It was heated at 200 °C in the dark for 53 h. It was monitored with ¹H NMR spectroscopy at particular time intervals and the NMR yields were taken. 4,4'-Dimethylbibenzyl **5** was formed in 30% yield. PCP was recovered in 51% yield.

Deuterium Labeling Experiments.

Catalytic Deuteration of [2.2]Paracyclophane with Ir^{III}(ttp)ⁱPr. Ir^{III}(ttp)ⁱPr (0.43 mg, 0.00048 mmol), D₂O (8.7 μL, 0.48 mmol) and benzene-*d*₆ stock solution (500 μL) of [2.2]paracyclophane (1.0 mg, 0.0048 mmol) were added successively to a NMR tube. The orange mixture was degassed for three freeze-pump-thaw cycles and the NMR tube was

flame-sealed under vacuum. It was heated at 200 °C in the dark for 47 h. It was monitored with ¹H NMR spectroscopy at particular time intervals and the NMR yields were taken. **5-d** was formed in 97% yield. Upon breaking the sealed NMR tube, **5-d** was isolated by column chromatography on silica gel eluting with hexane. ¹H NMR (C₆D₆, 400 MHz) δ 2.13 (s), 2.78 (s), 6.97 (s, 8 H). The internal benzylic D% = (1-3.596/4) x 100% = 10%. The terminal benzylic D% = (1-3.949/6) x 100% = 34%.

Benzylic H/D Exchange of 4,4'-Dimethylbibenzyl 5. Ir^{III}(ttp)ⁱPr (0.43 mg, 0.00048 mmol), D₂O (8.7 μL, 0.48 mmol) and benzene-*d*₆ stock solution (500 μL) of 4,4'-dimethylbibenzyl (1.0 mg, 0.0048 mmol) were added successively to a NMR tube. The orange mixture was degassed for three freeze-pump-thaw cycles and the NMR tube was flame-sealed under vacuum. It was heated at 200 °C in the dark for 48 h. It was monitored with ¹H NMR spectroscopy at particular time intervals and the NMR yields were taken. **5'-d** was formed in 99% yield. Upon breaking the sealed NMR tube, **5'-d** was isolated by column chromatography on silica gel eluting with hexane. ¹H NMR (CDCl₃, 400 MHz) δ 2.32 (s, 6 H), 2.83-2.86 (m), 7.09 (s, 8 H). The internal benzylic D% = (1-2.869/4) x 100% = 28%. The terminal benzylic D% = (1-6.039/6) x 100% ≈ 0%.

Reaction of Ir^{III}(ttp)(CO)Cl with [2.2]Paracyclophane. Ir^{III}(ttp)(CO)Cl (0.44 mg, 0.00048 mmol), KOH (0.27 mg, 0.0048 mmol), D₂O (8.7 μL, 0.48 mmol) and benzene-*d*₆ stock solution (500 μL) of [2.2]paracyclophane (1.0 mg, 0.0048 mmol) were added to a NMR tube. The orange mixture was degassed for three freeze-pump-thaw cycles and the NMR tube was flame-sealed under vacuum. It was heated in the dark from 60 °C to 150 °C. It was monitored with ¹H NMR spectroscopy at particular time intervals and the NMR yields were taken. Neither Ir^{III}(ttp)(cyclophanyl) intermediates nor deuterated PCP were observed. After heating at 130 °C for 1 d, CCA of PCP was occurred.

Hydrolysis of Ir^{III}(ttp)R.

Hydrolysis of Ir^{III}(ttp)Me. Ir^{III}(ttp)Me (0.42 mg, 0.00048 mmol) and H₂O (8.6 μL, 0.48 mmol) were added to a NMR tube, followed by addition of 500 μL benzene-*d*₆. The orange mixture was degassed for three freeze-pump-thaw cycles and the NMR tube was flame-sealed under vacuum. It was heated at 200 °C in the dark for 75 h. It was monitored with ¹H NMR spectroscopy at particular time intervals and the NMR yields were taken. Ir^{III}(ttp)H was formed in 8 % yield. Ir^{III}(ttp)CH₃ was recovered in 81% yield.

Hydrolysis of Ir^{III}(ttp)Bn. Ir^{III}(ttp)Bn (0.46 mg, 0.00048 mmol) and H₂O (8.6 μL, 0.48 mmol) were added to a NMR tube, followed by addition of 500 μL benzene-*d*₆. The orange mixture was degassed for three freeze-pump-thaw cycles and the NMR tube was flame-sealed under vacuum. It was heated at 200 °C in the dark for 43 h. It was monitored with ¹H NMR spectroscopy at particular time intervals and the NMR yields were taken. Ir^{III}(ttp)H and toluene were formed in 56% and 72% yields, respectively. Ir^{III}(ttp)Bn was recovered in 3 % yield.

Hydrolysis of Ir^{III}(ttp)^{*i*}Pr. Ir^{III}(ttp)^{*i*}Pr (0.43 mg, 0.00048 mmol) and H₂O (8.6 μL, 0.48 mmol) were added to a NMR tube, followed by addition of 500 μL benzene-*d*₆. The orange mixture was degassed for three freeze-pump-thaw cycles and the NMR tube was flame-sealed under vacuum. It was heated at 200 °C in the dark for 44 h. It was monitored with ¹H NMR spectroscopy at particular time intervals and the NMR yields were taken. Ir^{III}(ttp)H, propane and propene were formed in 76%, 26% and 68% yields, respectively.

Reaction of Ir^{III}(ttp)CD₃ with PCP. Ir^{III}(ttp)CD₃ (0.42 mg, 0.00048 mmol) and benzene-*d*₆ stock solution (500 μL) of [2.2]paracyclophane (1.0 mg, 0.0048 mmol) were added successively to a NMR tube. The orange mixture was degassed for three freeze-pump-thaw

cycles and the NMR tube was flame-sealed under vacuum. It was heated at 200 °C in the dark for 11 h. It was monitored with ^1H and ^2H NMR spectroscopy at particular time intervals.

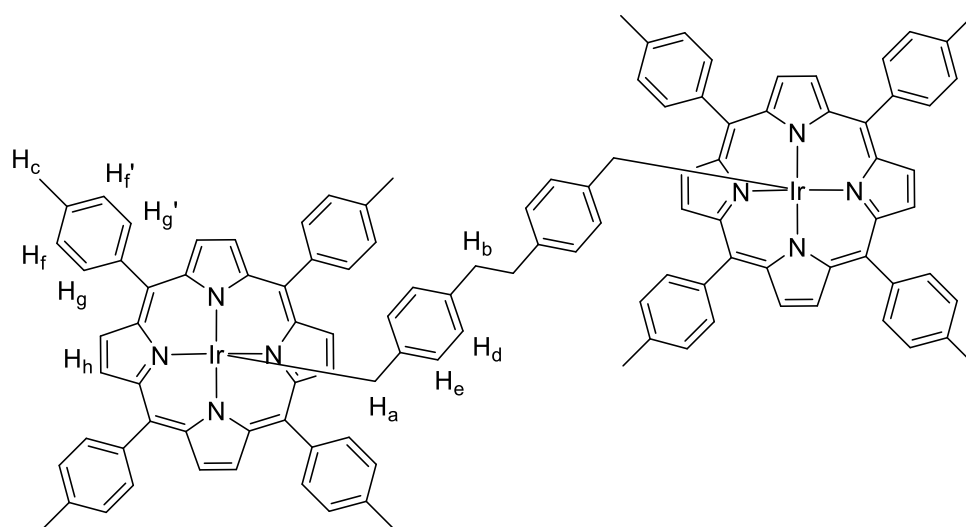
Initial Stage of Catalysis using $\text{Ir}^{\text{III}}(\text{ttp})^i\text{Pr}$ at 170 °C. $\text{Ir}^{\text{III}}(\text{ttp})^i\text{Pr}$ (0.43 mg, 0.00048 mmol), H_2O (8.6 μL , 0.48 mmol) and benzene- d_6 stock solution (500 μL) of [2.2]paracyclophane (1.0 mg, 0.0048 mmol) were added successively to a NMR tube. The orange mixture was degassed for three freeze-pump-thaw cycles and the NMR tube was flame-sealed under vacuum. It was heated at 170 °C in the dark for 36 h. It was monitored with ^1H NMR spectroscopy at particular time intervals and the NMR yields were taken. Di-Ir **7**, mono-Ir **8**, propane and propene were formed in 28%, 31%, 17% and 21% yields, respectively.

Reaction of $\text{Ir}^{\text{II}}_2(\text{ttp})_2$ with [2.2]Paracyclophane. $\text{Ir}^{\text{II}}_2(\text{ttp})_2$ (0.83 mg, 0.00048 mmol) and benzene- d_6 stock solution (500 μL) of [2.2]paracyclophane (0.5 mg, 0.0024 mmol) were added to a NMR tube under N_2 . The orange mixture was degassed for three freeze-pump-thaw cycles and the NMR tube was flame-sealed under vacuum. It was heated from 30 °C to 150 °C in the dark. It was monitored with ^1H NMR spectroscopy at particular time intervals and the NMR yields were taken. The CCA product di-Ir **7** was formed in 55% yield.

Reaction of $\text{Ir}^{\text{III}}(\text{ttp})\text{H}$ with [2.2]Paracyclophane. $\text{Ir}^{\text{III}}(\text{ttp})\text{H}$ (0.41 mg, 0.00048 mmol) and benzene- d_6 stock solution (500 μL) of [2.2]paracyclophane (1.0 mg, 0.0048 mmol) were added to a NMR tube under N_2 . The orange mixture was degassed for three freeze-pump-thaw cycles and the NMR tube was flame-sealed under vacuum. It was heated at 150 °C in the dark for 69 h. It was monitored with ^1H NMR spectroscopy at particular time intervals and the NMR yields were taken. The CCA products di-Ir **7** and mono-Ir **8** were formed in 50% and 33% yields, respectively.

In a separate experiment with identical conditions except that 1.4 mg Ir^{III}(ttp)H was used, **7** and **8** were isolated by dropper-scale column chromatography on silica gel eluting with DCM/hexane = 1:1 for characterizations.

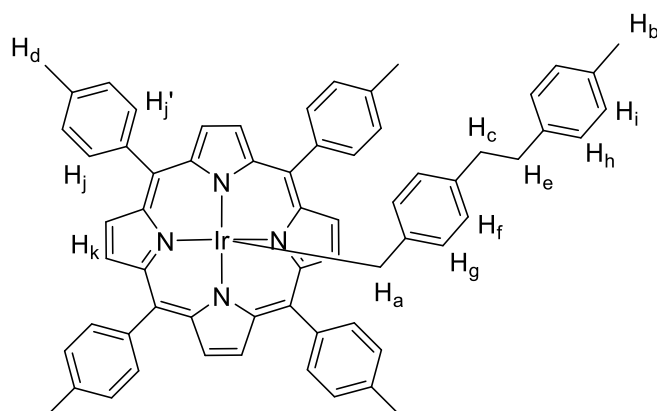
Compound **7**: $R_f = 0.71$ (CH₂Cl₂/hexane = 1:1). ¹H NMR (C₆D₆, 400 MHz) δ -3.67 (s, 4 H, H_a), 2.03 (s, 4 H, H_b), 2.42 (s, 24 H, H_c), 3.39 (d, ³J_{H-H} = 9.6 Hz, 4 H, H_d), 5.69 (d, ³J_{H-H} = 8.7 Hz, 4 H, H_e), 7.30 (d, ³J_{H-H} = 7.6 Hz, 8 H, H_f), 7.36 (peak overlapped with residual solvent, H_{f'}), 8.01 (d, ³J_{H-H} = 7.6 Hz, 8 H, H_g), 8.20 (d, ³J_{H-H} = 8.2 Hz, 8 H, H_{g'}), 8.73 (s, 16H, H_h). Attempted ¹³C{¹H} NMR measurement for overnight at r.t. resulted in complete decomposition of **7** and no characteristic porphyrin signals could be recorded. The ¹H NMR spectrum of **7** is closely similar to the rhodium analogue reported. HRMS calcd. for (C-₁₁₂H₈₈N₈Ir₂+H)⁺: m/z 1931.6484. Found: m/z 1931.6483.



Compound **8**: $R_f = 0.80$ (CH₂Cl₂/hexane = 1:1). ¹H NMR (C₆D₆, 400 MHz) δ -3.64 (s, 2 H, H_a), 2.10 (s, 3 H, H_b), 2.29 (t, ³J_{H-H} = 8.2 Hz, 2 H, H_c), 2.43 (s, 12 H, H_d), 2.54 (t, ³J_{H-H} = 8.4 Hz, 2 H, H_e), 3.45 (d, ³J_{H-H} = 8.0 Hz, 2 H, H_f), 5.83 (d, ³J_{H-H} = 7.8 Hz, 2 H, H_g), 6.85 (d, ³J_{H-H} = 8.2, 2 H, H_h), 6.92 (d, ³J_{H-H} = 8.0 Hz, 2 H, H_i), 8.07 (d, ³J_{H-H} = 7.8 Hz, 4 H, H_j), 8.20 (d, ³J_{H-H} = 7.7 Hz, 4 H, H_{j'}), 8.74 (s, 8H, H_k). There were 8 *meso*-aryl protons masked by the

residual solvent. HRMS calcd. for $(C_{64}H_{53}N_4Ir+H)^+$: m/z 1071.3978. Found: m/z 1071.3990.

Standing of this C_6D_6 solution for overnight at r.t. resulted in complete decomposition of **8**.



The mini-scale experiment and the close R_f values of **7**, **8** and PCP rendered difficulties in product purifications. Attempted column chromatography still retained some minor impurities and solvent peaks in their 1H NMR spectra.

Reaction of $Ir^{III}(ttp)H$ with [2.2]Paracyclophane with 3 mol% $Ir^{II}_2(ttp)_2$. $Ir^{III}(ttp)H$ (0.41 mg, 0.00048 mmol), $Ir^{II}_2(ttp)_2$ (0.02 mg, 1.4×10^{-5} mmol) and benzene- d_6 stock solution (500 μ L) of [2.2]paracyclophane (1.0 mg, 0.0048 mmol) were added to a NMR tube under N_2 . The orange mixture was degassed for three freeze-pump-thaw cycles and the NMR tube was flame-sealed under vacuum. It was heated at 150 $^\circ C$ in the dark for 98 h. The CCA products di-Ir **7** and mono-Ir **8** were formed in 49% and 39% yields, respectively. $Ir^{III}(ttp)H$ was recovered in 4% yield.

Bi-molecular Reductive Elimination from $Ir^{III}(ttp)H$ and $Ir^{III}(ttp)Bn$. $Ir^{III}(ttp)Bn$ (0.46 mg, 0.00048 mmol) and $Ir^{III}(ttp)H$ (0.41 mg, 0.00048 mmol) were added to a NMR tube, followed by addition of 500 μ L benzene- d_6 under N_2 . The orange mixture was degassed for three freeze-pump-thaw cycles and the NMR tube was flame-sealed under vacuum. It was

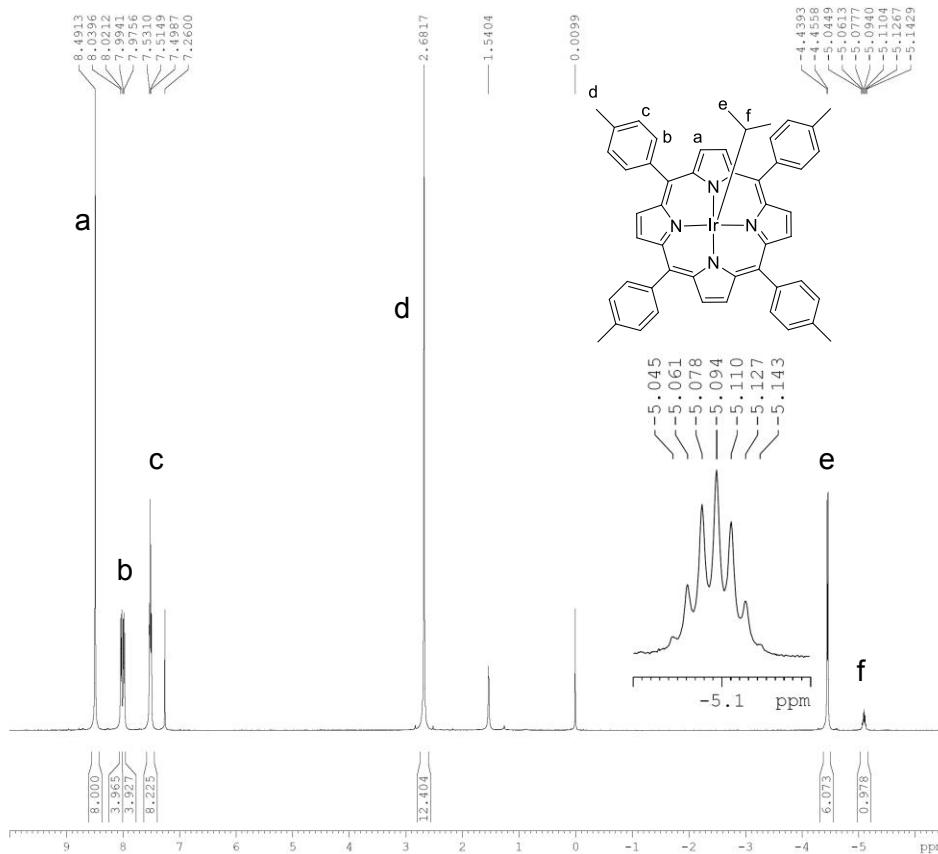
heated at 200 °C in the dark for 43 h. It was monitored with ^1H NMR spectroscopy at particular time intervals and the NMR yields were taken. Toluene was formed in 78% yield.

Reaction of $\text{Ir}^{\text{II}}_2(\text{ttp})_2$ with H_2O . $\text{Ir}^{\text{II}}_2(\text{ttp})_2$ (0.26 mg, 0.00015 mmol) and H_2O (8.6 μL , 0.48 mmol) were added to a NMR tube, followed by addition of 500 μL benzene- d_6 under N_2 . The orange mixture was degassed for three freeze-pump-thaw cycles and the NMR tube was flame-sealed under vacuum. It was heated in the dark from 27 °C to 50 °C for 209 h. It was monitored with ^1H NMR spectroscopy at particular time intervals and the NMR yields were taken. $\text{Ir}^{\text{III}}(\text{ttp})\text{H}$ was formed in 58% yield. $\text{Ir}^{\text{II}}_2(\text{ttp})_2$ was recovered in 8% yield.

Appendix I List of Spectra

No.	Spectra	Page
1	^1H NMR spectra of $\text{Ir}^{\text{III}}(\text{ttp})^i\text{Pr}$	160
2	$^{13}\text{C}\{^1\text{H}\}$ NMR spectrum of $\text{Ir}^{\text{III}}(\text{ttp})^i\text{Pr}$	161
3	^1H NMR spectrum of deuterated 5-d	161
4	^1H NMR spectrum of deuterated 5-d'	162
5	^1H NMR spectrum of di-Ir 7	163
6	^1H NMR spectrum of mono-Ir 8	164
7	HRMS spectrum of $\text{Ir}^{\text{III}}(\text{ttp})^i\text{Pr}$ (FAB)	165
8	HRMS spectrum of di-Ir 7 (FAB)	166
9	HRMS spectrum of mono-Ir 8 (FAB)	167

Ir^{III}(ttp)ⁱPr (CDCl₃, 400 MHz)



```

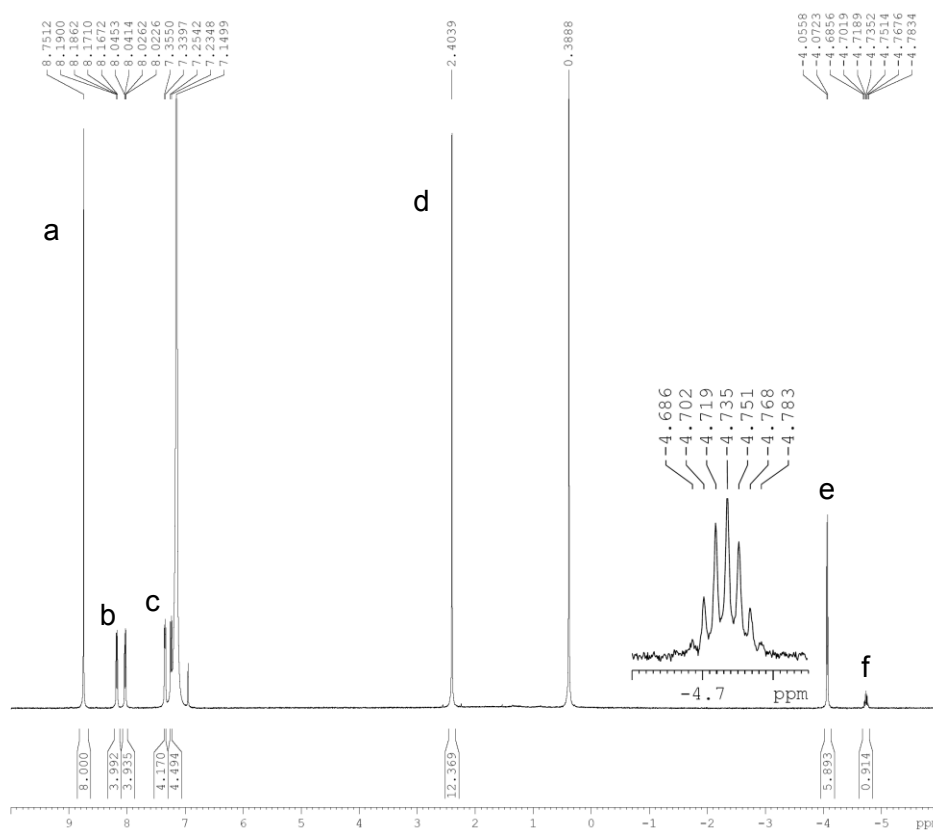
Current Data Parameters
NAME          CTT 452
EXPNO        1
PROCNO       1

F2 - Acquisition Parameters
Date_        20140216
Time_        20.43
INSTRUM      spect
PROBHD       5 mm PADDL 13C
PULPROG      zg30
TD            65536
SOLVENT      CDCl3
NS            32
DS            2
SWH           12019.230 Hz
FIDRES        0.183399 Hz
AQ            2.7263477 sec
RG            203
DW            41.600 usec
DE            6.50 usec
TE            294.8 K
D1            1.00000000 sec
TDO           1

----- CHANNEL f1 -----
NUC1          1H
P1            14.83 usec
PL1           0 dB
PL1W          -1.#IND0000 W
SFO1          400.1324708 MHz

F2 - Processing parameters
SI            32768
SF            400.1300094 MHz
WDW           EM
SSB           0
LB            0.30 Hz
GB            0
PC            1.00
    
```

Ir^{III}(ttp)ⁱPr (C₆D₆, 400 MHz)



```

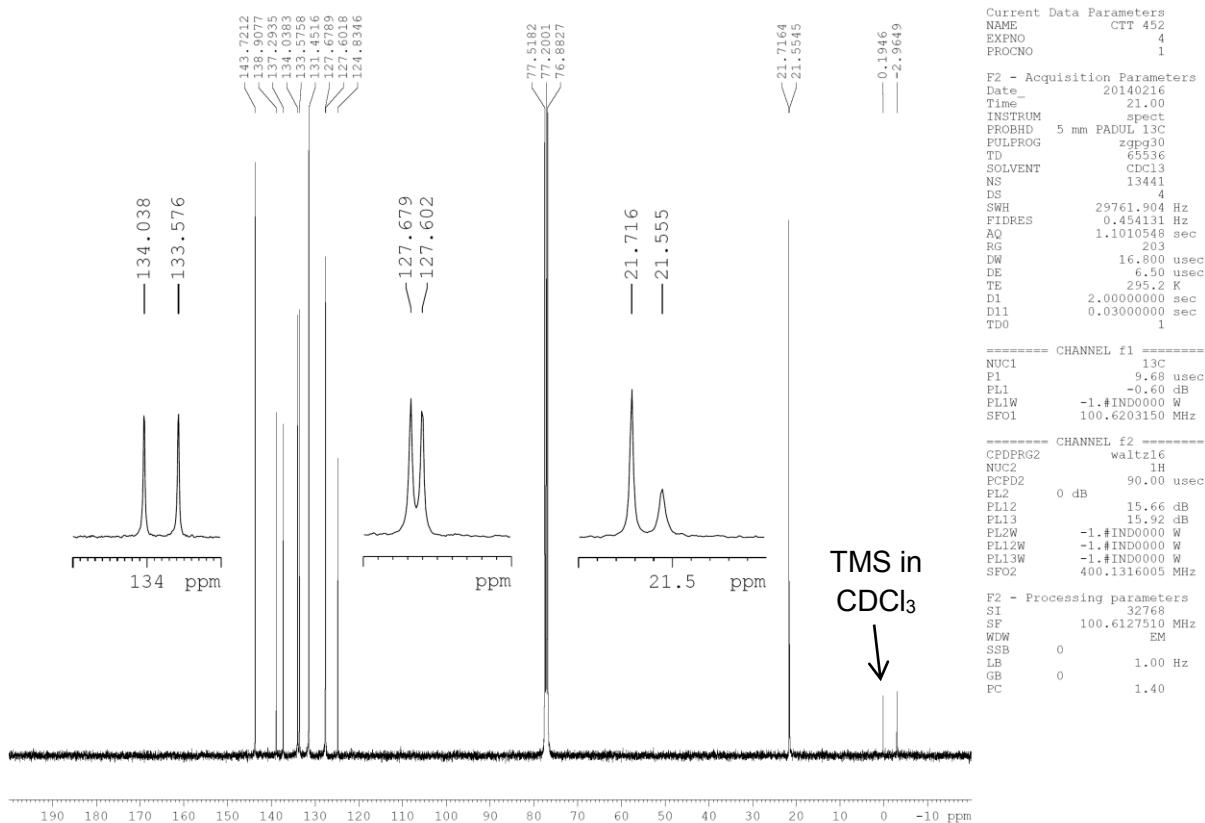
Current Data Parameters
NAME          CTT Ir(tp)iPr
EXPNO        5
PROCNO       1

F2 - Acquisition Parameters
Date_        20140212
Time_        9.34
INSTRUM      spect
PROBHD       5 mm PADDL 13C
PULPROG      zg30
TD            65536
SOLVENT      C6D6
NS            128
DS            2
SWH           12019.230 Hz
FIDRES        0.183399 Hz
AQ            2.7263477 sec
RG            203
DW            41.600 usec
DE            6.50 usec
TE            294.8 K
D1            1.00000000 sec
TDO           1

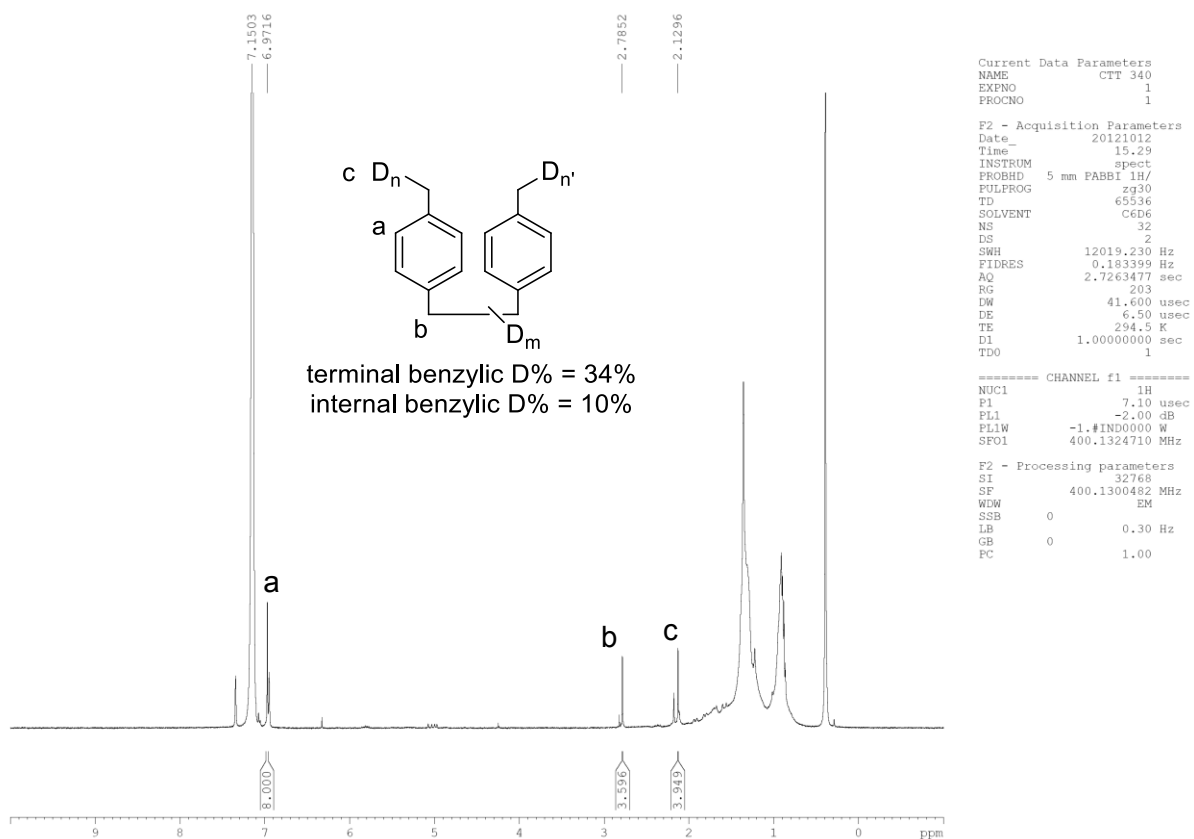
----- CHANNEL f1 -----
NUC1          1H
P1            14.83 usec
PL1           0 dB
PL1W          -1.#IND0000 W
SFO1          400.1324710 MHz

F2 - Processing parameters
SI            32768
SF            400.1300474 MHz
WDW           EM
SSB           0
LB            0.30 Hz
GB            0
PC            1.00
    
```

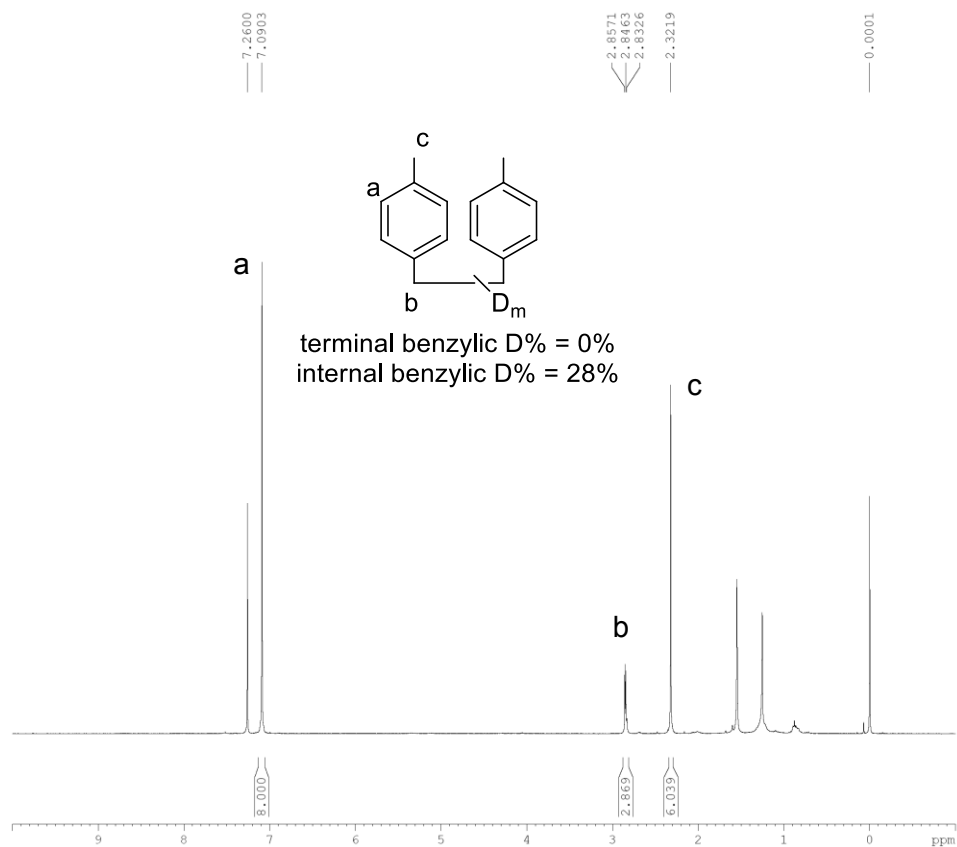
Ir^{III}(ttp)ⁱPr (¹³C{¹H}, CDCl₃, 100 MHz)



5-d (C₆D₆, 400 MHz)



5-d' (CDCl₃, 400 MHz)



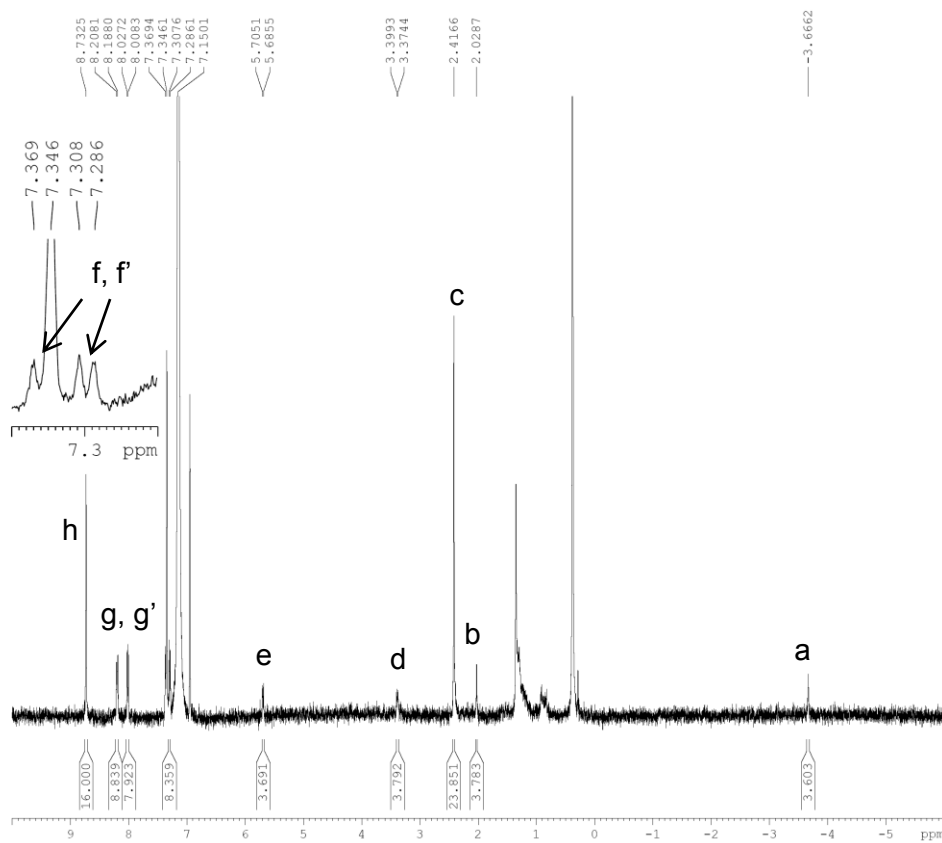
Current Data Parameters
NAME CTT 356
EXPNO 7
PROCNO 1

F2 - Acquisition Parameters
Date_ 20121212
Time_ 9.19
INSTRUM spect
PROBHD 5 mm P4UL 13C
PULPROG zg30
TD 65536
SOLVENT CDCl3
NS 32
DS 2
SWH 12019.230 Hz
FIDRES 0.183399 Hz
AQ 2.7263477 sec
RG 203
DW 41.600 usec
DE 6.50 usec
TE 295.2 K
D1 1.00000000 sec
TD0 1

----- CHANNEL f1 -----
NUC1 1H
P1 15.69 usec
PL1 0 dB
PL1W -1.#IND0000 W
SFO1 400.1324708 MHz

F2 - Processing parameters
SI 32768
SF 400.1300091 MHz
WDW EM
SSB 0
LB 0.30 Hz
GB 0
PC 1.00

Di-Ir 7 (C₆D₆, 400 MHz)



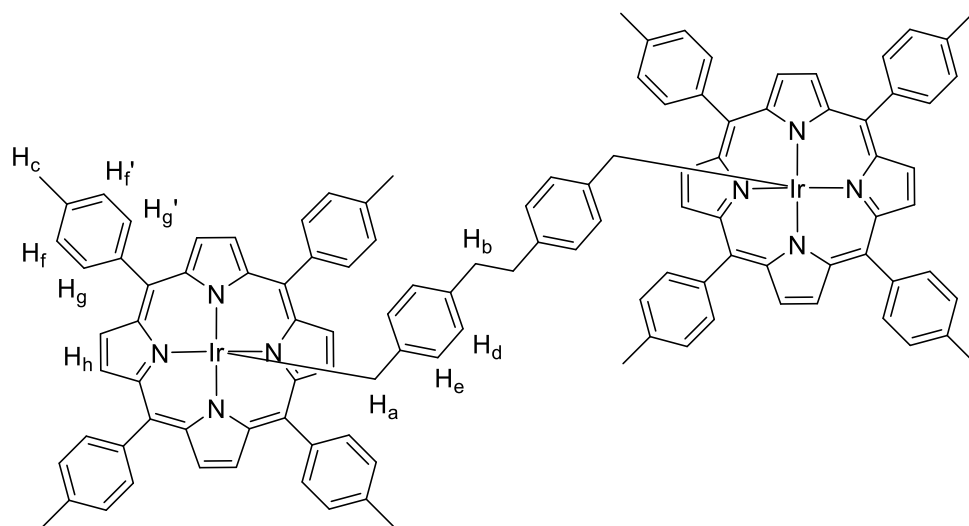
```

Current Data Parameters
NAME          CTT 485
EXPNO        19
PROCNO       1

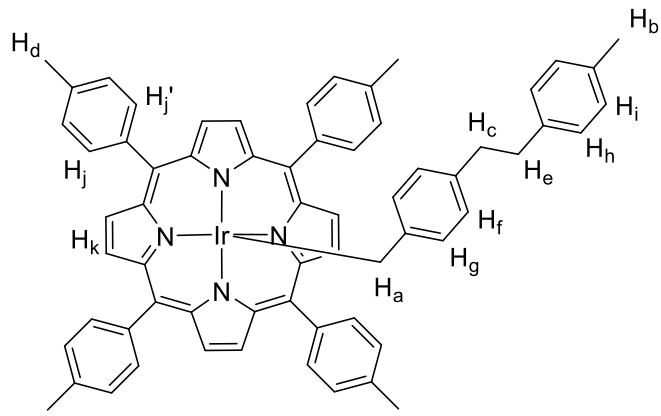
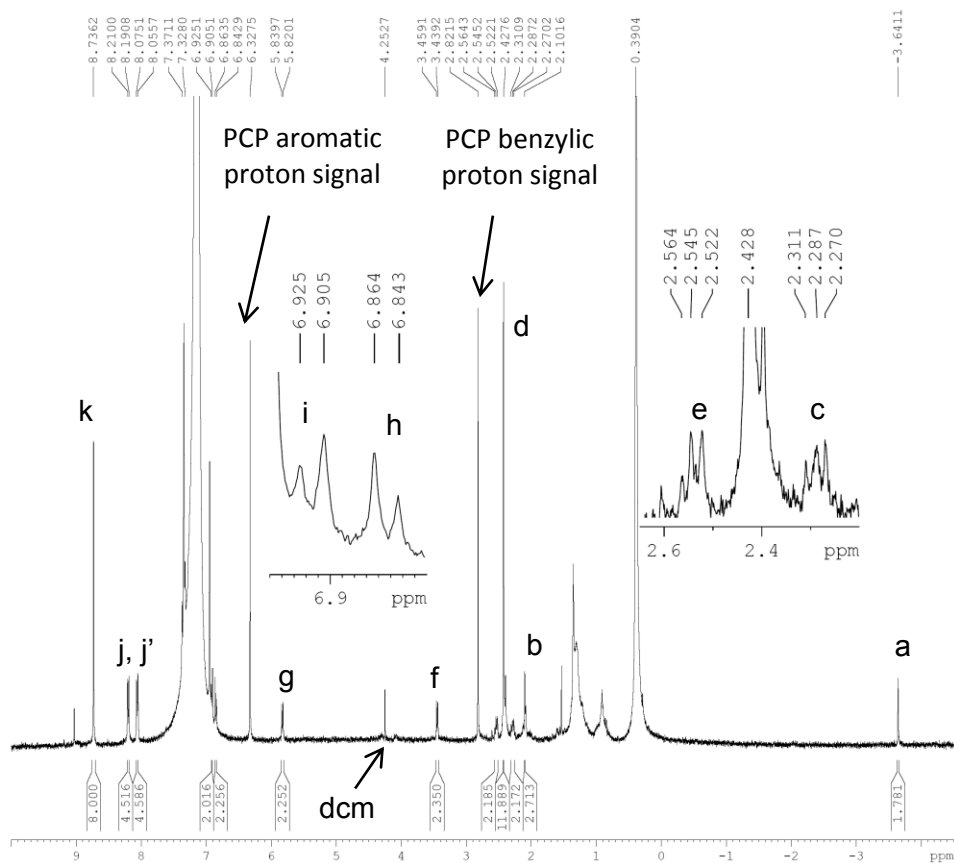
F2 - Acquisition Parameters
Date_         20140825
Time_        15.19
INSTRUM      spect
PROBHD       5 mm PADUL 13C
PULPROG      zg30
TD           65536
SOLVENT      C6D6
NS           40
DS           2
SWH          12019.230 Hz
FIDRES       0.183399 Hz
AQ           2.7263477 sec
RG           203
DW           41.600 usec
DE           6.50 usec
TE           293.9 K
D1           1.00000000 sec
TD0          1

===== CHANNEL f1 =====
NUC1          1H
P1            14.83 usec
PL1           0 dB
PL1W         -1.#IND0000 W
SFO1          400.1300000 MHz

F2 - Processing parameters
SI            32768
SF            400.1300472 MHz
WDW           EM
SSB           0
LB            0.30 Hz
GB            0
PC            1.00
    
```



Mono-Ir 8 (C₆D₆, 400 MHz)



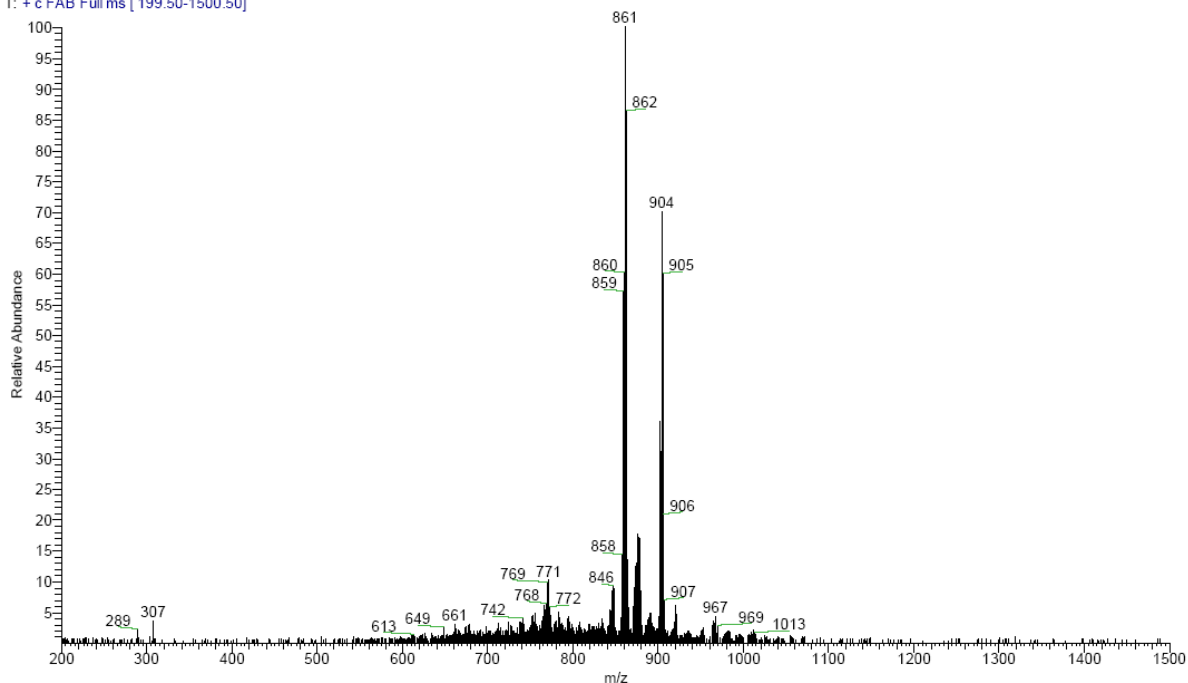
HRMS Spectra

Ir^{III}(ttp)ⁱPr (FAB)

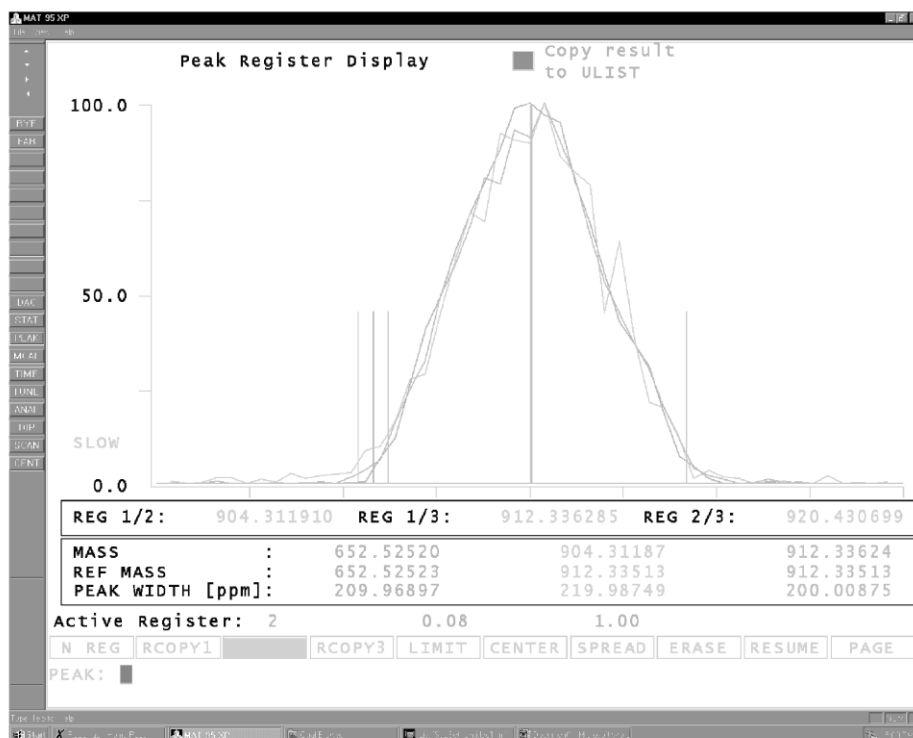
D:\MS_raw_data\ksc1304
fab_pos, 20kV, 4uA, NBA as matrix, unknown conc.
ksc1304 #5 RT: 0.42 AV: 1 NL: 2.57E5
T: + c FAB Full ms [199.50-1500.50]

03/03/14 04:41:21 PM

CTT452

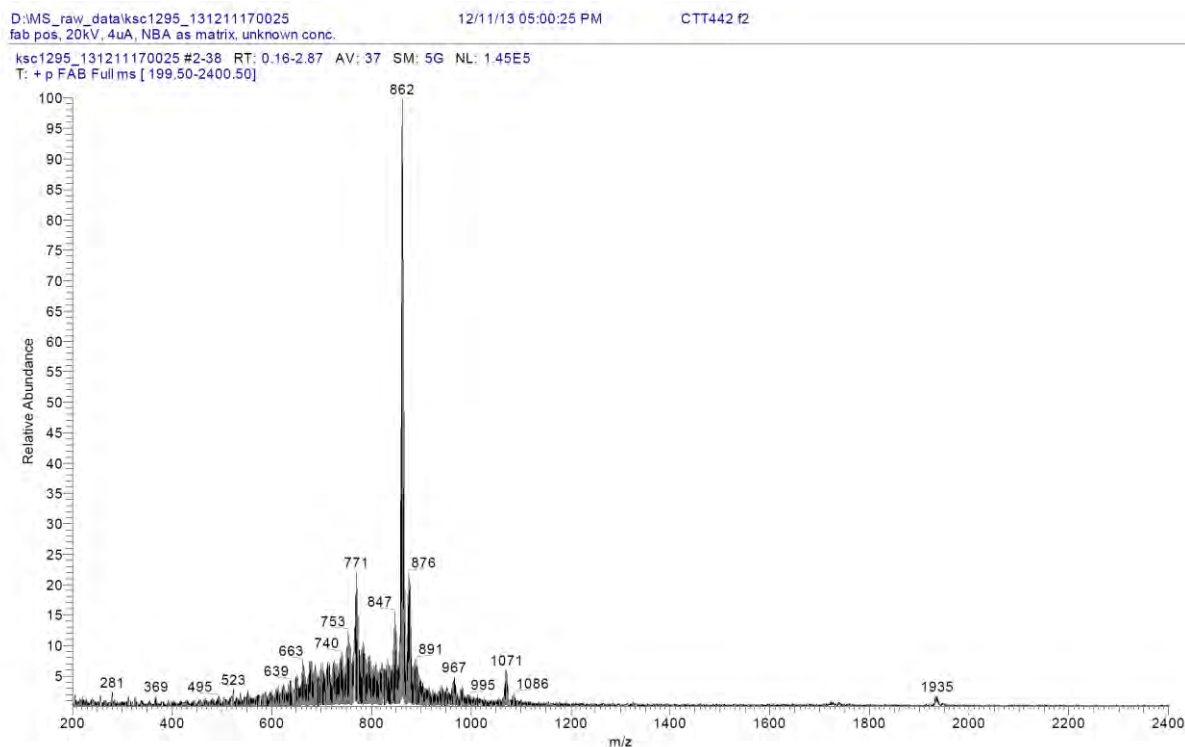


Accurate Mass Measurement

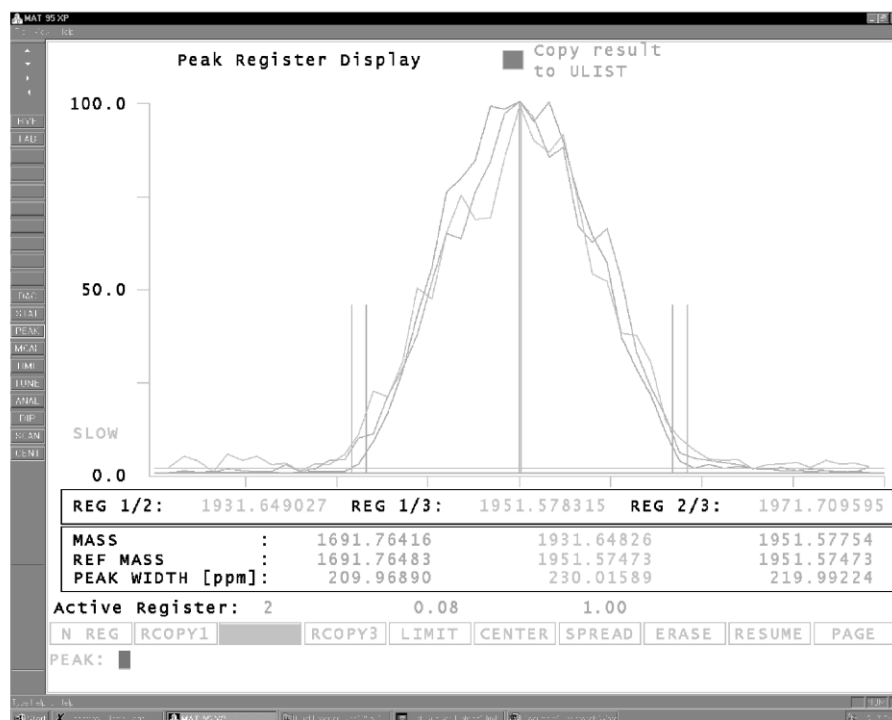


Molecular formula
C51H43N4Ir
[M]⁺ (theoretical)
= 904.3115

Di-Ir 7 (FAB)



Accurate Mass Measurement



Molecular formula
 $C_{112}H_{88}N_8Ir_2$
 $[M+H]^+$ (theoretical)
 = 1931.6484

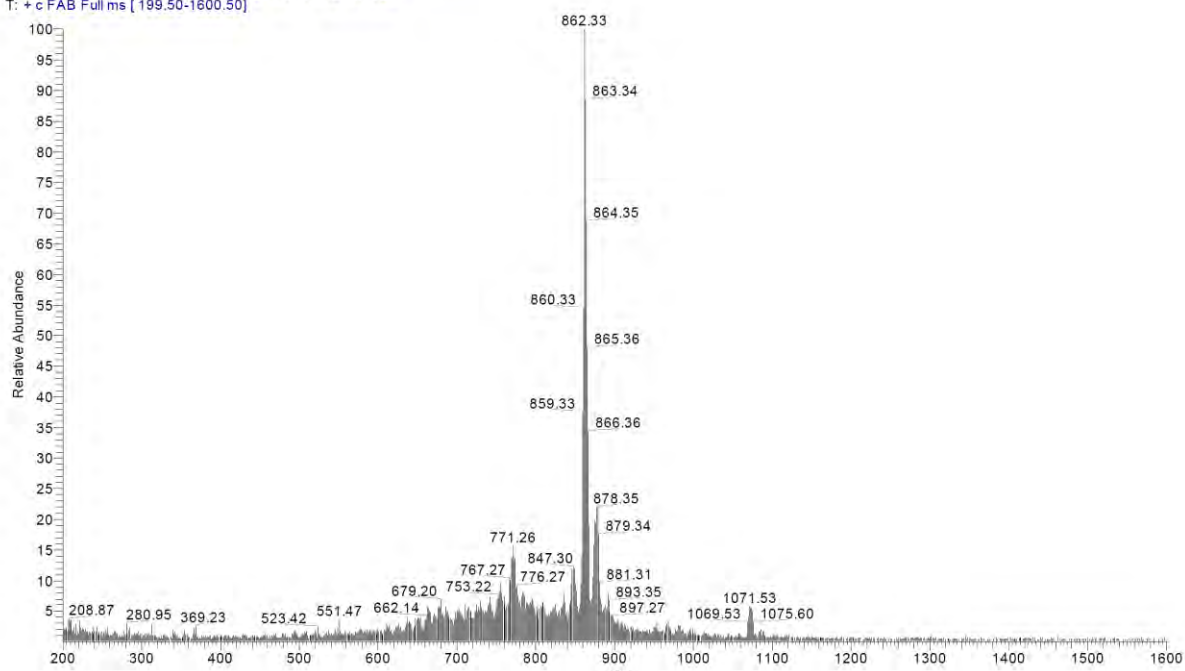
Mono-Ir 8 (FAB)

D:\MS_raw_data\ksc1294_131211132850
 fab pos. 20kV, 4uA, NBA as matrix, unknown conc.

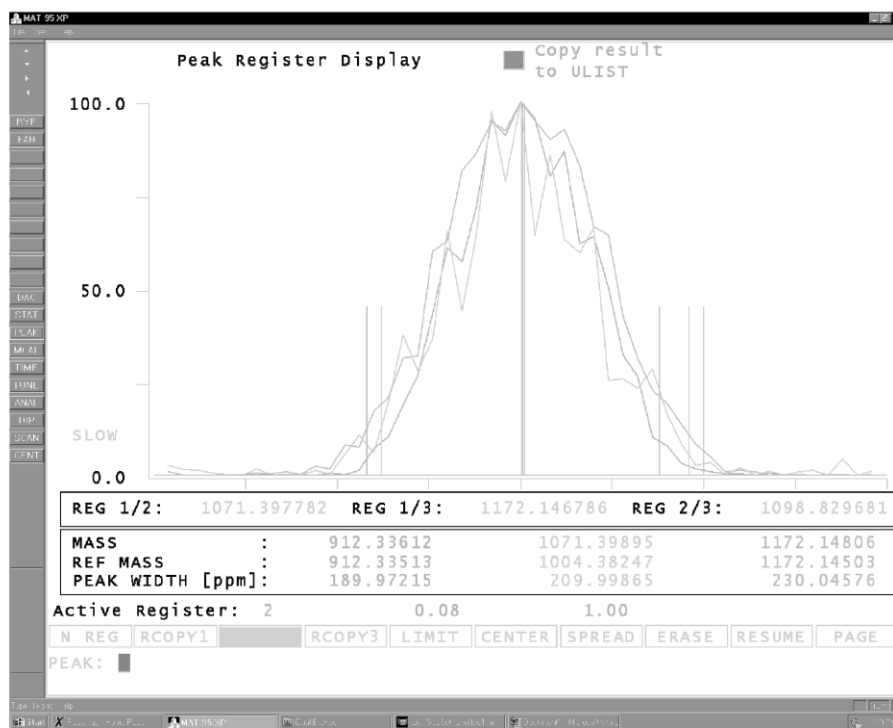
12/11/13 01:28:50 PM

CTT442 f1

ksc1294_131211132850 #1 RT: 0.12 AV: 1 NL: 4.15E5
 T: +c FAB Full ms [199.50-1600.50]



Accurate Mass Measurement



Molecular formula
 $C_{64}H_{53}N_4Ir$
 $[M+H]^+$ (theoretical)
 = 1071.3978

References

1. Cram, D. J.; Steinberg, H. *J. Am. Chem. Soc.* **1951**, *73*, 5691-5703.
2. Van der Ent, A.; Onderdelinden, A. L. *Inorg. Synth.* **1973**, *14*, 92-95.
3. (a) Ogoshi, H.; Setsune, J.-I.; Yoshida, Z.-I. *J. Organomet. Chem.* **1978**, *159*, 317-328. (b) Yeung, S. K.; Chan, K. S. *Organometallics* **2005**, *24*, 6426-6430.
4. Ogoshi, H.; Setsune, J.-I.; Omura, T.; Yoshida, Z.-I. *J. Am. Chem. Soc.* **1975**, *97*, 6461-6466.
5. Cheung, C. W.; Chan, K. S. *Organometallics* **2008**, *27*, 3043-3055.
6. Chan, K. S.; Leung, Y.-B. *Inorg. Chem.* **1994**, *33*, 3187.

Chapter 4 Catalytic Carbon-Carbon Bond Hydrogenation of [2.2]Paracyclophane with Water by Cobalt Porphyrin Complexes

4.1 Introduction

In the rhodium and iridium porphyrin catalyzed hydrogenation of PCP with water, activation of $M^{III}(ttp)R$ pre-catalyst to $M^{II}(ttp)$ for CCA is a prerequisite reaction step. In addition, $M^{II}(ttp)$ is in equilibrium with its dimer $M^{II}_2(ttp)_2$. The use of $M^{III}(ttp)R$ pre-catalyst is beneficial from easy reaction setup, it suffers the drawback of lengthened reaction time. Direct utilization of rhodium(II) or iridium(II) metalloporphyrin radicals as catalyst requires multistep preparation and extra manipulation precautions due to their air-sensitiveness.

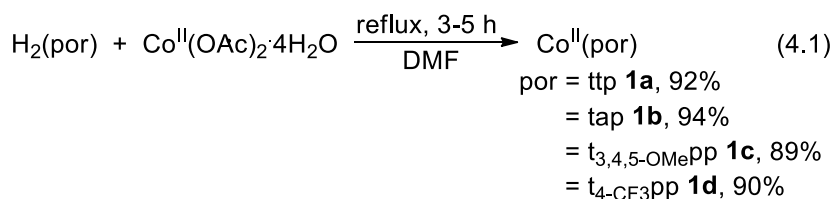
Cobalt(II) porphyrin complexes are attractive alternative choices of catalyst. They can be readily accessed by the simple metallation of free base porphyrins. They are air stable and allow easy reaction setup. Previously, the Chan group has successfully utilized the metalloradical character of cobalt(II) porphyrin complexes for stoichiometric and catalytic transformation of aryl C-X bond ($X = I$ and Br).¹ In addition, the economic competitiveness of cobalt compared with rhodium and iridium is of more practical use. In this chapter, the examination of cobalt(II) porphyrin catalyzed hydrogenation of PCP with H_2O is reported.

4.2 Objectives of the Work

We aim to develop a cheap and user-friendly cobalt porphyrin catalyzed C-C σ -bond hydrogenation protocol using H_2O .

4.3 Preparation of Cobalt(II) Porphyrins

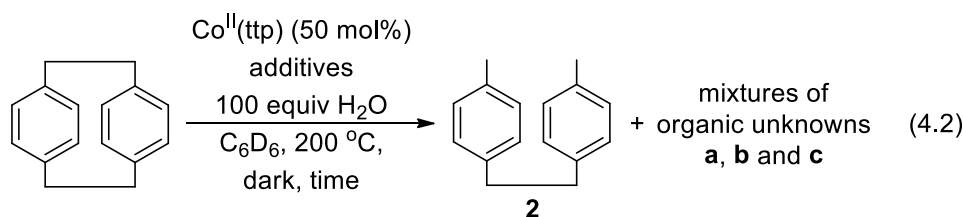
$Co^{II}(ttp)$, $Co^{II}(tap)$, $Co^{II}(t_{3,4,5-OMe}pp)$ and $Co^{II}(t_{4-CF_3}pp)$ were prepared in 92%, 94%, 89% and 90% yields, respectively, by refluxing $Co^{II}(OAc)_2 \cdot 4H_2O$ with the corresponding free base porphyrins in DMF according to the literature method (eq 4.1).²



4.4 Discovery of Selective Hydrogenation of PCP in DMF Solvent

Initially, we suspected that $\text{Co}^{\text{II}}(\text{ttp})$ would be less reactive than $\text{Rh}^{\text{II}}(\text{ttp})$ and $\text{Ir}^{\text{II}}(\text{ttp})$ in the CCA of PCP due to the formation of much weaker Co-C bond than Rh-C and Ir-C bonds.³ Hence, a high loading of $\text{Co}^{\text{II}}(\text{ttp})$, e.g. 50 mol%, was employed to investigate the catalytic hydrogenation of PCP with H_2O . The first attempt yielded only trace amount of the hydrogenation product **2**, together with a mixture of at least three organic unknowns **a**, **b** and **c** (Table 4.1, eq 4.2, entry 1). Preliminary information from their ^1H NMR spectra suggested that **a** and **b** were PCP ring-opening products due to the downfield shifted aromatic signals (Figure 4.1).⁴ The organic unknowns **a** and **b** were unlikely the dimer or trimer of **2** based on their ^1H NMR spectra (see experimental). $\text{Co}^{\text{II}}(\text{ttp})$ was successfully recovered in 80% yield, supporting its true catalyst nature.

Table 4.1 Catalytic Hydrogenation of PCP with H_2O .



entry	additives	Time / h	Total Organics / %	$\text{Co}^{\text{II}}(\text{ttp})$ recovery / %	Remarks
1	--	20	45	80	
2	5 mol% PPh_3	16	57	95	only trace amount of 2
3	2 equiv KOH	38	66	85	
4	DMF- <i>d</i> ₇ solvent	41	14	0	2 was formed selectively with trace unknown b

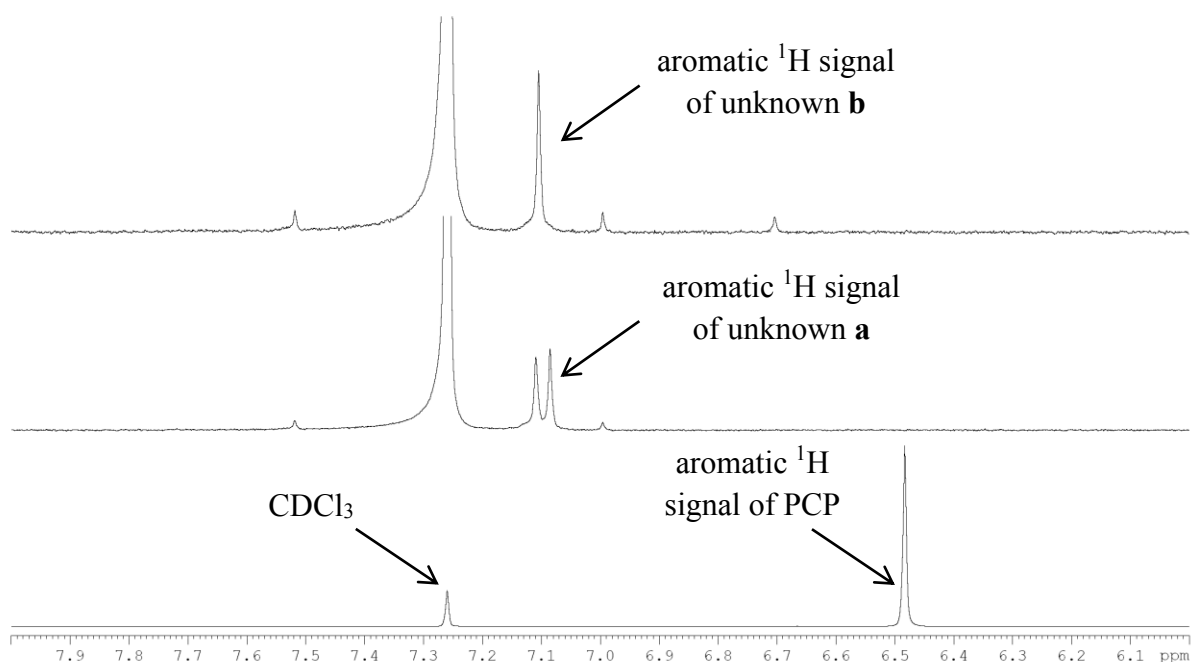
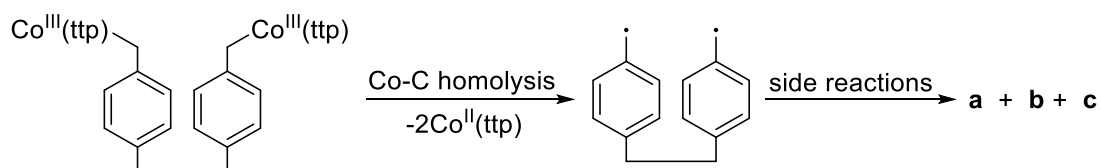


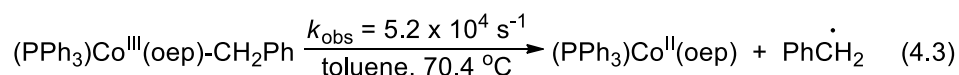
Figure 4.1 Expanded ^1H NMR Spectra of PCP, unknown **a** and **b** in CDCl_3 .

Addition of PPh_3 to generate the more electron rich $(\text{PPh}_3)\text{Co}^{\text{II}}(\text{ttp})$ in situ was attempted.⁵ The coordination of PPh_3 also helps stabilize the $\text{Co}(\text{III})$ state after the CCA step. However, the same mixture of organic products was still obtained with the addition of 5 mol% of PPh_3 (Table 4.1, entry 2, eq 4.2). Owing to the high reaction temperature at $200\text{ }^\circ\text{C}$ and low loading of PPh_3 , the concentration of $(\text{PPh}_3)\text{Co}^{\text{II}}(\text{ttp})$ was reasoned to be low in the reaction mixture.⁶

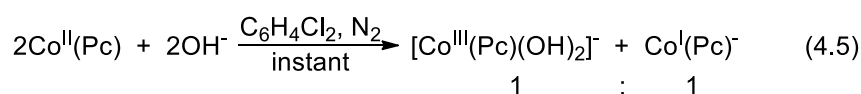
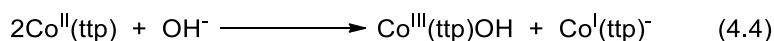
We reasoned that the organic products **a**, **b** and **c** were originated from the homolysis of Co-C bond in the CCA intermediates (Scheme 4.1). The Co-C bond is very weak with BDE reported as 23.8 kcal/mol in $(\text{PPh}_3)\text{Co}^{\text{III}}(\text{oep})\text{-Bn}$.⁷ Kinetic measurements by Halpern revealed fast homolysis rate constant $k_{\text{obs}} = 5.2 \times 10^4\text{ s}^{-1}$ at $70.4\text{ }^\circ\text{C}$ (eq 4.3).



Scheme 4.1 Decomposition of CCA Intermediates.



Thus, 2 equiv of KOH was added to promote the hydrolysis. However, the hydrogenation product **2** was not formed selectively with added KOH (Table 4.1, eq 4.2, entry 3). Moreover, the reaction time became longer. The addition of KOH might have promoted the ligand induced disproportionation of $\text{Co}^{\text{II}}(\text{ttp})$ to give $\text{Co}^{\text{I}}(\text{ttp})^-$ and $\text{Co}^{\text{III}}(\text{ttp})\text{OH}$ (eq 4.4). This significantly reduced the concentration of $\text{Co}^{\text{II}}(\text{ttp})$ for CCA of PCP. Analogous disproportionation of macrocyclic cobalt(II) tetra(neopentoxo)phthalocyanine, $\text{Co}^{\text{II}}(\text{Pc})$, in the presence of OH^- to give 1:1 mixture of $[\text{Co}^{\text{III}}(\text{Pc})(\text{OH})_2]^-$ and $\text{Co}^{\text{I}}(\text{Pc})^-$ has been reported (eq 4.5).⁸



Finally, we employed DMF-*d*₇ polar solvent to facilitate the hydrolysis. To our delight, PCP was catalytically hydrogenated to yield **2** selectively in 14% yield (Table 4.1, eq 4.2, entry 4). $\text{Co}^{\text{II}}(\text{ttp})$ could not be recovered after the catalysis. Although the reaction yield was low, it led to a correct direction to further optimize the cobalt(II) porphyrin catalyzed hydrogenation of PCP with H₂O. In order to minimize the cost of DMF-*d*₇ for further investigations, DMF was employed as the solvent and the reactions were monitored by TLC analysis.

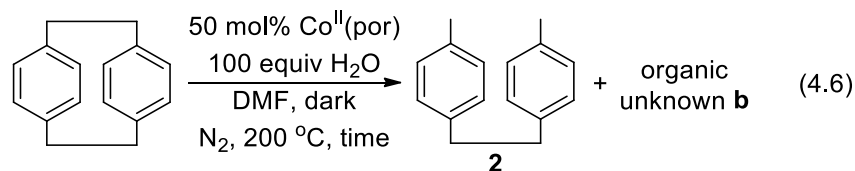
4.5 Optimization of Catalytic Hydrogenation of PCP with H₂O

4.5.1 Porphyrin Ligand Electronic Effects

We then examined the porphyrin ligand electronic effects. $\text{Co}^{\text{II}}(\text{ttp})$ and more electron rich $\text{Co}^{\text{II}}(\text{tap})$ catalysts performed similarly to give 29% and 28% yields of **2** selectively in 32

h (Table 4.2, eq 4.6, entries 1 and 2). $\text{Co}^{\text{II}}(\text{t}_4\text{-CF}_3\text{pp})$ dissolved poorly in DMF at r.t. and resulted in a longer reaction time (Table 4.2, eq 4.6, entry 3). Hence, no significant porphyrin electronic effects were observed and $\text{Co}^{\text{II}}(\text{ttp})$ was the most cost-effective catalyst.

Table 4.2 Porphyrin Ligand Electronic Effects.



entry	por	Time / h	GC yield / %			Co ^{II} (por) recovery / %	
			2	unknown b ^a	PCP recovery		total
1	ttp	32	29	2	1	32	0
2	tap	32	28	2	< 1	30	0
3	t ₄ -CF ₃ pp	48	35	1	0	36	0

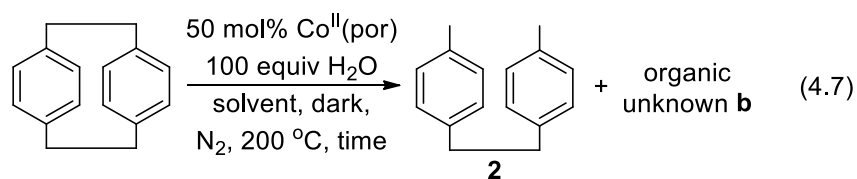
^a estimated from the ¹H NMR of crude reaction mixture

4.5.2 Solvent Effects

In view of the importance of DMF for achieving selective catalytic hydrogenation of PCP with H₂O, we investigated the potential of using other polar solvents, e.g. CH₃CN and *N*-methyl-2-pyrrolidone (NMP), to see whether the polar solvent effect was general. Due to the poor solubility of $\text{Co}^{\text{II}}(\text{ttp})$ in CH₃CN and NMP at r.t., $\text{Co}^{\text{II}}(\text{t}_{3,4,5}\text{-OMepp})$ and $\text{Co}^{\text{II}}(\text{tap})$ were utilized in CH₃CN and NMP solvents, respectively, to ensure complete solubility with the assumption of insignificant porphyrin ligand electronic effects based on previous results.⁹

The catalytic hydrogenation of PCP carried out in CH₃CN and NMP yielded only less than 10% of **2**, even though the corresponding $\text{Co}^{\text{II}}(\text{por})$ catalysts could be recovered (Table 4.3, entries 2 and 3, eq 4.7). The dielectric constants of DMF, CH₃CN and NMP are 38.3, 36.6 and 32.6, respectively, suggesting that they are similarly polar.¹⁰ Hence, the role of DMF was likely unique.

Table 4.3 Solvent Effects.



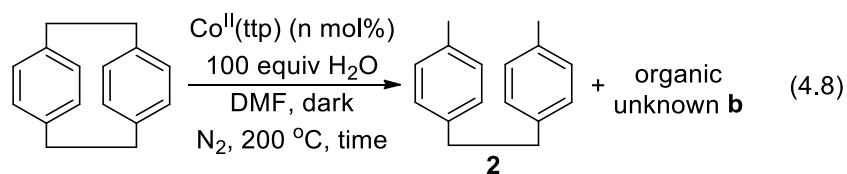
entry	por	solvent	Time / h	GC yield / %			Co ^{II} (por) recovery / %	
				2	unknown b ^a	PCP recovery		total
1	ttp	DMF	32	29	2	1	32	0
2	t _{3,4,5} -OMe ₃ pp	CH ₃ CN	60	trace	5	34	39	71
3	tap	NMP	48	7	0	1	8	91

^a estimated from the ¹H NMR of crude reaction mixture

4.5.3 Catalyst Loading Effects

The Co^{II}(ttp) catalyst loading effects were then examined. In general, the yields of hydrogenation product **2** increased with decreasing Co^{II}(ttp) loadings with the compromise of longer reaction times (Table 4.4, eq 4.8). At 10 mol% of Co^{II}(ttp) loading, a good mass balance of the reactants and products was observed (Table 4.4, eq 4.8, entry 1). On the contrary, employing 2 equiv of Co^{II}(ttp) led to almost complete decomposition of the organic compounds (Table 4.4, eq 4.8, entry 6). In addition, 41% total yield of Co^{II}(ttp) and suspected (DMF)Co^{II}(ttp) were recovered (Figure 4.2). Hence, the decomposition of Co^{II}(ttp) catalyst and the organic compounds was very likely in a stoichiometric relationships. The reactions carried out in air resulted in slightly lower yield of **2** (Table 4.4, entries 2 vs 3, eq 4.8).

Table 4.4 Co^{II}(ttp) Catalyst Loading Effects.



entry	Co ^{II} (ttp) mol%	time	GC yield / %				Co ^{II} (ttp) recovery / %
			2	unknown b ^a	PCP recovery	total	
1	10	4 d	38	0	34	72	0
2	20	3 d	44	1	5	50	0
3 ^b	20	2 d	31	1	2	34	0
4	50	32 h	29	2	1	32	0
5	100	19 h	13	1	< 1	14	0
6	200	19 h	3	N/A ^c	1	4	41 ^d

^a estimated from the ¹H NMR of crude reaction mixture

^b in air

^c unable to determine because of messy crude ¹H NMR spectrum

^d total yield of Co^{II}(ttp) and suspected (DMF)Co^{II}(ttp)

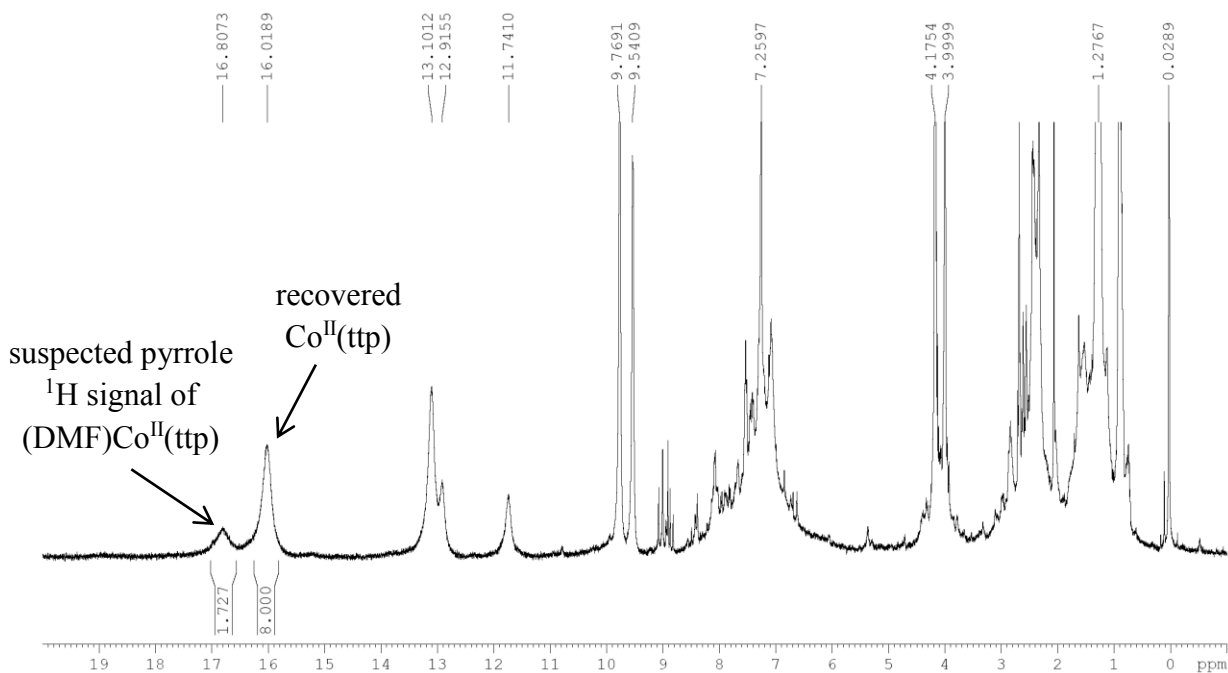


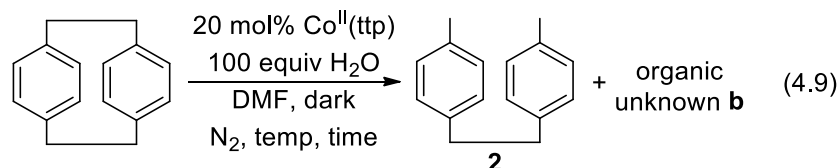
Figure 4.2 Suspected (DMF)Co^{II}(ttp) with Pyrrole ¹H Signal at $\delta = 16.81$ ppm in CDCl₃.

4.5.4 Temperature Effects

In order to minimize the excessive decompositions, the catalysis carried out at milder reaction temperatures was attempted. In addition, the loading of $\text{Co}^{\text{II}}(\text{ttp})$ catalyst was reduced to 20 mol%. At 150 °C, only trace amount of **2** was yielded with PCP recovered in 50% yield (Table 4.5, eq 4.9, entry 1). Moreover, an unknown $\text{Co}^{\text{III}}(\text{ttp})\text{R}$ or $(\text{DMF})\text{Co}^{\text{III}}(\text{ttp})\text{R}$ were observed from the ^1H NMR spectrum of crude reaction mixture with characteristic pyrrole ^1H signal at $\delta = 9.11$ ppm and upfield ^1H signals at $\delta = -2.43$, -3.84 and -6.79 ppm (Figure 4.3). It decomposed to intractable unknowns after purification by column chromatography in dark.

Catalytic hydrogenation of PCP carried out at 170 °C and 180 °C was very slow and yielded only 10% and 33% of **2**, respectively (Table 4.5, eq 4.9, entries 2 and 3). Therefore, milder reaction temperature was insufficient for the catalytic hydrogenation of PCP to occur.

Table 4.5 Temperature Effects.



entry	temp / °C	time / d	GC yield / %				$\text{Co}^{\text{II}}(\text{ttp})$ recovery / %
			2	unknown b ^a	PCP recovery	total	
1	150	2	trace	0	50	50	93 ^b
2	170	4	10	trace	24	34	0
3	180	5	33	1	6	40	0
4	200	3	44	1	5	50	0

^a estimated from the ^1H NMR of crude reaction mixture

^b together with decomposed unknowns

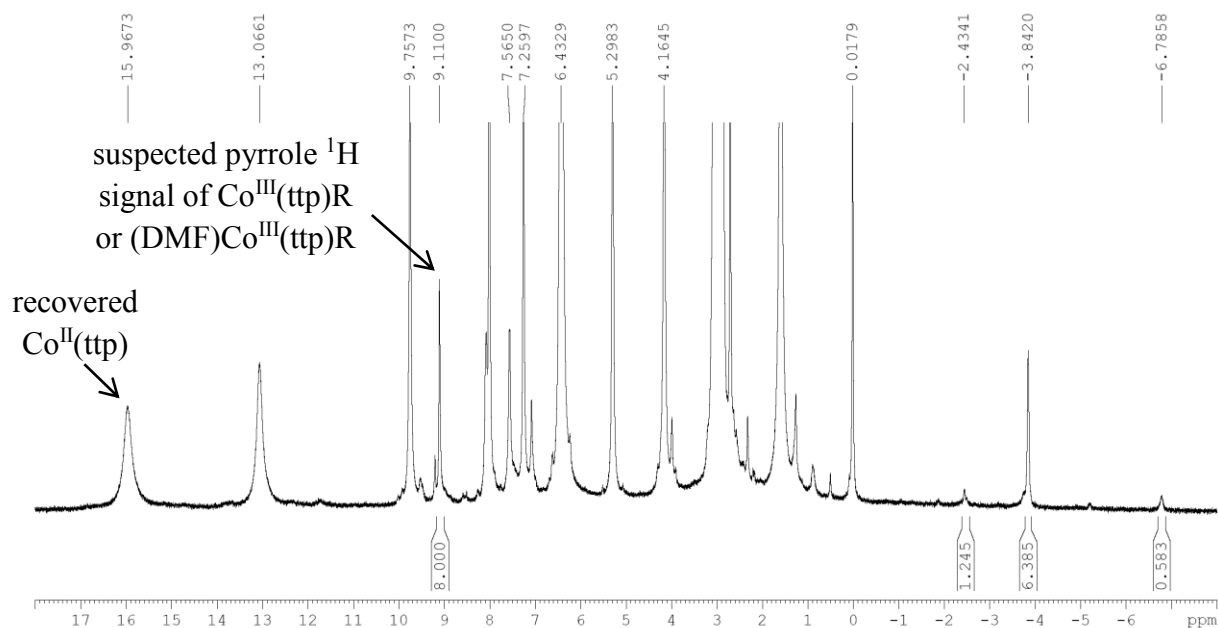


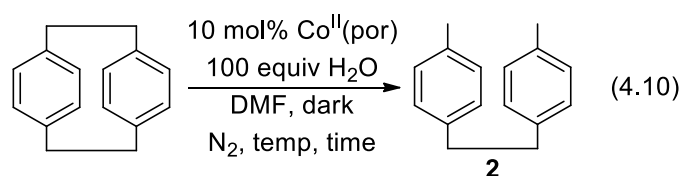
Figure 4.3 Suspected $\text{Co}^{\text{III}}(\text{tp})\text{R}$ or $(\text{DMF})\text{Co}^{\text{III}}(\text{tp})\text{R}$ Formation.

4.5.5 Improved Catalytic Hydrogenation of PCP at Higher Temperatures

From the results obtained in previous sections, two critical parameters were essential to the cobalt(II) porphyrin catalyzed hydrogenation of PCP: (1) low $\text{Co}^{\text{II}}(\text{tp})$ catalyst loading to achieve good mass balance; and (2) high temperature to give enough driving force. Therefore, we attempted to further increase the reaction temperature and to reduce the loading of $\text{Co}^{\text{II}}(\text{por})$ catalyst to 10 mol% to avoid any accelerated decomposition at the same time.

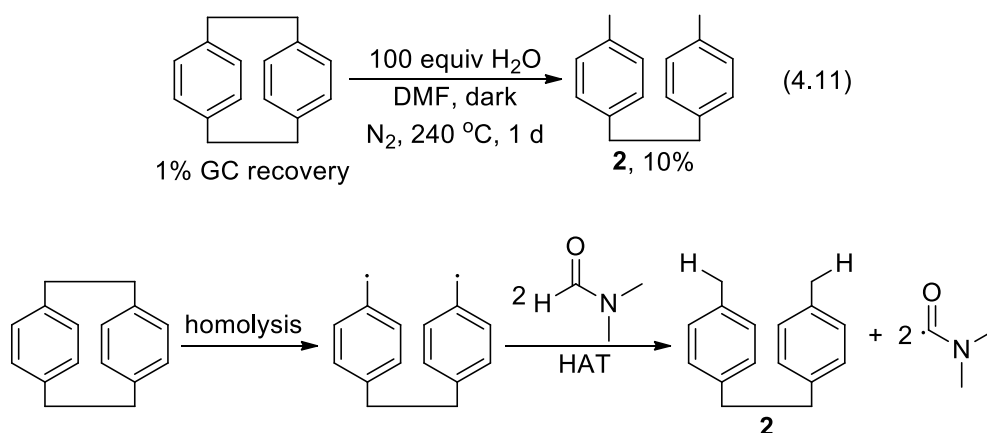
To our delight, PCP was successfully hydrogenated at 220 °C and 240 °C to yield 86% and 97% of **2** in 20 h, respectively (Table 4.6, eq. 4.10, entries 2 and 3). A longer reaction time at 240 °C led to decreased yield of **2** by about 10% (Table 4.6, eq 4.10, entry 4), suggesting that the decomposition of the organic compounds at high temperature. Re-examining the porphyrin ligand electronic effects revealed that both electron rich $\text{Co}^{\text{II}}(\text{tap})$ and electron poor $\text{Co}^{\text{II}}(\text{t}_4\text{-CF}_3\text{pp})$ were poorer catalysts than $\text{Co}^{\text{II}}(\text{tp})$ (Table 4.6, entries 5 and 6, eq 4.10).

Table 4.6 Improved Catalytic Hydrogenation of PCP at Higher Temperatures.



entry	por	temp / °C	time / h	GC yield / %			Co ^{II} (por) recovery / %
				2	PCP recovery	total	
1	ttp	200	72	44	5	50	0
2	ttp	220	20	86	3	89	0
3	ttp	240	20	97	1	98	0
4	ttp	240	48	84	0	84	0
5	tap	240	20	83	< 1	83	0
6	t ₄ -CF ₃ pp	240	20	72	0	72	0

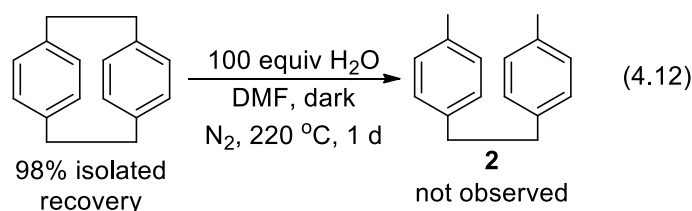
Control experiment at 240 °C showed that PCP was decomposed extensively and yielded 10% of the hydrogenation product **2** (eq 4.11). Homolysis of the weak benzylic carbon-carbon bond of PCP probably took place at 240 °C to form the bi-radical intermediate (Scheme 4.2). It then abstract hydrogen atoms, likely from the aldehydic hydrogen of DMF to form **2**. This process is thermodynamically favorable because the BDE of aldehydic C-H bond in DMF is 81.7 kcal/mol, while that of benzylic C-H bond in toluene is 89.7 kcal/mol. The fate of amino acyl radical is unclear. Fast decarbonylation of this radical is a possible decomposition pathway.¹¹



Scheme 4.2 Proposed Decomposition of PCP to **2** in DMF.

Fortunately, PCP was stable when heated with H₂O in DMF at 220 °C for 1 d (eq 4.12).

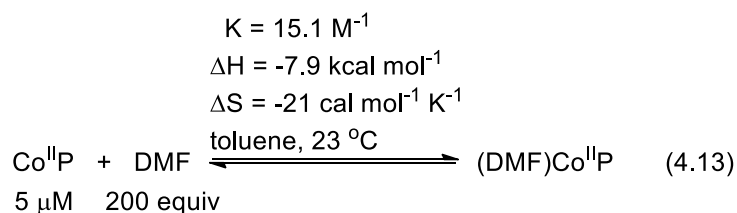
Formation of the hydrogenation product **2** was not observed.



4.6 Mechanistic Investigations

4.6.1 Pre-coordination of DMF to Co^{II}(ttp)

The binding constant of DMF to cobalt(II) protoporphyrin IX dimethyl ester (CoP) at 23 °C in toluene has been reported to be 15.1 M⁻¹ (eq 4.13).¹²



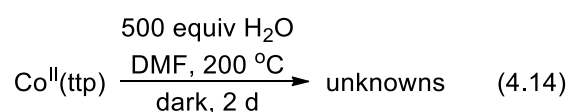
The corresponding binding free energy at 220 °C is estimated to be 2.5 kcal/mol and a weak binding constant of 0.082 M⁻¹. Assume the affinity of DMF towards Co^{II}P is similar to Co^{II}(ttp), the relative ratio of Co^{II}(ttp) and (DMF)Co^{II}(ttp) at 220 °C is only 1:1 for 10 mol% loading of Co^{II}(ttp) even though DMF is employed as the solvent. Therefore, both Co^{II}(ttp) and (DMF)Co^{II}(ttp) are likely the active catalysts in the hydrogenation of PCP.

4.6.2 Stability Test of Co^{II}(ttp) with H₂O in DMF

In view of the excessive Co^{II}(ttp) decomposition observed in most reactions examined, independent experiments were performed to investigate the stability of Co^{II}(ttp) with H₂O in DMF at elevated temperature. Co^{II}(ttp) was decomposed completely into brownish black

unknown solids at 200 °C in 2 d, regardless of N₂ or air atmosphere (Table 4.7, eq 4.14). The unknowns did not give characterizable signals in ¹H NMR analysis. Alternatively, the unknown products obtained from N₂ conditions were dissolved in CH₂Cl₂ for UV-Vis spectroscopic analysis. The Soret band at 409 nm was almost disappeared, supporting the decomposition of Co^{II}(ttp) (Figure 4.4). A new absorption peak at 509 nm was observed. However these data were insufficient to suggest structural assignment for the unknowns.

Table 4.7 Stability Test of Co^{II}(ttp) with H₂O in DMF.



entry	conditions	Co(ttp) recovery / %
1	Air	0
2	N ₂	0

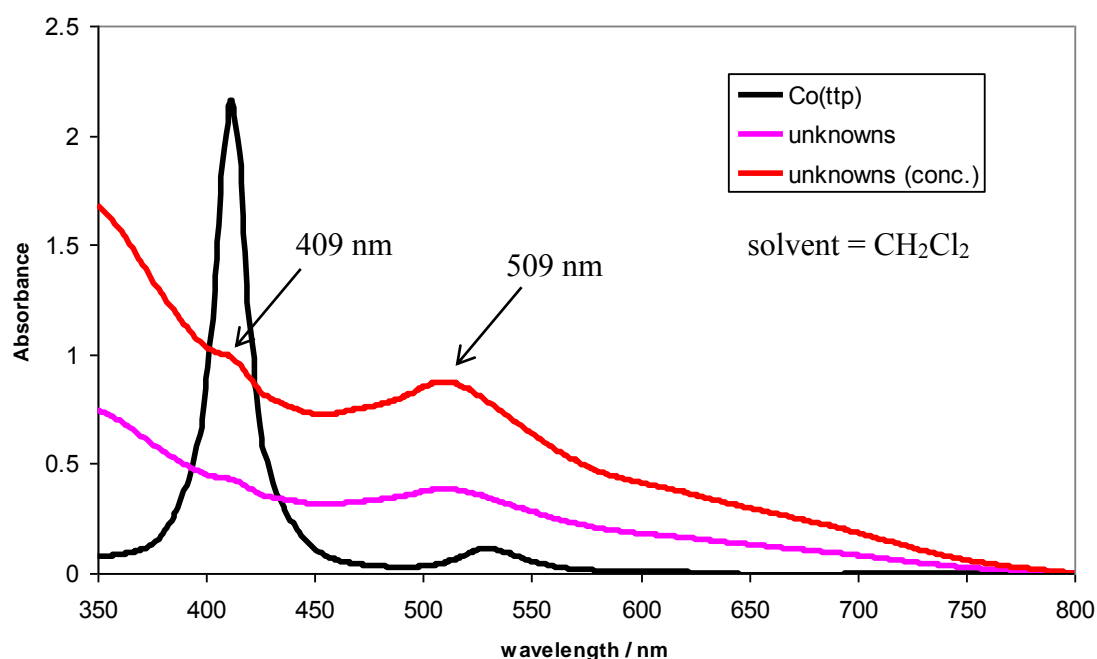


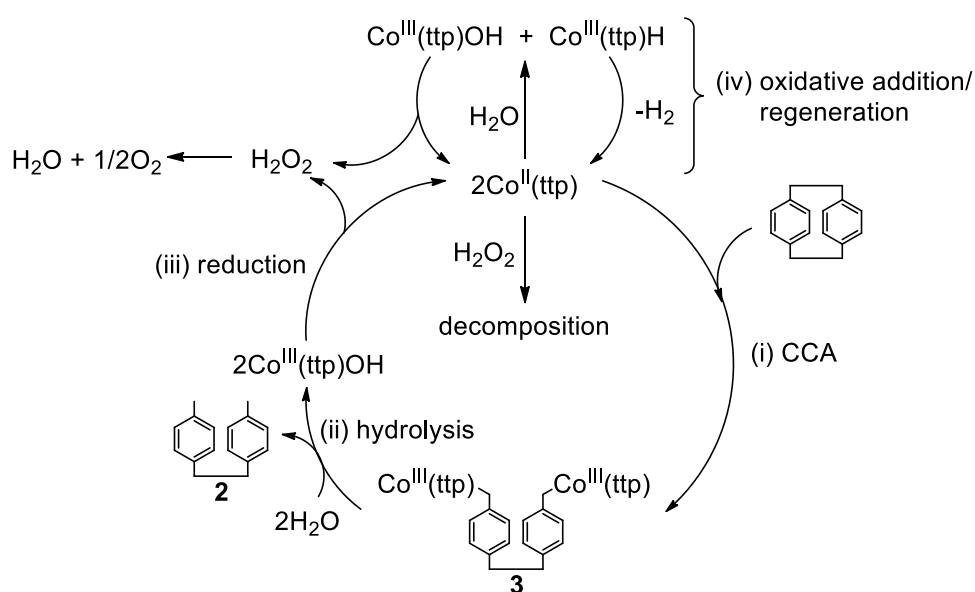
Figure 4.4 Comparison of UV-Vis Spectra of Co^{II}(ttp) and Unknowns.

The oxidative addition of H₂O with Co^{II}(ttp) to give Co^{III}(ttp)H and Co^{III}(ttp)OH in polar DMF may proceed much faster than in non-polar benzene. Coordination of DMF can stabilize the high valent Co(III) state. The oxidative addition of H₂O with Co^{II}(CN)₅³⁻ occurs

readily at 25 °C in aqueous medium.¹³ Dehydrogenation of $\text{Co}^{\text{III}}(\text{ttp})\text{H}$ produces H_2 and regenerates $\text{Co}^{\text{II}}(\text{ttp})$.¹⁴ $\text{Co}^{\text{III}}(\text{ttp})\text{OH}$ is quickly reduced by the OH^- ligand to give back $\text{Co}^{\text{II}}(\text{ttp})$ and produce H_2O_2 , which subsequently oxidizes $\text{Co}^{\text{II}}(\text{ttp})$. The oxidation of other cobalt(II) tetradentate- N_4 macrocycle by H_2O_2 has been suggested to occur by the OH^\cdot attack at the imine nitrogen.¹⁵

4.7 Proposed Mechanism

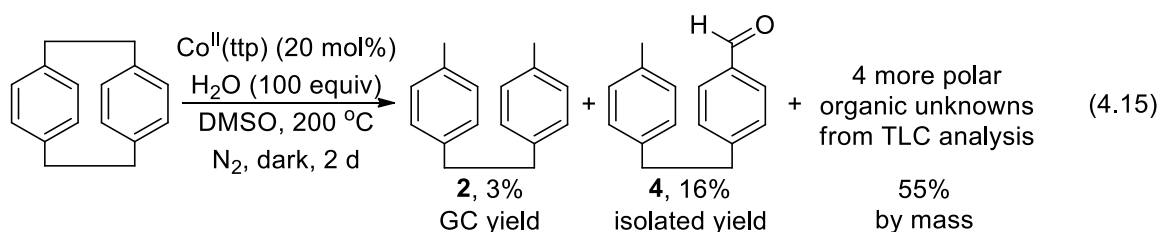
At this stage we lacked in-depth investigations on the cobalt(II) porphyrin catalyzed hydrogenation of PCP with H_2O . Based on the previous understanding on the rhodium and iridium porphyrin catalyzed protocols, a preliminary catalytic cycle is proposed for the cobalt system (Scheme 4.3). $\text{Co}^{\text{II}}(\text{ttp})$ first undergoes CCA with PCP to give the di-Co intermediate **3**, though not observed (step i). In polar DMF solvent, hydrolysis of **3** takes place readily to yield **2** and $\text{Co}^{\text{III}}(\text{ttp})\text{OH}$ (step ii). $\text{Co}^{\text{III}}(\text{ttp})\text{OH}$ is rapidly reduced to regenerate $\text{Co}^{\text{II}}(\text{ttp})$ and give H_2O_2 . At the same time, $\text{Co}^{\text{II}}(\text{ttp})$ reacts quickly with H_2O to produce $\text{Co}^{\text{III}}(\text{ttp})\text{OH}$ and $\text{Co}^{\text{III}}(\text{ttp})\text{H}$, facilitated by the DMF solvent (step iv). Dehydrogenation of $\text{Co}^{\text{III}}(\text{ttp})\text{H}$ affords $\text{Co}^{\text{II}}(\text{ttp})$ and H_2 . Finally, rapid production of H_2O_2 induces the decomposition of $\text{Co}^{\text{II}}(\text{ttp})$.



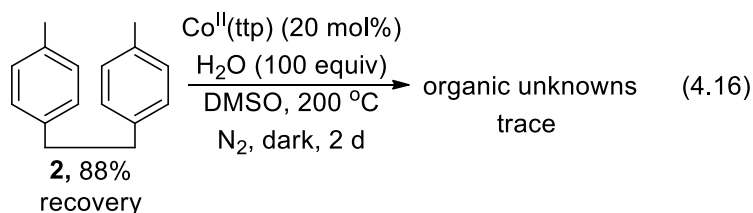
Scheme 4.3 Proposed Catalytic Cycle.

4.8 Co^{II}(ttp) Catalyzed Carbon-Carbon Bond Hydration in DMSO

As an extended study from the solvent effects, attempted catalytic hydrogenation of PCP in DMSO solvent gave unexpected results. When PCP was heated with 20 mol% of Co^{II}(ttp) and 100 equiv of H₂O at 200 °C in DMSO, **2** was formed in only 3% yield (eq 4.15). In addition, an oxygen incorporated product **4** was formed in 16% yield. ¹H NMR analysis of the isolated product suggested an aldehyde functionality. Further experiments are needed to investigate whether H₂O or DMSO act as the oxygen source and Co^{III}(ttp)OH is involved to cleave the benzylic carbon-carbon bond of PCP.



Control experiment was carried out to investigate whether the benzylic C-H bond of **2** could be oxidized in the reaction conditions. Conversion of **2** to **4** was not observed with 88% recovery yield of **2** (eq 4.16).



4.9 Conclusions

The economical Co^{II}(ttp) catalyst shows its promising ability in the catalytic hydrogenation of PCP. Deuterium labeling experiments using D₂O are needed to examine whether H₂O is acting as the hydrogen source. In addition, carbon-carbon σ -bond oxidation of hydrocarbon with H₂O is possible using PCP as the substrate.

References

1. (a) To, C. T.; Chan, T. L.; Li, B. Z.; Hui, Y. Y.; Kwok, T. Y.; Lam, S. Y.; Chan, K. S. *Tetrahedron Lett.* **2011**, *52*, 1023-1026. (b) Qian, Y. Y.; Wong, K. L.; Zhang, M. W.; Kwok, T. Y.; To, C. T.; Chan, K. S. *Tetrahedron Lett.* **2012**, *53*, 1571-1575. (c) Liu, C. R.; Qian, Y. Y.; Chan, K. S. *Dalton Trans.* **2014**, *43*, 7771-7779.
2. Adler, A. D.; Longo, F. R.; Kampas, F.; Kim, J. *J. Inorg. Nucl. Chem.* **1970**, *32*, 2445-2448.
3. Please refer to Chapter 3, section 3.1 for details.
4. The aromatic signal of PCP is more upfield than simple aromatics because of more alkene character due to its bent structure.
5. Wayland, B. B.; Sherry, A. E.; Bunn, A. G. *J. Am. Chem. Soc.* **1993**, *115*, 7675-7684.
6. The ΔH and ΔS of PPh_3 binding to cobalt(II) mesoporphyrin IX dimethyl ester in toluene at 26 °C has been reported to be $-7.0 \text{ kcal mol}^{-1}$ and $-17 \text{ cal mol}^{-1} \text{ K}^{-1}$, respectively. Hence, such binding at 200 °C is unfavorable with ΔG estimated to be $1.0 \text{ kcal mol}^{-1}$, which corresponds to a binding constant of 0.33 M^{-1} . See: Takayanagi, T.; Tamamoto, H.; Kwan, T. *Bull. Chem. Soc. Jpn.* **1975**, *48*, 2618-2622.
7. Geno, M. K.; Halpern, J. *J. Am. Chem. Soc.* **1987**, *109*, 1238-1240.
8. Liu, W.; Hempstead, M. R.; Nevin, W. A.; Melnik, M.; Lever, A. B. P.; Leznoff, C. C. *J. Chem. Soc., Dalton Trans.* **1987**, 2511-2518.
9. The solubility comparisons were based on visual observation at r.t after treating the $\text{Co}^{\text{II}}(\text{por})$ solutions with 47 kHz sonication for 1 min.
10. Marcus, Y. *The Properties of Solvents*, John Wiley & Sons., 1998.
11. The decarbonylation rate constants for simple alkyl acyl radicals are in the order of 10^4 to 10^8 in solutions at 23 °C. See: Chatgililoglu, C.; Crich, D.; Komatsu, M.; Ryu, I. *Chem. Rev.* **1999**, *99*, 1991-2070.

12. Stynes, D. V.; Stynes, H. C.; James, B. R.; Ibers, J. A. *J. Am. Chem. Soc.* **1973**, *95*, 1796-1801.
13. This has been discussed in details in Chapter 3, section 3.5.6. For reference, see: Sokol, C. S.; Brubaker, Jr. C. H. *J. Inorg. Nucl. Chem.* **1968**, *30*, 3267-3271.
14. Kellett, R. M.; Spiro, T. G. *Inorg. Chem.* **1985**, *24*, 2373-2377.
15. (a) Tait, A. M.; Hoffman, M. Z.; Hayon, E. *Int. J. Radiat. Phys. Chem.* **1976**, *8*, 691-696. (b) Heckman, R. A.; Espenson, J. H. *Inorg. Chem.* **1979**, *18*, 38-43.

Experimental Section

General Procedures

Unless otherwise specified, all reagents were purchased from commercial suppliers and directly used without further purification. Hexane for chromatography was distilled from anhydrous CaCl_2 . Benzene- d_6 was distilled from sodium under vacuum, degassed with three freeze-pump-thaw cycles and stored in a Teflon screw head stoppered flask under N_2 . Thin layer chromatography was performed on pre-coated silica gel 60 F₂₅₄ plates. Silica gel (Merck, 70-230 mesh) was used for column chromatography under air or N_2 .

Melting points were recorded on an MPA100 Automated Melting Point System. ^1H NMR spectra were recorded on a Bruker AV-400 MHz at 400 MHz. Chemical shifts were referenced internally to the residual solvent proton resonance in C_6D_6 ($\delta = 7.15$ ppm), CDCl_3 ($\delta = 7.26$ ppm) or with tetramethylsilane ($\delta = 0.00$ ppm) as the internal standard. Chemical shifts (δ) are reported in parts per million (ppm). Coupling constants (J) are reported in hertz (Hz).

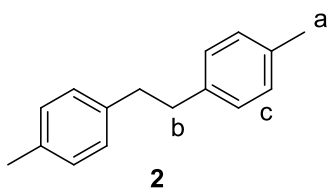
All reactions in 0.5 mL benzene- d_6 or 0.5 mL DMF- d_7 were carried out in a flame-sealed NMR tube in vacuum with the reaction mixture degassed with three freeze(77 K)-pump(0.005 mmHg)-thaw(r.t.) cycles, then heated in oven in dark and wrapped with aluminum foil to protect from exposure to room light before ^1H NMR measurements. The NMR yields were with benzene residue as the internal standard. GC yields were taken using naphthalene as internal standard. Aqueous stock solution of KOH was prepared separately, transferred to the reaction vessel and dried under vacuum at r.t. to obtain anhydrous starting materials. Benzene- d_6 and DMF- d_7 stock solutions of [2.2]paracyclophane were prepared separately, degassed and stored under N_2 before transferred to the reaction vessel. All the $\text{Co}^{\text{II}}(\text{por})$ complexes were prepared according to the literature procedures.¹

Experimental Procedures

Discovery of Selective Hydrogenation of PCP in DMF Solvent

In C₆D₆ without additives. Co^{II}(ttp) (1.7 mg, 0.0024 mmol), H₂O (8.6 μL, 0.48 mmol) and benzene-*d*₆ stock solution (500 μL) of [2.2]paracyclophane (1.0 mg, 0.0048 mmol) were added successively to a NMR tube. The orange mixture was degassed for three freeze-pump-thaw cycles and the NMR tube was flame-sealed under vacuum. It was heated at 200 °C in the dark for 20 h. It was monitored with ¹H NMR spectroscopy at particular time intervals. The organic products were isolated by column chromatography eluting with hexane to remove Co^{II}(ttp). Total yield was taken by mass balance. Product **2**, unknowns **a**, **b** and **c** were re-purified from TLC plate eluting with hexane for 4 times.

Product **2**: ¹H NMR (CDCl₃, 400 MHz) δ 2.32 (s, 6 H, H_a), 2.86 (s, 4 H, H_b), 7.09 (s, 8 H, H_c).



Unknown **a**: ¹H NMR (CDCl₃, 400 MHz) δ 2.32 (s, 3 H), 2.86 (s, 4 H), 3.96 (s, 2 H), 7.10 (d, *J* = 9.6 Hz, 8 H). The integration of proton numbers may reflect the empirical ratio only.

Unknown **b**: ¹H NMR (CDCl₃, 400 MHz) δ 2.86 (s, 8 H), 3.96 (s, 8 H), 6.70 (s, 1 H), 7.10 (s, 16 H). The integration of proton numbers may reflect the empirical ratio only.

Unknown **c**: ¹H NMR (C₆D₆, 400 MHz) δ 2.77 (s, 6 H), 2.79 (s, 7 H), 3.77 (s, 3 H), 4.25 (s, 1 H), 6.98 (s, 16 H). The integration of proton numbers may reflect the empirical ratio only.

In C₆D₆ with 5 mol% PPh₃. Co^{II}(ttp) (1.7 mg, 0.0024 mmol), PPh₃ (0.06 mg, 0.24 μmol), H₂O (8.6 μL, 0.48 mmol) and benzene-*d*₆ stock solution (500 μL) of [2.2]paracyclophane (1.0 mg, 0.0048 mmol) were added successively to a NMR tube. The orange mixture was degassed for three freeze-pump-thaw cycles and the NMR tube was flame-sealed under vacuum. It was heated at 200 °C in the dark for 16 h. It was monitored with ¹H NMR spectroscopy at particular

time intervals. The organic products were isolated by column chromatography eluting with hexane to remove $\text{Co}^{\text{II}}(\text{ttp})$. Total yield was taken by mass balance.

In C_6D_6 with 2 equiv of KOH. $\text{Co}^{\text{II}}(\text{ttp})$ (1.7 mg, 0.0024 mmol), KOH (0.54 mg, 0.0096 mmol), H_2O (8.6 μL , 0.48 mmol) and benzene- d_6 stock solution (500 μL) of [2.2]paracyclophane (1.0 mg, 0.0048 mmol) were added successively to a NMR tube. The orange mixture was degassed for three freeze-pump-thaw cycles and the NMR tube was flame-sealed under vacuum. It was heated at 200 °C in the dark for 38 h. It was monitored with ^1H NMR spectroscopy at particular time intervals. The organic products were isolated by column chromatography eluting with hexane to remove $\text{Co}^{\text{II}}(\text{ttp})$. Total yield was taken by mass balance.

In DMF- d_7 . $\text{Co}^{\text{II}}(\text{ttp})$ (1.7 mg, 0.0024 mmol), H_2O (8.6 μL , 0.48 mmol) and DMF- d_7 stock solution (500 μL) of [2.2]paracyclophane (1.0 mg, 0.0048 mmol) were added successively to a NMR tube. The orange mixture was degassed for three freeze-pump-thaw cycles and the NMR tube was flame-sealed under vacuum. It was heated at 200 °C in the dark for 41 h. It was monitored with ^1H NMR spectroscopy at particular time intervals. The organic products were isolated by column chromatography eluting with hexane. Total yield was taken by mass balance.

Porphyrin Ligand Electronic Effects

With $\text{Co}^{\text{II}}(\text{ttp})$ Catalyst. $\text{Co}^{\text{II}}(\text{ttp})$ (7.0 mg, 0.0096 mmol), H_2O (34 μL , 1.9 mmol) and [2.2]paracyclophane (4.0 mg, 0.019 mmol) were dissolved in 2 mL DMF in a rotaflo tube. The orange mixture was degassed for three freeze-pump-thaw cycles and flushed with N_2 . The tube was heated at 200 °C in the dark for 32 h. After complete consumption of PCP from TLC analysis, the reaction was extracted with CH_2Cl_2 and H_2O to remove DMF. The organic layer was collected and rotary evaporated. The crude mixture was purified by column chromatography eluting with hexane to afford the organic products. GC yields were taken.

With Co^{II}(tap) Catalyst. Co^{II}(ttp) (7.7 mg, 0.0096 mmol), H₂O (34 μL, 1.9 mmol) and [2.2]paracyclophane (4.0 mg, 0.019 mmol) were dissolved in 2 mL DMF in a rotaflo tube. The orange mixture was degassed for three freeze-pump-thaw cycles and flushed with N₂. The tube was heated at 200 °C in the dark for 32 h. After complete consumption of PCP from TLC analysis, the reaction was extracted with CH₂Cl₂ and H₂O to remove DMF. The organic layer was collected and rotary evaporated. The crude mixture was purified by column chromatography eluting with hexane to afford the organic products. GC yields were taken.

With Co^{II}(t₄-CF₃pp) Catalyst. Co^{II}(t₄-CF₃pp) (9.1 mg, 0.0096 mmol), H₂O (34 μL, 1.9 mmol) and [2.2]paracyclophane (4.0 mg, 0.019 mmol) were dissolved in 2 mL DMF in a rotaflo tube. The orange mixture was degassed for three freeze-pump-thaw cycles and flushed with N₂. The tube was heated at 200 °C in the dark for 32 h. After complete consumption of PCP from TLC analysis, the reaction was extracted with CH₂Cl₂ and H₂O to remove DMF. The organic layer was collected and rotary evaporated. The crude mixture was purified by column chromatography eluting with hexane to afford the organic products. GC yields were taken.

Solvent Effects.

With CH₃CN solvent. Co^{II}(t_{3,4,5}-OMe₆pp) (9.9 mg, 0.0096 mmol), H₂O (34 μL, 1.9 mmol) and [2.2]paracyclophane (4.0 mg, 0.019 mmol) were dissolved in 2 mL CH₃CN in a rotaflo tube. The orange mixture was degassed for three freeze-pump-thaw cycles and flushed with N₂. The tube was heated at 200 °C in the dark for 60 h. The reaction was then extracted with CH₂Cl₂ and H₂O to remove DMF. The organic layer was collected and rotary evaporated. The crude mixture was purified by column chromatography eluting with hexane to afford the organic products. GC yields were taken. Co^{II}(t_{3,4,5}-OMe₆pp) was recovered by eluting with CH₂Cl₂ (7.0 mg, 71%).

With NMP solvent. Co^{II}(tap) (7.7 mg, 0.0096 mmol), H₂O (34 μL, 1.9 mmol) and [2.2]paracyclophane (4.0 mg, 0.019 mmol) were dissolved in 2 mL NMP in a rotaflo tube. The orange mixture was degassed for three freeze-pump-thaw cycles and flushed with N₂. The tube was heated at 200 °C in the dark for 60 h. After complete consumption of PCP from TLC analysis, the reaction was extracted with CH₂Cl₂ and H₂O to remove DMF. The organic layer was collected and rotary evaporated. The crude mixture was purified by column chromatography eluting with hexane to afford the organic products. GC yields were taken. Co^{II}(tap) was recovered by eluting with CH₂Cl₂ (7.0 mg, 91%).

Co^{II}(ttp) Catalyst Loading Effects.

With 10 mol% Co^{II}(ttp). Co^{II}(ttp) (1.4 mg, 0.0019 mmol), H₂O (34 μL, 1.9 mmol) and [2.2]paracyclophane (4.0 mg, 0.019 mmol) were dissolved in 2 mL DMF in a rotaflo tube. The orange mixture was degassed for three freeze-pump-thaw cycles and flushed with N₂. The tube was heated at 200 °C in the dark for 4 d. The reaction was then extracted with CH₂Cl₂ and H₂O to remove DMF. The organic layer was collected and rotary evaporated. The crude mixture was purified by column chromatography eluting with hexane to afford the organic products. GC yields were taken.

With 20 mol% Co^{II}(ttp). Co^{II}(ttp) (2.8 mg, 0.0038 mmol), H₂O (34 μL, 1.9 mmol) and [2.2]paracyclophane (4.0 mg, 0.019 mmol) were dissolved in 2 mL DMF in a rotaflo tube. The orange mixture was degassed for three freeze-pump-thaw cycles and flushed with N₂. The tube was heated at 200 °C in the dark for 3 d. After complete consumption of PCP from TLC analysis, the reaction was extracted with CH₂Cl₂ and H₂O to remove DMF. The organic layer was collected and rotary evaporated. The crude mixture was purified by column chromatography eluting with hexane to afford the organic products. GC yields were taken.

With 20 mol% Co^{II}(ttp) in air. Co^{II}(ttp) (2.8 mg, 0.0038 mmol), H₂O (34 μL, 1.9 mmol) and [2.2]paracyclophane (4.0 mg, 0.019 mmol) were dissolved in 2 mL DMF in a rotaflo tube. The tube was heated at 200 °C in the dark for 2 d. After complete consumption of PCP from TLC analysis, the reaction was extracted with CH₂Cl₂ and H₂O to remove DMF. The organic layer was collected and rotary evaporated. The crude mixture was purified by column chromatography eluting with hexane to afford the organic products. GC yields were taken.

With 100 mol% Co^{II}(ttp). Co^{II}(ttp) (14.0 mg, 0.019 mmol), H₂O (34 μL, 1.9 mmol) and [2.2]paracyclophane (4.0 mg, 0.019 mmol) were dissolved in 2 mL DMF in a rotaflo tube. The orange mixture was degassed for three freeze-pump-thaw cycles and flushed with N₂. The tube was heated at 200 °C in the dark for 19 h. After complete consumption of PCP from TLC analysis, the reaction was extracted with CH₂Cl₂ and H₂O to remove DMF. The organic layer was collected and rotary evaporated. The crude mixture was purified by column chromatography eluting with hexane to afford the organic products. GC yields were taken.

With 200 mol% Co^{II}(ttp). Co^{II}(ttp) (28.0 mg, 0.038 mmol), H₂O (34 μL, 1.9 mmol) and [2.2]paracyclophane (4.0 mg, 0.019 mmol) were dissolved in 2 mL DMF in a rotaflo tube. The orange mixture was degassed for three freeze-pump-thaw cycles and flushed with N₂. The tube was heated at 200 °C in the dark for 19 h. After complete consumption of PCP from TLC analysis, the reaction was extracted with CH₂Cl₂ and H₂O to remove DMF. The organic layer was collected and rotary evaporated. The crude mixture was purified by column chromatography eluting with hexane to afford the organic products. GC yields were taken. Cobalt(II) porphyrin complexes were recovered by eluting with CH₂Cl₂ (11.5 mg, 41%).

Temperature Effects.

At 150 °C. Co^{II}(ttp) (2.8 mg, 0.0038 mmol), H₂O (34 μL, 1.9 mmol) and [2.2]paracyclophane (4.0 mg, 0.019 mmol) were dissolved in 2 mL DMF in a rotaflo tube. The orange mixture was

degassed for three freeze-pump-thaw cycles and flushed with N₂. The tube was heated at 150 °C in the dark for 2 d. The reaction was then extracted with CH₂Cl₂ and H₂O to remove DMF. The organic layer was collected and rotary evaporated. The crude mixture was purified by column chromatography eluting with hexane to afford the organic products. GC yields were taken. Cobalt porphyrin complexes were recovered by eluting with CH₂Cl₂ (2.6 mg, 93%).

At 170 °C. Co^{II}(ttp) (2.8 mg, 0.0038 mmol), H₂O (34 μL, 1.9 mmol) and [2.2]paracyclophane (4.0 mg, 0.019 mmol) were dissolved in 2 mL DMF in a rotaflo tube. The orange mixture was degassed for three freeze-pump-thaw cycles and flushed with N₂. The tube was heated at 170 °C in the dark for 4 d. The reaction was then extracted with CH₂Cl₂ and H₂O to remove DMF. The organic layer was collected and rotary evaporated. The crude mixture was purified by column chromatography eluting with hexane to afford the organic products. GC yields were taken.

At 180 °C. Co^{II}(ttp) (2.8 mg, 0.0038 mmol), H₂O (34 μL, 1.9 mmol) and [2.2]paracyclophane (4.0 mg, 0.019 mmol) were dissolved in 2 mL DMF in a rotaflo tube. The orange mixture was degassed for three freeze-pump-thaw cycles and flushed with N₂. The tube was heated at 180 °C in the dark for 5 d. After complete consumption of PCP from TLC analysis, the reaction was extracted with CH₂Cl₂ and H₂O to remove DMF. The organic layer was collected and rotary evaporated. The crude mixture was purified by column chromatography eluting with hexane to afford the organic products. GC yields were taken.

Improved Catalytic Hydrogenation of PCP at Higher Temperatures

At 220 °C. Co^{II}(ttp) (1.4 mg, 0.0019 mmol), H₂O (34 μL, 1.9 mmol) and [2.2]paracyclophane (4.0 mg, 0.019 mmol) were dissolved in 2 mL DMF in a rotaflo tube. The orange mixture was degassed for three freeze-pump-thaw cycles and flushed with N₂. The tube was heated at 220

°C in the dark for 20 h. After complete consumption of PCP from TLC analysis, the reaction was extracted with CH₂Cl₂ and H₂O to remove DMF. The organic layer was collected and rotary evaporated. The crude mixture was purified by column chromatography eluting with hexane to afford the organic products. GC yields were taken.

At 240 °C for 20 h. Co^{II}(ttp) (1.4 mg, 0.0019 mmol), H₂O (34 μL, 1.9 mmol) and [2.2]paracyclophane (4.0 mg, 0.019 mmol) were dissolved in 2 mL DMF in a rotaflo tube. The orange mixture was degassed for three freeze-pump-thaw cycles and flushed with N₂. The tube was heated at 240 °C in the dark for 20 h. After complete consumption of PCP from TLC analysis, the reaction was extracted with CH₂Cl₂ and H₂O to remove DMF. The organic layer was collected and rotary evaporated. The crude mixture was purified by column chromatography eluting with hexane to afford the organic products. GC yields were taken.

At 240 °C for 48 h. Co^{II}(ttp) (1.4 mg, 0.0019 mmol), H₂O (34 μL, 1.9 mmol) and [2.2]paracyclophane (4.0 mg, 0.019 mmol) were dissolved in 2 mL DMF in a rotaflo tube. The orange mixture was degassed for three freeze-pump-thaw cycles and flushed with N₂. The tube was heated at 240 °C in the dark for 48 h. After complete consumption of PCP from TLC analysis, the reaction was extracted with CH₂Cl₂ and H₂O to remove DMF. The organic layer was collected and rotary evaporated. The crude mixture was purified by column chromatography eluting with hexane to afford the organic products. GC yields were taken.

At Co^{II}(tap). Co^{II}(tap) (1.5 mg, 0.0019 mmol), H₂O (34 μL, 1.9 mmol) and [2.2]paracyclophane (4.0 mg, 0.019 mmol) were dissolved in 2 mL DMF in a rotaflo tube. The orange mixture was degassed for three freeze-pump-thaw cycles and flushed with N₂. The tube was heated at 240 °C in the dark for 20 h. After complete consumption of PCP from TLC analysis, the reaction was extracted with CH₂Cl₂ and H₂O to remove DMF. The organic layer was collected and rotary evaporated. The crude mixture was purified by column chromatography eluting with hexane to afford the organic products. GC yields were taken.

At Co^{II}(t₄-CF₃pp). Co^{II}(t₄-CF₃pp) (1.8 mg, 0.0019 mmol), H₂O (34 μL, 1.9 mmol) and [2.2]paracyclophane (4.0 mg, 0.019 mmol) were dissolved in 2 mL DMF in a rotaflo tube. The orange mixture was degassed for three freeze-pump-thaw cycles and flushed with N₂. The tube was heated at 240 °C in the dark for 20 h. After complete consumption of PCP from TLC analysis, the reaction was extracted with CH₂Cl₂ and H₂O to remove DMF. The organic layer was collected and rotary evaporated. The crude mixture was purified by column chromatography eluting with hexane to afford the organic products. GC yields were taken.

Control Experiment at 240 °C. H₂O (34 μL, 1.9 mmol) and [2.2]paracyclophane (4.0 mg, 0.019 mmol) were dissolved in 2 mL DMF in a rotaflo tube. The colorless solution was degassed for three freeze-pump-thaw cycles and flushed with N₂. The tube was heated at 240 °C in the dark for 1 d. After complete consumption of PCP from TLC analysis, the reaction was extracted with CH₂Cl₂ and H₂O to remove DMF. The organic layer was collected and rotary evaporated. The crude mixture was purified by column chromatography eluting with hexane to afford the organic products. GC yields were taken.

Control Experiment at 220 °C. H₂O (34 μL, 1.9 mmol) and [2.2]paracyclophane (4.0 mg, 0.019 mmol) were dissolved in 2 mL DMF in a rotaflo tube. The colorless solution was degassed for three freeze-pump-thaw cycles and flushed with N₂. The tube was heated at 220 °C in the dark for 1 d. The reaction was then extracted with CH₂Cl₂ and H₂O to remove DMF. The organic layer was collected and rotary evaporated. The crude mixture was purified by column chromatography eluting with hexane to recover the PCP (3.9 mg, 98%).

Stability Test of Co^{II}(ttp).

Under air. Co^{II}(tp) (2.8 mg, 0.0019 mmol) and H₂O (34 μL, 1.9 mmol) were dissolved in 2 mL DMF in a rotaflo tube. The tube was heated at 200 °C in the dark for 2 d. After complete

consumption of $\text{Co}^{\text{II}}(\text{tp})$ from TLC analysis, the reaction was extracted with CH_2Cl_2 and H_2O to remove DMF. The organic layer was collected and rotary evaporated to afford crude solids.

Under N_2 . $\text{Co}^{\text{II}}(\text{tp})$ (2.8 mg, 0.0019 mmol) and H_2O (34 μL , 1.9 mmol) were dissolved in 2 mL DMF in a rotaflo tube. The orange mixture was degassed for three freeze-pump-thaw cycles and flushed with N_2 . The tube was heated at 200 $^\circ\text{C}$ in the dark for 2 d. After complete consumption of $\text{Co}^{\text{II}}(\text{tp})$ from TLC analysis, the reaction was extracted with CH_2Cl_2 and H_2O to remove DMF. The organic layer was collected and rotary evaporated to afford crude solids. The solids were dissolved in CH_2Cl_2 for UV-Vis spectroscopic analysis.

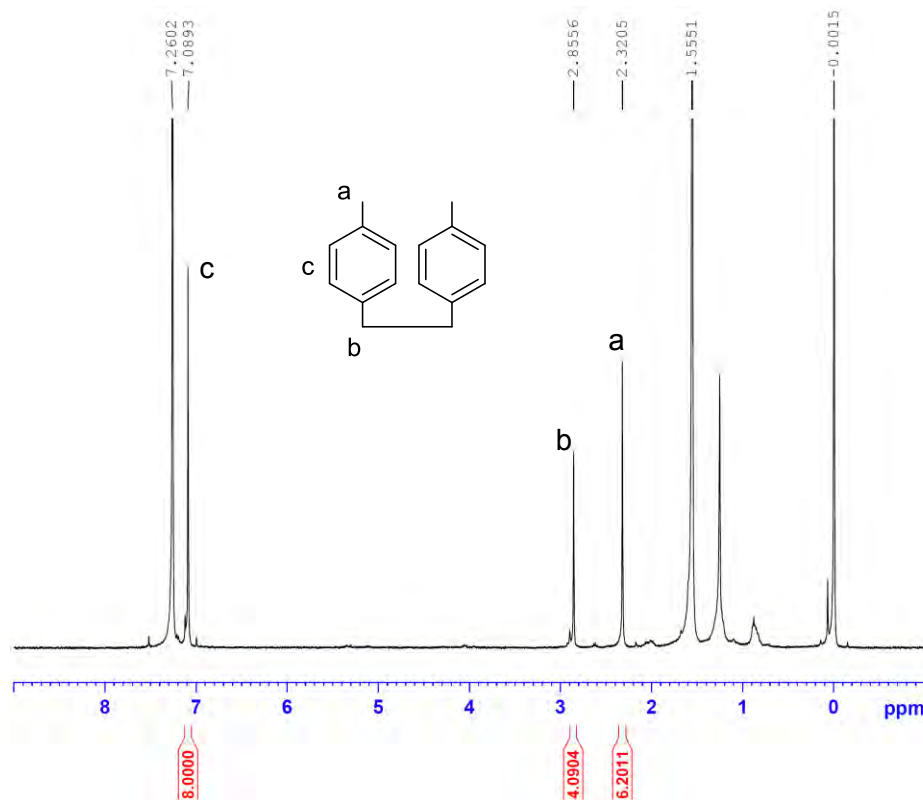
Catalytic Hydration of PCP in DMSO. $\text{Co}^{\text{II}}(\text{tp})$ (2.8 mg, 0.0038 mmol), H_2O (34 μL , 1.9 mmol) and [2.2]paracyclophane (4.0 mg, 0.019 mmol) were dissolved in 2 mL DMSO in a rotaflo tube. The orange mixture was degassed for three freeze-pump-thaw cycles and flushed with N_2 . The tube was heated at 200 $^\circ\text{C}$ in the dark for 2 d. After complete consumption of PCP from TLC analysis, the reaction was extracted with ethyl acetate and H_2O to remove DMSO. The organic layer was collected and rotary evaporated. **2** was first purified by column chromatography eluting with hexane, then **4** was obtained by eluting with hexane/ CH_2Cl_2 = 2:1, finally the unknowns were collected by eluting with CH_2Cl_2 . GC yield was taken for **2**. Isolated yields were taken for **4** (0.7 mg, 16%) and the organic unknowns (2.2 mg, 55%).

Control Experiment of **2.** $\text{Co}^{\text{II}}(\text{tp})$ (2.8 mg, 0.0038 mmol), H_2O (34 μL , 1.9 mmol) and 4,4'-dimethylbibenzyl **2** (4.0 mg, 0.019 mmol) were dissolved in 2 mL DMSO in a rotaflo tube. The orange mixture was degassed for three freeze-pump-thaw cycles and flushed with N_2 . The tube was heated at 200 $^\circ\text{C}$ in the dark for 2 d. The reaction was then extracted with ethyl acetate and H_2O to remove DMSO. The organic layer was collected and rotary evaporated. The crude mixture was purified by column chromatography eluting with hexane to afford the organic products. GC yields were taken.

Appendix I List of Spectra

No.	Spectra	Page
1	¹ H NMR spectra of 2	196
2	¹ H NMR spectra of unknown a	196
3	¹ H NMR spectra of unknown b	197
4	¹ H NMR spectra of unknown c	197
5	¹ H NMR spectrum of 4	198
6	GCMS spectrum of 4	199

2 (CDCl₃, 400 MHz)



```

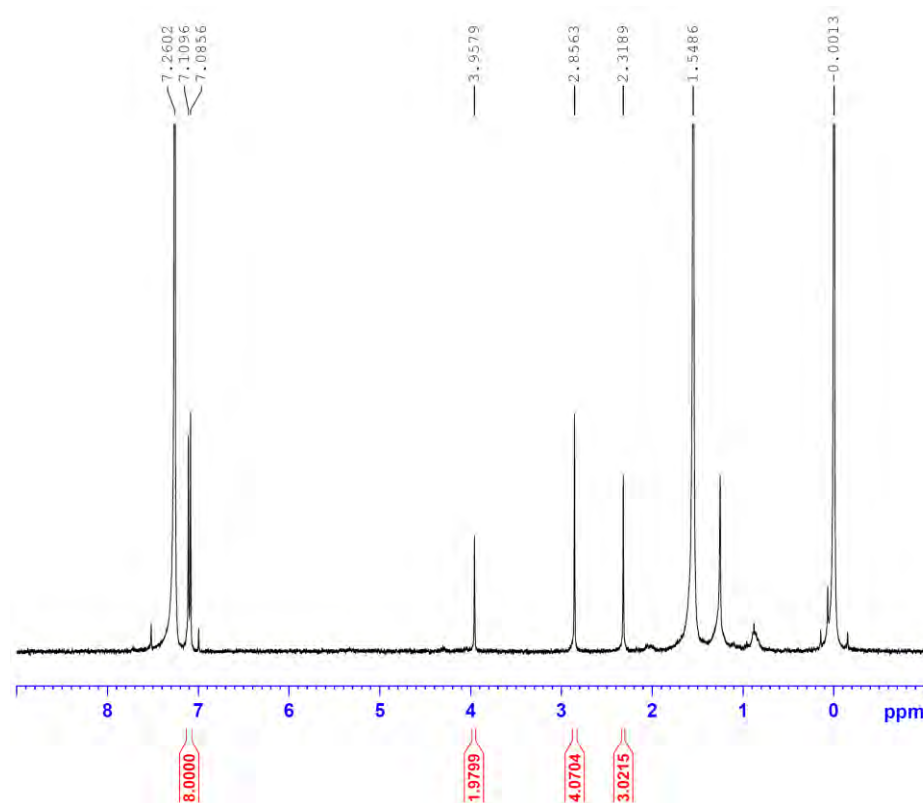
Current Data Parameters
NAME          CTT 273
EXPNO        10
PROCNO       1

F2 - Acquisition Parameters
Date_        20120313
Time_        14.40
INSTRUM      spect
PROBHD       5 mm PABBI 1H/
PULPROG      zg30
TD           65536
SOLVENT      CDCl3
NS           32
DS           2
SWH          12019.230 Hz
FIDRES       0.183399 Hz
AQ           2.7263477 sec
RG           203
DW           41.600 usec
DE           6.50 usec
TE           295.4 K
D1           1.00000000 sec
TD0          1

===== CHANNEL f1 =====
NUC1         1H
P1           7.10 usec
PL1          -2.00 dB
PL1W        -1.4IND0000 W
SFO1         400.1324710 MHz

F2 - Processing parameters
SI           32768
SF           400.1300100 MHz
WDW          EM
SSB          0
LB           0.30 Hz
GB           0
PC           1.00
    
```

unknown a (CDCl₃, 400 MHz)



```

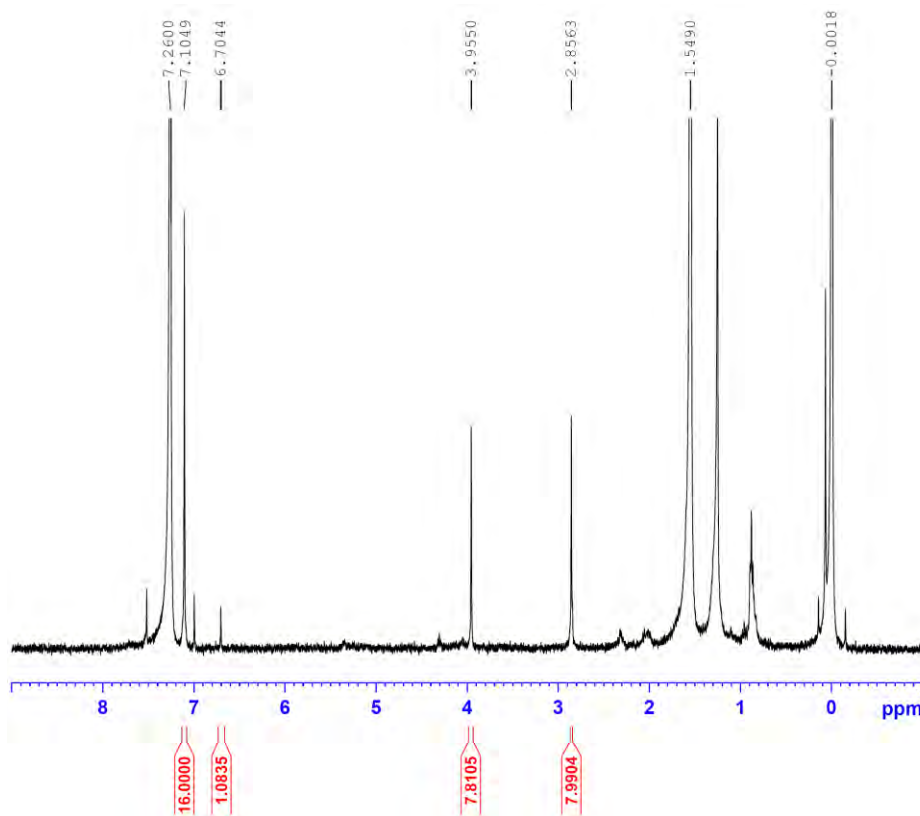
Current Data Parameters
NAME          CTT 272
EXPNO        7
PROCNO       1

F2 - Acquisition Parameters
Date_        20120305
Time_        12.50
INSTRUM      spect
PROBHD       5 mm PABBI 1H/
PULPROG      zg30
TD           65536
SOLVENT      CDCl3
NS           32
DS           2
SWH          12019.230 Hz
FIDRES       0.183399 Hz
AQ           2.7263477 sec
RG           203
DW           41.600 usec
DE           6.50 usec
TE           295.6 K
D1           1.00000000 sec
TD0          1

===== CHANNEL f1 =====
NUC1         1H
P1           7.10 usec
PL1          -2.00 dB
PL1W        -1.4IND0000 W
SFO1         400.1324710 MHz

F2 - Processing parameters
SI           32768
SF           400.1300100 MHz
WDW          EM
SSB          0
LB           0.30 Hz
GB           0
PC           1.00
    
```


unknown b (CDCl₃, 400 MHz)



```

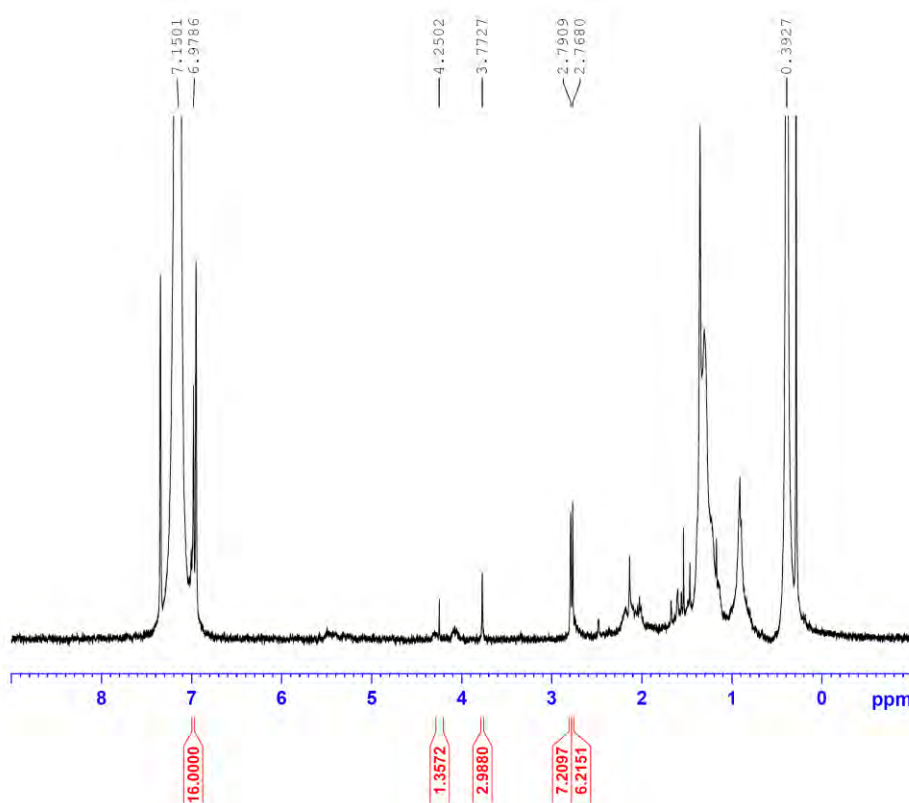
Current Data Parameters
NAME          CTT 272
EXPNO         8
PROCNO        1

F2 - Acquisition Parameters
Date_         20120305
Time          13.01
INSTRUM       spect
PROBHD        5 mm PABAI 1H/
PULPROG       zg30
TD            65536
SOLVENT       CDCl3
NS            32
DS            2
SWH           12019.230 Hz
FIDRES        0.183399 Hz
AQ            2.7263477 sec
RG            203
DW            41.600 usec
DE            6.50 usec
TE            295.4 K
D1            1.00000000 sec
TD0           1

===== CHANNEL f1 =====
NUC1           1H
P1             7.10 usec
PL1            -2.00 dB
PL1W          -1.#IND0000 W
SFO1           400.1324710 MHz

F2 - Processing parameters
SI             32768
SF            400.1300100 MHz
WDW            EM
SSB            0
LB             0.30 Hz
GB             0
PC             1.00
    
```

unknown c (C₆D₆, 400 MHz)



```

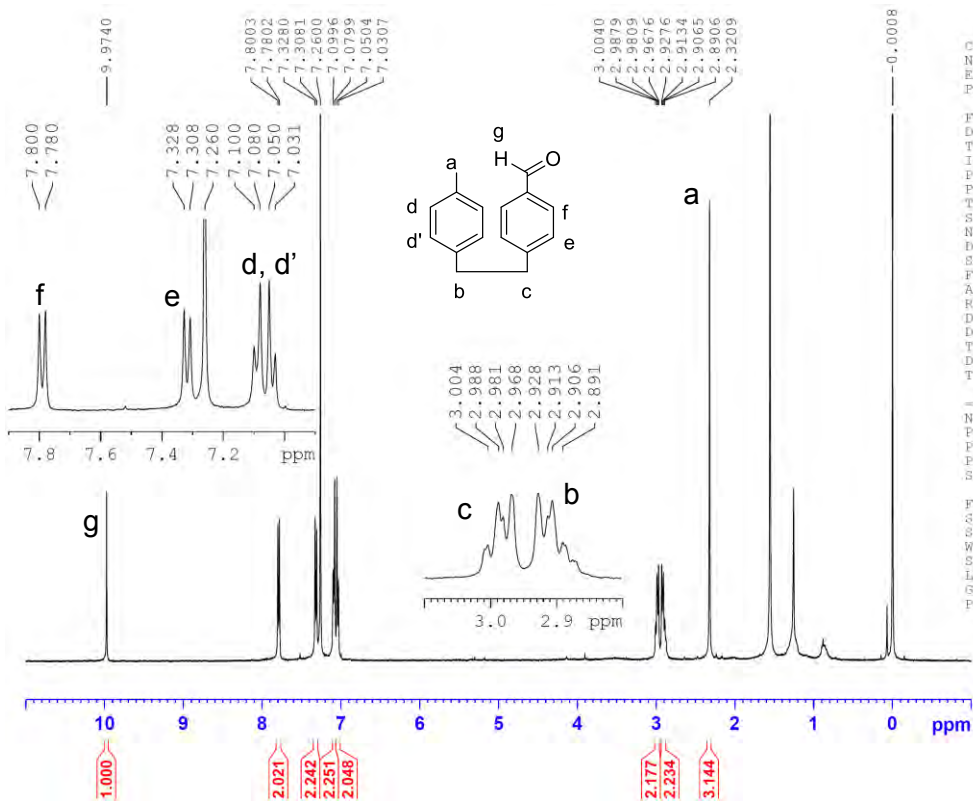
Current Data Parameters
NAME          CTT 272
EXPNO         6
PROCNO        1

F2 - Acquisition Parameters
Date_         20120229
Time          17.08
INSTRUM       spect
PROBHD        5 mm PABAI 1H/
PULPROG       zg30
TD            65536
SOLVENT       C6D6
NS            32
DS            2
SWH           12019.230 Hz
FIDRES        0.183399 Hz
AQ            2.7263477 sec
RG            203
DW            41.600 usec
DE            6.50 usec
TE            295.2 K
D1            1.00000000 sec
TD0           1

===== CHANNEL f1 =====
NUC1           1H
P1             7.10 usec
PL1            -2.00 dB
PL1W          -1.#IND0000 W
SFO1           400.1324710 MHz

F2 - Processing parameters
SI             32768
SF            400.1300482 MHz
WDW            EM
SSB            0
LB             0.30 Hz
GB             0
PC             1.00
    
```

4 (CDCl₃, 400 MHz)



```

Current Data Parameters
NAME      CTT 363
EXNO      6
PROCNO    1

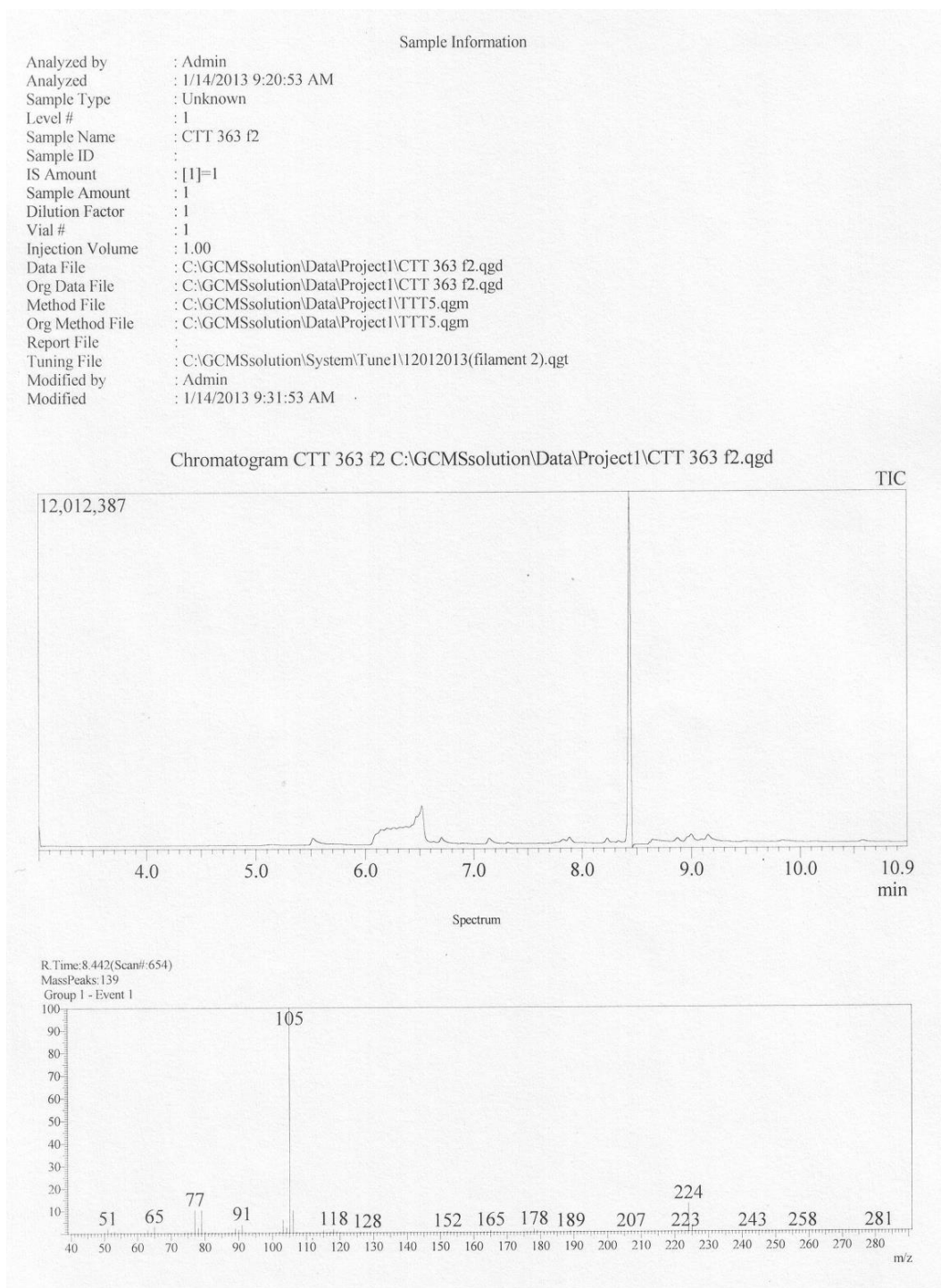
F2 - Acquisition Parameters
Date_     20130118
Time      16.50
INSTRUM   spect
PROBHD    5 mm PABBO BB-
PULPROG   zg30
TD         65536
SOLVENT   CDCl3
NS         24
DS         2
SWH        12019.230 Hz
FIDRES     0.183399 Hz
AQ         2.7263477 sec
RG         181
DW         41.600 usec
DE         8.50 usec
TE         296.2 K
D1         1.00000000 sec
TD0        1

----- CHANNEL F1 -----
NUC1       1H
P1         14.00 usec
PL1        -1.00 dB
PL1W       -1.#IND00000 W
SFO1       400.1924712 MHz

F2 - Processing parameters
SI         32768
SF         400.1900146 MHz
WDW        EM
SSB        0
LB         0.30 Hz
GB         0
PC         1.00
    
```

GCMS Spectra of 4

The peak at $m/z = 224$ agrees with the molecular mass of 4



References

1. Adler, A. D.; Longo, F. R.; Kampas, F.; Kim, J. J. *Inorg. Nucl. Chem.* **1970**, *32*, 2445-2448.

Chapter 5 Analysis on the Carbon-Carbon Bond Activation with Group 9 Metalloporphyrins

5.1 Introduction

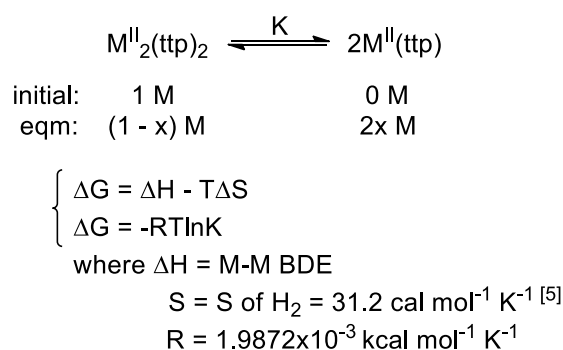
There are two reported CCA of unfunctionalized hydrocarbons with detailed experimental investigations: (1) Rh^{II}(ttp)-catalyzed 1,2-addition of Rh^{III}(ttp)H with *c*-octane¹ and (2) Rh^{II}(tmp) bi-metalloradical CCA of PCP.² This chapter will discuss these two modes of CCA in a more general approach based on the reaction thermodynamics and kinetics. Secondly, the bi-molecular reductive elimination between M^{III}(ttp)H and M^{III}(ttp)R to generate R-H and M^{II}₂(ttp)₂ will also be discussed as an alternative hydrogenation process. Finally, the reduction potentials of M^{III}(por)L complexes (M = Co, Rh and Ir) will be compared in relation to CCA.

5.2 Thermodynamics

5.2.1 Equilibrium Concentration of M^{II}(ttp) Metalloradical

Sterically non-bulky rhodium(II) and iridium(II) porphyrin radicals, e.g. Rh^{II}(ttp) and Ir^{II}(ttp), are in thermal equilibrium with its dimer in solutions.³ The degree of dimer dissociation to give the monomer increases with temperatures. Due to the much stronger (ttp)Ir-Ir(ttp) bond (20 kcal/mol) than the (ttp)Rh-Rh(ttp) bond (12 kcal/mol),⁴ Rh^{II}₂(ttp)₂ dissociates to give high concentration of Rh^{II}(ttp) than the iridium analogue under the same temperature. Table 5.1 tabulates the selected ΔG , K, [M^{II}(ttp)] at equilibrium and [Rh^{II}(ttp)]/[Ir^{II}(ttp)] ratio at equilibrium using 1 M Rh^{II}₂(ttp)₂ and Ir^{II}₂(ttp)₂ at initial as the examples from 0 °C to 200 °C.

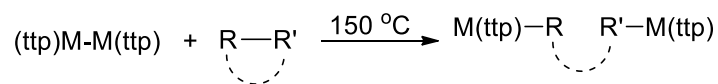
Table 5.1 Selected Equilibria of $M^{II}_2(tp)_2$ and $M^{II}(tp)$ from 0 °C to 200 °C (M = Rh and Ir).



T / °C	M = Rh			M = Ir			Rh ^{II} /Ir ^{II} ratio
	$\Delta G /$ kcal mol ⁻¹	K	2x / M	$\Delta G /$ kcal mol ⁻¹	K	2x / M	
0	3.5	0.0016	0.04	11.5	6.4×10^{-10}	2.5×10^{-5}	1577
20	2.9	0.0074	0.08	10.9	8.0×10^{-9}	8.9×10^{-5}	942
25	2.7	0.0104	0.10	10.7	1.4×10^{-8}	1.2×10^{-4}	836
40	2.2	0.0275	0.16	10.2	7.1×10^{-8}	2.7×10^{-4}	596
60	1.6	0.0877	0.28	9.6	4.9×10^{-7}	7.0×10^{-4}	392
80	1.0	0.2451	0.44	9.0	2.7×10^{-6}	1.7×10^{-3}	265
100	0.4	0.6133	0.64	8.4	1.3×10^{-5}	3.5×10^{-3}	182
120	-0.3	1.3979	0.88	7.7	5.0×10^{-5}	7.0×10^{-3}	125
140	-0.9	2.9419	1.13	7.1	1.7×10^{-4}	0.013	87
160	-1.5	5.7801	1.36	6.5	5.3×10^{-4}	0.023	59
180	-2.1	10.6988	1.55	5.9	0.0015	0.038	41
200	-2.8	18.7987	1.69	5.2	0.0038	0.061	28

5.2.2 Reaction Free Energy Estimations

The thermodynamic feasibilities of bi-metalloradical CCA with $Co^{II}(tp)$, $Rh^{II}_2(tp)_2$ and $Ir^{II}_2(tp)_2$ at 150 °C are estimated from the bond energy approach. In order to achieve a complete reaction, it is assumed that the reaction equilibrium constant must be greater than 100. This corresponds to a reaction free energy lower than -4 kcal/mol at 150 °C. Scheme 5.1 illustrates the estimation method. Similarly, scheme 5.2 illustrates the estimation for the $M^{II}(tp)$ -catalyzed 1,2-addition of $M^{III}(tp)H$.



at 150 °C, for a complete reaction with $K > 100$, then $\Delta G < -4$ kcal/mol

for non-ring substrate, $\Delta S \sim 0$

$$\Delta H = (\text{M}-\text{M}) + (\text{C}-\text{C}) - 2(\text{M}-\text{C})$$

$$\Delta G = \Delta H - T\Delta S$$

$$-4 > (\text{M}-\text{M}) + (\text{C}-\text{C}) - 2(\text{M}-\text{C})$$

$$2(\text{M}-\text{C}) > (\text{M}-\text{M}) + (\text{C}-\text{C}) + 4$$

for ring substrate with ring opening, $T\Delta S \sim -13$ kcal/mol

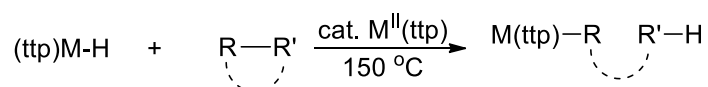
$$\Delta G = \Delta H - T\Delta S$$

$$-4 > (\text{M}-\text{M}) + (\text{C}-\text{C}) - 2(\text{M}-\text{C}) + 13$$

$$2(\text{M}-\text{C}) > (\text{M}-\text{M}) + (\text{C}-\text{C}) + 17$$

* there is no (M-M) term for Co(tp)

Scheme 5.1 Thermodynamic Estimation for the Bi-metalloradical CCA.



at 150 °C, for a complete reaction with $K > 100$, then $\Delta G < -4$ kcal/mol

for non-ring substrate, $\Delta S \sim 0$

$$\Delta H = (\text{M}-\text{H}) + (\text{C}-\text{C}) - (\text{M}-\text{C}) - (\text{C}-\text{H})$$

$$\Delta G = \Delta H - T\Delta S$$

$$-4 > (\text{M}-\text{H}) + (\text{C}-\text{C}) - (\text{M}-\text{C}) - (\text{C}-\text{H})$$

$$(\text{M}-\text{C}) + (\text{C}-\text{H}) > (\text{M}-\text{H}) + (\text{C}-\text{C}) + 4$$

for ring substrate with ring opening, $T\Delta S \sim -13$ kcal/mol

$$\Delta G = \Delta H - T\Delta S$$

$$-4 > (\text{M}-\text{H}) + (\text{C}-\text{C}) - (\text{M}-\text{C}) - (\text{C}-\text{H}) + 13$$

$$(\text{M}-\text{C}) + (\text{C}-\text{H}) > (\text{M}-\text{H}) + (\text{C}-\text{C}) + 17$$

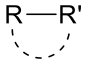
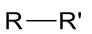
Scheme 5.2 Thermodynamic Estimation for the $\text{M}^{\text{II}}(\text{ttp})$ -Catalyzed 1,2-Addition of $\text{M}^{\text{III}}(\text{ttp})\text{H}$.

Substituting the bond energies of M-M and M-H bonds in $M^{II}_2(tp)_2$ and $M^{III}(tp)-H$, respectively, listed in Table 5.2 into Scheme 5.1 and Scheme 5.2, the minimum free energies estimated for the corresponding CCA reaction to occur are summarized in Table 5.3.

Table 5.2 Summary of the M-M and M-H Bond Energies.

M(tp)-X	Bond Energy (kcal/mol)	
	X = M(tp)	X = H
Co(tp)-X	N/A	52
Rh(tp)-X	12	60
Ir(tp)-X	20	70

Table 5.3 Estimations of the Energetic Requirement for the Two Types of CCA.

Substrate	Free Energy Estimation / kcal mol ⁻¹					
	M ^{II} (tp) bi-metalloradical CCA 2(M-C) > (C-C)			M ^{II} (tp)-catalyzed 1,2-addition of M ^{III} (tp)H (M-C) + (C-H) > (C-C)		
	Co	Rh	Ir	Co	Rh	Ir
	17	29	37	69	77	87
	4	16	24	56	64	74

Comparing rhodium and iridium in the bi-metalloradical CCA, despite the apparently thermodynamic more demanding for $Ir^{II}_2(tp)_2$, the Ir-C bond formed is stronger than the Rh-C bond formed by about 5 kcal/mol.^{4b} It sums up to 10 kcal/mol for two Ir-C bonds formation. It is well enough to compensate for the breaking of Ir-Ir bond which is 8 kcal/mol stronger than the Rh-Rh bond. Therefore, the bi-metalloradical CCA with $Ir^{II}_2(tp)_2$ is thermodynamically more favorable than with $Rh^{II}_2(tp)_2$.

$Co^{II}(tp)$ is considered a special case because it exists as a monomer without the need to break the M-M bond. Therefore, it only requires the two M-C bonds formed in total to be 4 kcal/mol stronger than the C-C bond being broken in order for the non-ring opening CCA to occur.

In the $M^{II}(ttp)$ -catalyzed 1,2-addition of $M^{III}(ttp)H$, the estimated trend in energetic requirements increases with the M-H bond energy in $M^{III}(ttp)-H$.

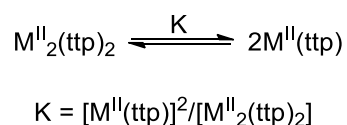
5.3 Kinetics

The proposed rate laws of $M^{II}(por)$ bi-metalloradical CCA and $M^{II}(por)$ -catalyzed 1,2-addition of $M^{III}(por)H$ with a hydrocarbon substrate in a general case are expressed in eqs 5.1 and 5.2, respectively.² Although the rate law for the latter reaction has not yet been measured experimentally for both Rh and Ir, we assumed that it follows a radical chain type reaction (for which $M^{II}_2(por)_2$ dimer exist) and 1st order in both $[M^{II}(por)]$ and $[M^{III}(por)H]$.⁶

$$\text{rate} = k[M^{II}(por)]^2[\text{substrate}] \quad (5.1)$$

$$\text{rate} = k[M^{II}(por)][M^{III}(por)H][\text{substrate}] \quad (5.2)$$

The two equations above is general to $M^{II}(por)$ that only exists as monomer, e.g. $Rh^{II}(tmp)$. For $M^{II}_2(por)_2$ which is in equilibrium with $M^{II}(por)$, e.g. $Rh^{II}_2(tmp)_2$, Scheme 5.3 applies. Therefore, the corresponding rate laws for $M^{II}_2(tmp)_2$ now become eqs 5.3 and 5.4.



Scheme 5.3 Equilibrium of $M^{II}_2(tmp)_2$ and $M^{II}(tmp)$.

$$\text{rate} = K^{1/2}k[M^{II}_2(tmp)_2]^{1/2}[\text{substrate}] \quad (5.3)$$

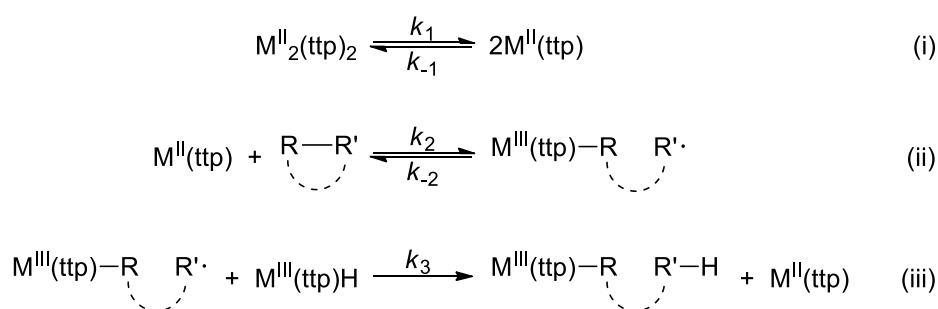
$$\text{rate} = K^{1/2}k[M^{II}_2(por)_2]^{1/2}[M^{III}(por)H][\text{substrate}] \quad (5.4)$$

Apart from the 1st order dependence on the substrate, the rate of bi-metalloradical CCA is 2nd order dependent on $M^{II}(tmp)$, which requires high temperatures to facilitate the $M^{II}_2(tmp)_2$ dimer dissociation. Although rate enhancement effect is significant with increased $[M^{II}(tmp)]$,

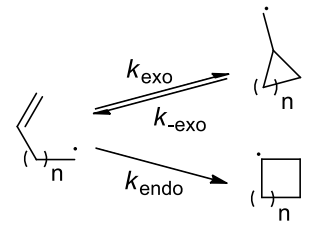
it also promotes the bi-metalloradical CHA at the same time.⁷ In other words, the bi-metalloradical CCA is more practical for CHA inactive substrates, for example [2.2]paracyclophane.

Such drawback is minimized in the M^{II} -catalyzed 1,2-addition of $M^{III}(ttp)H$ since it is 1st order dependent on $M^{II}(ttp)$. Alternatively, the reaction rate can be increased by employing a higher $[M^{III}(ttp)H]$. This combination allows milder reaction temperatures and probably lower operating $[M^{II}(ttp)]$. The extensive thermal dehydrogenation of $M^{III}(ttp)H$ and bi-molecular CHA can be avoided.

Unlike the $M^{II}(ttp)$ bi-metalloradical CCA, the $M^{II}(ttp)$ -catalyzed 1,2-addition of $M^{III}(ttp)H$ is essentially a three-step reaction (Scheme 5.4).¹ $M^{II}_2(ttp)_2$ first dissociates to give $M^{II}(ttp)$ (step i). After the initial CCA with $M^{II}(ttp)$ to generate a $M^{III}(ttp)$ -alkyl radical, it must possess sufficient life time to undergo the subsequent H atom abstraction from $M^{III}(ttp)H$ to furnish the reaction (step iii), otherwise it cyclizes back to regenerate the reactants (step ii). Since the values for k_1 , k_2 and k_3 are not reported, the rate constants of olefin-radical cyclization and H atom abstraction from common H atom sources are compared for reference (Tables 5.4 and 5.5).



Scheme 5.4 Stepwise $M^{II}(ttp)$ -Catalyzed 1,2-Addition of $M^{III}(ttp)H$.

Table 5.4 Rate Constants of *exo* and *endo* Cyclization of Olefin Alkyl Radicals at 25 °C.⁸


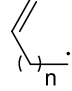
	$k_{\text{exo}} / \text{s}^{-1}$	$k_{-\text{exo}} / \text{s}^{-1}$	$k_{\text{endo}} / \text{s}^{-1}$
n = 1	1.8×10^4	2.0×10^8	not observed
n = 2	1.0	4.7×10^3	not observed
n = 3	2.3×10^5	--	4.1×10^3
n = 4	5.2×10^3	--	8.3×10^2
n = 5	<70	--	1.2×10^5

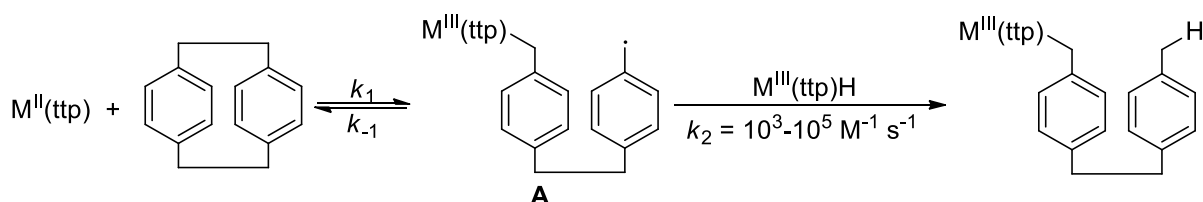
 Table 5.5 Rate Constants of H Atom Abstraction of 1°, 2°, 3° Alkyl and Benzylic Radicals at 25-30 °C.⁸

H Atom Source	X-H BDE ⁸ / kcal mol ⁻¹	$k / \text{M}^{-1} \text{s}^{-1}$			
		RCH ₂ ·	R ₂ CH·	R ₃ C·	PhCH ₂ ·
PhS-H	83.5	9.2×10^7	1.1×10^8	1.5×10^8	3.0×10^5
Et ₃ Si-H	94.6	7.0×10^3	N/A	3.0×10^3	N/A
Cy ₂ P-H	86.2	1.0×10^6	N/A	2.5×10^3	2.5×10^3
<i>n</i> -Bu ₃ Ge-H	~86	1.0×10^5	N/A	N/A	N/A
<i>n</i> -Bu ₃ Sn-H	78.0	2.7×10^6	1.5×10^6	1.7×10^6	3.6×10^4
1,4-cyclohexadiene	74.3	4.8×10^5	N/A	9.4×10^3	1.0×10^2

The rate constants of intramolecular cyclization are in the range of 10^3 to 10^5 s^{-1} (Table 5.4). The bi-molecular rate constants of H atom abstraction from non C-H sources are in the range of 10^3 to $10^8 \text{ M}^{-1} \text{ s}^{-1}$ (Table 5.5). Abstraction of H atom from donor with weaker X-H bond tends to be faster. Rh^{III}(ttp)H and Ir^{III}(ttp)H with M-H BDE to be 60 kcal/mol and 70 kcal/mol, respectively, serve as the much better H atom donors. Therefore, the latter process can compete with the cyclization in the presence of sufficient H atom donor.

The benzylic radical undergoes slower H atom abstraction than the 1°, 2° and 3° alkyl radicals by 2 to 3 orders of magnitude, probably due to the formation of weaker benzylic C-H bond (89.7 kcal/mol) than a typical alkyl C-H bond (~100 kcal/mol).⁹ Therefore in the CCA of

PCP, even though $M^{II}(ttp)$ cleaves the benzylic C-C bond of PCP bi-molecularly to form the $M^{III}(ttp)$ -terminal benzylic radical intermediates **A**, it may re-cyclize much faster than abstracting a H atom from $M^{III}(ttp)H$, e.g. $k_{-1}[A] \gg k_2[A][M^{III}(ttp)H]$ (Scheme 5.5). CCA of PCP via $M^{II}(ttp)$ -catalyzed 1,2-addition of $M^{III}(ttp)H$ will not be observed. In contrast, the CCA of *c*-octane proceeds smoothly via the $Rh^{II}(ttp)$ -catalyzed 1,2-addition of $Rh^{III}(ttp)H$ pathway as it involves the H atom abstraction by 1° alkyl radical intermediate.

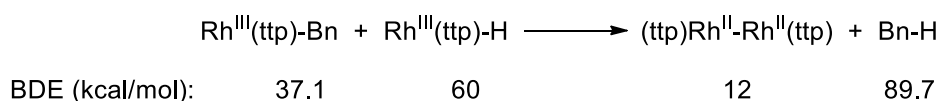


Scheme 5.5 Absence of $M^{II}(ttp)$ -Catalyzed 1,2-Addition of $M^{III}(ttp)H$ for PCP.

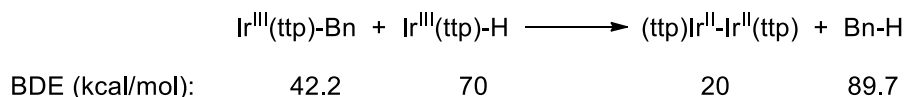
5.4 Bi-molecular Reductive Elimination with $M^{III}(ttp)H$

In Chapter 3, the reductive elimination of toluene and $Ir^{II}_2(ttp)_2$ from $Ir^{III}(ttp)Bn$ and $Ir^{III}(ttp)H$ is discussed. Here, the reaction thermodynamics will be analyzed as well as for the analogous reaction with rhodium porphyrin complexes.

Using the BDE values of $Rh^{III}(ttp)-Bn$ (37.1 kcal/mol),¹⁰ $Rh^{III}(ttp)-H$ (60 kcal/mol),^{4a} $(ttp)Rh^{II}-Rh^{II}(ttp)$ (12 kcal/mol)^{4a} and $Bn-H$ (89.7 kcal/mol),⁹ this yields the free energy of -4.6 kcal/mol for the reaction with rhodium porphyrin complexes (Scheme 5.6). The corresponding reaction free energy for iridium porphyrin complexes is estimated to be 2.5 kcal/mol, which is endergonic.



Assume $T\Delta S \sim 0$
then $\Delta G = \Delta H$
 $= 37.1 + 60 - 12 - 89.7$
 $= -4.6 \text{ kcal/mol}$



Assume $T\Delta S \sim 0$
then $\Delta G = \Delta H$
 $= 42.2 + 70 - 20 - 89.7$
 $= 2.5 \text{ kcal/mol}$

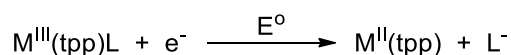
Scheme 5.6 Thermodynamic Estimations for the Bi-molecular Reductive Eliminations.

This surprising results suggest that the bi-molecular reductive elimination of toluene and $\text{Rh}^{\text{II}}_2(\text{ttp})_2$ from $\text{Rh}^{\text{III}}(\text{ttp})\text{Bn}$ and $\text{Rh}^{\text{III}}(\text{ttp})\text{H}$ may occur more readily than the iridium system studied. In the rhodium porphyrin catalytic hydrogenation of PCP with H_2O , the di-Rh and mono-Rh CCA intermediates may react with $\text{Rh}^{\text{III}}(\text{ttp})\text{H}$ as an alternative hydrogenation pathway, in analogous to the iridium porphyrin system discussed in Chapter 3.

5.5 Redox Potentials of Group 9 Metalloporphyrins

The reduction potentials of group 9 metal(III) porphyrin complexes provide another useful insight on their reactivities in the CCA reactions. For example, the bi-metalloradical CCA of PCP with $\text{Rh}^{\text{II}}(\text{tmp})$ accompanies the metal center oxidation from Rh(II) to Rh(III). This process would be more favorable with a more negative Rh(III)/Rh(II) reduction potential, suggesting a more stable Rh(III) state. Table 5.6 lists the reduction potentials of $\text{M}^{\text{III}}(\text{ttp})\text{L}$ and $\text{M}^{\text{III}}(\text{oep})\text{L}$ ($\text{M} = \text{Co}, \text{Rh}$ and Ir) as the references.

Table 5.6 Comparison on the Reduction Potentials of M^{III}(por)L.



M	por	L	solvent	temp / °C	E ^o vs SCE / V
Co		Cl	CH ₂ Cl ₂	N/A	-0.055 ¹¹
Rh	tpp	Cl	THF	23	-1.01 ¹²
Ir		(CO)Cl	THF	22	-1.17 ¹³
Co		Br	CH ₂ Cl ₂ :MeOH (4:1)	N/A	-1.05 ¹⁴
Rh	oep	Cl	THF	23	-1.30 ¹²
Ir		(CO)Cl	THF	22	-1.49 ¹³

The tendency for the reduction of M^{III}(por)L to M^{II}(por) follows a general trend for both tpp and oep ligands: Co > Rh > Ir. As the electron richness increases down the group, the high valent M(III) oxidation state can be better stabilized. The reducing property is further enhanced with more electron rich oep ligand. This facilitates the oxidation of M^{II}(por).

From the above table, it suggested that iridium(II) porphyrins are the most reducing. In other words, CCA using iridium(II) porphyrins will be thermodynamically more favorable than rhodium(II) and cobalt(II) porphyrins. This agrees with the energetic estimation discussed in section 5.2.2 for bi-metalloradical CCA process. In addition, electron rich porphyrin ligand increases the LUMO energy and the metalloradical character of Ir^{II}(por)

The reduction potentials of Co(III)/Co(II) reported varies greatly in the literatures, from +0.01 V to -1.05 V. Alternative report suggests that the reduction of Co^{III}(tpp)R (R = Me, Et and CH₂Cl) occurs at the porphyrin ligand instead of the Co(III) center to form porphyrin π radical anion only at potentials from -1.37 V to -1.42 V (vs SCE) in THF or CH₂Cl₂.¹⁵ These examples showed that cobalt porphyrins exhibit distinct reactivity depending on the reaction conditions. In contrast, the 1st oxidation potentials of Co^{II}(tpp) from two separate reports are similar, e.g. +0.58 V and +0.52V (vs SCE), giving metal center oxidized [Co^{III}(tpp)]⁺ complex.^{16,17}

5.6 Conclusions

The $M^{II}(\text{por})$ bi-metalloradical CCA and $M^{II}(\text{por})$ -catalyzed 1,2-addition of $M^{III}(\text{por})\text{H}$ were analyzed from the thermodynamic and kinetic points of view. The $M^{II}(\text{por})$ bi-metalloradical CCA is ideal for CHA inactive hydrocarbon substrate. This process is thermodynamically more favorable with $\text{Ir}^{II}_2(\text{ttp})_2$, in agreement with the estimation using the 1st reduction potentials of $M^{III}(\text{por})\text{L}$. Alternatively, the $M^{II}(\text{por})$ -catalyzed 1,2-addition of $M^{III}(\text{por})\text{H}$ pathway avoids the bi-metalloradical CHA process by kinetic control. The bimolecular reductive elimination with $M^{III}(\text{ttp})\text{H}$ as an alternative hydrogenation process is thermodynamically more favorable for rhodium porphyrin complexes.

References

1. Chan, Y. W.; Chan, K. S. *J. Am. Chem. Soc.* **2010**, *132*, 6920-6922.
2. To, C. T.; Choi, K. S.; Chan, K. S. *J. Am. Chem. Soc.* **2012**, *134*, 11388-11391.
3. Cui, W.; Li, S.; Wayland, B. B. *J. Organomet. Chem.* **2007**, *692*, 3198-3206.
4. (a) Wayland, B. B.; Ba, S.; Sherry, A. E. *J. Am. Chem. Soc.* **1991**, *113*, 5305-5311. (b) Wayland, B. B. *Personal Communication*, Temple University, Philadelphia, PA, 2008.
5. Chase, M. W., Jr. *J. Phys. Chem. Ref. Data, Monograph 9* **1998**, 1-1951.
6. Espenson, J. *Chemical Kinetics and Reaction Mechanisms*, 2nd Ed., McGraw-Hill Companies, Inc., USA, 2002.
7. (a) Wayland, B. B.; Ba, S.; Sherry, A. E. *J. Am. Chem. Soc.* **1991**, *113*, 5305-5311. (b) Wayland, B. B.; Ba, S.; Sherry, A. E. *Inorg. Chem.* **1992**, *31*, 148-150.
8. Fossey, J.; Lefort, D.; Sorba, J. *Free Radicals in Organic Chemistry*, John Wiley & Sons, Masson, Paris, 1997.
9. Luo, Y. R. *Comprehensive Handbook of Chemical Bond Energies*, CRC Press, Boca Raton, FL, 2007.
10. Cui, W.; Wayland, B. B. *J. Am. Chem. Soc.* **2004**, *126*, 8266-8274.
11. Huet, J.; Gaudemer, A.; Boucly-Goester, C.; Boucly, P. *Inorg. Chem.* **1982**, *21*, 3413-3419.
12. Liu, Y. H.; Anderson, J. E.; Kadish, K. M. *Inorg. Chem.* **1988**, *27*, 2320-2325.
13. Swistak, C.; Cornilion, J.-L.; Anderson, J. E.; Kadish, K. M. *Organometallics* **1987**, *6*, 2146-2150.
14. Johnson, A. W.; Ward, D.; Batten, P.; Hamilton, A. L.; Shelton, G.; Elson, C. M. *J. Chem. Soc., Perkin Trans. 1* **1975**, 2076-2085.
15. Kadish, K. M.; Han, B. C.; Endo, A. *Inorg. Chem.* **1991**, *30*, 4502-4506.
16. Tezuka, M.; Ohkatsu, Y.; Osa, T. *Bull. Chem. Soc. Jpn.* **1976**, *49*, 1435-1436.

17. D'Souza, F.; Villard, A.; Van Caemelbecke, E.; Franzen, M.; Boschi, T.; Tagliatesta, P.; Kadish, K. M. *Inorg. Chem.* **1993**, *32*, 4042-4048.